


國立交通大學

機械工程學系  
碩士論文

使用平行化直接模擬蒙地卡羅法初步模擬在稀薄流體  
範圍時瞬間啟動的空穴超音速流場

**Preliminary Simulation of Instantaneously Started  
Supersonic Driven Cavity Flows in the Rarefied Gas  
Regimes Using the Parallel Direct Simulation Monte Carlo  
Method**



研究生：洪維呈

指導教授：吳宗信 博士

中華民國九十六年七月

使用平行化直接模擬蒙地卡羅法初步模擬在稀薄流體範圍時瞬間啟動的空

穴超音速流場

Preliminary Simulation of Instantaneously Started Supersonic Driven Cavity

Flows in the Rarefied Gas Regime Using the Parallel Direct Simulation Monte

Carlo Method

研究生：洪維呈

Student: Wei-Cheng Hung

指導教授：吳宗信 博士

Advisor: Dr. Jong-Shinn Wu



A Thesis

Submitted to Institute of Mechanical Engineering

College of Engineering

National Chiao Tung University

in partial Fulfillment of the Requirements

for the Degree of

Master of Science

in

Mechanical Engineering

July 2007

Hsinchu, Taiwan

中華民國九十六年七月

## 致謝

在交大兩年的求知路程，特別感謝指導教授吳宗信老師的照顧，讓我在學習過程及生活方面都得到不少獲益。在研究及做學問方面，與老師的知識交流實令我感到獲益匪淺，讓我能順利的踏入研究的領域並且不斷地成長。還有老師愛台灣精神及推廣本土文化不遺餘力也在我心中根深蒂固。同時也感謝口試委員黃俊誠老師、郭添全博士、陳明志老師在口試時提供的寶貴意見，使得本論文更加充實完備。另外特別感謝曾坤璋學長長期發展關於此篇論文中所用到的程式之辛勞，且在最後兩個月不吝於付出時間與心力來教導我於研究中所遭遇的問題，以及蔡哥、凱文兄在研究上啟發教導及生活上的鼓勵幫助，在此一併致謝。

要感謝的人太多，邵雲龍、許國賢、陳育進、梁偉豪、陳百彥等已畢業的學長，還有 APPL 實驗室的成員，李允民、周欣芸、李富利、洪捷祭、許哲維、鄭凱文、胡孟樺、邱沅明、江明鴻學長姊指導受益良多，盧勁全、謝昇汎、林宗漢、陳又寧、王柏勝同學，與你們努力奮鬥相處的時光將是我最美好的回憶，正勤、士傑、志良、玫琪、丞志、政霖、育宗等學弟妹們協助，以及來自紐西蘭的訪問學者 Hadley M. Cave (瓦片)，使我這兩年過得相當充實且溫馨，並能順利完成學業。

此外最後特別感謝我的大學指導教授牛仰堯導師，感謝他對我的期許鼓勵及愛護，我會更加努力朝向目標邁進，以及陪伴我的家人，辛苦了。在這離別季節，大家各自奔向前程，希望大家追求自己的夢想前進，擁有光明未來和生活。

洪維呈 謹誌

九六年七月于風城

# 使用平行化直接模擬蒙地卡羅法初步模擬在稀薄流體範圍時瞬間

## 啟動的空穴超音速流場

學生：洪維呈

指導教授：吳宗信

國立交通大學機械工程學系

### 摘要

空穴流場是一個很基本的流體力學問題，在過去也有很多人做過相關的研究。但是大多數人都是討論連續及不可壓縮流流場，較少數人針對連續流到稀薄流體區的流場作研究。因此我們對此做一系列的探討。

本文的目的為使用直接模擬蒙地卡羅法及非結構性網格來模擬從自由分子流到接近連體流體範圍瞬間啟動的空穴超音速流場。傳統上在模擬稀薄區中，非穩態流場較少人研究，也較困難。我們先運用非穩態的時間平均取樣方法來模擬，但發現有大量 scatter 現象。因而我們運用 DSMC-DREAM (Rapid Ensembled Average Method) [Cave et al., 2007] 可運用在減少統計時產生的 scatter 時間平均的 DSMC 資料，也為了確保能在較鄰近的分子發生碰撞，運用 transient sub-cells 在非結構性網格功能，使得同時降低計算負荷及記憶體使用量。

模擬且比較在 quasi-1D 不可壓縮 Couette 流體分析資料來驗證程式。結果發現 DREAM 能夠大量地減低在使用非穩態 DSMC 技術時產生的統計 scatter。最後，模擬非



穩態驅動空穴流場條件包含上板驅動速度馬赫數 4 和 Knudsen 數(與平均自由路徑和空穴大小有關)由 10 到 0.0033。

結果顯示其速度滑動現象會在 Knudsen 數的影響中表現的很明顯。在 Knudsen 數 0.1，0.01 和 0.0033 的渦流幾何中心隨時間改變後會朝向幾何中心；但 Knudsen 數 10 和 1 則往上板移動。而由於本文為初步模擬在非穩態的流場現象，所以先模擬在高馬赫 4 的流體。然而模擬此空穴超音速流場仍然有些統計樣本造成的 scatter 誤差現象。所以在未來會使用 temporal variable time step 來減少計算時間，及同時增加 DSMC-DREAM (Rapid Ensembled Average Method) [Cave et al., 2007] 循環次數，來大大減低此 scatter 誤差現象。



# **Preliminary Simulation of Instantaneously Started Supersonic Driven Cavity Flows in the Rarefied Gas Regime Using the Parallel Direct Simulation Monte Carlo Method**

Student: Wei-Cheng Hung

Advisor: Dr. Jong-Shinn Wu

Department of Mechanical Engineering  
National Chiao-Tung University

## **Abstract**

The driven cavity flow is one of the fundamental problems in the fluid dynamics. The kind of topic establishes the foundation in computational fluid dynamics and its simple geometry. However they have been completely studied in the literature, most of researches focused on incompressible or continuum compressible regime. Very few researches have been done in the rarefied and near continuum regimes. It may serve as the benchmarking problem in these regimes. Therefore, this thesis reports the simulation of instantaneously started supersonic driven cavity flows from the free-molecular to near-continuum regime using the parallel direct Monte Carlo method using unstructured grids. A special technique called DSMC-DREAM (Rapid Ensembled Average Method) was applied to reduce the statistical scatter of time-averaging DSMC data. To ensure nearest-neighbor collision, transient sub-cells are also implemented on an unstructured grid. Implementation was verified by comparing the simulation results of a quasi-1D incompressible Couette flow with the analytical data. Result shows that the DREAM can greatly reduce the statistical scatter with

an acceptable runtime for unsteady flow simulation using DSMC technique. Simulation conditions for the unsteady top driven cavity flows include  $Ma=4$  of the speed of top driven plate and  $Kn=10-0.0033$  based on the mean free path of wall temperature and size of the cavity. Results show that the velocity slips along the solid walls increase with increase Knudsen number at the same Mach number ( $M=4$ ). Center of the primary vortex during one time moves towards the geometric center with Knudsen number is 0.1, 0.01 and 0.0033. Other cases move toward the upper wall with Knudsen number is 10 and 1. Because the thesis is preliminary study on unsteady flow, thus we focus on supersonic flow ( $M=4$ ). There are scatter on simulation supersonic cavity flow; hence it will use temporal variable time step to induce computational cost and increase DSMC-DREAM (Rapid Ensembled Average Method) run times. Further, the imperfection of results are on Knudsen number 10 (free molecular flow), 1 and 0.1 because of the mean free path larger than characteristic length. Thus, particles could collisionless of a square driven cavity.



# Table of Contents

|   |      |
|---|------|
| 致謝 .....  | I    |
| 摘要 .....  | II   |
| Abstract.....   | IV   |
| Table of Contents.....  | VI   |
| List of Tables .....  | VIII |
| List of Figures.....  | IX   |
| Nomenclature.....   | XV   |
| Chapter 1 Introduction.....   | 1    |
| 1.1. Motivation and Background .....  | 1    |
| 1.1.1 Importance of Driven Cavity Flows .....   | 1    |
| 1.1.2 Classification of Rarefaction .....   | 2    |
| 1.1.3 Direct Simulation Monto Carlo Method.....   | 3    |
| 1.2. Literature Survey .....  | 5    |
| 1.3. Specific Objectives of the Thesis .....  | 7    |
| Chapter 2 Numerical Methods.....  | 8    |
| 2.1. The Boltzmann Equation .....   | 8    |
| 2.2. General Description of the standard DSMC.....  | 10   |
| 2.3. General Description of the PDSC.....   | 15   |
| 2.4. General Description of Unsteady Sampling Method in DSMC [JCP paper<br>submitted in June 2007]..... | 18   |
| 2.5. DSMC Rapid Ensemble Averaging Method (DREAM) [JCP paper submitted in<br>June 2007] .....           | 19   |
| Chapter 3 Results and Discussion .....  | 21   |
| 3.1. Quasi 1-D Couette Flows .....  | 21   |
| 3.1.1. Problem Description and Test Conditions .....  | 22   |
| 3.1.2. Verifications of Unsteady Sample Method.....   | 22   |
| 3.1.3. Verifications of DSMC Rapid Ensemble Average Method (DREAM) ....                                 | 23   |
| 3.1.4. Benchmark of the Transient Sub-Cell Method.....  | 24   |
| 3.2. Instantaneously Started Driven Cavity Flows .....  | 26   |
| 3.2.1. Problem Description and Test Conditions .....  | 26   |
| 3.2.2. Effects of Knudsen Number .....  | 27   |
| 3.2.2.1. General Simulation Results .....   | 27   |
| 3.2.2.1.1. Supersonic Moving Plate (M=4) .....  | 27   |
| 3.2.2.2. Property Distributions Across Cavity Centroid.....   | 30   |
| 3.2.2.2.1. Supersonic Moving Plate (M=4) .....  | 30   |
| 3.2.2.3. Property Distributions Near Solid Walls .....  | 34   |
| 3.2.2.3.1. Supersonic Moving Plate (M=4) .....  | 34   |

|   |    |
|---|----|
| 3.2.2.4. Recirculation Center Position.....                   | 36 |
| Chapter 4 Conclusions and Recommendation of Future Work ..... | 39 |
| 4.1. Summary.....   | 39 |
| 4.2. Recommendation of Future Work .....                      | 39 |
| References .....  | 41 |



## List of Tables

|           |  |    |
|-----------|--|----|
| Table I   | Flow and simulation condition for 1-D Couette flow.....      | 43 |
| Table II  | The grid sizes of distinct driven cavity cases. ....         | 44 |
| Table III | The time steps of distinct driven cavity cases. ....         | 45 |
| Table IV  | The initial conditions of distinct driven cavity cases. .... | 46 |
| Table V   | The other conditions of distinct driven cavity cases.....    | 47 |
| Table VI  | Positions of properties distributions across .....           | 48 |



## List of Figures

|                  |   |    |
|------------------|---|----|
| <b>Fig. 2.1</b>  | Classifications of Gas Flows .....  | 49 |
| <b>Fig. 2.2</b>  | Flow chart of the DSMC method .....   | 50 |
| <b>Fig. 2.3</b>  | Simplified flow chart of the parallel DSMC method for np processors....   | 51 |
| <b>Fig. 2.4</b>  | The additional schemes in the parallel DSMC code.....   | 52 |
| <b>Fig. 2.5</b>  | Sampling method in DSMC include (a) steady sampling (b) unsteady ensemble sampling (c) unsteady time averaging. ....  | 53 |
| <b>Fig. 2.6</b>  | Simplified flow chart of the unsteady parallel DSMC method. ....  | 54 |
| <b>Fig. 2.7</b>  | Simplified flow chart of the DSMC Rapid Ensemble Averaging Method (DREAM).....  | 55 |
| <b>Fig. 3.1</b>  | Computational domains for the developing Couette flow. ....   | 56 |
| <b>Fig. 3.2</b>  | The mesh (100x100) for M=0.3, Kn=0.02 Couette flow.....   | 57 |
| <b>Fig. 3.3</b>  | Contours of velocity for M=0.3, Kn=0.02 Couette flow from unsteady DSMC technique at normalized time (a) t=1; (b) t=3; (c) t=7; (d) t=16; (e) t=32.....                   | 58 |
| <b>Fig. 3.4</b>  | Comparison of for M=0.3, Kn=0.02 Couette flow development by unsteady DSMC (symbols) with the exact Navier-Stokes solution (lines).....                                   | 59 |
| <b>Fig. 3.5</b>  | Contours of velocity for for M=0.3, Kn=0.02 Couette flow from DREAM technique at normalized time (a) t=1; (b) t=3; (c) t=7; (d) t=16; (e) t=32                            | 60 |
| <b>Fig. 3.6</b>  | Comparison of for M=0.3, Kn=0.02 Couette flow development by unsteady DSMC with the DREAM technique at normalized time (a) t=1; (b) t=3; (c) t=7; (d) t=16; (e) t=32..... | 61 |
| <b>Fig. 3.7</b>  | Comparison of for M=0.3, Kn=0.02 Couette flow development by unsteady DSMC with the DREAM technique (symbols) with the exact Navier-Stokes solution (lines). ....         | 62 |
| <b>Fig. 3.8</b>  | The mesh for $\frac{\Delta x}{\lambda} = \frac{\Delta y}{\lambda} = 0.25$ for M=0.3, Kn=0.02 Couette flow. ....   | 63 |
| <b>Fig. 3.9</b>  | Contours of velocity for $\frac{\Delta x}{\lambda} = \frac{\Delta y}{\lambda} = 0.25$ , for M=0.3, Kn=0.02 Couette flow. ....   | 64 |
| <b>Fig. 3.10</b> | Contours of mcs/mfps for $\frac{\Delta x}{\lambda} = \frac{\Delta y}{\lambda} = 0.25$ , for M=0.3, Kn=0.02 Couette flow. ....   | 65 |
| <b>Fig. 3.11</b> | the mesh for $\frac{\Delta x}{\lambda} = \frac{\Delta y}{\lambda} = 1$ for M=0.3, Kn=0.02 Couette flow. ....  | 66 |
| <b>Fig. 3.12</b> | Contours of mcs/mfps for $\frac{\Delta x}{\lambda} = \frac{\Delta y}{\lambda} = 1$ , for M=0.3, Kn=0.02 Couette flow. ....  | 67 |

|                  |   |    |
|------------------|---|----|
| <b>Fig. 3.14</b> | Comparison of Couette flow development by $\frac{\Delta x}{\lambda} = \frac{\Delta y}{\lambda} = 0.25$ with $\frac{\Delta x}{\lambda} = \frac{\Delta y}{\lambda} = 1$ .....                                       | 69 |
| <b>Fig. 3.15</b> | The 2D square (L/H=1) driven cavity flow with moving top plate.....   | 70 |
| <b>Fig. 3.16</b> | the mesh (40x40) for Kn=10, 1, 0.1 driven cavity flow. ....   | 71 |
| <b>Fig. 3.17</b> | the mesh (100x100) for Kn=0.01 driven cavity flow. ....   | 72 |
| <b>Fig. 3.18</b> | the mesh (300x300) for Kn=0.0033 driven cavity flow. ....   | 73 |
| <b>Fig. 3.19</b> | Contours of u-velocity for M=4, Kn=10 at (a) t =50 $\mu$ s; (b) t =125 $\mu$ s; (c) t =225 $\mu$ s; (d) t =325 $\mu$ s; (e) t =425 $\mu$ s; (f) t =600 $\mu$ s; (g) t =1500 $\mu$ s; (h) t =3000 $\mu$ s .....    | 74 |
| <b>Fig. 3.20</b> | Contours of u-velocity for M=4, Kn=1 at (a) t =40 $\mu$ s; (b) t =100 $\mu$ s; (c) t =180 $\mu$ s; (d) t =320 $\mu$ s; (e) t =480 $\mu$ s; (f) t =700 $\mu$ s; (g) t =1100 $\mu$ s; (h) t =1800 $\mu$ s .....     | 75 |
| <b>Fig. 3.21</b> | Contours of u-velocity for M=4, Kn=0.1 at (a) t =10 $\mu$ s; (b) t =50 $\mu$ s; (c) t =150 $\mu$ s; (d) t =300 $\mu$ s; (e) t =500 $\mu$ s; (f) t =900 $\mu$ s; (g) t =2500 $\mu$ s; (h) t =4500 $\mu$ s .....    | 76 |
| <b>Fig. 3.22</b> | Contours of u-velocity for M=4, Kn=0.01 at (a) t =10 $\mu$ s; (b) t =75 $\mu$ s; (c) t =175 $\mu$ s; (d) t =300 $\mu$ s; (e) t =500 $\mu$ s; (f) t =900 $\mu$ s; (g) t =1750 $\mu$ s; (h) t =3750 $\mu$ s .....   | 77 |
| <b>Fig. 3.23</b> | Contours of u-velocity for M=4, Kn=0.0033 at (a) t =10 $\mu$ s; (b) t =40 $\mu$ s; (c) t =120 $\mu$ s; (d) t =400 $\mu$ s; (e) t =800 $\mu$ s; (f) t =1200 $\mu$ s; (g) t =1800 $\mu$ s; (h) t =2650 $\mu$ s..... | 78 |
| <b>Fig. 3.24</b> | Contours of v-velocity for M=4, Kn=10 at (a) t =50 $\mu$ s; (b) t =125 $\mu$ s; (c) t =225 $\mu$ s; (d) t =325 $\mu$ s; (e) t =425 $\mu$ s; (f) t =600 $\mu$ s; (g) t =1500 $\mu$ s; (h) t =3000 $\mu$ s .....    | 79 |
| <b>Fig. 3.25</b> | Contours of v-velocity for M=4, Kn=1 at (a) t =40 $\mu$ s; (b) t =100 $\mu$ s; (c) t =180 $\mu$ s; (d) t =320 $\mu$ s; (e) t =480 $\mu$ s; (f) t =700 $\mu$ s; (g) t =1100 $\mu$ s; (h) t =1800 $\mu$ s .....     | 80 |
| <b>Fig. 3.26</b> | Contours of v-velocity for M=4, Kn=0.1 at (a) t =10 $\mu$ s; (b) t =50 $\mu$ s; (c) t =150 $\mu$ s; (d) t =300 $\mu$ s; (e) t =500 $\mu$ s; (f) t =900 $\mu$ s; (g) t =2500 $\mu$ s; (h) t =4500 $\mu$ s .....    | 81 |
| <b>Fig. 3.27</b> | Contours of v-velocity for M=4, Kn=0.01 at (a) t =10 $\mu$ s; (b) t =75 $\mu$ s; (c) t =175 $\mu$ s; (d) t =300 $\mu$ s; (e) t =500 $\mu$ s; (f) t =900 $\mu$ s; (g) t =1750 $\mu$ s; (h) t =3750 $\mu$ s .....   | 82 |
| <b>Fig. 3.28</b> | Contours of v-velocity for M=4, Kn=0.0033 at (a) t =10 $\mu$ s; (b) t =40 $\mu$ s; (c) t =120 $\mu$ s; (d) t =400 $\mu$ s; (e) t =800 $\mu$ s; (f) t =1200 $\mu$ s; (g) t =1800 $\mu$ s; (h) t =2650 $\mu$ s..... | 83 |



|                  |  |    |
|------------------|--|----|
| <b>Fig. 3.29</b> | Contours of Mach number for $M=4$ , $Kn=10$ at (a) $t=50 \mu s$ ; (b) $t=125 \mu s$ ; (c) $t=225 \mu s$ ; (d) $t=325 \mu s$ ; (e) $t=425 \mu s$ ; (f) $t=600 \mu s$ ; (g) $t=1500 \mu s$ ; (h) $t=3000 \mu s$ .....        | 84 |
| <b>Fig. 3.30</b> | Contours of Mach number for $M=4$ , $Kn=1$ at (a) $t=40 \mu s$ ; (b) $t=100 \mu s$ ; (c) $t=180 \mu s$ ; (d) $t=320 \mu s$ ; (e) $t=480 \mu s$ ; (f) $t=700 \mu s$ ; (g) $t=1100 \mu s$ ; (h) $t=1800 \mu s$ .....         | 85 |
| <b>Fig. 3.31</b> | Contours of Mach number for $M=4$ , $Kn=0.1$ at (a) $t=10 \mu s$ ; (b) $t=50 \mu s$ ; (c) $t=150 \mu s$ ; (d) $t=300 \mu s$ ; (e) $t=500 \mu s$ ; (f) $t=900 \mu s$ ; (g) $t=2500 \mu s$ ; (h) $t=4500 \mu s$ .....        | 86 |
| <b>Fig. 3.32</b> | Contours of Mach number for $M=4$ , $Kn=0.01$ at (a) $t=10 \mu s$ ; (b) $t=75 \mu s$ ; (c) $t=175 \mu s$ ; (d) $t=300 \mu s$ ; (e) $t=500 \mu s$ ; (f) $t=900 \mu s$ ; (g) $t=1750 \mu s$ ; (h) $t=3750 \mu s$ .....       | 87 |
| <b>Fig. 3.33</b> | Contours of Mach number for $M=4$ , $Kn=0.0033$ at (a) $t=10 \mu s$ ; (b) $t=40 \mu s$ ; (c) $t=120 \mu s$ ; (d) $t=400 \mu s$ ; (e) $t=800 \mu s$ ; (f) $t=1200 \mu s$ ; (g) $t=1800 \mu s$ ; (h) $t=2650 \mu s$ .....    | 88 |
| <b>Fig. 3.34</b> | Contours of number density for $M=4$ , $Kn=10$ at (a) $t=50 \mu s$ ; (b) $t=125 \mu s$ ; (c) $t=225 \mu s$ ; (d) $t=325 \mu s$ ; (e) $t=425 \mu s$ ; (f) $t=600 \mu s$ ; (g) $t=1500 \mu s$ ; (h) $t=3000 \mu s$ .....     | 89 |
| <b>Fig. 3.35</b> | Contours of number density for $M=4$ , $Kn=1$ at (a) $t=40 \mu s$ ; (b) $t=100 \mu s$ ; (c) $t=180 \mu s$ ; (d) $t=320 \mu s$ ; (e) $t=480 \mu s$ ; (f) $t=700 \mu s$ ; (g) $t=1100 \mu s$ ; (h) $t=1800 \mu s$ .....      | 90 |
| <b>Fig. 3.36</b> | Contours of number density for $M=4$ , $Kn=0.1$ at (a) $t=10 \mu s$ ; (b) $t=50 \mu s$ ; (c) $t=150 \mu s$ ; (d) $t=300 \mu s$ ; (e) $t=500 \mu s$ ; (f) $t=900 \mu s$ ; (g) $t=2500 \mu s$ ; (h) $t=4500 \mu s$ .....     | 91 |
| <b>Fig. 3.37</b> | Contours of number density for $M=4$ , $Kn=0.01$ at (a) $t=10 \mu s$ ; (b) $t=75 \mu s$ ; (c) $t=175 \mu s$ ; (d) $t=300 \mu s$ ; (e) $t=500 \mu s$ ; (f) $t=900 \mu s$ ; (g) $t=1750 \mu s$ ; (h) $t=3750 \mu s$ .....    | 92 |
| <b>Fig. 3.38</b> | Contours of number density for $M=4$ , $Kn=0.0033$ at (a) $t=10 \mu s$ ; (b) $t=40 \mu s$ ; (c) $t=120 \mu s$ ; (d) $t=400 \mu s$ ; (e) $t=800 \mu s$ ; (f) $t=1200 \mu s$ ; (g) $t=1800 \mu s$ ; (h) $t=2650 \mu s$ ..... | 93 |
| <b>Fig. 3.39</b> | Contours of temperature for $M=4$ , $Kn=10$ at (a) $t=50 \mu s$ ; (b) $t=125 \mu s$ ; (c) $t=225 \mu s$ ; (d) $t=325 \mu s$ ; (e) $t=425 \mu s$ ; (f) $t=600 \mu s$ ; (g) $t=1500 \mu s$ ; (h) $t=3000 \mu s$ .....        | 94 |
| <b>Fig. 3.40</b> | Contours of temperature for $M=4$ , $Kn=1$ at (a) $t=40 \mu s$ ; (b) $t=100 \mu s$ ; (c) $t=180 \mu s$ ; (d) $t=320 \mu s$ ; (e) $t=480 \mu s$ ; (f) $t=700 \mu s$ ; (g) $t=1100 \mu s$ ; (h) $t=1800 \mu s$ .....         | 95 |
| <b>Fig. 3.41</b> | Contours of temperature for $M=4$ , $Kn=0.1$ at (a) $t=10 \mu s$ ; (b) $t=50 \mu s$ ; (c) $t=150 \mu s$ ; (d) $t=300 \mu s$ ; (e) $t=500 \mu s$ ; (f) $t=900 \mu s$ ; (g) $t=2500 \mu s$ ; (h) $t=4500 \mu s$ .....        |    |

|                  |   |     |
|------------------|---|-----|
|                  | =4500 $\mu$ s .....   | 96  |
| <b>Fig. 3.42</b> | Contours of temperature for $M=4$ , $Kn=0.01$ at (a) $t=10 \mu$ s; (b) $t=75 \mu$ s; (c) $t=175 \mu$ s; (d) $t=300 \mu$ s; (e) $t=500 \mu$ s; (f) $t=900 \mu$ s; (g) $t=1750 \mu$ s; (h) $t=3750 \mu$ s .....   | 97  |
| <b>Fig. 3.43</b> | Contours of temperature for $M=4$ , $Kn=0.0033$ at (a) $t=10 \mu$ s; (b) $t=40 \mu$ s; (c) $t=120 \mu$ s; (d) $t=400 \mu$ s; (e) $t=800 \mu$ s; (f) $t=1200 \mu$ s; (g) $t=1800 \mu$ s; (h) $t=2650 \mu$ s..... | 98  |
| <b>Fig. 3.44</b> | Profiles of u-velocity for $M=4$ , $Kn=10$ along vertical lines through geometric center ( $x/L=0.5$ ) at $t=50 \sim 3000 \mu$ s.....   | 99  |
| <b>Fig. 3.45</b> | Profiles of u-velocity for $M=4$ , $Kn=1$ along vertical lines through geometric center ( $x/L=0.5$ ) at $t=40 \sim 1800 \mu$ s.....  | 100 |
| <b>Fig. 3.46</b> | Profiles of u-velocity for $M=4$ , $Kn=0.1$ along vertical lines through geometric center ( $x/L=0.5$ ) at $t=10 \sim 4500 \mu$ s.....  | 101 |
| <b>Fig. 3.47</b> | Profiles of u-velocity for $M=4$ , $Kn=0.01$ along vertical lines through geometric center ( $x/L=0.5$ ) at $t=10 \sim 3750 \mu$ s.....   | 102 |
| <b>Fig. 3.48</b> | Profiles of u-velocity for $M=4$ , $Kn=0.0033$ along vertical lines through geometric center ( $x/L=0.5$ ) at $t=10 \sim 2600 \mu$ s.....   | 103 |
| <b>Fig. 3.49</b> | Profiles of v-velocity for $M=4$ , $Kn=10$ along vertical lines through geometric center ( $x/L=0.5$ ) at $t=50 \sim 3000 \mu$ s.....   | 104 |
| <b>Fig. 3.50</b> | Profiles of v-velocity for $M=4$ , $Kn=1$ along vertical lines through geometric center ( $x/L=0.5$ ) at $t=40 \sim 1800 \mu$ s.....  | 105 |
| <b>Fig. 3.51</b> | Profiles of v-velocity for $M=4$ , $Kn=0.1$ along vertical lines through geometric center ( $x/L=0.5$ ) at $t=10 \sim 4500 \mu$ s.....  | 106 |
| <b>Fig. 3.52</b> | Profiles of v-velocity for $M=4$ , $Kn=0.01$ along vertical lines through geometric center ( $x/L=0.5$ ) at $t=10 \sim 3750 \mu$ s.....   | 107 |
| <b>Fig. 3.53</b> | Profiles of v-velocity for $M=4$ , $Kn=0.0033$ along vertical lines through geometric center ( $x/L=0.5$ ) at $t=10 \sim 2600 \mu$ s.....   | 108 |
| <b>Fig. 3.54</b> | Profiles of number density for $M=4$ , $Kn=10$ along vertical lines through geometric center ( $x/L=0.5$ ) at $t=50 \sim 3000 \mu$ s.....   | 109 |
| <b>Fig. 3.55</b> | Profiles of number density for $M=4$ , $Kn=1$ along vertical lines through geometric center ( $x/L=0.5$ ) at $t=40 \sim 1800 \mu$ s.....  | 110 |
| <b>Fig. 3.56</b> | Profiles of number density for $M=4$ , $Kn=0.1$ along vertical lines through geometric center ( $x/L=0.5$ ) at $t=10 \sim 4500 \mu$ s.....  | 111 |
| <b>Fig. 3.57</b> | Profiles of number density for $M=4$ , $Kn=0.01$ along vertical lines through geometric center ( $x/L=0.5$ ) at $t=10 \sim 3750 \mu$ s.....   | 112 |
| <b>Fig. 3.58</b> | Profiles of number density for $M=4$ , $Kn=0.0033$ along vertical lines through geometric center ( $x/L=0.5$ ) at $t=10 \sim 2600 \mu$ s.....   | 113 |
| <b>Fig. 3.59</b> | Profiles of temperature for $M=4$ , $Kn=10$ along vertical lines through  |     |

|                  |  |     |
|------------------|--|-----|
|                  | geometric center ( $x/L=0.5$ ) at $t=50 \sim 3000 \mu s$ .....   | 114 |
| <b>Fig. 3.60</b> | Profiles of temperature for $M=4$ , $Kn=1$ along vertical lines through geometric center ( $x/L=0.5$ ) at $t=40 \sim 1800 \mu s$ .....         | 115 |
| <b>Fig. 3.61</b> | Profiles of temperature for $M=4$ , $Kn=0.1$ along vertical lines through geometric center ( $x/L=0.5$ ) at $t=10 \sim 4500 \mu s$ .....       | 116 |
| <b>Fig. 3.62</b> | Profiles of temperature for $M=4$ , $Kn=0.01$ along vertical lines through geometric center ( $x/L=0.5$ ) at $t=10 \sim 3750 \mu s$ .....      | 117 |
| <b>Fig. 3.63</b> | Profiles of temperature for $M=4$ , $Kn=0.0033$ along vertical lines through geometric center ( $x/L=0.5$ ) at $t=10 \sim 2600 \mu s$ .....    | 118 |
| <b>Fig. 3.64</b> | Profiles of u-velocity for $M=4$ , $Kn=10$ along horizontal lines through geometric center ( $y/L=0.5$ ) at $t=50 \sim 3000 \mu s$ .....       | 119 |
| <b>Fig. 3.65</b> | Profiles of u-velocity for $M=4$ , $Kn=1$ along horizontal lines through geometric center ( $y/L=0.5$ ) at $t=40 \sim 1800 \mu s$ .....        | 120 |
| <b>Fig. 3.66</b> | Profiles of u-velocity for $M=4$ , $Kn=0.1$ along horizontal lines through geometric center ( $y/L=0.5$ ) at $t=10 \sim 4500 \mu s$ .....      | 121 |
| <b>Fig. 3.67</b> | Profiles of u-velocity for $M=4$ , $Kn=0.01$ along horizontal lines through geometric center ( $y/L=0.5$ ) at $t=10 \sim 3750 \mu s$ .....     | 122 |
| <b>Fig. 3.68</b> | Profiles of u-velocity for $M=4$ , $Kn=0.0033$ along horizontal lines through geometric center ( $y/L=0.5$ ) at $t=10 \sim 2600 \mu s$ .....   | 123 |
| <b>Fig. 3.69</b> | Profiles of v-velocity for $M=4$ , $Kn=10$ along horizontal lines through geometric center ( $y/L=0.5$ ) at $t=50 \sim 3000 \mu s$ .....       | 124 |
| <b>Fig. 3.70</b> | Profiles of v-velocity for $M=4$ , $Kn=1$ along horizontal lines through geometric center ( $y/L=0.5$ ) at $t=40 \sim 1800 \mu s$ .....        | 125 |
| <b>Fig. 3.71</b> | Profiles of v-velocity for $M=4$ , $Kn=0.1$ along horizontal lines through geometric center ( $y/L=0.5$ ) at $t=10 \sim 4500 \mu s$ .....      | 126 |
| <b>Fig. 3.72</b> | Profiles of v-velocity for $M=4$ , $Kn=0.01$ along horizontal lines through geometric center ( $y/L=0.5$ ) at $t=10 \sim 3750 \mu s$ .....     | 127 |
| <b>Fig. 3.73</b> | Profiles of v-velocity for $M=4$ , $Kn=0.0033$ along horizontal lines through geometric center ( $y/L=0.5$ ) at $t=10 \sim 2600 \mu s$ .....   | 128 |
| <b>Fig. 3.74</b> | Profiles of number density for $M=4$ , $Kn=10$ along horizontal lines through geometric center ( $y/L=0.5$ ) at $t=50 \sim 3000 \mu s$ .....   | 129 |
| <b>Fig. 3.75</b> | Profiles of number density for $M=4$ , $Kn=1$ along horizontal lines through geometric center ( $y/L=0.5$ ) at $t=40 \sim 1800 \mu s$ .....    | 130 |
| <b>Fig. 3.76</b> | Profiles of number density for $M=4$ , $Kn=0.1$ along horizontal lines through geometric center ( $y/L=0.5$ ) at $t=10 \sim 4500 \mu s$ .....  | 131 |
| <b>Fig. 3.77</b> | Profiles of number density for $M=4$ , $Kn=0.01$ along horizontal lines through geometric center ( $y/L=0.5$ ) at $t=10 \sim 3750 \mu s$ ..... | 132 |
| <b>Fig. 3.78</b> | Profiles of number density for $M=4$ , $Kn=0.0033$ along horizontal lines  |     |

|                  |   |     |
|------------------|---|-----|
|                  | through geometric center ( $y/L=0.5$ ) at $t=10 \sim 2600 \mu s$ .....  | 133 |
| <b>Fig. 3.79</b> | Profiles of temperature for $M=4$ , $Kn=10$ along horizontal lines through geometric center ( $y/L=0.5$ ) at $t=50 \sim 3000 \mu s$ .....     | 134 |
| <b>Fig. 3.80</b> | Profiles of temperature for $M=4$ , $Kn=1$ along horizontal lines through geometric center ( $y/L=0.5$ ) at $t=40 \sim 1800 \mu s$ .....      | 135 |
| <b>Fig. 3.81</b> | Profiles of temperature for $M=4$ , $Kn=0.1$ along horizontal lines through geometric center ( $y/L=0.5$ ) at $t=10 \sim 4500 \mu s$ .....    | 136 |
| <b>Fig. 3.82</b> | Profiles of temperature for $M=4$ , $Kn=0.01$ along horizontal lines through geometric center ( $y/L=0.5$ ) at $t=10 \sim 3750 \mu s$ .....   | 137 |
| <b>Fig. 3.83</b> | Profiles of temperature for $M=4$ , $Kn=0.0033$ along horizontal lines through geometric center ( $y/L=0.5$ ) at $t=10 \sim 2600 \mu s$ ..... | 138 |
| <b>Fig. 3.84</b> | Profiles of u-velocity for $M=4$ , $Kn=10$ along horizontal lines through upper wall ( $y/L=0.9875$ ) at $t=50 \sim 3000 \mu s$ .....         | 139 |
| <b>Fig. 3.85</b> | Profiles of u-velocity for $M=4$ , $Kn=1$ along horizontal lines through upper wall ( $y/L=0.9875$ ) at $t=40 \sim 1800 \mu s$ .....          | 140 |
| <b>Fig. 3.86</b> | Profiles of u-velocity for $M=4$ , $Kn=0.1$ along horizontal lines through upper wall ( $y/L=0.9875$ ) at $t=10 \sim 4500 \mu s$ .....        | 141 |
| <b>Fig. 3.87</b> | Profiles of u-velocity for $M=4$ , $Kn=0.01$ along horizontal lines through upper wall ( $y/L=0.995$ ) at $t=10 \sim 3750 \mu s$ .....        | 142 |
| <b>Fig. 3.88</b> | Profiles of u-velocity for $M=4$ , $Kn=0.0033$ along horizontal lines through upper wall ( $y/L=0.9983$ ) at $t=10 \sim 2600 \mu s$ .....     | 143 |
| <b>Fig. 3.89</b> | Profiles of v-velocity for $M=4$ , $Kn=10$ along horizontal lines through upper wall ( $y/L=0.9875$ ) at $t=50 \sim 3000 \mu s$ .....         | 144 |
| <b>Fig. 3.90</b> | Profiles of v-velocity for $M=4$ , $Kn=1$ along horizontal lines through upper wall ( $y/L=0.9875$ ) at $t=40 \sim 1800 \mu s$ .....          | 145 |
| <b>Fig. 3.91</b> | Profiles of v-velocity for $M=4$ , $Kn=0.1$ along horizontal lines through upper wall ( $y/L=0.9875$ ) at $t=10 \sim 4500 \mu s$ .....        | 146 |
| <b>Fig. 3.92</b> | Profiles of v-velocity for $M=4$ , $Kn=0.01$ along horizontal lines through upper wall ( $y/L=0.995$ ) at $t=10 \sim 3750 \mu s$ .....        | 147 |
| <b>Fig. 3.93</b> | Profiles of v-velocity for $M=4$ , $Kn=0.0033$ along horizontal lines through upper wall ( $y/L=0.9983$ ) at $t=10 \sim 2600 \mu s$ .....     | 148 |
| <b>Fig. 3.94</b> | Profiles of number density for $M=4$ , $Kn=10$ along horizontal lines through upper wall ( $y/L=0.9875$ ) at $t=50 \sim 3000 \mu s$ .....     | 149 |
| <b>Fig. 3.95</b> | Profiles of number density for $M=4$ , $Kn=1$ along horizontal lines through upper wall ( $y/L=0.9875$ ) at $t=40 \sim 1800 \mu s$ .....      | 150 |
| <b>Fig. 3.96</b> | Profiles of number density for $M=4$ , $Kn=0.1$ along horizontal lines through upper wall ( $y/L=0.9875$ ) at $t=10 \sim 4500 \mu s$ .....    | 151 |
| <b>Fig. 3.97</b> | Profiles of number density for $M=4$ , $Kn=0.01$ along horizontal lines   |     |

|                   |   |     |
|-------------------|---|-----|
|                   | through upper wall ( $y/L=0.995$ ) at $t = 10 \sim 3750 \mu s$ .....  | 152 |
| <b>Fig. 3.98</b>  | Profiles of number density for $M=4$ , $Kn=0.0033$ along horizontal lines through upper wall ( $y/L=0.9983$ ) at $t = 10 \sim 2600 \mu s$ ..... | 153 |
| <b>Fig. 3.99</b>  | Profiles of temperature for $M=4$ , $Kn=10$ along horizontal lines through upper wall ( $y/L=0.9875$ ) at $t = 50 \sim 3000 \mu s$ .....        | 154 |
| <b>Fig. 3.100</b> | Profiles of temperature for $M=4$ , $Kn=1$ along horizontal lines through upper wall ( $y/L=0.9875$ ) at $t = 40 \sim 1800 \mu s$ .....         | 155 |
| <b>Fig. 3.101</b> | Profiles of temperature for $M=4$ , $Kn=0.1$ along horizontal lines through upper wall ( $y/L=0.9875$ ) at $t = 10 \sim 4500 \mu s$ .....       | 156 |
| <b>Fig. 3.102</b> | Profiles of temperature for $M=4$ , $Kn=0.01$ along horizontal lines through upper wall ( $y/L=0.995$ ) at $t = 10 \sim 3750 \mu s$ .....       | 157 |
| <b>Fig. 3.103</b> | Profiles of temperature for $M=4$ , $Kn=0.0033$ along horizontal lines through upper wall ( $y/L=0.9983$ ) at $t = 10 \sim 2600 \mu s$ .....    | 158 |
| <b>Fig. 3.105</b> | Positions of the center of the vortex for $M=4$ , $Kn=10$ at $1000 \sim 3000 \mu s$ .....   | 160 |
| <b>Fig. 3.106</b> | Positions of the center of the vortex for $M=4$ , $Kn=1$ at $1000 \sim 1800 \mu s$ .....  | 160 |
| <b>Fig. 3.107</b> | Positions of the center of the vortex for $M=4$ , $Kn=0.1$ at $2000 \sim 4500 \mu s$ .....  | 161 |
| <b>Fig. 3.108</b> | Positions of the center of the vortex for $M=4$ , $Kn=0.01$ at $1000 \sim 3750 \mu s$ .....   | 161 |
| <b>Fig. 3.109</b> | Positions of the center of the vortex for $M=4$ , $Kn=0.0033$ at $1200 \sim 2600 \mu s$ .....   | 162 |
| <b>Fig. 3.110</b> | Positions of the center of the vortex with $M=4$ for values of $x/L$ and Knudsen number .....   | 163 |
| <b>Fig. 3.111</b> | Positions of the center of the vortex with $M=4$ for values of $y/L$ and Knudsen number .....   | 163 |

## Nomenclature

|                     |  |
|---------------------|--|
| $\lambda$           | : mean free path                                       |
| $\rho$              | : density  |
| $\sigma$            | : the differential cross section                       |
| $\omega$            | : viscosity temperature exponent                       |
| $\Omega$            | : space domain   |
| $\varepsilon_{rot}$ | : rotational energy                                    |
| $\varepsilon_v$     | : vibrational energy                                   |
| $\zeta_{rot}$       | : rotational degree of freedom                         |
| $\zeta_v$           | : vibrational degree of freedom                        |
| $\Delta t$          | : time-step  |
| $\sigma_T$          | : the total cross section                              |
| $c$                 | : the total velocity                                   |
| $c'$                | : random velocity                                      |
| $c_o$               | : mean velocity  |
| $c_r$               | : relative speed                                       |
| $d$                 | : molecular diameter                                   |
| $D$                 | : the throat diameter of the twin-jet interaction      |
| $d_{ref}$           | : reference diameter                                   |
| $E$                 | : energy   |
| $k$                 | : the Boltzmann constant                               |
| $Kn$                | : Knudsen number                                       |
| $Kn_{max}$          | : continuum breakdown parameter                        |
| $Kn_{max}^{Thr.}$   | : the threshold value of continuum breakdown parameter |
| $Kn_Q$              | : local Knudsen numbers based on flow property Q       |
| $L$                 | : characteristic length;                               |
| $m$                 | : molecule mass  |
| $M_\infty$          | : free-stream mach number                              |



- $n$  : number density
- $P_{Tne}$  : thermal non-equilibrium indicator
- $P_{Tne}^{Thr.}$  : the threshold value of thermal non-equilibrium indicator
- $Re$  : Reynolds number
- $T_o$  : stagnation temperature
- $T_\infty$  : free-stream temperature
- $T_{ref}$  : reference temperature
- $T_{rot}$  : rotational temperature
- $T_{tot}$  : total temperature
- $T_{tr}$  : translational temperature
- $T_v$  : vibrational temperature
- $T_w$  : wall temperature



# Chapter 1

## Introduction

### 1.1. Motivation and Background

#### 1.1.1 Importance of Driven Cavity Flows

The driven cavity flow is one of the fundamental problems in the fluid dynamics. The kind of topic establishes the foundation of fluid dynamic theory and its geometry simple, but having singular points at the corners, which may cause difficulties in numerical simulations. In addition, fluid flows involved in micro-electrical-mechanical devices, vacuum systems, and high altitude aerodynamics do not have local equilibrium. In these applications, gas flows in channels, tubes, and ducts due to pressure and temperature gradients in the flow direction are very common. Several practical applications require understanding of this kind of flows in detail. However they have been completely studied in the literature, most of researches focused on incompressible or continuum compressible regime [Karniadakis, 2001] or compared the geometry type of the cavity and effect on fluid model which based on Reynolds number is all numerous contribution. Very few researches have been done in the rarefied and near continuum regimes, where the understanding may become important in micro- and nano-scale gas flows that are often encountered in MEMS and NEMS related devices. It may serve as the benchmarking problem in these regimes, where standard Navier-Stokes equation



fails to describe the flow accurately. Therefore, an accurate numerical solution of a driven cavity flow in the rarefied and near-continuum regime is required.

### 1.1.2 Classification of Rarefaction

Knudsen number ( $Kn=\lambda/L$ ) is usually used to indicate the degree of rarefaction. Note that the mean free path  $\lambda$  is the average distance traveled by molecules before collision and  $L$  is the flow characteristic length. In general, flows are divided into four regimes and three solutions. When the local  $Kn$  number approaches zero, the flow reaches inviscid limit and can be solved by Euler equation. As local  $Kn$  increases, molecular nature of the gas becomes dominated. Hence, when the flow is close to the continuum regime ( $Kn$  approach 0.01), the well known Navier-Stokes equation may be applied to yield accurate result for engineering purposes. For  $Kn$  larger than 0.01, continuum assumption begins to break down and the particle-based method is necessary and a kinetic approach, based on the Boltzmann equation [Cercignani, 1998]. It is important to note that the kinetic approach is valid in the whole range of the gas rarefaction. This is an important advantage when systems with multiscale physics are investigated; however it is rarely used to numerically solve the practical problems because of two major difficulties. They include higher dimensionality (up to seven) of the Boltzmann equation and the difficulties of correctly modeling the integral collision term. The well known direct simulation Monte Carlo (DSMC) method [Bird, 1994] is also a powerful computational scheme.

### 1.1.3 Direct Simulation Monte Carlo Method

Direct Simulation Monte Carlo (DSMC), was proposed by Bird to solve the Boltzmann equation using direct simulation of particle collision kinetics, and the associated monograph was published in 1994 [Bird's book]. Later on, both Nanbu [1986] and Wagner [1992] were able to demonstrate mathematically that the DSMC method is equivalent to solving the Boltzmann equation as the simulated number of particles becomes large. The DSMC method is a particle method for the simulation of gas flows. The gas is modeled at the microscopic level using simulated particles, which each represents a large number of physical molecules or atoms. The physics of the gas are modeled through the motion of particles and collisions between them. Mass, momentum and energy transports between particles are considered at the particle level. The method is statistical in nature and depends heavily upon pseudo-random number sequences for simulation. Physical events such as collisions are handled probabilistically using largely phenomenological models, which are designed to reproduce real fluid behavior when examined at the macroscopic level. This method has become a widely used computational tool for the simulation of gas flows in the transitional flow regime, in which molecular effects become important.

The DSMC method becomes very time-consuming as the flow approaches continuum regime since the sampling cell size has to be much smaller than the local mean free path for the solution to be accurate. Several remedies in speeding up the DSMC computation include:

(1) parallel computing [Robinson, 1996-1998]; (2) variable time-step scheme for steady flows [Kannenbergh, 2000]; (3) sub-cells within each sampling cell [Bird's book, 1994], and (4) unsteady flows sampling. Details of the "parallel computing", "variable time-step scheme" and "sub-cell" can be found in those references cited in the above and are not described here for brevity. Only "unsteady flows sampling" concept is described here since it was rarely discussed in detail in the literature. Unsteady flow simulations have difficulties in DSMC sampling, Cave, *et al.* [2007] developed new model for under-expanded jets from sonic nozzles during the start up of rocket nozzles and during the injection phase of the Pulsed Pressure Chemical Vapor Deposition (PP-CVD) process. But sampling over a small time interval requires either a very large number of simulated molecules or the average of a large number of separate simulations ("ensemble-averaging"). The costs high computational expense and large memory. Xu [1993] used one method of decreasing the statistical scatter of the results is to using statistical smoothing procedures in two dimensional unsteady problems. Wagner [1992] proved Bird's two-dimensional axis-symmetric code which incorporates unsteady sampling techniques in which a number of time intervals close to the sampling point are averaged ("time-averaging"); however this is single processor code. The increased computational capacities of parallel-DSMC techniques have the potential to enable the simulation of time-dependent flow problems at the near-continuum regime.

Accordingly, in this thesis develops an unsteady time-averaging sampling method [Cave,

*et al.*, 2007] for transient cavity flow and uses DSMC rapid ensemble averaging method (DREAM) to reduce the statistical scatter with an acceptable runtime for unsteady flow simulation.

## 1.2. Literature Survey

Driven flows are encountered in systems not in equilibrium. Proto-type flows of this kind are the Couette flow problem in one dimension and the driven cavity flow problem in two or three dimensions. The Couette flow problem has been studied [Cercignani, 1994]. It is clarified that in the fluid dynamics, the cavity problem is a well known typical benchmark problem for testing and verifying continuum solvers and has been thoroughly studied [Hou, *et al.*, 1995]. However, the research work for the same flow pattern in the free molecular, transient, and slip regimes is very limited. Recently, the two-dimensional cavity flow problem was studied using lattice Boltzmann method with slip conditions.

Huang, *et al.* [2003] validated one dimensional incompressible Couette flow by Navier-Stokes equations. He used forth Runge-Kutta method and compared with exact solution. In this thesis, we will also use the result to validate unsteady sampling method. Ghia, *et al.* [1982] used the 2D incompressible Navier-Stokes equation to study the laminar incompressible flow in a square cavity whose top wall moves with a uniform velocity. The Reynolds number in their study is varied from  $Re=100$  to  $Re=10,000$ . They presented the

velocity along vertical and horizontal line through geometry center of cavity and the primary vortex position. Until very recently, Naris and Valougeorgis [2005] used BGK model to simulate the driven cavity flow over the whole range of the Knudsen number. They presented the simulation data over the whole range of the Knudsen number and various aspect ratio (height/width). However, simulation results by Naris and Valougeorgis [2005] were only good for low speed rarefied gas flows since the BGK Boltzmann equation was used. In addition, no data were validated by comparing with experiments or solution from direct Boltzmann equation, such as DSMC method.

Cave *et al.*, [2007] developed a unsteady sampling procedures for the parallel direction simulation Monte Carlo method. This paper is simulations of a shock tube and the development of Couette flow are then carried out as validation studies. To overcome the large computational expense and memory requirements usually involved in DSMC simulations of unsteady flows. “Time-averaging” method was implemented which has considerable computational advantages over ensemble-averaging a large number of separate runs. Also, in order to reduce the statistical scatter with an acceptable runtime for unsteady flow simulation using DSMC technique. DSMC-DREAM (Rapid Ensembled Average Method) was developed whereby a combination of time- and ensemble-averaged data was build up by regenerating the particle data a short time prior to the sampling point of interesting, assuming a Maxwell-Boltzmann distribution of particle velocities. In this thesis, we used this method

and validated this code.

### **1.3. Specific Objectives of the Thesis**

The current objectives of the thesis are summarized as follows:

1. To verify of the unsteady sampling and DREAM techniques in a parallelized DSMC code (PDSC).
2. To verify of the transient sub-cell technique in a parallelized DSMC code (PDSC).
3. To simulate driven cavity flows, including  $Ma=4$  of the speed of top driven plate and  $Kn=10-0.0033$ , based on the average number density and wall temperature.
4. To discuss the effects of Knudsen Number of the driven plate on the flow fields.

The organization of the thesis is stated as follows: Chapter 1 describes the Introduction, Chapter 2 describes the Numerical Method, Chapter 3 describes the verification of implementation of unsteady sampling and DREAM techniques, and followed by the Results and Discussion, and finally Chapter 4 describes the conclusion and recommendation of future work.

# Chapter 2

## Numerical Methods

### 2.1. The Boltzmann Equation

The Knudsen number (Kn) is used to indicate the degree of rarefaction. In Fig. 2.1, flows are divided into four regimes and three solutions. We have found the Boltzmann equation is valid for all flow regimes which from 10 to 0.0001. It is one of the most important transport equations in non-equilibrium statistical mechanics, which deals with systems far from thermodynamics equilibrium. There are some assumptions made in the derivation of the Boltzmann equation which defines limits of applicability. They are summarized as follows:

1. Molecular chaos is assumed which is valid when the intermolecular forces are short range. It allows the representation of the two particles distribution function as a product of the two single particle distribution functions.
2. Distribution functions do not change before particle collision. This implies that the encounter is of short time duration in comparison to the mean free collision time.
3. All collisions are binary collisions.
4. Particles are uninfluenced by intermolecular potentials external to an interaction.

According to these assumptions, the Boltzmann equation is derived and shown as Eq. (2.1)

$$\frac{\partial(nf)}{\partial t} + u_i \frac{\partial(nf)}{\partial x_i} + F_i \frac{\partial(nf)}{\partial u_i} = \frac{\partial f}{\partial x_i} \Big|_c = \int_{-\infty}^{\infty} \int_0^{4\pi} n^2 (f' f_1' - f f_1) g \sigma d\Omega dU \quad (2.1)$$

Meaning of particle phase-space distribution function  $f$  is the number of particles with center of mass located within a small volume  $d^3r$  near the point  $r$ , and velocity within a range  $d^3u$ , at time  $t$ .  $F_i$  is an external force per unit mass and  $t$  is the time and  $u_i$  is the molecular velocity.  $\sigma$  is the differential cross section and  $d\Omega$  is an element of solid angle. The prime denotes the post-collision quantities and the subscript 1 denotes the collision partner. Meaning of each term in Eq. (2.1) is described in the following;

1. The first term on the left hand side of the equation represents the time variation of the distribution function of the particles (unsteady term).
2. The second term gives the spatial variation of the distribution function (flux term).
3. The third term describes the effect of a force on the particles (force term).
4. The term at right hand side of the equation is called the collision integral (collision term). It is the source of most of the difficulties in obtaining solutions of the Boltzmann equation.

In general, it is difficult to solve the Boltzmann equation directly using numerical method because the difficulties of correctly modeling the integral collision term. Instead, the DSMC method was used to simulated problems involving rarefied gas dynamics, which is the main topic in the current thesis.



## 2.2. General Description of the standard DSMC

In order to the expected rarefaction caused by the rarefied gas flows, the direct simulation Monte Carlo (DSMC) method which is a particle-based method developed by Bird during the 1960s and is widely used an efficient technique to simulate rarefied gas regime [Bird, 1976 and Bird, 1994]. In the DSMC method, a large number of particles are generated in the flow field to represent real physical molecules rather than a mathematical foundation and it has been proved that the DSMC method is equivalent to solving the Boltzmann equation [Nanbu, 1986 and Wagner, 1992]. The assumptions of molecular chaos and a dilute gas are required by both the Boltzmann formulation and the DSMC method [Bird, 1976 and Bird, 1994]. An important feature of DSMC is that the molecular motion and the intermolecular collisions are uncoupled over the time intervals that are much smaller than the mean collision time. Both the collision between molecules and the interaction between molecules and solid boundaries are computed on a probabilistic basis and, hence, this method makes extensive use of random numbers. In most practical applications, the number of simulated molecules is extremely small compared with the number of real molecules. The general procedures of the DSMC method are described in the next section, and the consequences of the computational approximations can be found in Bird [Bird, 1976 and Bird, 1994].

In DSMC, there are three molecular collision models for real physical behavior and imitate the real particle collision, which are the Hard Sphere (HS), Variable Hard Sphere (VHS) and

Variable Soft Sphere (VSS) molecular models, in the standard DSMC method [Bird, 1994].

The collision pairs then are chosen by the acceptance-rejection method. The no time counter (NTC) method is an efficient method for molecular collision. This method yield the exact collision rate in both simple gases and gas mixtures, and under either equilibrium or non-equilibrium conditions.

Fig. 2.2 is a general flowchart of the DSMC method. Important steps of the DSMC method include setting up the initial conditions, moving all the simulated particles, indexing (or sorting) all the particles, colliding between particles and sampling the molecules within cells to determine the macroscopic quantities. The details of each step will be described in the

following;



- **Initialization**

The first step to use the DSMC method in simulating flows is to set up the geometry and flow conditions. A physical space is discretized into a network of cells and the domain boundaries have to be assigned according to the flow conditions. An important feature has to be noted is the size of the computational cell should be smaller than the mean free path, and the distance of the molecular movement per time step should be smaller than the cell dimension. After the data of geometry and flow conditions have been read in the code, the numbers of each cell is calculated according to the free-stream number density and the current cell volume. The initial particle velocities are assigned to each particle based on the

Maxwell-Boltzmann distribution according to the free-stream velocities and temperature, and the positions of each particle are randomly allocated within the cells.

- **Molecular Movement**

After initialization process, the molecules begin move one by one, and the molecules move in a straight line over the time step if it did not collide with solid surface. For the standard DSMC code by Bird [Bird, 1976 and Bird, 1994], the particles are moved in a structured mesh. There are two possible conditions of the particle movement. First is the particle movement without interacting with solid wall. The particle location can be easy located according to the velocity and initial locations of the particle. Second is the case that the particle collides with solid boundary. The velocity of the particle is determined by the boundary type. Then, the particle continues its journey from the intersection point on the cell surface with its new absolute velocity until it stops. Although it is easier to implement by using structured mesh, it is difficult for those flows with complex geometry.

- **Indexing**

The location of the particle after movement with respect to the cell is important information for particle collisions. The relations between particles and cells are reordered according to the order of the number of particles and cells. Before the collision process, the collision partner will be chosen by a random method in the current cell. And the number of the collision partner can be easy determined according to this numbering system.

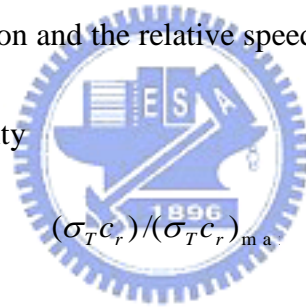
- **Gas-Phase Collisions**

The other most important phase of the DSMC method is gas phase collision. The current DSMC method uses the no time counter (NTC) method to determine the correct collision rate in the collision cells. The number of collision pairs within a cell of volume  $V_c$  over a time interval  $\Delta t$  is calculated by the following equation;

$$\frac{1}{2} N \bar{N} F_N (\sigma_T c_r)_{\max} \Delta t / V_c \quad (2.2)$$

$N$  and  $\bar{N}$  are fluctuating and average number of simulated particles, respectively.  $F_N$  is the particle weight, which is the number of real particles that a simulated particle represents.

$\sigma_T$  and  $c_r$  are the cross section and the relative speed, respectively. The collision for each pair is computed with probability



$$(\sigma_T c_r) / (\sigma_T c_r)_{\max} \quad (2.3)$$

The collision is accepted if the above value for the pair is greater than a random fraction.

Each cell is treated independently and the collision partners for interactions are chosen at random, regardless of their positions within the cells. The collision process is described sequentially as follows:

1. The number of collision pairs is calculated according to the NTC method, Eq. (2.2), for each cell.
2. The first particle is chosen randomly from the list of particles within a collision cell.
3. The other collision partner is also chosen at random within the same cell.

4. The collision is accepted if the computed probability, Eq (2.3), is greater than a random number.
5. If the collision pair is accepted then the post-collision velocities are calculated using the mechanics of elastic collision. If the collision pair is not to collide, continue choosing the next collision pair.
6. If the collision pair is polyatomic gas, the translational and internal energy can be redistributed by the Larsen-Borgnakke model [Borgnakke and Larsen, 1975], which assumes in equilibrium.

The collision process will be finished until all the collision pairs are handled for all cells and then progress to the next step.

- **Sampling**



After the particle movement and collision process finish, the particle has updated positions and velocities. The macroscopic flow properties in each cell are assumed to be constant over the cell volume and are sampled from the microscopic properties of each particle within the cell. The macroscopic properties, including density, velocities and temperatures, are calculated in the following equations [Bird, 1976 and Bird, 1994];

$$\rho = nm \tag{2.4a}$$

$$c_o = \bar{c} = \bar{c}_o + \bar{c}' \tag{2.4b}$$

$$\frac{3}{2}kT_r = \frac{1}{2}m(\overline{u'^2} + \overline{v'^2} + \overline{w'^2}) \tag{2.4c}$$

$$T_{rot} = \frac{2}{k}(\varepsilon_{rot}/\zeta_r) \quad (2.4d)$$

$$T_v = \frac{2}{k}(\varepsilon_v/\zeta_v) \quad (2.4e)$$

$$T_{tot} = (3T_{tr} + \zeta_{rot}T_{rot} + \zeta_vT_v)/(3 + \zeta_{rot} + \zeta_v) \quad (2.4f)$$

$n$ ,  $m$  are the number density and molecule mass, respectively.  $c$ ,  $c_o$ , and  $c'$  are the total velocity, mean velocity, and random velocity, respectively. In addition,  $T_{tr}$ ,  $T_{rot}$ ,  $T_v$  and  $T_{tot}$  are translational, rotational, vibration and total temperature, respectively.  $\varepsilon_{rot}$  and  $\varepsilon_v$  are the rotational and vibration energy, respectively.  $\zeta_{rot}$  and  $\zeta_v$  are the number of degree of freedom of rotation and vibration, respectively.

If the simulated particle is monatomic gas, the translational temperature is regarded simply as total temperature. Vibration effect can be neglect if the temperature of the flow is low enough.

The flow will be monitored if steady state is reached. If the flow is under unsteady situation, the sampling of the properties should be reset until the flow reaches steady state.

As a rule of thumb, the sampling of particles starts when the number of molecules in the calculation domain becomes approximately constant.

### 2.3. General Description of the PDSC

Although the large number of molecules in a real gas is replaced with a reduced number of model particles, there are still a large number of particles must be simulated, leading to tremendous computer power requirements and needing to cost a lot of computational time. As a result, parallel DSMC method is developed to solve the problem. Fig. 2.3 illustrates a

simplified flow chart of the parallel DSMC method used in the current study. The DSMC algorithm is readily parallelized through physical domain decomposition. The cells of the computational grid are distributed among the processors. Each processor executes the DSMC algorithm in serial for all particles and cells in its domain. Data communication occurs when particles cross the domain (processor) boundaries and are then transferred between processors.

**Parallel DSMC Code (PDSC)** is the main solver used in this thesis, which utilizes unstructured tetrahedral mesh. Fig. 2.4 is the features of PDSC and brief introduction is listed in the following paragraphs.

1. *2D/2D-axisymmetric/3-D unstructured-grid topology*: PDSC can accept either 2D/2D-axisymmetric (triangular, quadrilateral or hybrid triangular-quadrilateral) or 3D (tetrahedral, hexahedral or hybrid tetrahedral-hexahedral) mesh [Wu et al.'s JCP paper, 2006]. Computational cost of particle tracking for the unstructured mesh is generally higher than that for the structured mesh. However, the use of the unstructured mesh, which provides excellent flexibility of handling boundary conditions with complicated geometry and of parallel computing using dynamic domain decomposition based on load balancing, is highly justified.
2. *Parallel computing using dynamic domain decomposition*: Load balancing of PDSC is achieved by repeatedly repartitioning the computational domain using a multi-level graph-partitioning tool, PMETIS [Wu and Tseng, 2005] by taking advantage of the unstructured mesh topology employed in the code. A decision policy for repartition with a concept of Stop-At-Rise (SAR) [Wu and Tseng, 2005]

or constant period of time (fixed number of time steps) can be used to decide when to repartition the domain. Capability of repartitioning of the domain at constant or variable time interval is also provided in PDSC. Resulting parallel performance is excellent if the problem size is comparably large. Details can be found in Wu and Tseng [Wu and Tseng, 2005].

3. *Spatial variable time-step scheme*: PDSC employs a spatial variable time-step scheme (or equivalently a variable cell-weighting scheme), based on particle flux (mass, momentum, energy) conservation when particles pass interface between cells. This strategy can greatly reduce both the number of iterations towards the steady state, and the required number of simulated particles for an acceptable statistical uncertainty. Past experience shows this scheme is very effective when coupled with an adaptive mesh refinement technique [Wu et al.'s CPC paper, 2004].
4. *Unsteady flow simulation*: An unsteady sampling routine is implemented in PDSC, allowing the simulation of time-dependent flow problems in the near continuum range [JCP paper submitted in June 2007]. A post-processing procedure called DSMC Rapid Ensemble Averaging Method (DREAM) is developed to improve the statistical scatter in the results while minimizing both memory and simulation time. In addition, a temporal variable time-step (TVTS) scheme is also developed to speed up the unsteady flow simulation using PDSC. More details can be found in [JCP paper submitted in June 2007]. Details of the idea and implementation are described next.
5. *Transient Sub-cells*: Recently, transient sub-cells are implemented in PDSC directly on the unstructured grid, in which the nearest-neighbor collision can be enforced, whilst maintaining minimal computational overhead [JFM paper under preparation, 2007].



## 2.4. General Description of Unsteady Sampling Method in DSMC [JCP paper submitted in June 2007]

In section 2.3, the PDSC code has been specifically designed for simulating steady flows, therefore some modification is need for unsteady sampling. The **unsteady sampling method** has been described in detail in the paper [Cave, *et al.*, 2007].

There are two methods for unsteady sampling, the differences illustrated in Fig. 2.5 and the details will be described in the following;

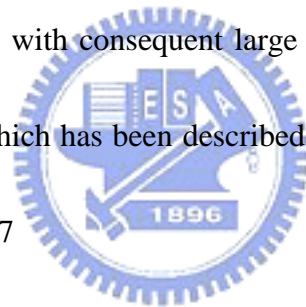
1. The “Ensemble-Average” method, require multiple simulation runs. The flow flied is sampled at the suitable sampling times during the run. The sampling simulation outputs from each run are averaged over the runs. There the results are vary precise, but the method is very computational expensive. Because a large of runs is required to reduce the statistical scatter to smooth data and a large amount of memory is needed to record the sampling data for each simulation.
2. The “Time-Average” method, require one simulation run. It averages a number of time steps over an interval before the sampling time. However it suffers a potential disadvantage in that the results will be “smeared” over the time over which samples are taken. Hence the sample time must be sufficiently short to minimizes time “smearing” and yet long enough to obtain a good statistical sample. This method of time averaging has been used previously by Auld to model shock tube flow [Auld, 1992]

In PDSC, the method of time-averaging was implemented [Cave, *et al.*, 2007]. Fig. 2.6

shows the flow chart of the PDSC method with the unsteady sampling procedures implemented. Here  $M$  is the output matrix for sampling interval  $M$ . Most parts of the procedure are the same as the steady simulation except the sampling data must be reset after completing each simulation interval.

## **2.5. DSMC Rapid Ensemble Averaging Method (DREAM) [JCP paper submitted in June 2007]**

Because reducing the statistical scatter greatly, in time-average data requires a very large number of simulation particles with consequent large computational times. In the thesis, we have adapted DREAM code which has been described in detail in this paper by [Cave, *et al.*, 2007]. The illustrated in Fig. 2.7



First, we select a raw data set  $X-n$  produced by PDSC  $n$  sampling intervals prior to the sampling interval of interest  $X$ . New particle data is generated from the macroscopic properties in data set  $X-n$  by assuming a Maxwellian distribution of velocities. The standard PDSC algorithm is then used to simulate forward in time until the sampling period of interest  $X$  is reached. The time steps close to the sampling point are time-averaged in the same way as in PDSC and this process is repeated a number of times, thus building up a combination of ensemble-averaged and time-averaged data without having to simulate from zero flow time for each run. This process reduces the statistical scatter in the results by adding to the number

of particles in the sample, rather than by some artificial smoothing process. Because only a short period of the flow is processed in this way, the scheme has significant memory and computational advantages over both ensemble-averaging and using a greater number of particles in the time-averaging scheme.

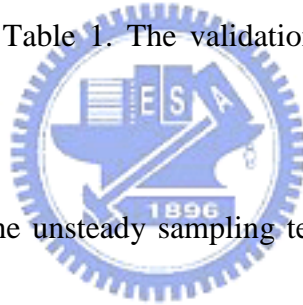


# Chapter 3

## Results and Discussion

### 3.1. Quasi 1-D Couette Flows

Although this thesis is concerned with supersonic square driven cavity flows in rarefied regime, a subsonic flow case with  $M=0.3$  and  $Kn=0.02$  is used as the benchmark case. The rationale is that a subsonic flow represents a more stringent test problem than a supersonic flow for the DSMC method in terms of statistical uncertainties. Flow and simulation conditions are summarized in Table 1. The validation process is described sequentially as follows:



First, as a validation of the unsteady sampling techniques in the PDSC code, we have used the test problem of quasi 1-D Couette flows. We have adapted Huang's paper [[2003]]. The simulation results of a quasi-1D incompressible Couette flow with the analytical data.

Second, use DREAM techniques [Cave, *et al.*, 2007] and simulate the same conditions in the PDSC code which compare the result.

Third, as a validation of transient sub-cell techniques in the PDSC code, we have use the different  $\Delta x/\lambda$  and try to find optimal  $\Delta x/\lambda$  .

### 3.1.1. Problem Description and Test Conditions

The computational domain for this simulation is shown in Fig. 3.1. Although this problem is quasi 1-D, we used 100 x 100 cell was used to validate the code. This grid spacing was chosen to be half of the mean free path in the undisturbed gas. The mesh is show in Fig. 3.2. Here argon gas is initially at rest between two parallel diffuse plates at the same uniform temperature as the gas, in this case 300K. At time  $t=0$  the upper plate begins moving instantaneously at speed  $U_\infty=96.6$  m/s. These conditions correspond to a Mach 0.3 flow with a Knudsen number of 0.02. The simulation time step was set at  $3.11 \times 10^{-5}$ s and used 100 sampling times.

In Huang's paper [2003], a continuum solution for the velocity at the vertical position  $y$  and time  $t$  can be obtained from the incompressible Navier-Stokes equations:

$$\frac{U(y,t)}{U_\infty} = \sum_{n=0}^{\infty} \text{erfc}[2n\eta_1 + \eta] + \sum_{n=0}^{\infty} \text{erfc}[2(n+1)\eta_1 - \eta] \quad (3-1)$$

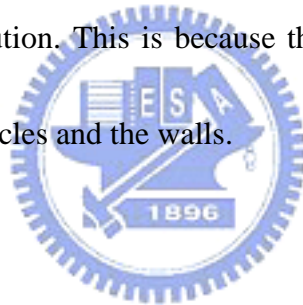
where  $\eta = y/2\sqrt{\nu t}$ ,  $\eta_1 = H/2\sqrt{\nu t}$ ,  $\text{erfc}$  is the complementary error function and  $\nu$  is the kinematics viscosity.

### 3.1.2. Verifications of Unsteady Sample Method

Fig. 3.3 (a)-(e) shows the velocity contour from the DSMC data on normalized time from  $t=1$  to  $t=36$ , in all cases time has been normalized such that  $t = t^*U_\infty/L.$ , where  $t^*$  is real time,  $U_\infty$  is sound of speed,  $L$  is dimension of plate. In these figures,  $\mathbf{u}_p$  and  $\mathbf{L}$  represents the top

plate speed and length (also width) of the driven cavity, respectively. The upper plate suddenly starts the velocity and conducts kinetic energy to lower plate gradually. However, the DSMC data exhibit the statistical scatter with an acceptable runtime for unsteady flow simulation.

Compare Huang's paper [2003] which introduces Couette flow exact solution. Fig. 3.4 shows the u-velocity profiles along the  $x/L=0.5$  line for a number of flow times as the Couette flow developed. Result show that lines (analytical in compressible Navier- Stokes solution) close to symbol point from DSMC data approximately, but the DSMC solution lags the incompressible continuum solution. This is because the high level of rarefaction effectively results in slip between gas particles and the walls.



### **3.1.3. Verifications of DSMC Rapid Ensemble Average Method (DREAM)**

In order to reduce the statistical scatter for unsteady flow simulation, use DSMC Rapid Ensemble Average Method [Cave, *et al.*, 2007]. Fig. 3.5 (a)-(e) shows the velocity contour from the DREAM data on normalized time from  $t = 1$  to  $t = 36$ . Result show that the DREAM can greatly reduce the statistical scatter for unsteady flow simulation using DSMC technique. Fig. 3.6 (a)-(e) shows a comparison of the velocity profile from the unsteady DSMC data and the data after processing by DREAM as the flow from  $t = 1$  to  $t = 32$ , illustrating the reduction in statistical scatter achieved by using DREAM. Fig. 3.7 shows the velocity profiles for a

number of flow times as the Couette flow developed. All data has been processed by DREAM and also exhibits the expected phenomenon of velocity slip at the walls.

### 3.1.4. Benchmark of the Transient Sub-Cell Method

In the section, obtain optimal sub-cell [Tesng, *et al.*, 2007] to allow the maintenance of good collision quality within the simulation. Even for grids which are “under-resolved” (that is, if the sampling cells are bigger than the recommended setting of  $1/3 \sim 1$  times the local mean free path). Running simulations with under-resolved sampling cells which employ sub-cells results in a reduction in the computational and memory requirements of the simulation, albeit at the cost of a reduction in the possible sampling resolution of the macroscopic properties, but without sacrificing simulation accuracy. In order to obtain optimal and verification, compare coarse mesh with transient sub-cell with finer mesh without transient sub-cell.

First, use finer mesh to simulate Couette flow. These conditions correspond to a Mach 0.3 flow with a Knudsen number of 0.02. The mesh for this simulation is shown in Fig. 3.8.

This grid spacing was chosen to be  $\frac{\Delta x}{\lambda} = \frac{\Delta y}{\lambda} = 0.25$  and the domain 1m x 0.025m. Here argon gas is initially at rest between two parallel diffuse plates at the same uniform temperature as the gas, in this case 300K. At time  $t=0$  the upper plate begins moving instantaneously at speed  $U_{\infty}=96.6$  m/s. The simulation time step was set at  $3.11 \times 10^{-5}$ s and used 100 sampling

times. Fig 3.9 shows the velocity contour on normalized time from  $t = 7$ . The data has been processed by DREAM. Fig. 3.10 shows the merit of collision (=mean collision distance/local mean free path), which represents the quality of collisions in a DSMC simulation. The average data is about 0.12; this is good for collision in each cell.

Second, use coarse mesh to simulate Couette flow. These conditions correspond to a Mach 0.3 flow with a Knudsen number of 0.02. The mesh for this simulation is shown in Fig.

3.11. This grid spacing was chosen to be  $\frac{\Delta x}{\lambda} = \frac{\Delta y}{\lambda} = 1$  and the domain 1m x 0.1m. Here argon

gas is initially at rest between two parallel diffuse plates at the same uniform temperature as

the gas, in this case 300K. At time  $t=0$  the upper plate begins moving instantaneously at speed

$U_{\infty}=96.6$  m/s. The simulation time step was set at  $3.11 \times 10^{-5}$ s and used 100 sampling times.

Fig. 3.12 shows the velocity contour on normalized time from  $t = 7$ . The data has been

processed by DREAM. Fig. 3.13 shows the merit of collision (=mean collision distance/local

mean free path), which represents the quality of collisions in a DSMC simulation. The

average data is about 0.15; this is good for collision in each cell.

Finally, compare these results. Fig. 3.14 shows the  $\frac{\Delta x}{\lambda} = \frac{\Delta y}{\lambda} = 0.25$  simulation compare to  $\frac{\Delta x}{\lambda} = \frac{\Delta y}{\lambda} = 1$ . Result show the simulation used coarse mesh with transient sub-cell

approximate that used finer mesh without transient sub-cell. In addition, result with transient

sub-cell could improve near lower plate effect. Therefore, the simulation with transient

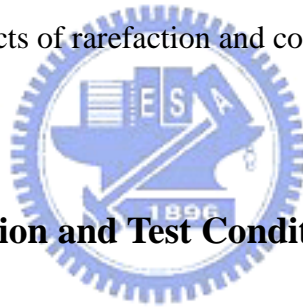
sub-cell keeping minimal computational overhead and memory requirement simultaneously,



but still has simulation accuracy.

## 3.2. Instantaneously Started Driven Cavity Flows

According to previous section, result show that the DREAM can greatly reduce the statistical scatter with an acceptable runtime for unsteady flow simulation using DSMC technique. Future, the transient sub-cell method can greatly reduce the computational cost and still has good quality of solution. In this section, we have used this benchmark and to simulate instantaneously started driven cavity flows in a systematic way. Thus, the result can understand more about the effects of rarefaction and compressibility in such conditions.



### 3.2.1. Problem Description and Test Conditions

Fig. 3.15 sketch of the 2D square ( $L/H=1$ ) driven cavity flow with moving top plate.

Initially, we use argon gas at rest inside the cavity and at the same uniform temperature 300K.

At time  $t = 0$  the upper plate begins moving instantaneously at speed  $Ma=4$  and  $Kn=10-0.0033$

based on the mean free path of wall temperature and size of the cavity. Table I shows the grid

sizes of these cases. This grid spacing was chosen to be equal of the mean free path for

$Kn=0.01, 0.0033$ , others cases are setting  $40 \times 40$ . The mesh in Knudsen number 10, 1, 0.1

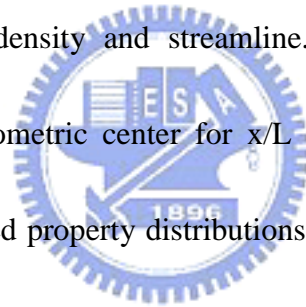
was  $40 \times 40$  showed in Fig. 3.16. The mesh in Knudsen number 0.01 was  $100 \times 100$  showed

in Fig. 3.17. The mesh in Knudsen number 0.00033 was  $300 \times 300$  showed in Fig. 3.18.

Particle per cell are 100, 100, 25, 25, 25 with Knudsen number 0.0033, 0.01, 0.1, 1, 10. Table III shows the time step of these cases. The simulation time step was correspond in Knudsen number, the speed of the top driven plate and the sampling times. All cases use 50 sampling times

### 3.2.2. Effects of Knudsen Number

In this section, we were observed effects of Knudsen number in the same Mach number ( $Ma=4$ ). First, we were showed general simulation results include u-direction, v-direction, Mach number, temperature, density and streamline. Second, we were showed property distributions across cavity geometric center for  $x/L = 0.5m$ ,  $y/L = 0$  to  $1m$  and  $y/L = 0.5m$ ,  $x/L = 0$  to  $1m$ . Third, we showed property distributions near the solid walls. Finally, we were observed the recirculation center position in different cases.



#### 3.2.2.1. General Simulation Results

##### 3.2.2.1.1. Supersonic Moving Plate ( $M=4$ )

Fig. 3.19 - Fig. 3.23 (a)-(h) show that u-velocity contour during started driven upper plate to steady state for  $Ma=4$ , and Knudsen number 10, 1, 0.1, 0.01 and 0.0033 respectively. In these figures,  $u_p$  and  $L$  represents the top plate speed and length (also width) of the driven cavity, respectively. The upper plate instantaneously started to flow steady. The u-velocity

normalizes to divide by the upper plate velocity. As time increase, the velocity extends gradually on upper plate and the value higher than other regime. The maximum u-velocity values are about 0.45, 0.55, 0.7, 0.8, and 0.9 with Knudsen number 10, 1, 0.1, 0.01 and 0.0033, respectively. Because of rarefaction effect caused slip phenomenon and the slip velocity along the solid walls increase with Knudsen number at the same Mach number.

Fig. 3.24 - Fig. 3.28 (a)-(h) show that v-velocity contour during started driven upper plate to steady state for  $Ma=4$ , and Knudsen number 10, 1, 0.1, 0.01 and 0.0033 respectively.

The normalization v-velocity divides by the upper plate velocity. As time goes on, the driven plate move from left to right wall, an ultra high v-velocity region appears at the left-hand upper corner and low-velocity corner appears at the right-hand upper region. Because of the particles collide with the right wall ( $x/L = 1$ ) and cause the particles to move along bottom plate. Hence, the v-velocity greatly decreases on right wall. Further, the particles proceed to move and come back on the left-hand upper corner eventually. Therefore, the v-velocity greatly increases on left wall.

Fig. 3.29 - Fig. 3.33 (a)-(h) show that Mach contour during started driven upper plate to steady state for  $Ma=4$ , and Knudsen number 10, 1, 0.1, 0.01 and 0.0033 respectively.

Fig. 3.34 - Fig. 3.38 (a)-(h) show that number density contour during started driven upper plate to steady state for  $Ma=4$  and Knudsen number 10, 1, 0.1, 0.01 and 0.0033 respectively. These values normalize to divide by initial number densities. The driven plate

instantaneously starts and carries a large number of particles to right-hand corner. Thus, there are obviously variations on the upper corner. An ultra high-density region appears at the very right-hand upper corner due to the high-speed moving plate at the upper of the cavity. These values rise on right-hand upper corner and vary with time. In addition, there are low densities at the left-hand upper corner because of a great deal of particles leave for right-hand corner.

Fig. 3.39 - Fig. 3.43 (a)-(h) show that temperature contour during started driven upper plate to steady state for  $Ma=4$ , and Knudsen number 10, 1, 0.1, 0.01 and 0.0033 respectively. Normalized temperature divides by the initial temperature 300K. An ultra high-temperature region appears at the very right-hand upper corner due to high-density region. This corner has many particles than other region. A large number of particles collide to each other and cause this region to increase temperature which varies with time increase.

In Knudsen number 10 (free-molecular flow regime), 1 and 0.1 (transient regime), there are not smooth and many crack in a square cavity. Because of the particle per cell less than other Knudsen number. This could cause deficient sampling on statistics. The other reason is Knudsen number 10 and 1 which the mean free paths are 10 and 1, these value large than characteristic length. Thus, particles could not effective collision (collisionless) of a square driven cavity.

As mentioned above, we can be briefly summarized as follows:

1. The slip velocity along the solid walls increases with increase Knudsen number at the

same Mach number.

2. An ultra high-density region appears at the very right-hand upper corner due to the high-speed moving plate at the upper of the cavity.
3. An ultra high-temperature region appears at the very right-hand upper corner due to high-density region.

### **3.2.2.2. Property Distributions Across Cavity Centroid**

#### **3.2.2.2.1. Supersonic Moving Plate (M=4)**

Fig. 3.44 - Fig. 3.48 (a)-(h) show that profiles of u-velocity along vertical lines through geometric center ( $x/L=0.5$ ) during started driven upper plate to steady state for  $Ma=4$ , and Knudsen number 10, 1, 0.1, 0.01 and 0.0033 respectively. As time goes on, the velocity enlarges gradually on upper plate and the values higher than other regime. Fig. 3.44 shows Knudsen number 10 (free molecular regime), the u-velocity values on the upper wall almost from 0.12 to 0.42 vary with time. On the other region, the values are approximately zero, but these values are quite vibration. Finally, because the primary vortex on the cavity. Thus, there are minimum value about -0.18 along vertical lines through geometric center ( $x/L=0.5$ ). This value represent left velocity, when the particle collide the right-hand wall caused the particles rebound. Fig. 3.45 shows Knudsen number 1, the u-velocity values on the upper wall almost from 0.1 to 0.45 vary with time. Except upper wall, the values are around zero, but these

values are quite vibration. There are minimum value about -0.12 along vertical lines through geometric center ( $x/L=0.5$ ). Fig. 3.46 shows Knudsen number 0.1, the u-velocity values on the upper wall almost from 0.05 to 0.65 vary with time. Except upper wall, the values are around zero, but these values are quite vibration than  $Kn=10$  and 1. Normally, the value on Knudsen number 0.1 should be smooth than Knudsen number 10, and 1. There is still unknown and study in the future. There are minimum value about -0.1 along vertical lines through geometric center ( $x/L=0.5$ ). Fig. 3.47 shows Knudsen number 0.01, the u-velocity values on the upper wall almost from 0.07 to 0.85 vary with time. There are minimum value about -0.18 along vertical lines through geometric center ( $x/L=0.5$ ). Fig. 3.48 shows Knudsen number 0.0033 (near-continuum regime), the u-velocity values on the upper wall almost from 0.2 to 0.9 vary with time. The maximum u-velocity on  $Kn=0.0033$  at the same Mach number is highest than other cases. There are minimum value about -0.15 along vertical lines through geometric center ( $x/L=0.5$ ).

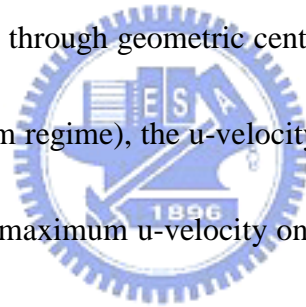


Fig. 3.49 - Fig. 3.53 (a)-(h) show that profiles of v-velocity along vertical lines through geometric center ( $x/L= 0.5$ ) during started driven upper plate to steady state for  $Ma=4$ , and Knudsen number 10, 1, 0.1, 0.01 and 0.0033 respectively. For the beginning, the values are about zero along vertical lines through geometric center; as time goes on, the value very nearly on the primary vortex.

Fig. 3.54 - Fig. 3.58 (a)-(h) show that profiles of number density along vertical lines

through geometric center ( $x/L=0.5$ ) during started driven upper plate to steady state for  $Ma=4$  and Knudsen number 10, 1, 0.1, 0.01 and 0.0033 respectively. At the start, the number densities are about 1; as time goes, the values along vertical lines through geometric center ( $x/L=0.5$ ) are change slightly.

Fig. 3.59 - Fig. 3.63 (a)-(h) show that profiles of temperature along vertical lines through geometric center ( $x/L=0.5$ ) during started driven upper plate to steady state for  $Ma=4$ , and Knudsen number 10, 1, 0.1, 0.01 and 0.0033 respectively. Fig. 3.59 shows Knudsen number 10 (free molecular regime), the temperature values on the upper wall almost from 2.1 to 4 times initial temperature 300K vary with time. On the other region, the values are approximately 1. Fig. 3.60 shows Knudsen number 1 (transient regime), the temperature values on the upper wall almost from 1.7 to 3.6 times initial temperature 300K vary with time. On the other region, the values are approximately 1. Fig. 3.61 shows Knudsen number 0.1 (transient regime), the temperature values on the upper wall almost from 1.2 to 3.3 times initial temperature 300K vary with time. Fig. 3.61 shows Knudsen number 0.01 (transient regime), the temperature values on the upper wall almost from 1.6 to 2 times initial temperature 300K vary with time. Because of these cases have temperature jump, the jump along the solid walls increase with decrease Knudsen number at the same Mach number.

Fig. 3.64 - Fig. 3.68 (a)-(h) show that profiles of u-velocity along horizontal lines through geometric center ( $y/L=0.5$ ) during started driven upper plate to steady state for  $Ma=4$ ,

and Knudsen number 10, 1, 0.1, 0.01 and 0.0033 respectively. At the beginning, the values are zero along the horizontal lines through geometric center ( $y/L=0.5$ ). Later, the primary vortex form of the cavity; the values are less than zero about on the primary vortex position. The position discuss in detail in the section 3.2.2.4. Further, the values are approximately -0.05, -0.05, -0.1, -0.15, and -0.14 with Knudsen number 10, 1, 0.1, 0.01 and 0.0033, separately.

Fig. 3.69 - Fig. 3.73 (a)-(h) show that profiles of v-velocity along horizontal lines through geometric center ( $y/L= 0.5$ ) during started driven upper plate to steady state for  $Ma=4$ , and Knudsen number 10, 1, 0.1, 0.01 and 0.0033 respectively. As time goes on, an ultra high v-velocity region appears at the left-hand region and low-velocity corner appears at the right-hand region.



Fig. 3.74 - Fig. 3.78 (a)-(h) show that profiles of number density along horizontal lines through geometric center ( $y/L= 0.5$ ) during started driven upper plate to steady state for  $Ma=4$  and Knudsen number 10, 1, 0.1, 0.01 and 0.0033 respectively. These values around 1 times initial number density on all cases. But with Knudsen number 0.01, the left-hand wall and right-hand wall are approximately 1.5 times initial number density in Fig. 3.77. With Knudsen number 0.0033, they are also about 1.5 times initial condition in Fig. 3.78.

Fig. 3.79 - Fig. 3.83 (a)-(h) show that profiles of temperature along horizontal lines through geometric center ( $y/L= 0.5$ ) during started driven upper plate to steady state for  $Ma=4$ ,



and Knudsen number 10, 1, 0.1, 0.01 and 0.0033 respectively. These values around 1 times initial temperature on all cases. But with Knudsen number 0.01, the left-hand wall and right-hand wall are approximately 2 times initial temperature in Fig. 3.82. With Knudsen number 0.0033, they are also about 1.8 times initial condition in Fig. 3.83.

### **3.2.2.3. Property Distributions Near Solid Walls**

#### **3.2.2.3.1. Supersonic Moving Plate (M=4)**

Usually, the simulation data save in the cell center for DSMC technique. Thus, observation cell center data properties are average and correct. The positions are show in Table VI. Fig. 3.84-Fig. 3.86 (a)-(h) show that profiles of u-velocity along horizontal lines through upper wall ( $y/L= 0.9875$ ) during started driven upper plate to steady state for  $Ma=4$ , and Knudsen number 10, 1 and 0.1 respectively. Fig. 3.87 (a)-(h) shows that profile of u-velocity along horizontal lines through upper wall ( $y/L= 0.995$ ) during started driven upper plate to steady state for  $Ma=4$ , and Knudsen number 0.01. Fig. 3.88 (a)-(h) shows that profile of u-velocity along horizontal lines through upper wall ( $y/L= 0.9983$ ) during started driven upper plate to steady state for  $Ma=4$ , and Knudsen number 0.0033. As time increase, the velocities enlarge gradually on the upper walls. Each maximum values are 0.4, 0.5, 0.65, 0.8, and 0.9 with Knudsen number 10, 1, 0.1, 0.01 and 0.0033, separately. Because of rarefaction effect caused slip phenomenon and the slip velocity along the upper solid walls increase with

Knudsen number at the same Mach number.

Fig. 3.89-Fig. 3.91 (a)-(h) show that profiles of  $v$ -velocity along horizontal lines through upper wall ( $y/L= 0.9875$ ) during started driven upper plate to steady state for  $Ma=4$ , and Knudsen number 10, 1 and 0.1 respectively. Fig. 3.92 (a)-(h) shows that profile of  $v$ -velocity along horizontal lines through upper wall ( $y/L= 0.995$ ) during started driven upper plate to steady state for  $Ma=4$ , and Knudsen number 0.01. Fig. 3.93 (a)-(h) shows that profile of  $v$ -velocity along horizontal lines through upper wall ( $y/L= 0.9983$ ) during started driven upper plate to steady state for  $Ma=4$ , and Knudsen number 0.0033. As time goes on, the driven plate move from left to right wall, an ultra high  $v$ -velocity region appears at the left-hand upper corner. These values are 0.65, 0.09, 0.11, 0.11 and 0.2 with Knudsen number 10, 1, 0.1, 0.01 and 0.0033, separately.

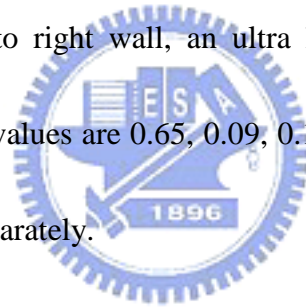


Fig. 3.94-Fig. 3.96 (a)-(h) show that profiles of number density along horizontal lines through upper wall ( $y/L= 0.9875$ ) during started driven upper plate to steady state for  $Ma=4$ , and Knudsen number 10, 1 and 0.1 respectively. Fig. 3.97 (a)-(h) shows that profile of number density along horizontal lines through upper wall ( $y/L= 0.995$ ) during started driven upper plate to steady state for  $Ma=4$ , and Knudsen number 0.01. Fig. 3.98 (a)-(h) shows that profile of number density along horizontal lines through upper wall ( $y/L= 0.9983$ ) during started driven upper plate to steady state for  $Ma=4$ , and Knudsen number 0.0033. The driven plate instantaneously starts and brings a great deal of particles to right-hand corner. An ultra

high-density region appears at the very right-hand upper corner due to the high-speed moving plate at the upper of the cavity. These values rise on right-hand upper corner and are 10, 10, 7, 7.5, and 12 times initial number density.

Fig. 3.99-Fig. 3.101 (a)-(h) show that profiles of temperature along horizontal lines through upper wall ( $y/L= 0.9875$ ) during started driven upper plate to steady state for  $Ma=4$ , and Knudsen number 10, 1 and 0.1 respectively. Fig. 3.102 (a)-(h) shows that profile of temperature along horizontal lines through upper wall ( $y/L= 0.995$ ) during started driven upper plate to steady state for  $Ma=4$ , and Knudsen number 0.01. Fig. 3.103 (a)-(h) shows that profile of temperature along horizontal lines through upper wall ( $y/L= 0.9983$ ) during started driven upper plate to steady state for  $Ma=4$ , and Knudsen number 0.0033. In Fig. 3.102, an ultra high-temperature region appears at the very right-hand upper corner which is value 4.8 times initial temperature 300K due to high-density region. In Fig. 3.103, an ultra high-temperature value is 3.2 times initial temperature 300K due to high-density region. The number density at the very right-hand upper corner with the Knudsen number 0.0033 larger than Knudsen number 0.01, but temperature does not direct proportion. That is still unknown and study in the future.

#### **3.2.2.4. Recirculation Center Position**

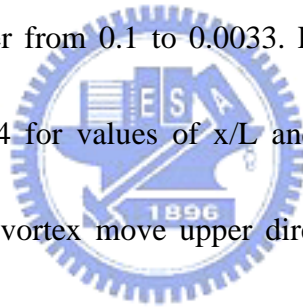
Fig. 3.104 (a) - (e) show that streamline for  $Ma=4$ , and Knudsen number 10, 1, 0.1, 0.01

and 0.0033 respectively. Result show Knudsen number 10, 1 and 0.1, the streamlines are crack. Because of simulation transient regime and data are not fine when using DSMC technique.

Fig. 3.105 shows that position of the center of the vortex during started driven upper plate at  $t = 1000 \sim 3000 \mu s$  for  $Ma=4$ , and Knudsen number 10. Result show that the positions of vortex center move from right-hand upper wall ( $y/L=0.8, x/L=0.75$ ) to near center upper wall ( $y/L=0.88, x/L=0.6$ ). The positions of center move toward upper wall and right wall gradually during form vortex center. Fig. 3.106 shows that position of the center of the vortex during started driven upper plate at  $t = 1000 \sim 1800 \mu s$  for  $Ma=4$ , and Knudsen number 1. Result show that the positions of vortex center move from right-hand upper wall ( $y/L=0.77, x/L=0.75$ ) to near upper wall ( $y/L=0.9, x/L=0.7$ ). The positions of center move toward upper wall gradually during form vortex center. Fig. 3.107 shows that position of the center of the vortex during started driven upper plate at  $t = 2000 \sim 4500 \mu s$  for  $Ma=4$ , and Knudsen number 0.1. Result show that the positions of vortex center move from right-hand upper wall ( $y/L=0.8, x/L=0.8$ ) to near center upper wall ( $y/L=0.8, x/L=0.6$ ). The positions of center move toward geometric center gradually during form vortex center. Fig. 3.108 shows that position of the center of the vortex during started driven upper plate at  $t = 1000 \sim 3750 \mu s$  for  $Ma=4$ , and Knudsen number 0.01. Result show that the positions of vortex center move from right-hand upper wall ( $y/L=0.82, x/L=0.78$ ) to near center upper wall ( $y/L=0.75, x/L=0.6$ ). The

positions of center move toward geometric center gradually during form vortex center. Fig. 3.109 shows that position of the center of the vortex during started driven upper plate at  $t = 1100 \sim 2600 \mu s$  for  $Ma=4$ , and Knudsen number 0.0033. Result show that the positions of vortex center move from right-hand upper wall ( $y/L=0.9$ ,  $x/L=0.85$ ) to near center upper wall ( $y/L=0.85$ ,  $x/L=0.75$ ). The positions of center move toward geometric center gradually during form vortex center.

Fig. 3.110 shows that positions of the center of the vortex with  $M=4$  for values of  $x/L$  and Knudsen number. Result show that positions of the center of the vortex move left direction with decrease Knudsen number from 0.1 to 0.0033. Fig. 3.111 shows that positions of the center of the vortex with  $M=4$  for values of  $x/L$  and Knudsen number. Result show that positions of the center of the vortex move upper direction with increase Knudsen number from 0.01 to 1.



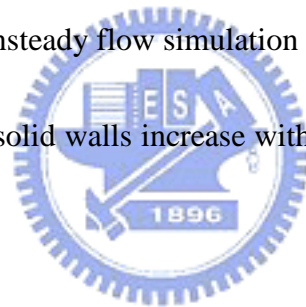
## Chapter 4

### Conclusions and Recommendation of Future Work

#### 4.1. Summary

The current study carries out the simulations of top driven supersonic ( $M=4$ ) cavity flow at various Knudsen numbers using a parallelized DSMC code (PDSC) with unsteady sampling and DREAM technique. Important conclusions are summarized as follows:

1. Use of the DREAM technique can greatly reduce the statistical scatter with an acceptable runtime for unsteady flow simulation using DSMC technique.
2. Velocity slips along the solid walls increase with increase Knudsen number at the same Mach number ( $M=4$ ).
3. Center of the primary vortex during one time moves towards the geometric center with Knudsen number is 0.1, 0.01 and 0.0033. Other cases move toward the upper wall with Knudsen number is 10 and 1.



#### 4.2. Recommendation of Future Work

Based on this study, future work is suggested as follows:

1. To use a “temporal variable time step” scheme in which the time step is increased when the flow is not being sampled to further decrease computational time;
2. To extend sampling time or sample particle per cell to improve the simulation result.

3. To simulate the driven cavity flow in  $Ma=1.1$  and  $Ma=2$ .
4. To simulate the driven cavity flow in subsonic region.
5. To simulate the driven cavity flow with oscillatory top moving plate.



## References

- [1] Auld, D. J., "Direct molecular simulation (DSMC) of shock tube flow", in Proc. First European Computational Fluid Dynamics Conference, Brussels, Belgium, September, 1992.
- [2] Bird, G. A., Molecular Gas Dynamics, Clarendon Press, Oxford, UK, 1976.
- [3] Bird, G. A., "Monte Carlo Simulation in an Engineering Context", Progr. Astro. Aero, 74, pp.239-255, 1981.
- [4] Bird, G. A., "Definition of Mean Free Path for Real Gases", Phys. Fluids, 26, pp.3222-3223, 1983.
- [5] Bird, G. A., Molecular Gas Dynamics and the Direct Simulation of Gas Flows, Oxford University Press, New York, 1994.
- [6] Borgnakke, C. and Larsen, P. S., "Statistical Collision Model for Monte Carlo Simulation of Polyatomic Gas Mixture", Journal of Computational Physics, 18, pp. 405-420, 1975.
- [7] Cercignani, C. and Cortese, S., "Validation of a Monte Carlo simulation of the plate Couette flow of a rarefied gas", J. Stat. Phys. 75, 817, 1994.
- [8] Cercignani, C., The Boltzmann Equation and Its Application, Springer, New York, 1998.
- [9] Cave, H. M., Krumdieck, S.P., and Jermy, M.C., "Development of a model for high precursor conversion efficiency pulsed-pressure chemical vapor deposition (PP-CVD) processing", Chem. Eng. J., 2007 (in press).
- [10] Cave, H. M., Tseng, K.-C., Wu, J.-S., Jermy, M. C., Huang, J.-C. and Krumdieck, S. P., "Implementation of Unsteady Sampling Procedures for the Parallel Direct Simulation Monte Carlo Method", J. of Computational Physics, 2007 (submitted).
- [11] Ghia, U., Ghia, K.N., and Shin, C.T., "High  $-Re$  solutions for incompressible flow using the Navier-Stokes equations and a multigrid method". J. of Computational Physics, 48, pp.387-411, 1982.
- [12] Hou, S., Zou, Q., Chen, S., and Doolen, G., "Simulation of cavity flow by the lattice Boltzmann method", J. Comput. Phys. 118, 329, 1995.
- [13] Huang, J.-C., "A study of instantaneous starting cylinder and shock impinging over wedge flow", in Proc. 10<sup>th</sup> National Computational Fluid Dynamics Conference, Hua-Lien, Taiwan, August 2003 (in Chinese).
- [14] Kannenberg, K. and Boyd, I. D., "Strategies for Efficient Particle Resolution in the Direct Simulation Monte Carlo Method", Journal of Computational Physics, 157, pp. 727-745, 2000.
- [15] Karniadakis, G.E., and Beskok, A., Micro Flows. Fundamentals and Simulation, Springer, New York, 2001.
- [16] Nanbu, K., "Theoretical Basis on the Direct Monte Carlo Method", Rarefied Gas Dynamics, 1, Boffi, V. and Cercignani, C. (editor), Teubner, Stuttgart, 1986.
- [17] Naris, S., and Valougeorgis, D., "The driven cavity flow over the whole range of the Knudsen



- number”, *Physics of Fluids*, 17, 2005.
- [18] Robinson, C. D., and Harvey, J. k., “ A parallel DSMC Implementation on Unstructured Meshes with Adaptive Domain Decomposition”, *Proceeding of 20<sup>th</sup> International Symposium on Rarefied Gas Dynamics*, pp. 227-232, Shen, C. (editor), Peking University Press, 1996.
- [19] Robinson, C. D., and Harvey, J. k., “Adaptive Domain Decomposition for Unstructured Meshes Applied to the Direct Simulation Monte Carlo Method”, *Parallel Computational Fluid Dynamics: Algorithm and Results using Advanced Computers*, pp. 469-476, 1997.
- [20] Robinson, C. D., Particle Simulations on Parallel Computers with Dynamic Load Balancing, Imperial College of Science, Technology and Medicine, UK, Ph.D. Thesis, 1998.
- [21] Tseng, K.-C., Cave, H. M., Wu, J.-S., Huang, J.-C., Lian, Y.-Y., Jermy, M. C. and Krumdieck, S. P., “Implementation of Transient Sub-Cells on Unstructured Grids for the Parallel Direct Simulation Monte Carlo Method”, *Journal of Computational Physics*, 2007 (submitted)
- [22] Wagner, W., “A convergence proof for Bird’s Direct simulation Monte Carlo method for the Boltzmann equation”, *Journal State Physics*, 66(3/4), pp. 1011-1044, 1992.
- [23] Wu, J.-S., and Tseng, K.-C., “Parallel DSMC Method Using Dynamic Domain Decomposition”, *International Journal for Numerical Methods in Engineering*, Vol. 63, pp. 37-76, 2005.
- [24] Wu, J.-S., Lee, W.-S., Lee, Fred and Wong, S.-C., “Pressure Boundary Treatment In Micromechanical Devices Using Direct Simulation Monte Carlo Method”, *JSME International Journal, Series B*, 44(3), pp. 439-450, 2001.
- [25] Wu, J.-S., and Hsu Y.-L., “Derivation of Variable Soft Sphere Model Parameters in Direct-Simulation Monte Carlo Method Using Quantum Chemistry Computation”, *Japanese Journal of Applied Physics*, 42, pp. 7574-7575, 2003.
- [26] Wu, J.-S., Tseng, K.-C., and Wu, F.-Y., “Parallel Three Dimensional Simulation Monte Carlo Method Using Adaptive Mesh and Variable Time Step“, *Computer Physics Communications*”, Vol. 162, No. 3, pp. 166-187, 2004.
- [27] Wu, J.-S., Lian, Y.-Y., Cheng, G., Koomullil, R. P., and Tseng, K.-C., “Development and Verification of a Coupled DSMC-NS Scheme Using Unstructured Mesh“, *Journal of Computational Physics*, Vol. 219, No. 2, pp. 579-607, 2006.
- [28] Xu, D.Q., Honma, H., and Abe, T., “DSMC approach to nonstationary Mach reflection of strong incoming shock waves using a smoothing technique”, *Shock Waves*, 3(1), 67, 1993.

## Tables

Table I Flow and simulation condition for 1-D Couette flow.

| condition\case                                     | Mesh (100 x100) | Mesh (100x100)<br>Fine grid | Mesh(100x100)<br>Coarse grid |
|--|-----------------|-----------------------------|------------------------------|
| Knudsen number                                     | 0.02            | 0.02                        | 0.02                         |
| Mach number  | 0.3             | 0.3                         | 0.3                          |
| Mesh   | 100 x100        | 200 x 5                     | 5 x 5                        |
| Grid size of the each cell                         | 0.01            | 0.025                       | 0.1                          |
| Velocity (m/s)                                     | 96.6            | 96.6                        | 96.6                         |
| Temperature (K)                                    | 300             | 300                         | 300                          |
| Number Density                                     | 6.457E+19       | 6.457E+19                   | 6.457E+19                    |
| Particle per cell (#)                              | 100             | 100                         | 100                          |
| the number of DTM time steps between samplings (#) | 100             | 100                         | 100                          |
| Timestep   | 3.11e-5         | 3.11e-5                     | 3.11e-5                      |

Table II The grid sizes of distinct driven cavity cases.

| Knudsen number | Mach number | Mesh      | Grid size of the each cell |
|----------------|-------------|-----------|----------------------------|
| 10             | 4           | 40 x 40   | 0.025                      |
| 1              | 4           | 40 x 40   | 0.025                      |
| 0.1            | 4           | 40 x 40   | 0.025                      |
| 0.01           | 4           | 100 x 100 | 0.01                       |
| 0.0033         | 4           | 300 x 300 | 3.33e-3                    |

Table III The time steps of distinct driven cavity cases.

| Knudsen number | Mach number | Time step (s) |
|----------------|-------------|---------------|
| 10             | 4           | $5e-7$        |
| 1              | 4           | $4e-7$        |
| 0.1            | 4           | $1e-7$        |
| 0.01           | 4           | $1e-7$        |
| 0.0033         | 4           | $4e-8$        |

Table IV The initial conditions of distinct driven cavity cases.

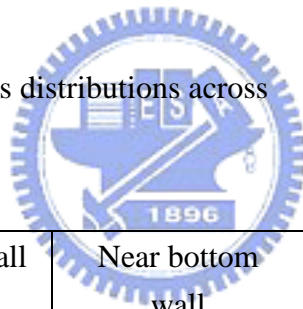
| Case\Condition | Driven Plate Velocity (m/s) | Temperature (K) | Number Density | Particle per cell (#) | Mesh      | Grid size of the each cell | Time step (s) | the number of DTM time steps between samplings (#) |
|----------------|-----------------------------|-----------------|----------------|-----------------------|-----------|----------------------------|---------------|--|
| Kn10M4         | 1288                        | 300             | 1.29438E+17    | #25                   | 40 x 40   | 0.025                      | 5e-7          | 50   |
| Kn1M4          | 1288                        | 300             | 1.29438E+18    | #25                   | 40 x 40   | 0.025                      | 4e-7          | 50   |
| Kn0.1M4        | 1288                        | 300             | 1.29438E+19    | #25                   | 40 x 40   | 0.025                      | 1e-7          | 50   |
| Kn0.01M4       | 1288                        | 300             | 1.29438E+20    | #100                  | 100 x 100 | 0.01                       | 1e-7          | 50   |
| Kn0.0033M4     | 1288                        | 300             | 3.88314E+20    | #100                  | 300 x 300 | 3.33e-3                    | 4e-8          | 50   |



Table V The other conditions of distinct driven cavity cases.

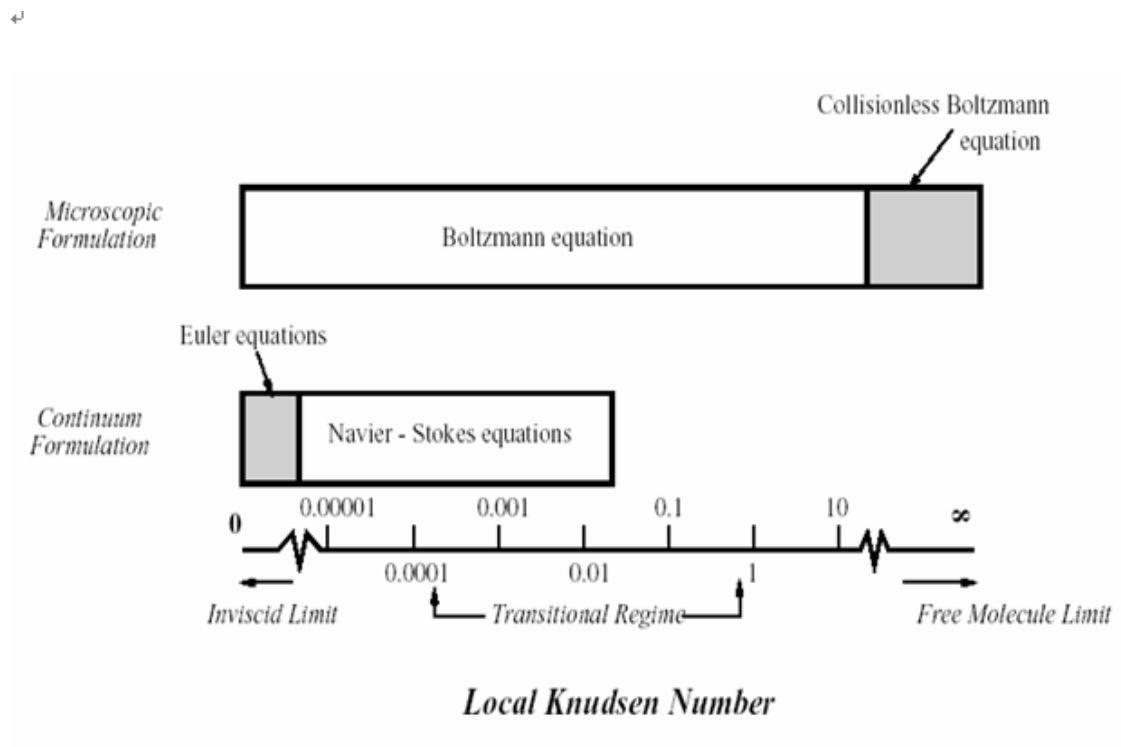
| Case\Condition | Sub-Cell (in a cell) | DREAM (Ensemble time) |
|----------------|----------------------|-----------------------|
| Kn10M4         | 5 x 5                | 10                    |
| Kn1M4          | 5 x 5                | 10                    |
| Kn0.1M4        | 5 x 5                | 10                    |
| Kn0.01M4       | 10 x 10              | 10                    |
| Kn0.0033M4     | 10 x 10              | 10                    |

Table VI Positions of properties distributions across



| Knudsen number | Near top wall | Near bottom wall | Near left wall | Near right wall |
|----------------|---------------|------------------|----------------|-----------------|
| 10             | $y/L=0.9875$  | $y/L=0.0125$     | $x/L=0.0125$   | $x/L=0.9875$    |
| 1              | $y/L=0.9875$  | $y/L=0.0125$     | $x/L=0.0125$   | $x/L=0.9875$    |
| 0.1            | $y/L=0.9875$  | $y/L=0.0125$     | $x/L=0.0125$   | $x/L=0.9875$    |
| 0.01           | $y/L=0.995$   | $y/L=0.005$      | $x/L=0.995$    | $x/L=0.995$     |
| 0.0033         | $y/L=0.9967$  | $y/L=0.0033$     | $x/L=0.0033$   | $x/L=0.9967$    |

# Figures



**Fig. 2.1** Classifications of Gas Flows



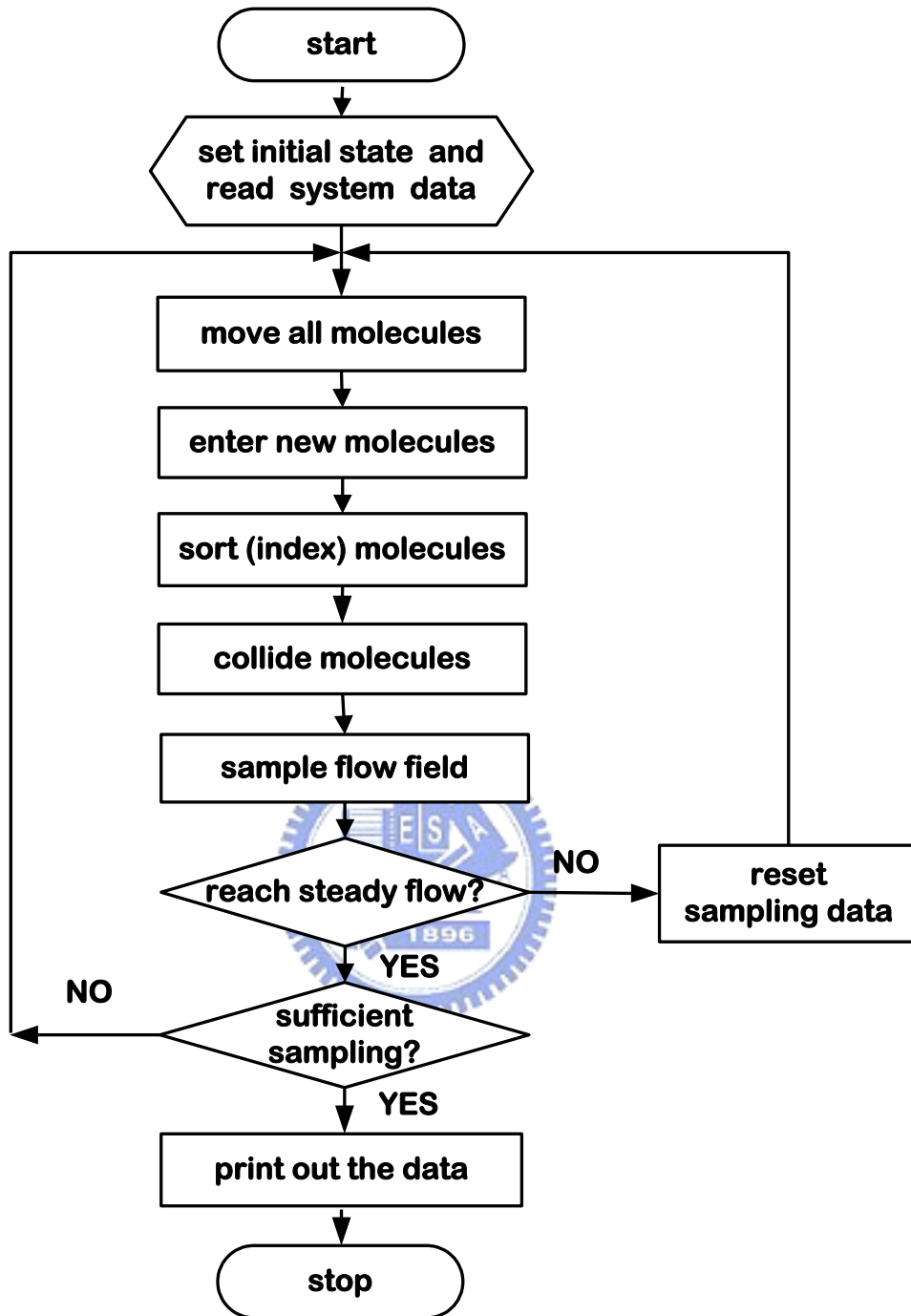


Fig. 2.2 Flow chart of the DSMC method

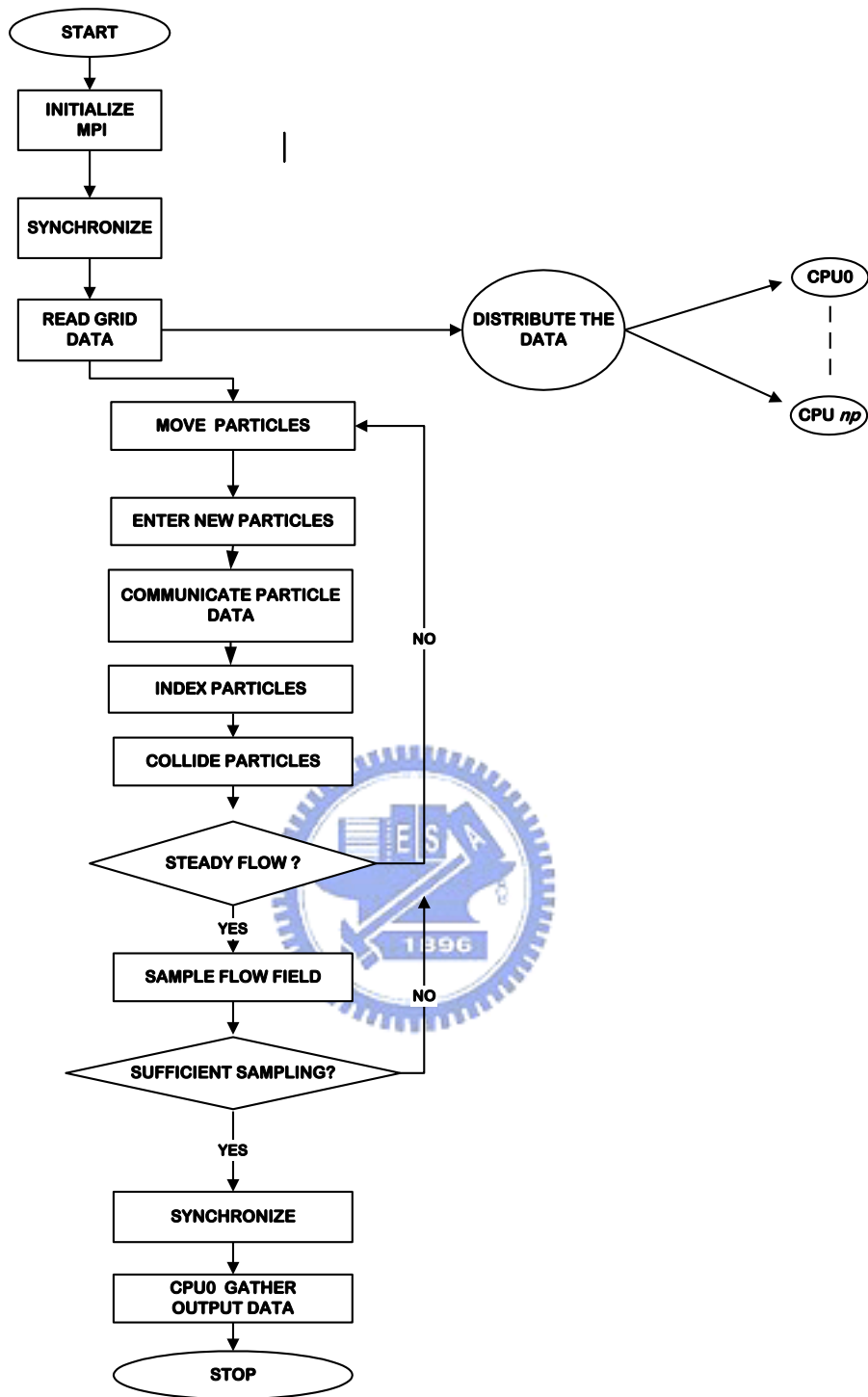
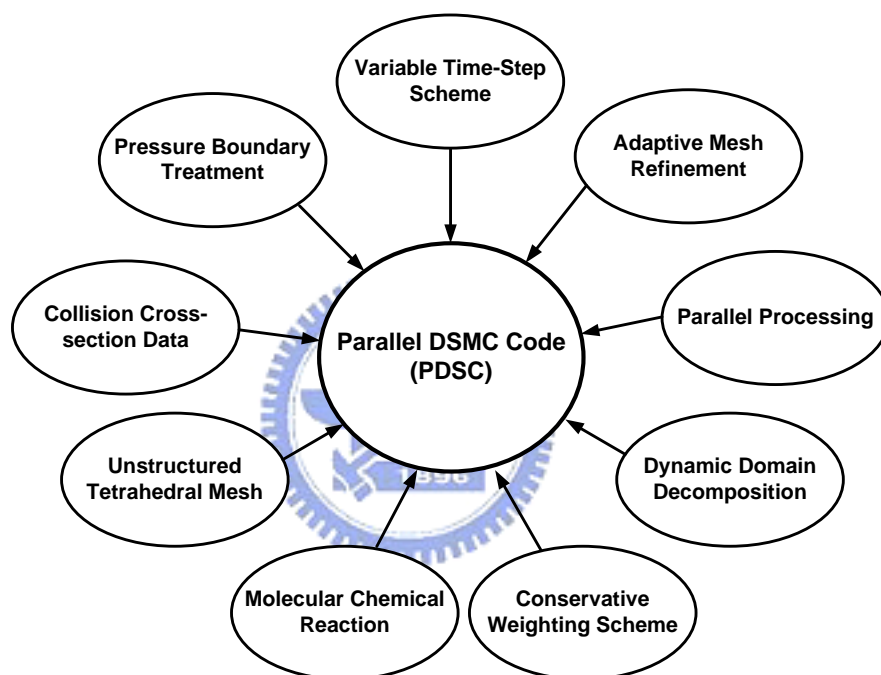
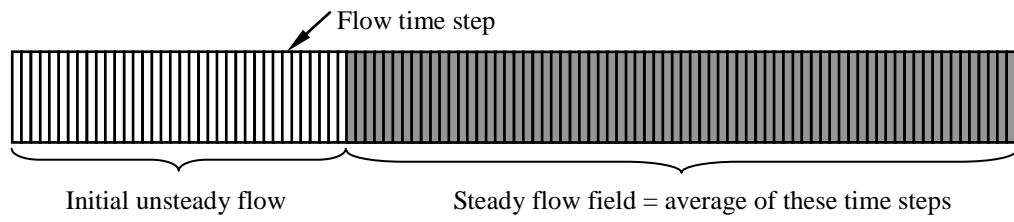


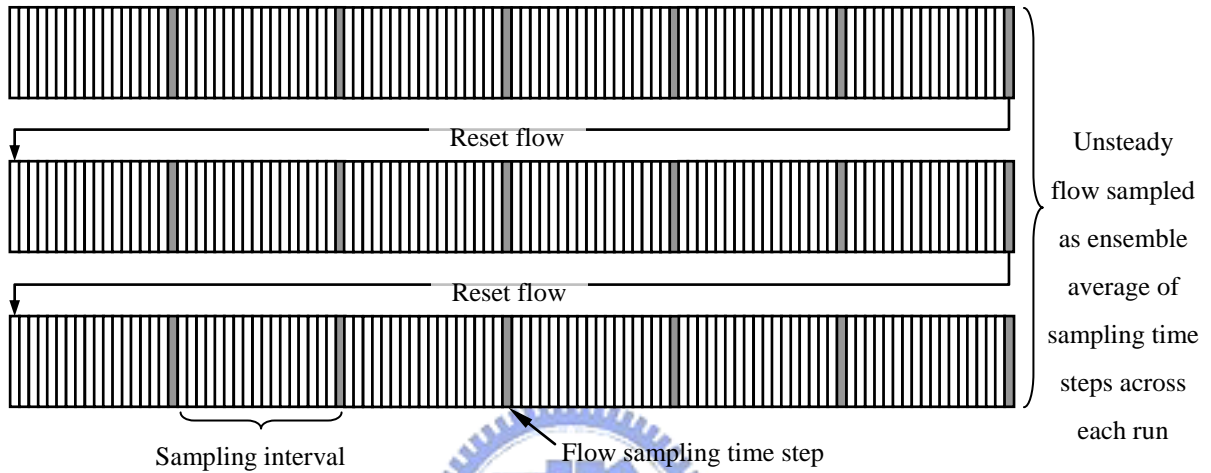
Fig. 2.3 Simplified flow chart of the parallel DSMC method for  $np$  processors.



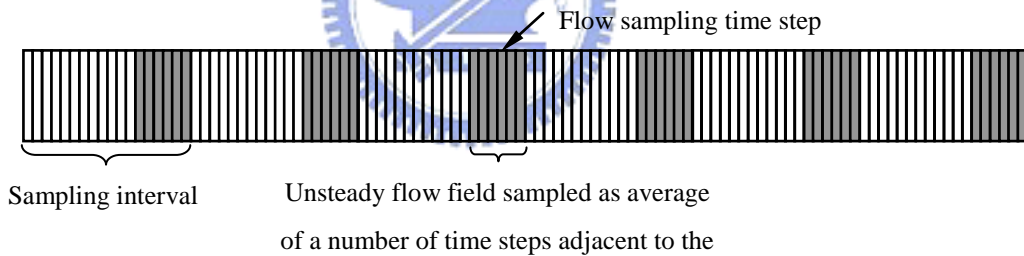
**Fig. 2.4** The additional schemes in the parallel DSMC code.



(a)



(b)



(c)

**Fig. 2.5** Sampling method in DSMC include (a) steady sampling (b) unsteady ensemble sampling (c) unsteady time averaging.

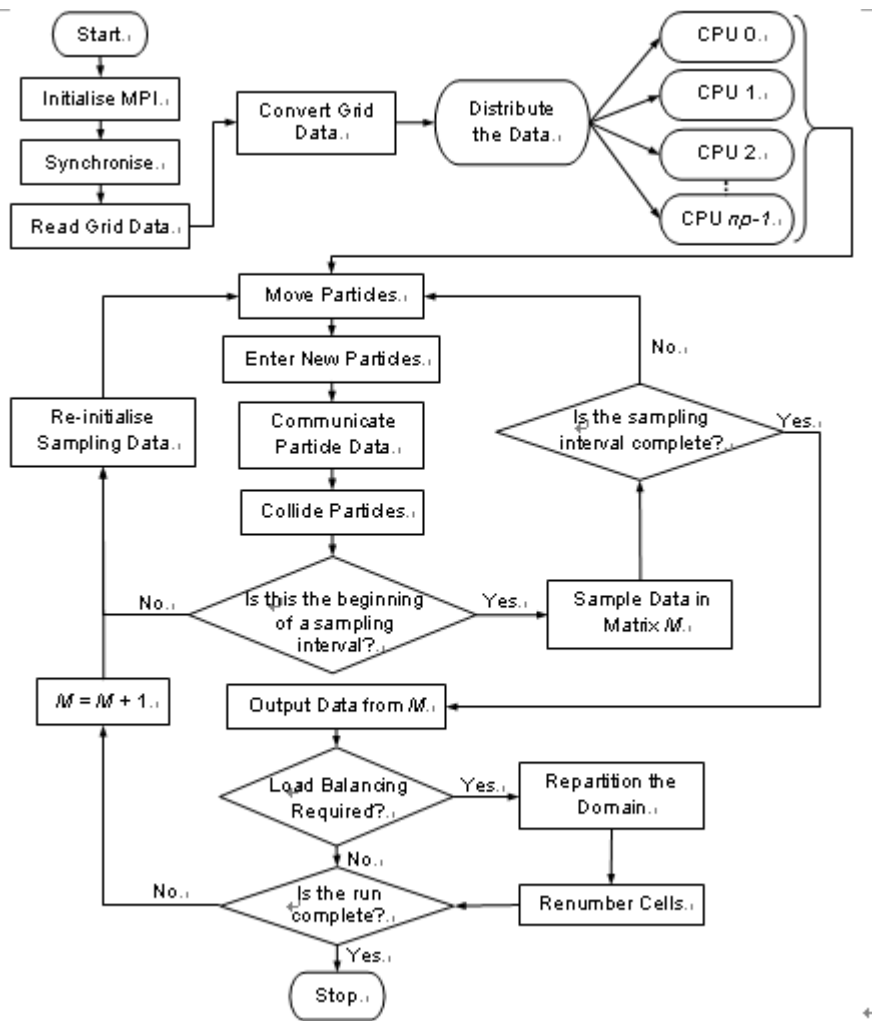


**Fig. 2.6** Simplified flow chart of the unsteady parallel DSMC method.

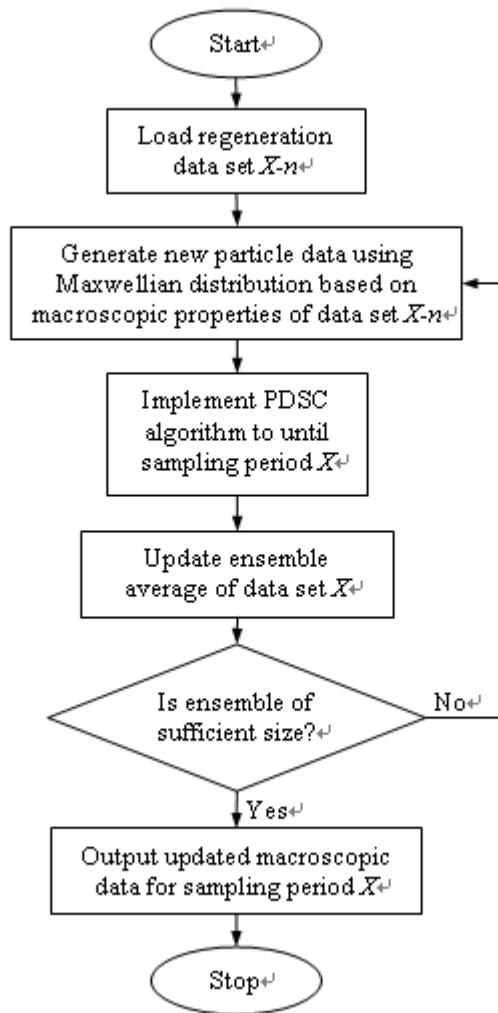


**Fig. 2.7** Simplified flow chart of the DSMC Rapid Ensemble Averaging Method (DREAM)

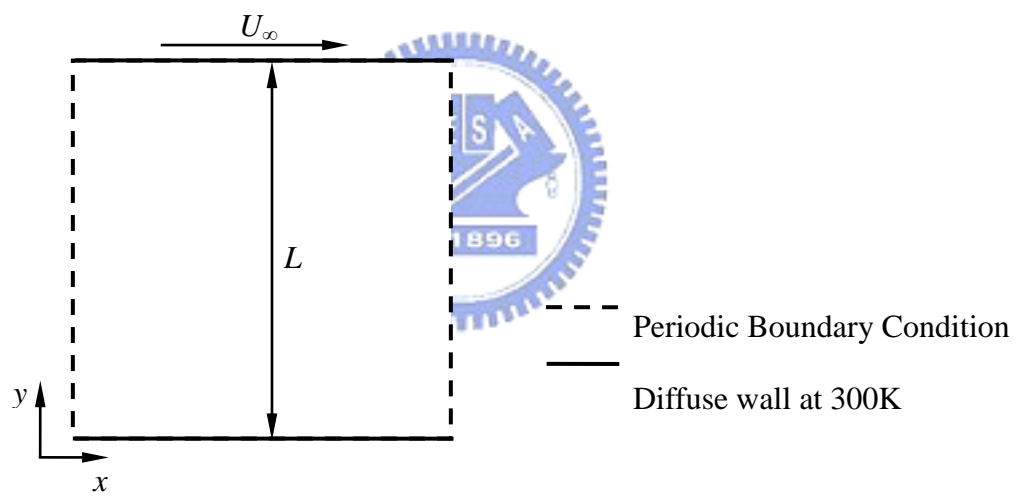


**Fig. 3.1** Computational domains for the developing Couette flow.

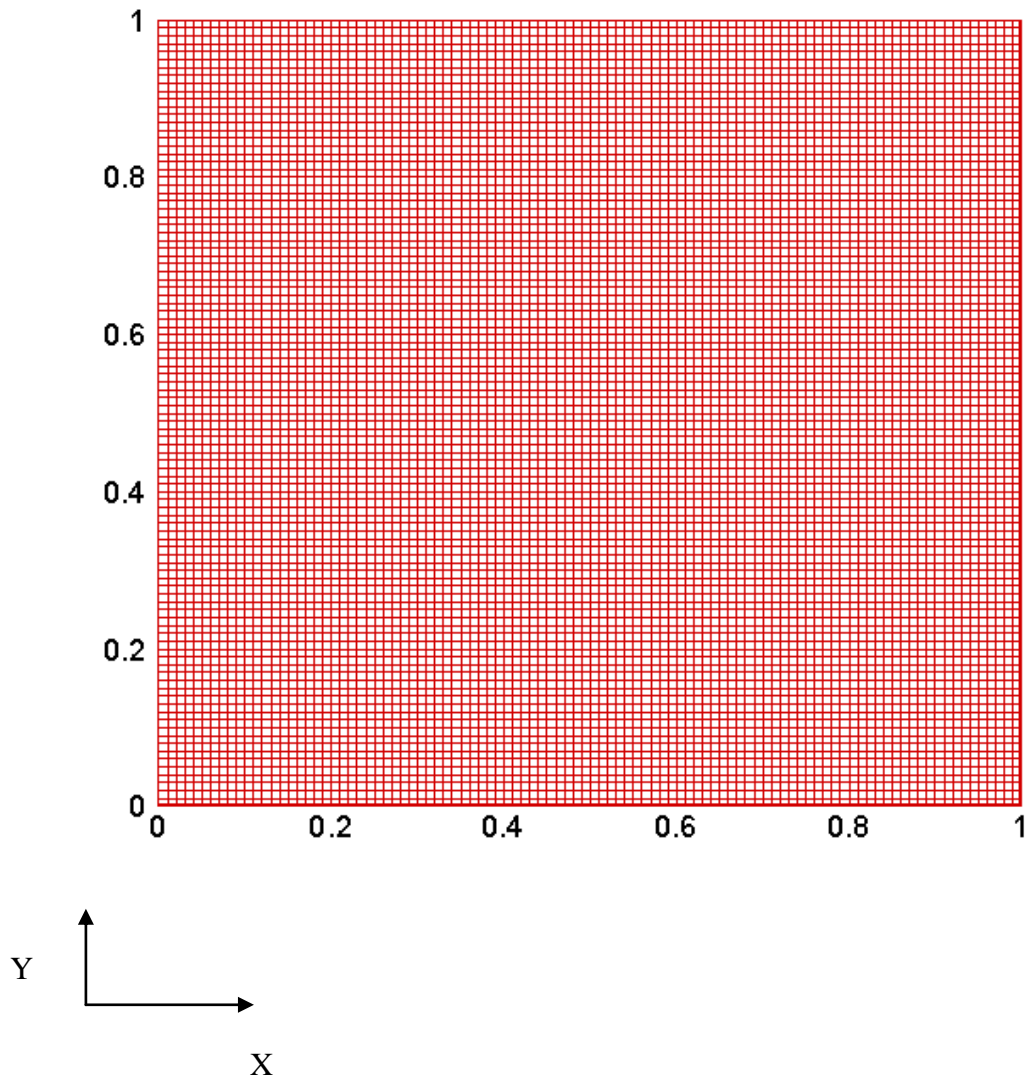


**Fig. 3.2** The mesh (100x100) for  $M=0.3$ ,  $Kn=0.02$  Couette flow.



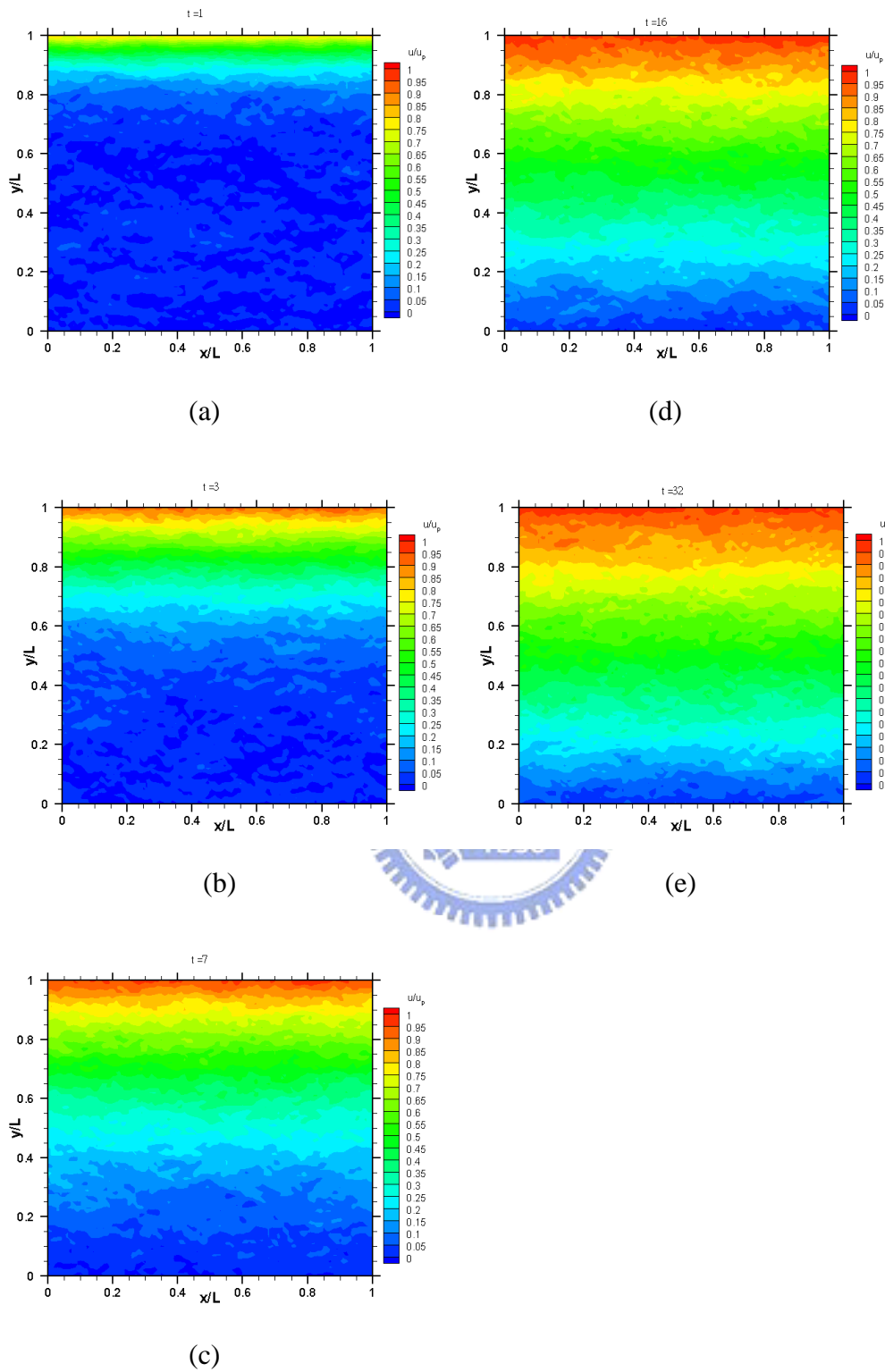


**Fig. 3.3** Contours of velocity for  $M=0.3$ ,  $Kn=0.02$  Couette flow from unsteady DSMC technique at normalized time (a)  $t=1$ ; (b)  $t=3$ ; (c)  $t=7$ ; (d)  $t=16$ ; (e)  $t=32$

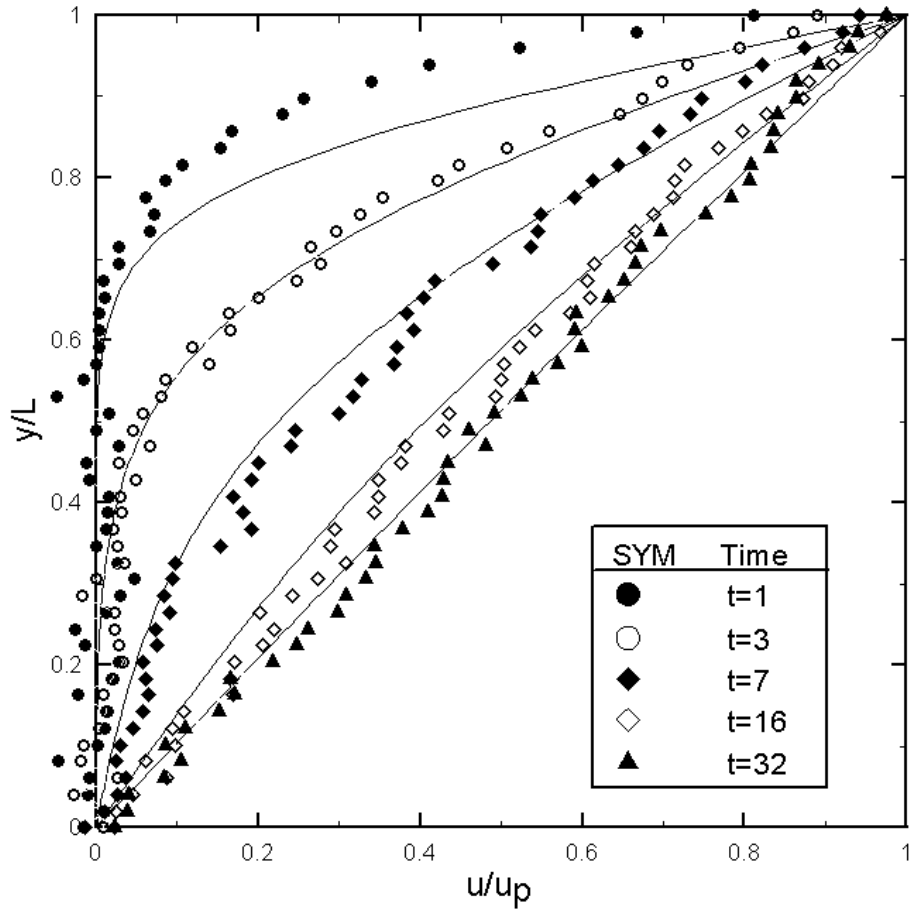


**Fig. 3.4** Comparison of for  $M=0.3$ ,  $Kn=0.02$  Couette flow development by unsteady DSMC (symbols) with the exact Navier-Stokes solution (lines).

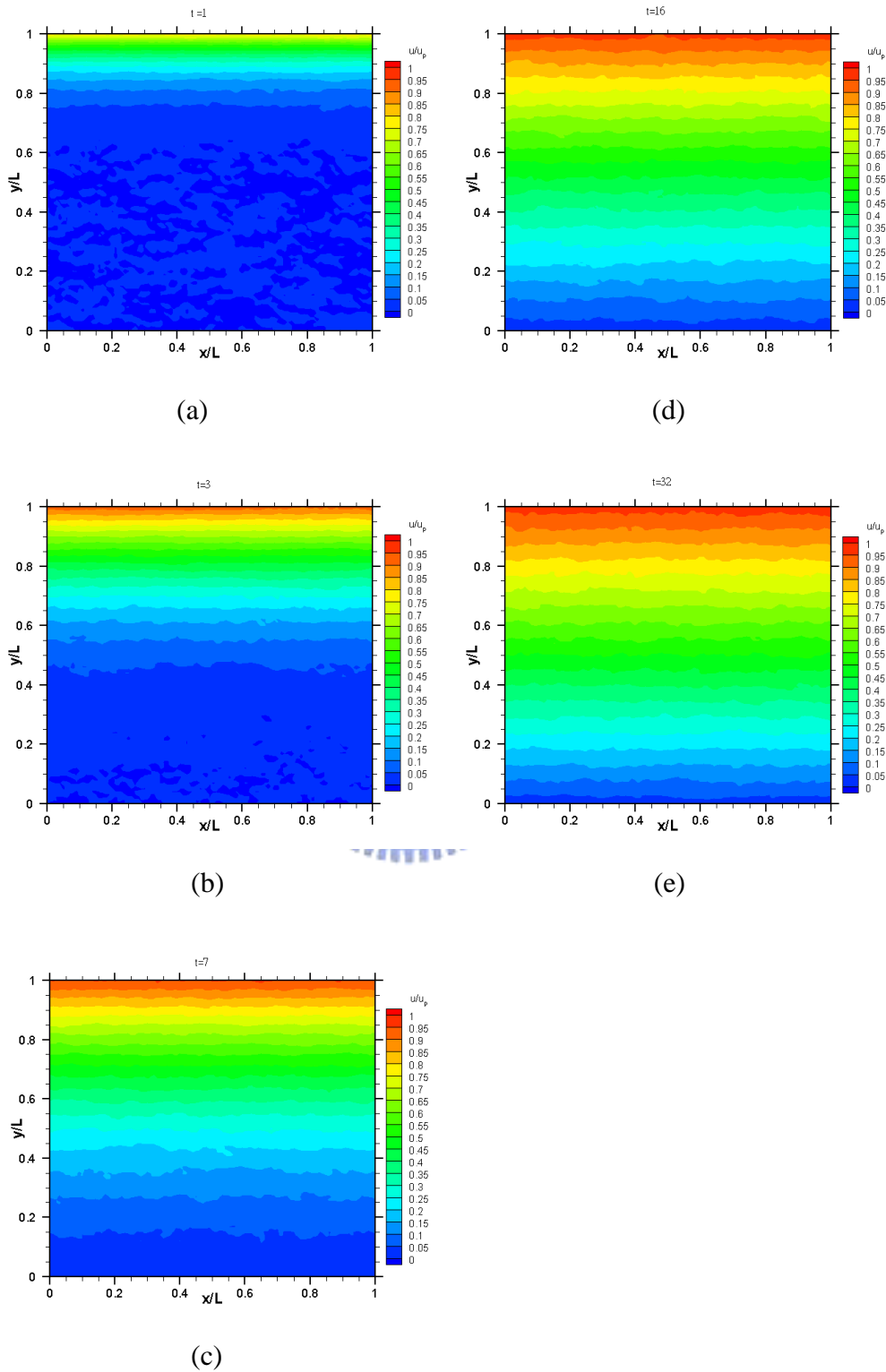


**Fig. 3.5** Contours of velocity for for  $M=0.3$ ,  $Kn=0.02$  Couette flow from DREAM technique at normalized time (a)  $t=1$ ; (b)  $t=3$ ; (c)  $t=7$ ; (d)  $t=16$ ; (e)  $t=32$

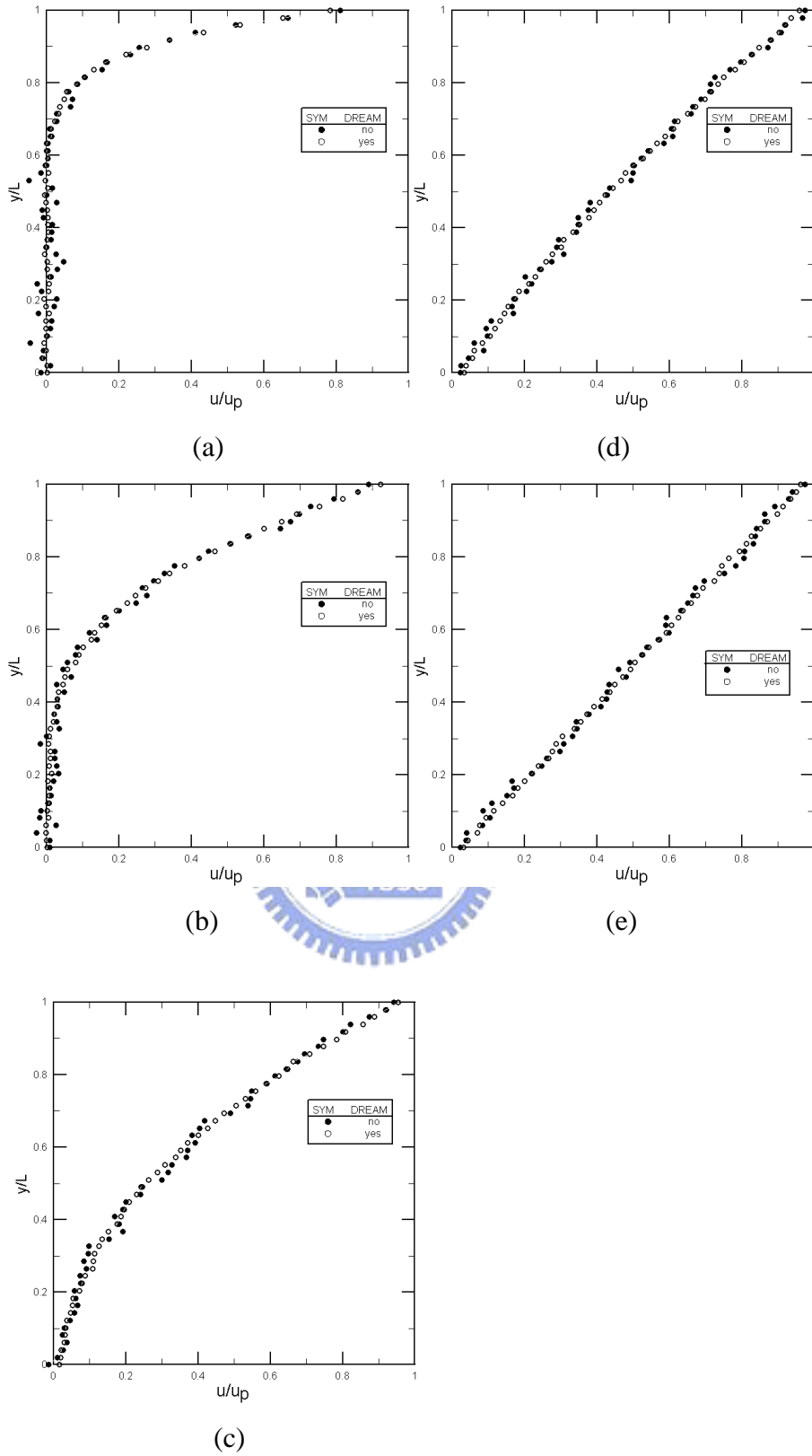


**Fig. 3.6** Comparison of for  $M=0.3$ ,  $Kn=0.02$  Couette flow development by unsteady DSMC with the DREAM technique at normalized time (a)  $t=1$ ; (b)  $t=3$ ; (c)  $t=7$ ; (d)  $t=16$ ; (e)  $t=32$

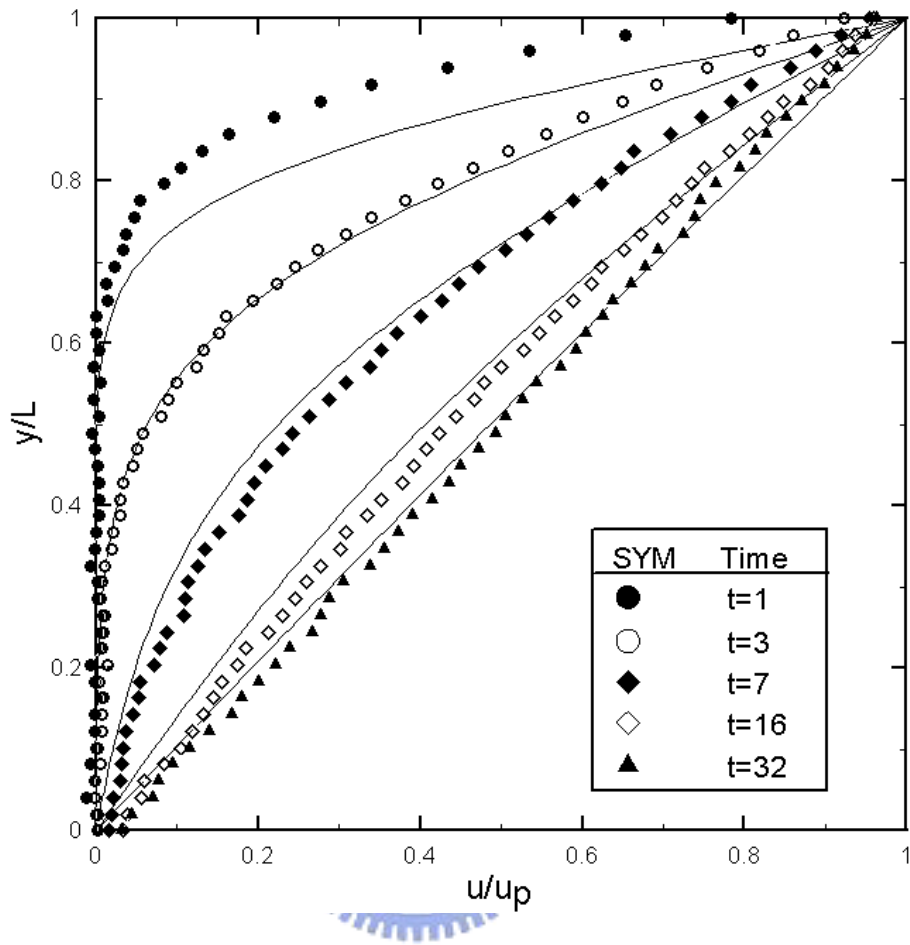


**Fig. 3.7** Comparison of for  $M=0.3$ ,  $Kn=0.02$  Couette flow development by unsteady DSMC with the DREAM technique (symbols) with the exact Navier-Stokes solution (lines).

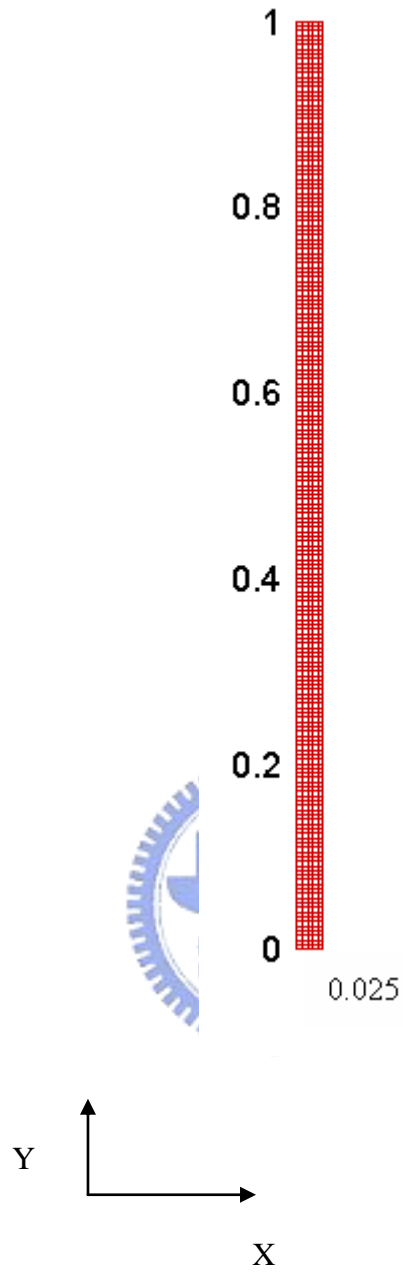


**Fig. 3.8** The mesh for  $\frac{\Delta x}{\lambda} = \frac{\Delta y}{\lambda} = 0.25$  for  $M=0.3$ ,  $Kn=0.02$  Couette flow.

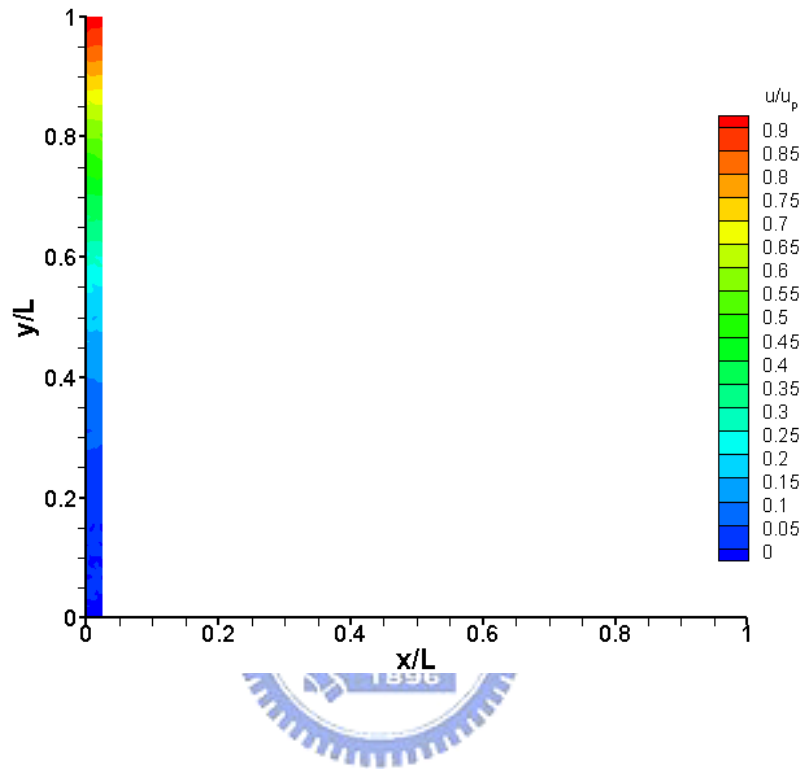


**Fig. 3.9** Contours of velocity for  $\frac{\Delta x}{\lambda} = \frac{\Delta y}{\lambda} = 0.25$ , for  $M=0.3$ ,  $Kn=0.02$  Couette flow.

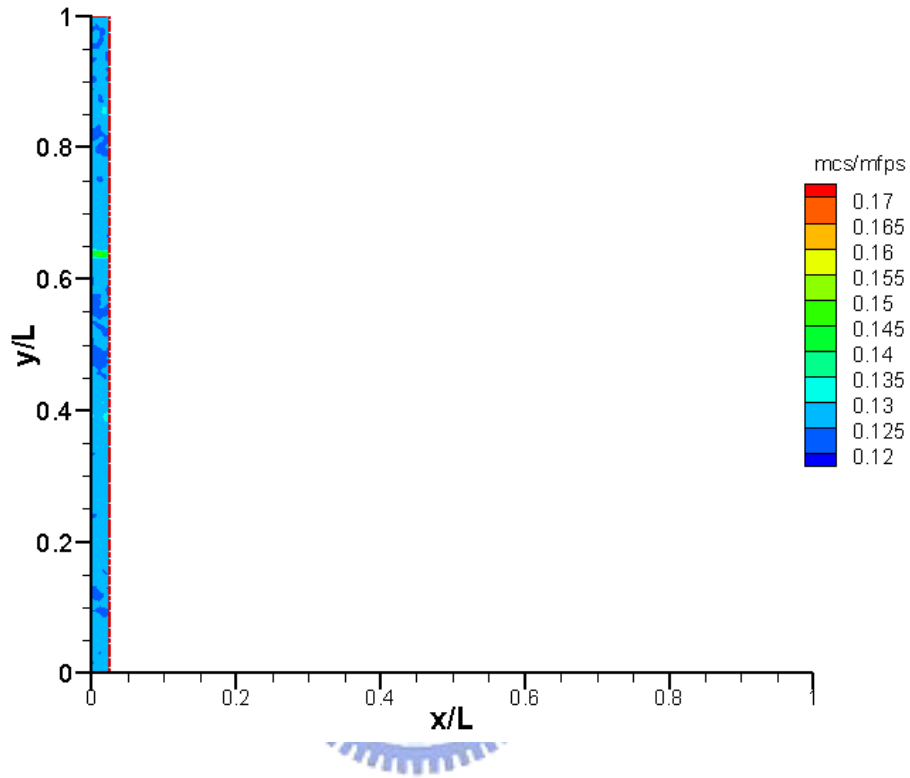


**Fig. 3.10** Contours of  $mcs/mfps$  for  $\frac{\Delta x}{\lambda} = \frac{\Delta y}{\lambda} = 0.25$ , for  $M=0.3$ ,  $Kn=0.02$  Couette flow.



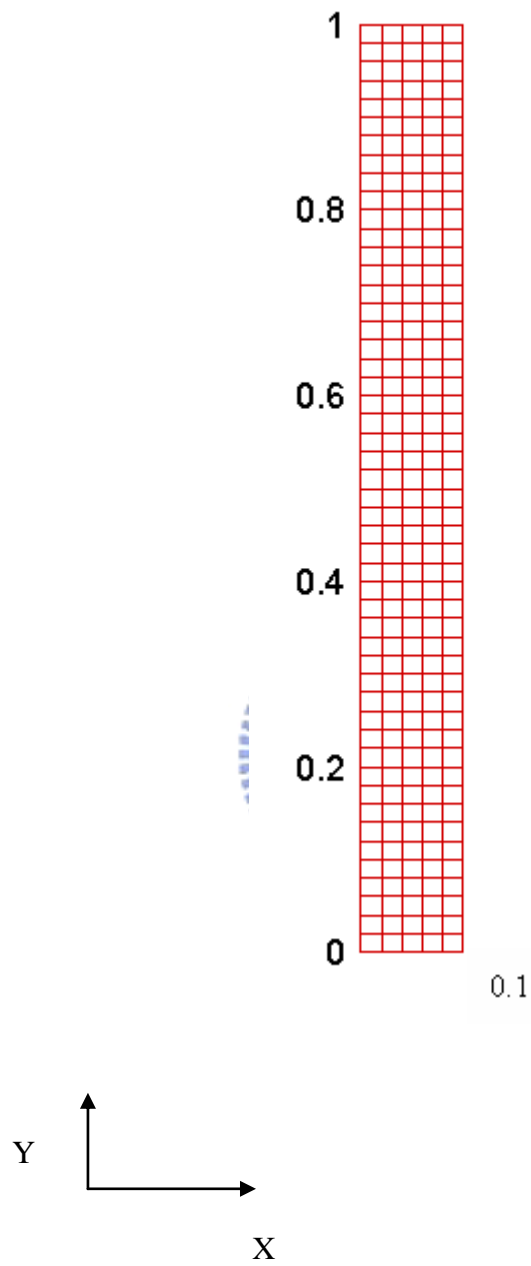


**Fig. 3.11** the mesh for  $\frac{\Delta x}{\lambda} = \frac{\Delta y}{\lambda} = 1$  for  $M=0.3$ ,  $Kn=0.02$  Couette flow.

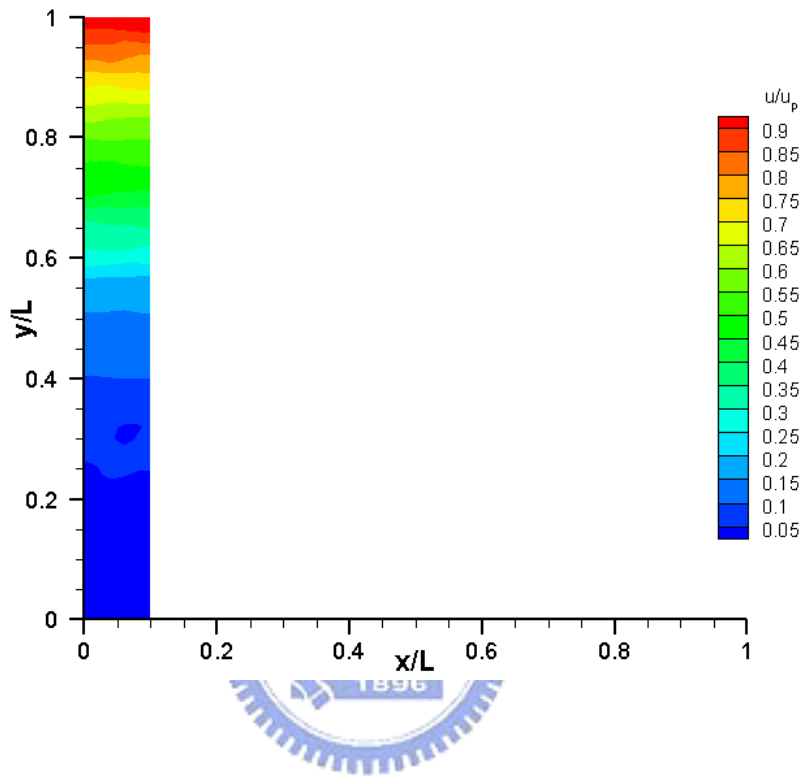


**Fig. 3.12** Contours of mcs/mfps for  $\frac{\Delta x}{\lambda} = \frac{\Delta y}{\lambda} = 1$ , for  $M=0.3$ ,  $Kn=0.02$  Couette flow.

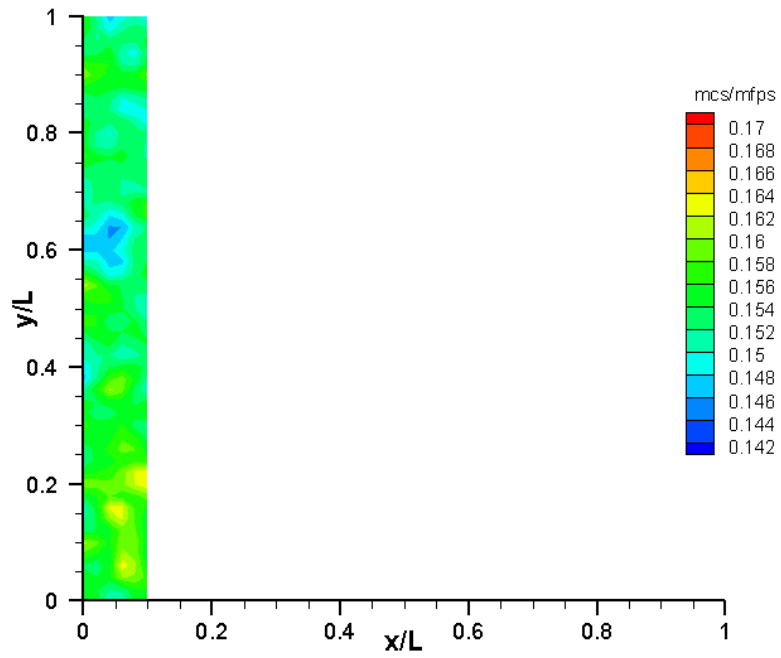


**Fig. 3.13** Contours of  $mcs/mfps$  for  $\frac{\Delta x}{\lambda} = \frac{\Delta y}{\lambda} = 1$ , for  $M=0.3$ ,  $Kn=0.02$  Couette flow.

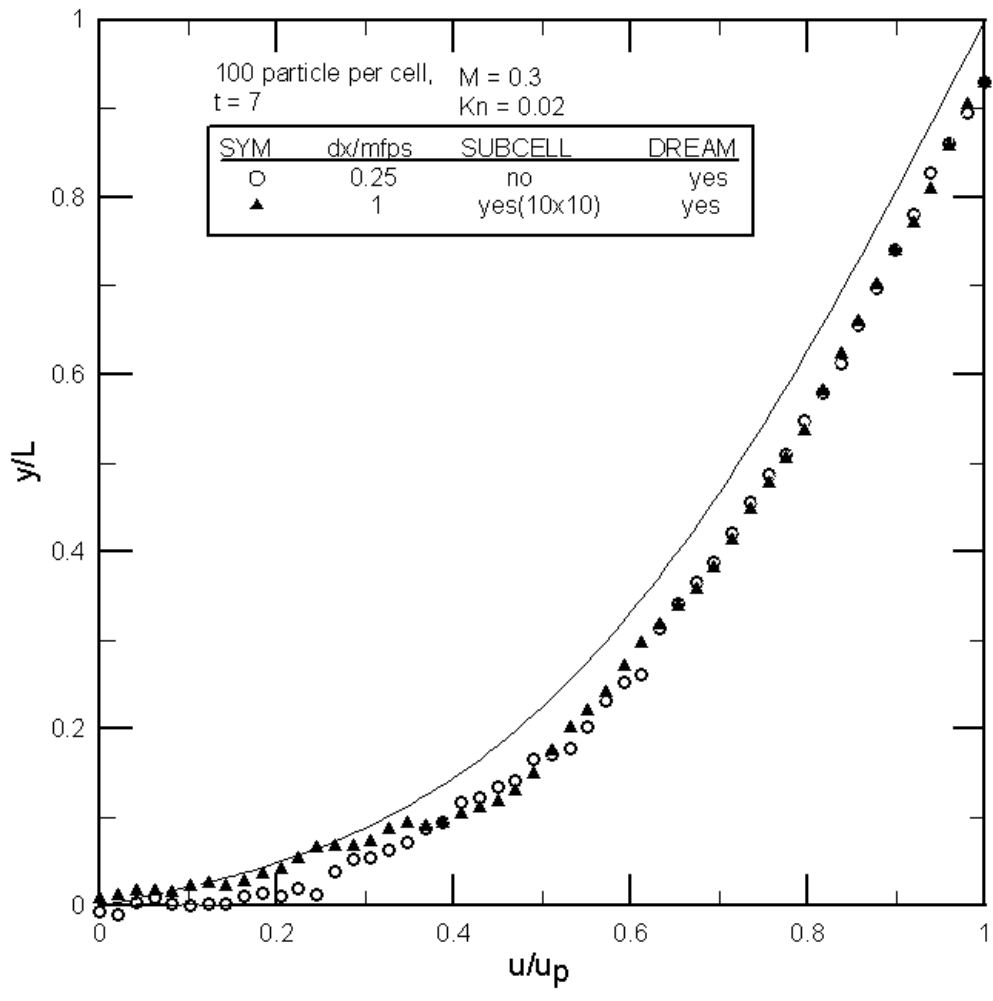


**Fig. 3.14** Comparison of Couette flow development by  $\frac{\Delta x}{\lambda} = \frac{\Delta y}{\lambda} = 0.25$  with  $\frac{\Delta x}{\lambda} = \frac{\Delta y}{\lambda} = 1$ .

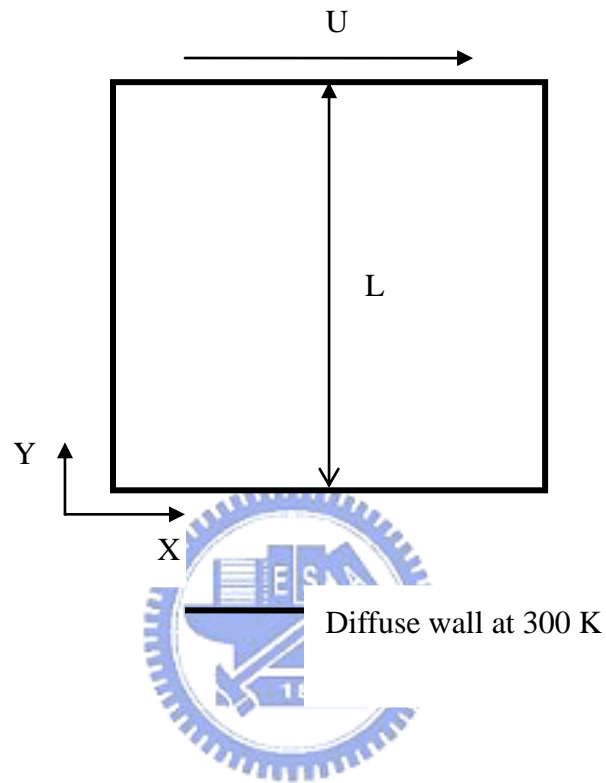


**Fig. 3.15** The 2D square ( $L/H=1$ ) driven cavity flow with moving top plate.

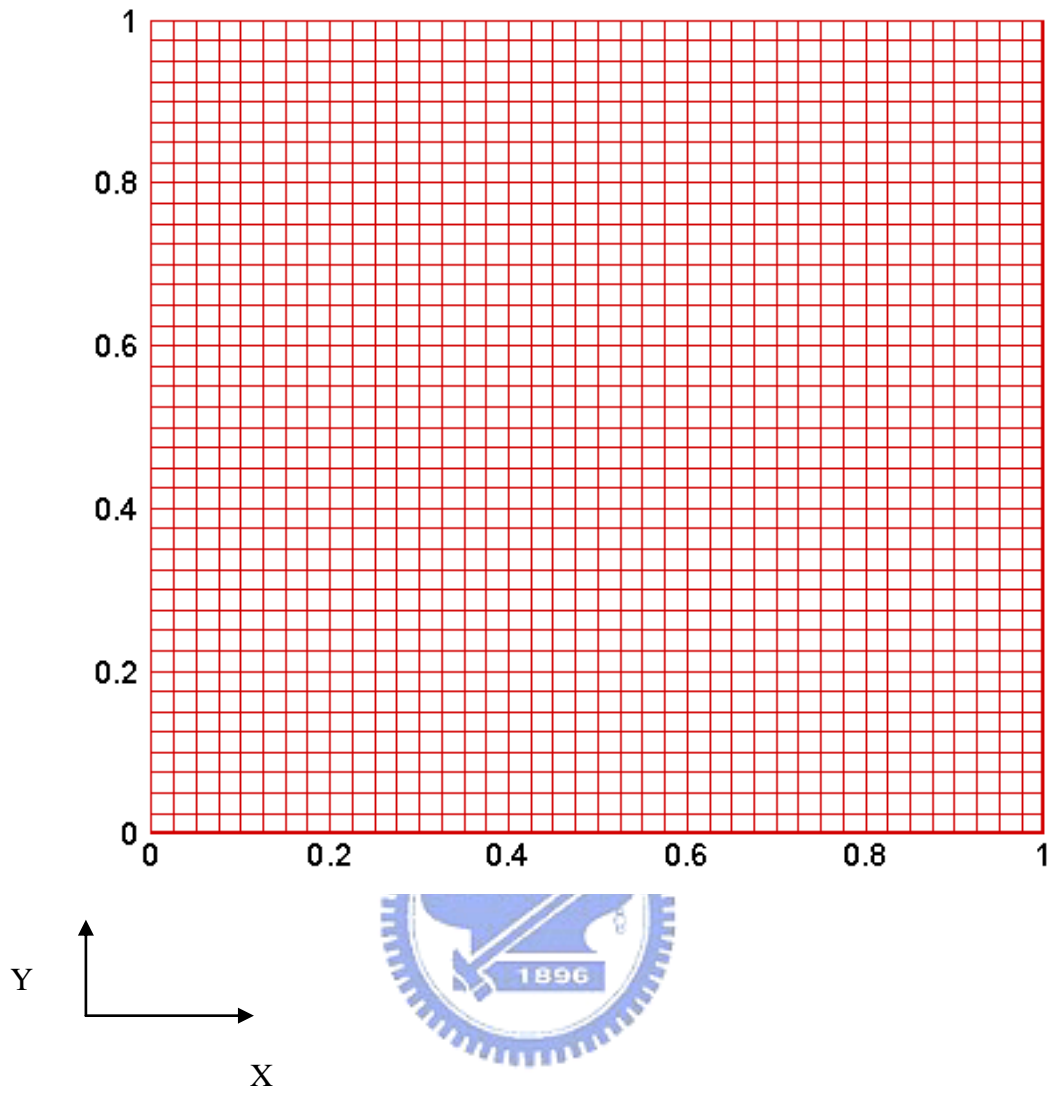


**Fig. 3.16** the mesh (40x40) for  $Kn=10, 1, 0.1$  driven cavity flow.

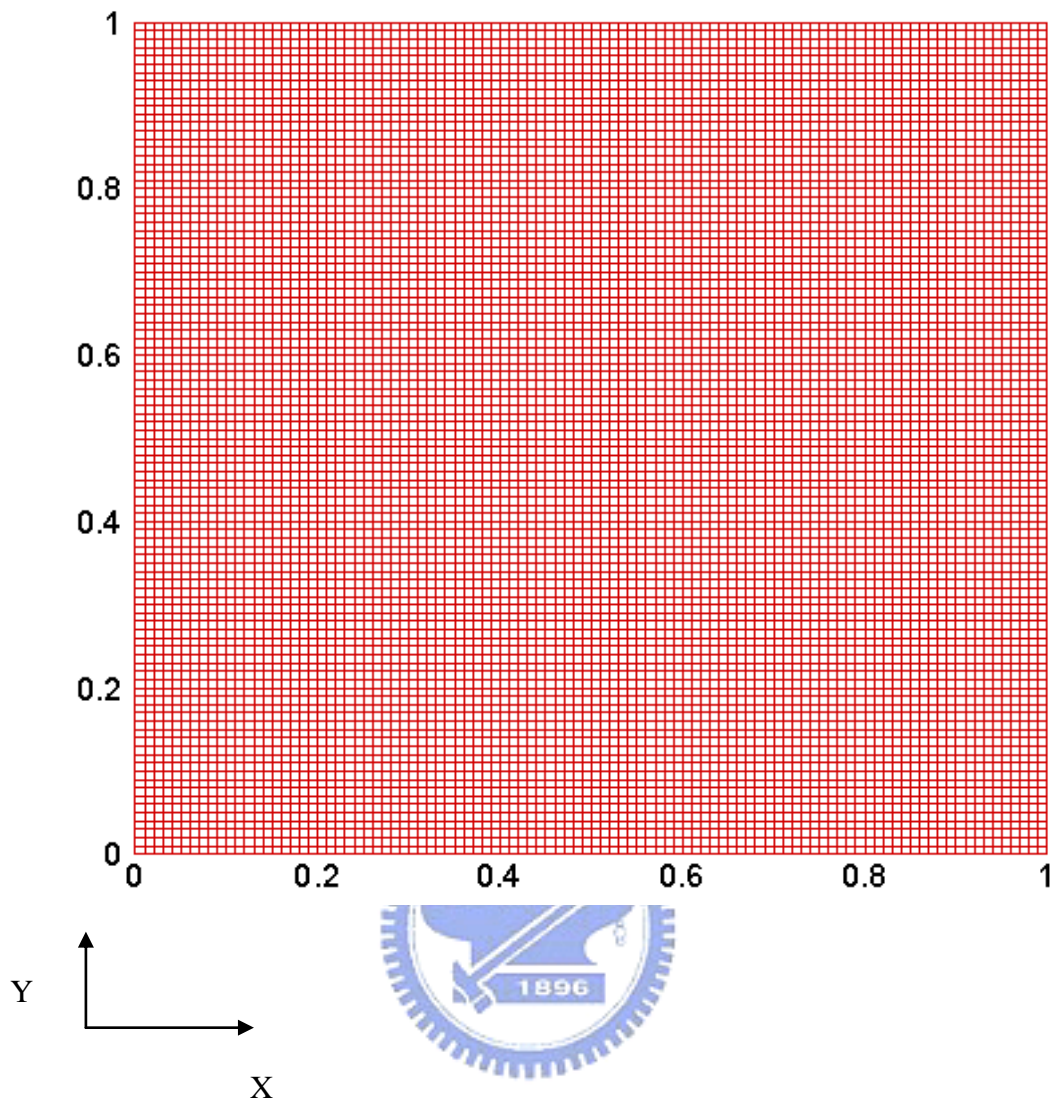


**Fig. 3.17** the mesh (100x100) for  $Kn=0.01$  driven cavity flow.

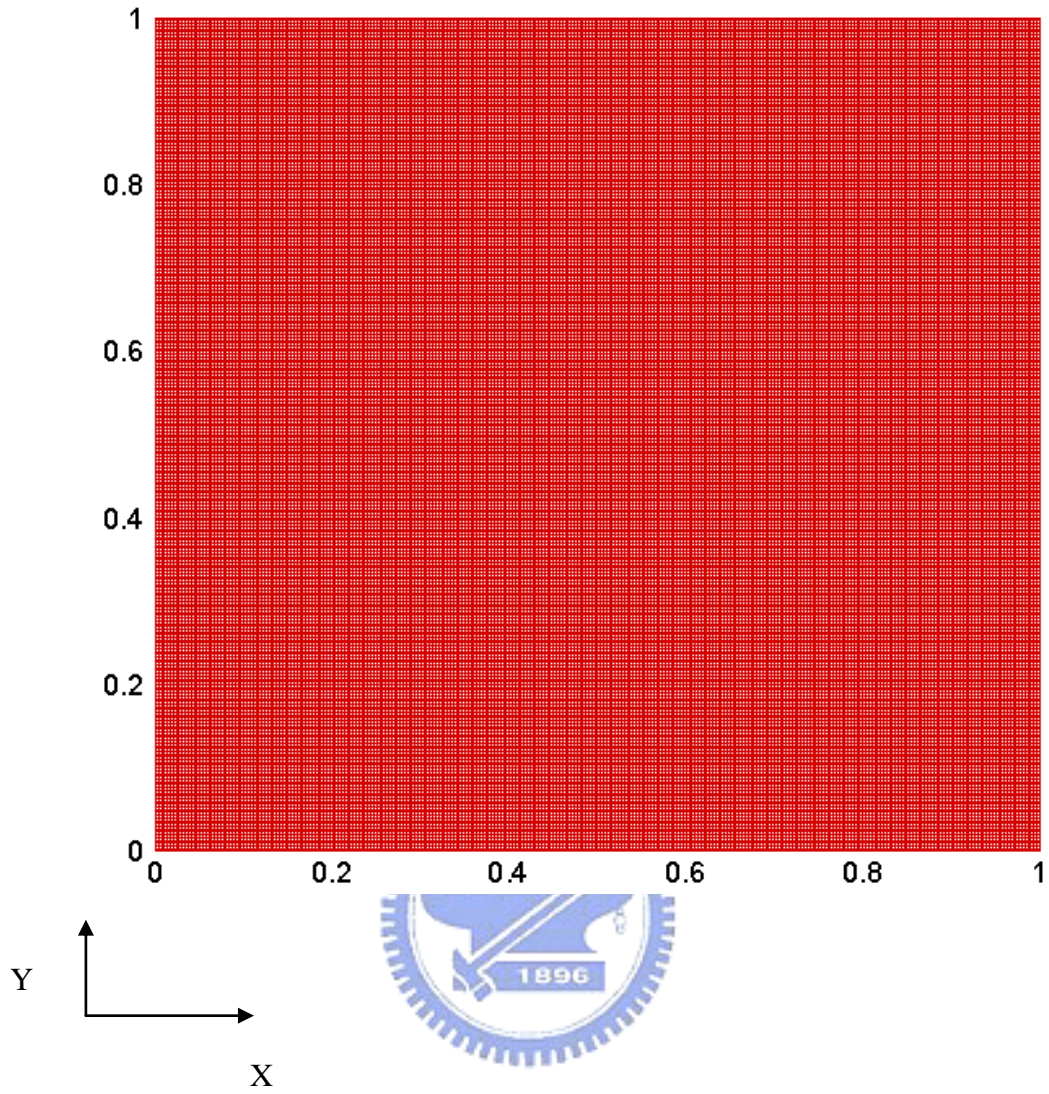


**Fig. 3.18** the mesh (300x300) for  $Kn=0.0033$  driven cavity flow.



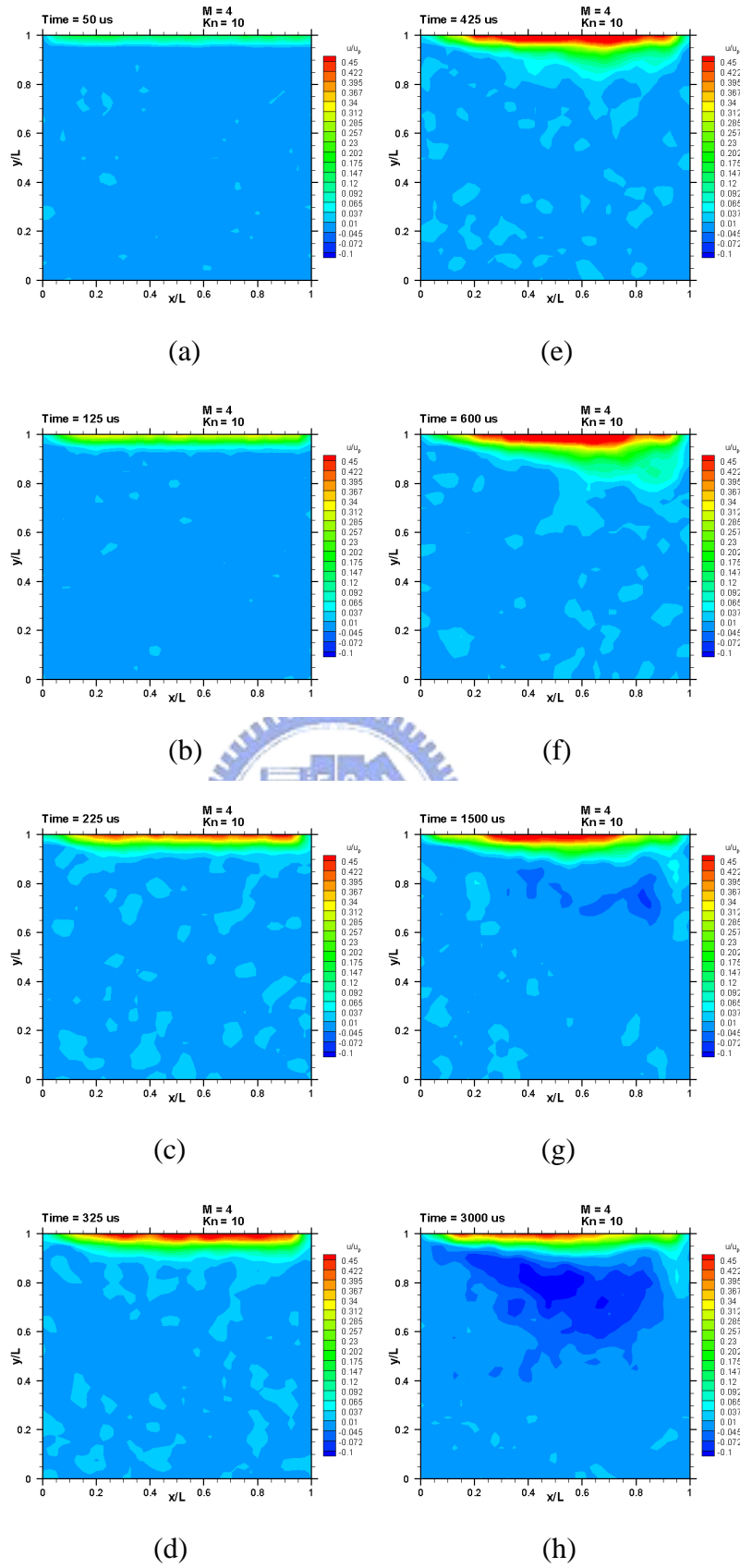


**Fig. 3.19** Contours of u-velocity for  $M=4$ ,  $Kn=10$  at (a)  $t=50 \mu s$ ; (b)  $t=125 \mu s$ ; (c)  $t=225 \mu s$ ; (d)  $t=325 \mu s$ ; (e)  $t=425 \mu s$ ; (f)  $t=600 \mu s$ ; (g)  $t=1500 \mu s$ ; (h)  $t=3000 \mu s$

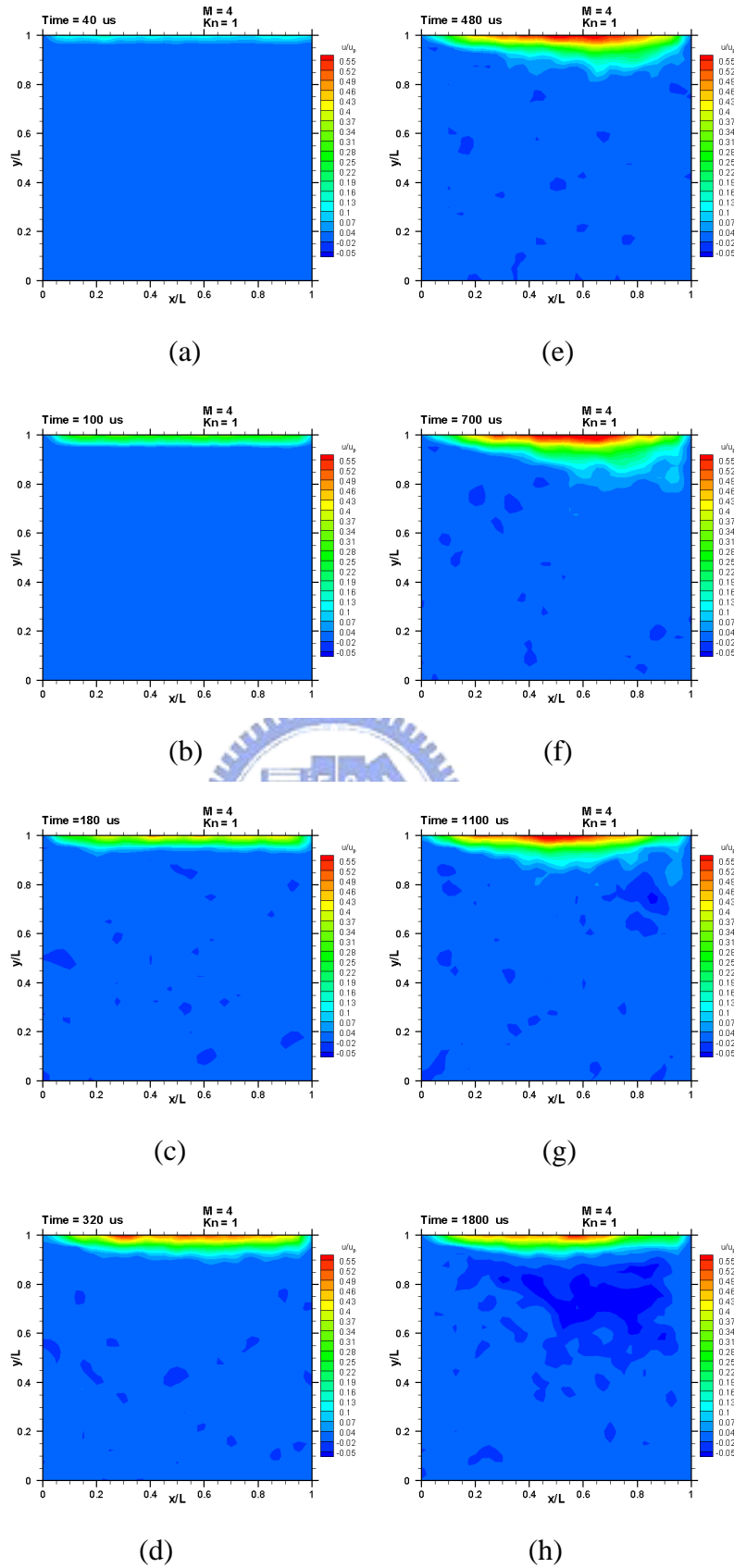


**Fig. 3.20** Contours of  $u$ -velocity for  $M=4$ ,  $Kn=1$  at (a)  $t=40 \mu s$ ; (b)  $t=100 \mu s$ ; (c)  $t=180 \mu s$ ; (d)  $t=320 \mu s$ ; (e)  $t=480 \mu s$ ; (f)  $t=700 \mu s$ ; (g)  $t=1100 \mu s$ ; (h)  $t=1800 \mu s$

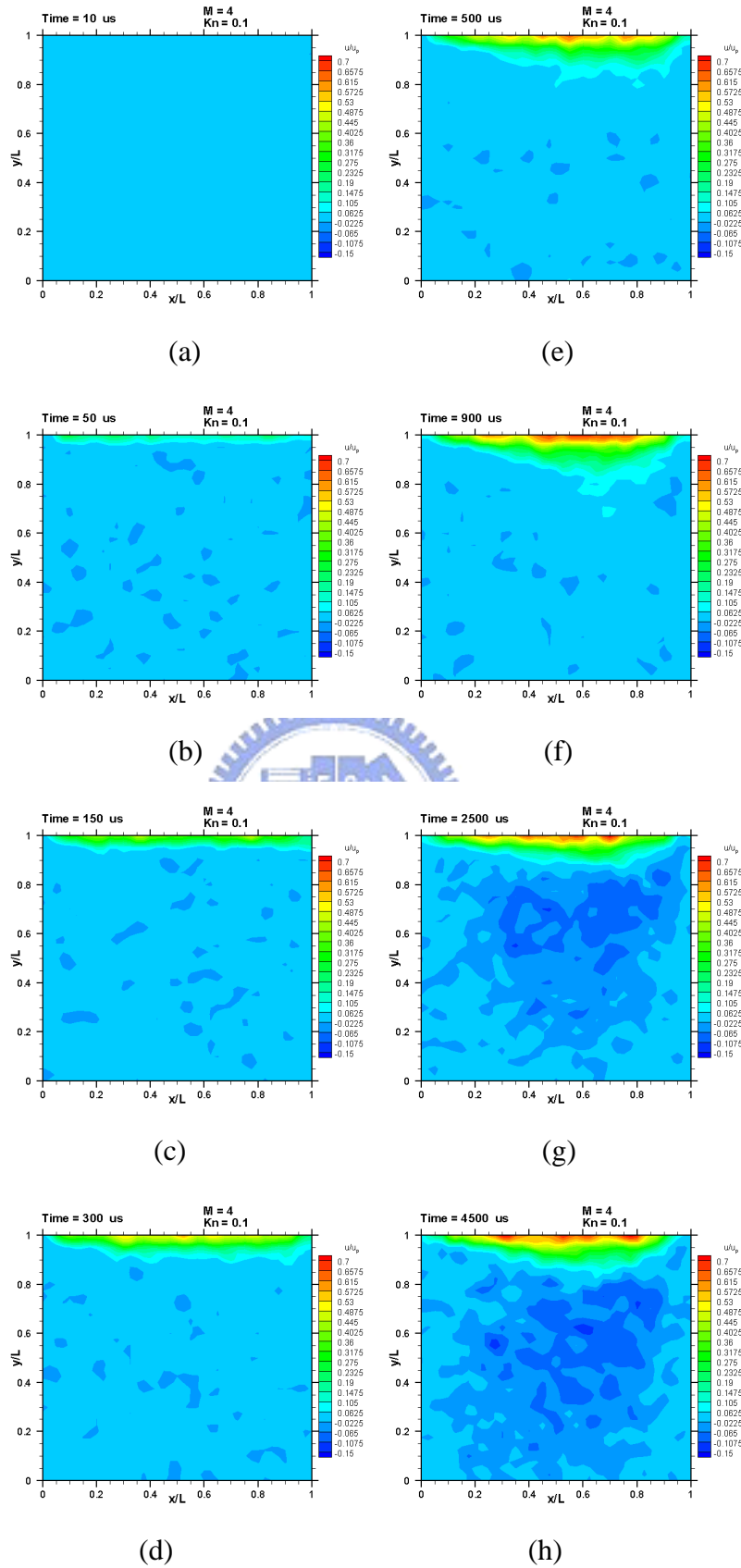


**Fig. 3.21** Contours of u-velocity for  $M=4$ ,  $Kn=0.1$  at (a)  $t = 10 \mu s$ ; (b)  $t = 50 \mu s$ ; (c)  $t = 150 \mu s$ ; (d)  $t = 300 \mu s$ ; (e)  $t = 500 \mu s$ ; (f)  $t = 900 \mu s$ ; (g)  $t = 2500 \mu s$ ; (h)  $t = 4500 \mu s$

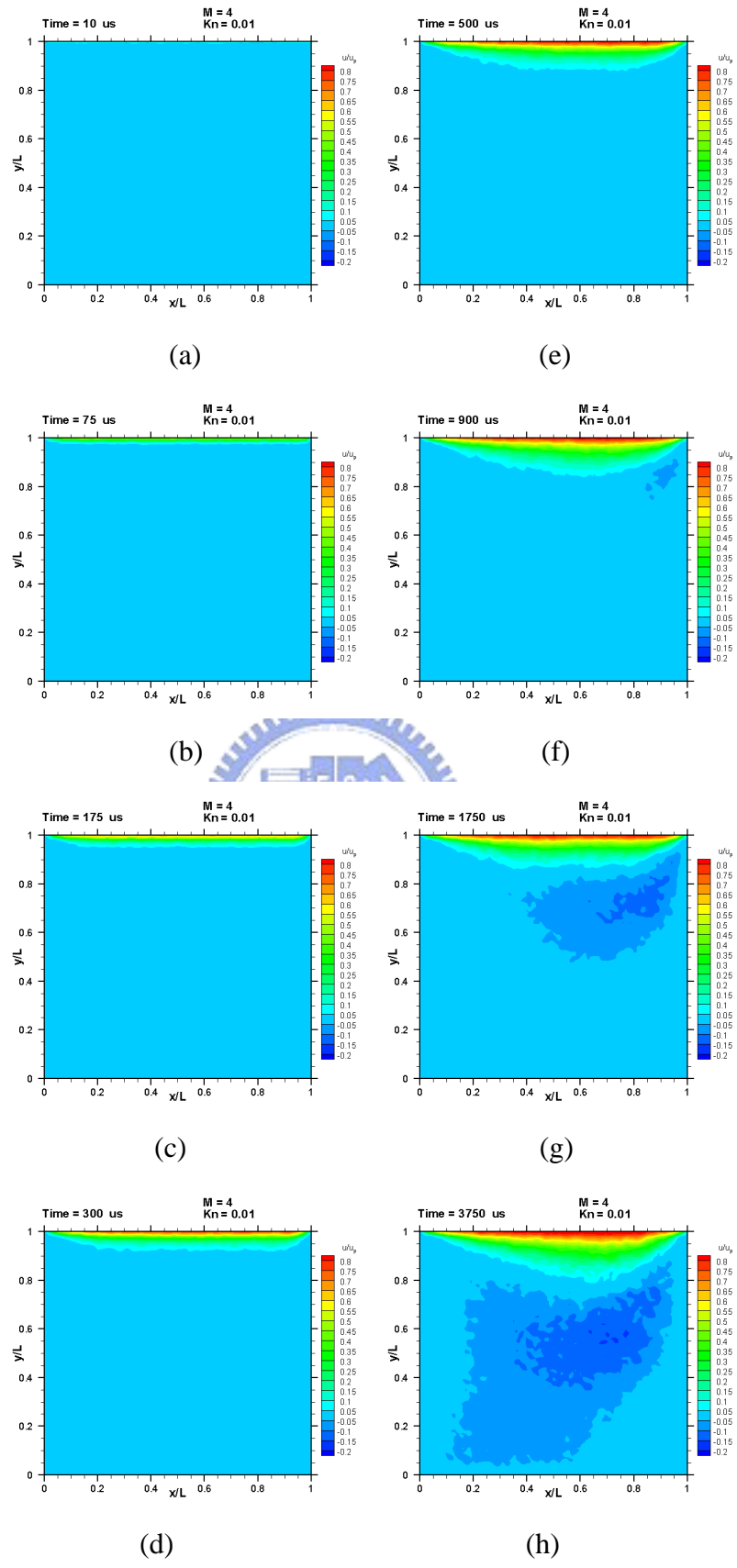


**Fig. 3.22** Contours of u-velocity for  $M=4$ ,  $Kn=0.01$  at (a)  $t=10 \mu s$ ; (b)  $t=75 \mu s$ ; (c)  $t=175 \mu s$ ; (d)  $t=300 \mu s$ ; (e)  $t=500 \mu s$ ; (f)  $t=900 \mu s$ ; (g)  $t=1750 \mu s$ ; (h)  $t=3750 \mu s$

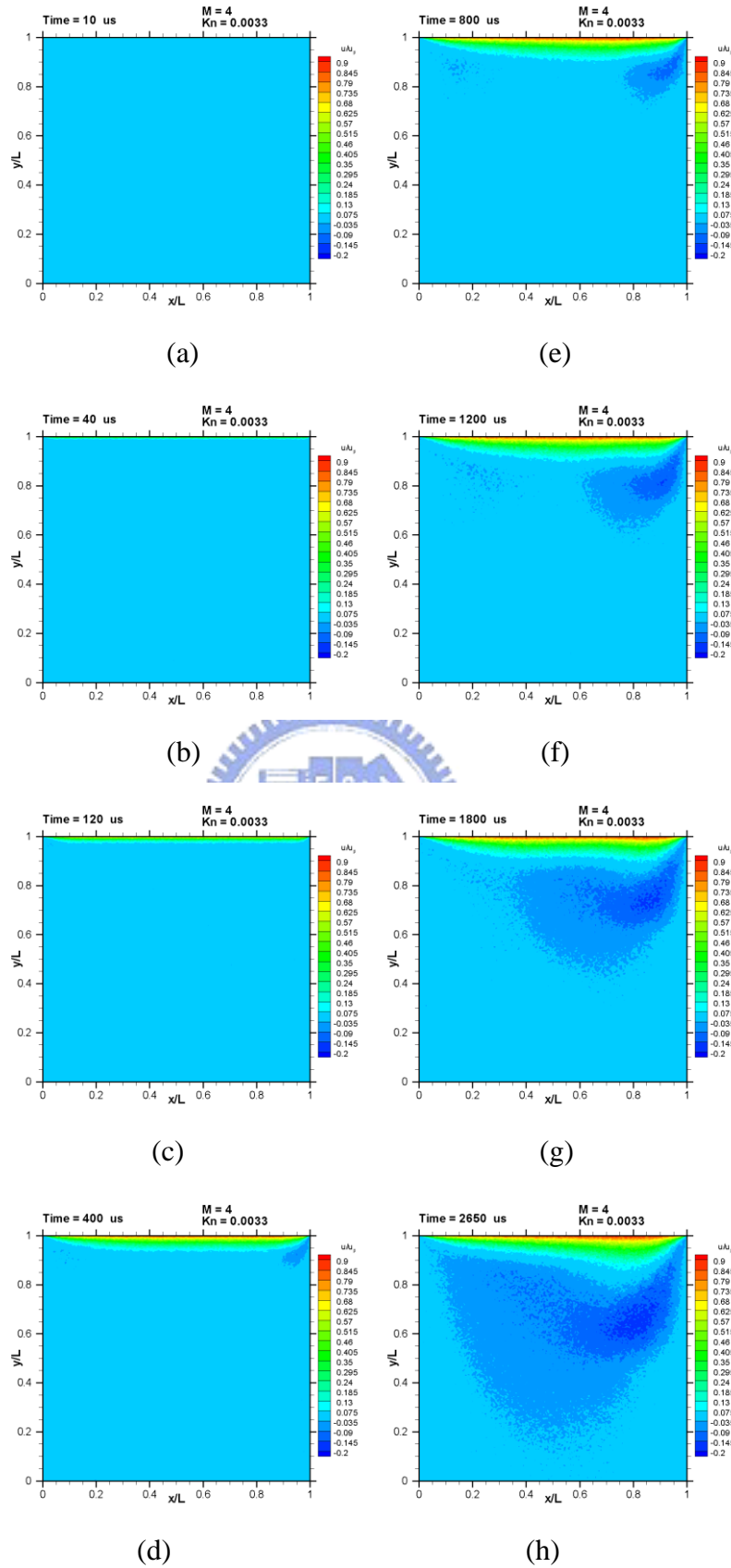


**Fig. 3.23** Contours of u-velocity for  $M=4$ ,  $Kn=0.0033$  at (a)  $t=10 \mu$ s; (b)  $t=40 \mu$ s; (c)  $t=120 \mu$ s; (d)  $t=400 \mu$ s; (e)  $t=800 \mu$ s; (f)  $t=1200 \mu$ s; (g)  $t=1800 \mu$ s; (h)  $t=2650 \mu$ s

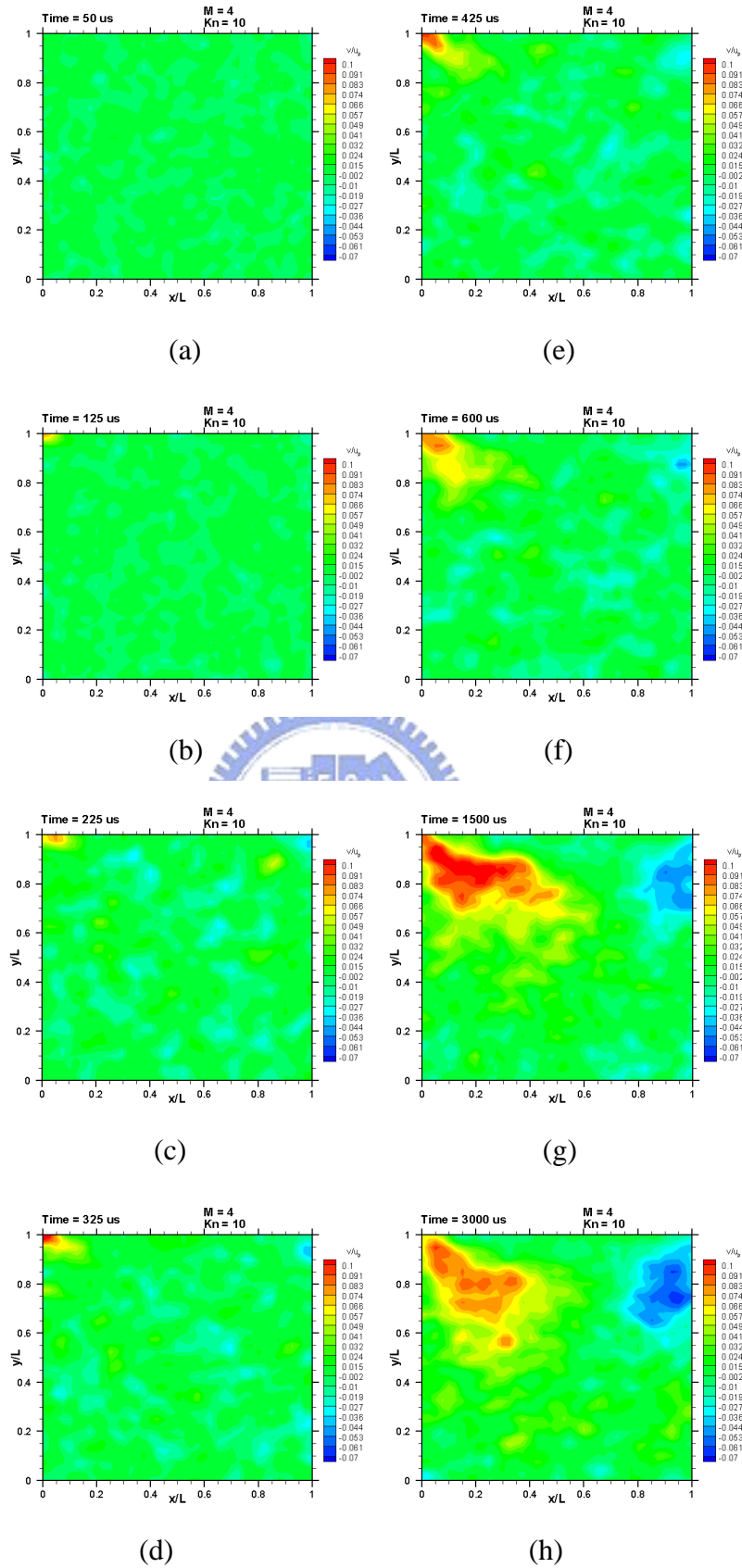


**Fig. 3.24** Contours of v-velocity for  $M=4$ ,  $Kn=10$  at (a)  $t=50 \mu s$ ; (b)  $t=125 \mu s$ ; (c)  $t=225 \mu s$ ; (d)  $t=325 \mu s$ ; (e)  $t=425 \mu s$ ; (f)  $t=600 \mu s$ ; (g)  $t=1500 \mu s$ ; (h)  $t=3000 \mu s$

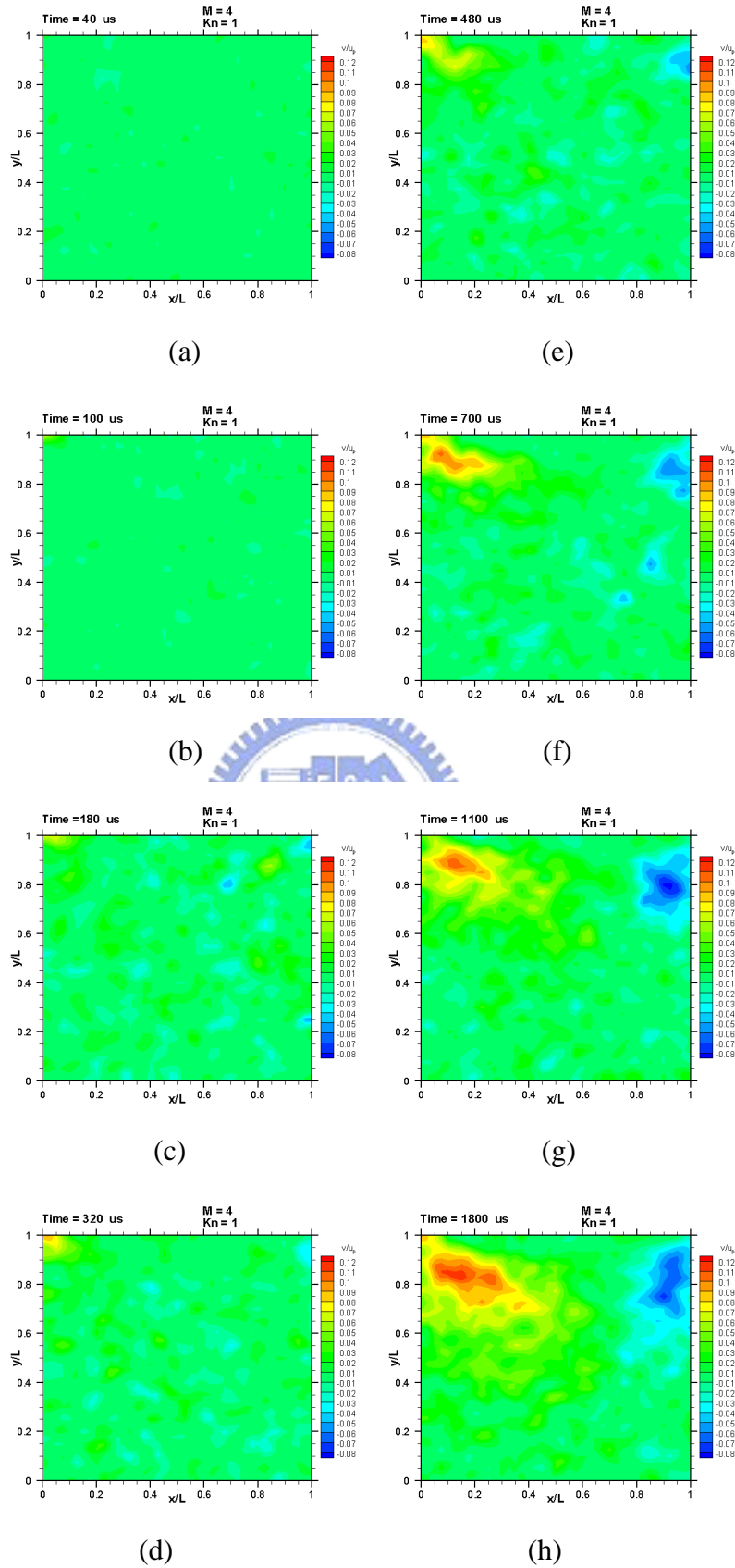


**Fig. 3.25** Contours of v-velocity for  $M=4$ ,  $Kn=1$  at (a)  $t=40 \mu s$ ; (b)  $t=100 \mu s$ ; (c)  $t=180 \mu s$ ; (d)  $t=320 \mu s$ ; (e)  $t=480 \mu s$ ; (f)  $t=700 \mu s$ ; (g)  $t=1100 \mu s$ ; (h)  $t=1800 \mu s$

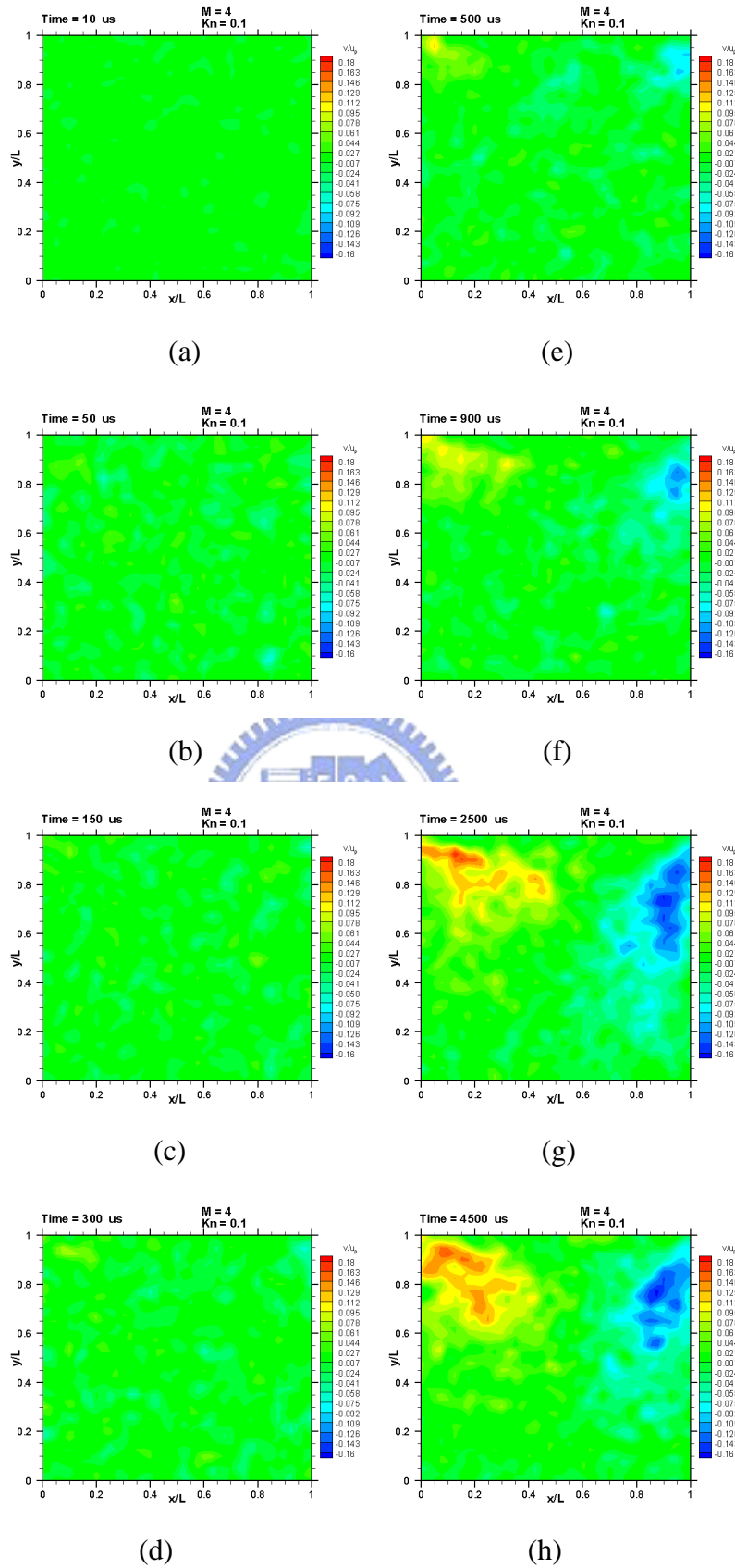


**Fig. 3.26** Contours of v-velocity for  $M=4$ ,  $Kn=0.1$  at (a)  $t=10 \mu s$ ; (b)  $t=50 \mu s$ ; (c)  $t=150 \mu s$ ; (d)  $t=300 \mu s$ ; (e)  $t=500 \mu s$ ; (f)  $t=900 \mu s$ ; (g)  $t=2500 \mu s$ ; (h)  $t=4500 \mu s$



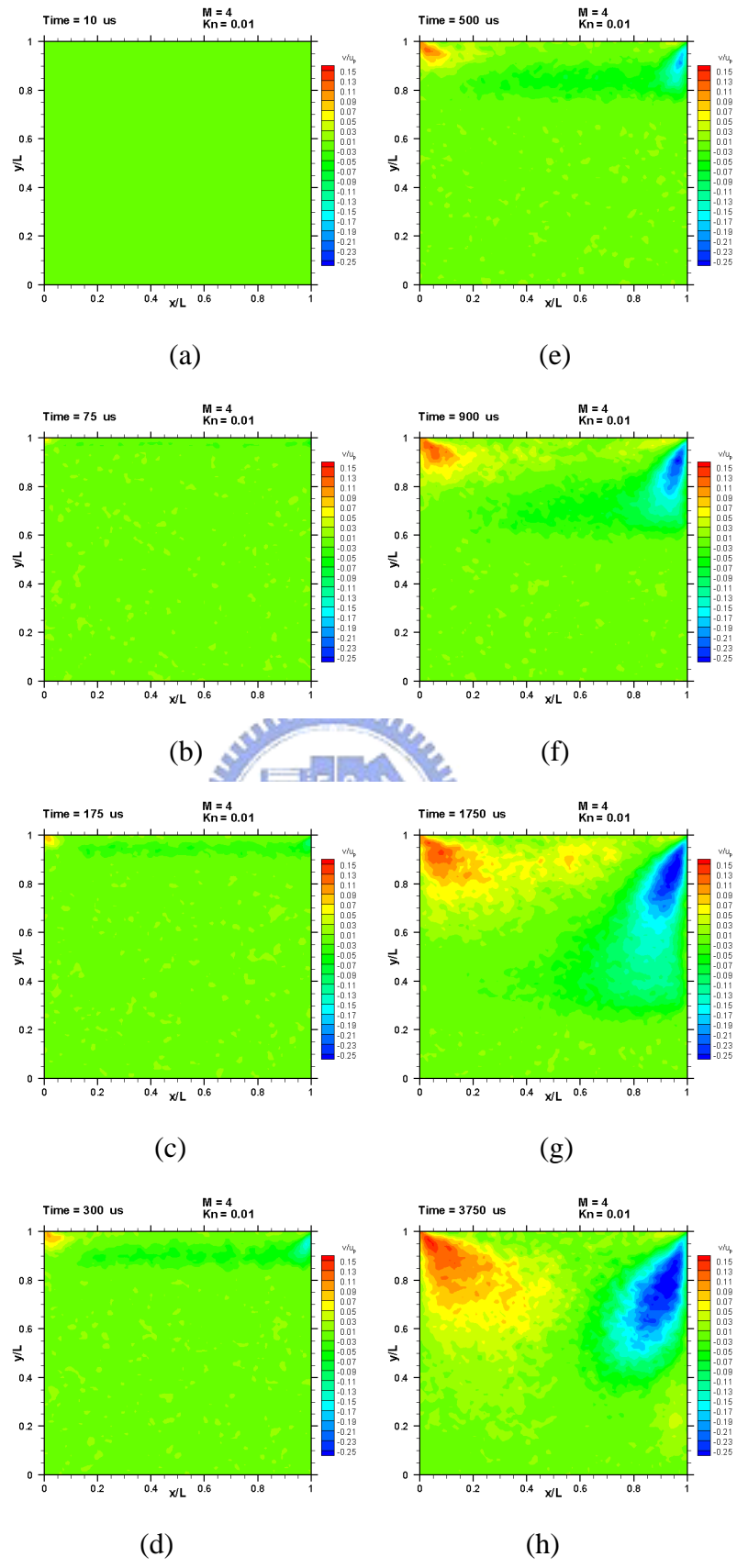


**Fig. 3.27** Contours of v-velocity for  $M=4$ ,  $Kn=0.01$  at (a)  $t=10 \mu$ s; (b)  $t=75 \mu$ s; (c)  $t=175 \mu$ s; (d)  $t=300 \mu$ s; (e)  $t=500 \mu$ s; (f)  $t=900 \mu$ s; (g)  $t=1750 \mu$ s; (h)  $t=3750 \mu$ s

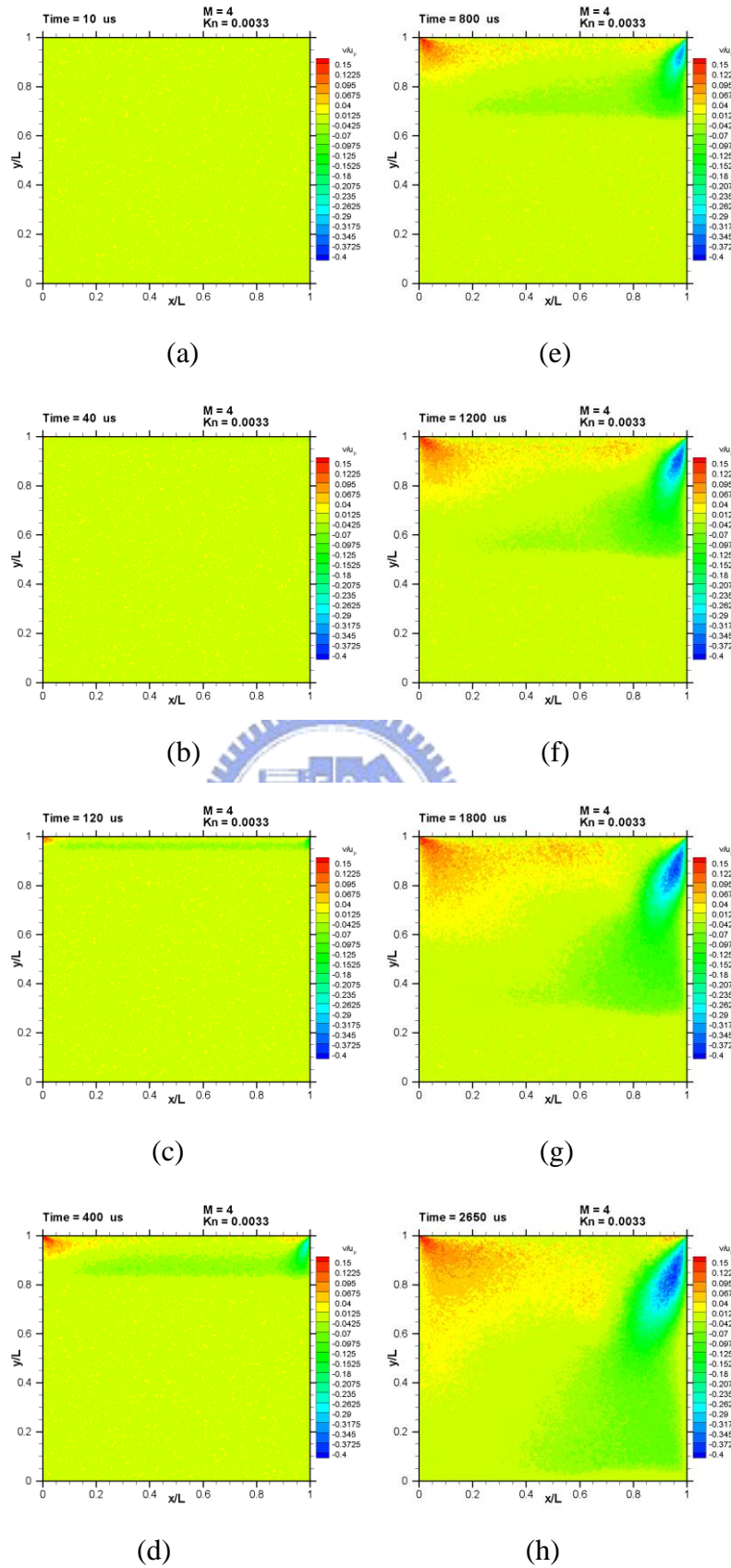


**Fig. 3.28** Contours of v-velocity for  $M=4$ ,  $Kn=0.0033$  at (a)  $t=10 \mu s$ ; (b)  $t=40 \mu s$ ; (c)  $t=120 \mu s$ ; (d)  $t=400 \mu s$ ; (e)  $t=800 \mu s$ ; (f)  $t=1200 \mu s$ ; (g)  $t=1800 \mu s$ ; (h)  $t=2650 \mu s$

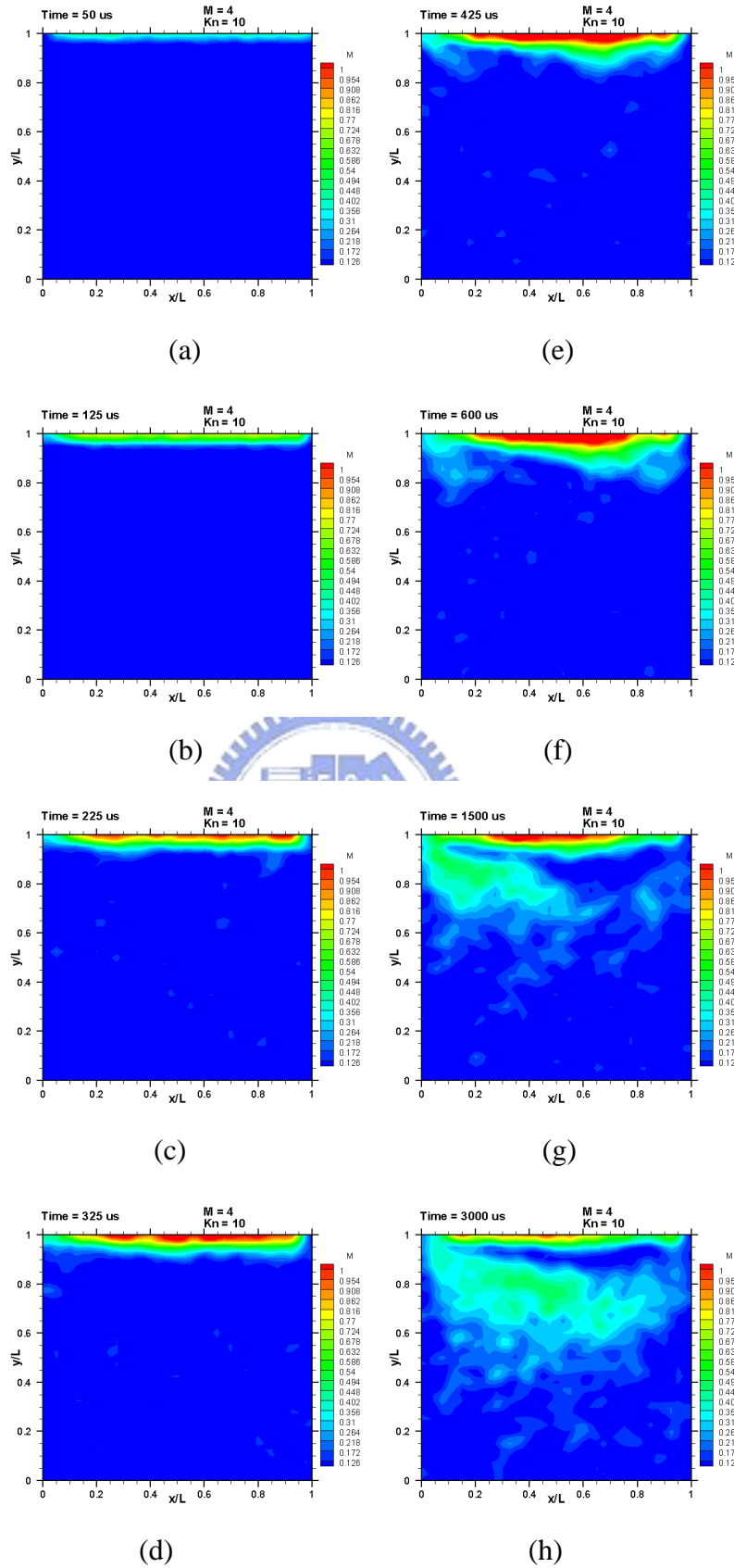


**Fig. 3.29** Contours of Mach number for  $M=4$ ,  $Kn=10$  at (a)  $t=50 \mu s$ ; (b)  $t=125 \mu s$ ; (c)  $t=225 \mu s$ ; (d)  $t=325 \mu s$ ; (e)  $t=425 \mu s$ ; (f)  $t=600 \mu s$ ; (g)  $t=1500 \mu s$ ; (h)  $t=3000 \mu s$

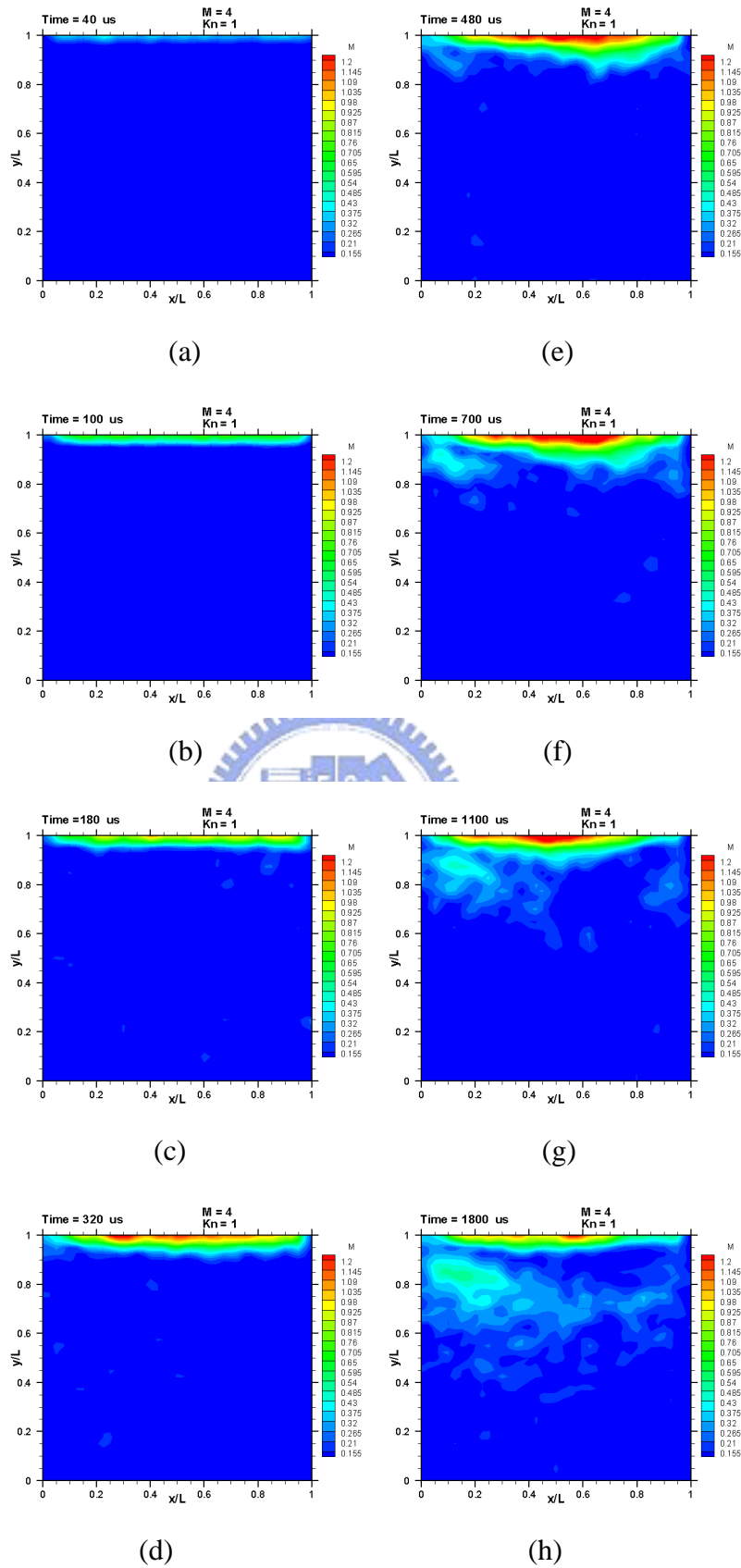


**Fig. 3.30** Contours of Mach number for  $M=4$ ,  $Kn=1$  at (a)  $t=40 \mu s$ ; (b)  $t=100 \mu s$ ; (c)  $t=180 \mu s$ ; (d)  $t=320 \mu s$ ; (e)  $t=480 \mu s$ ; (f)  $t=700 \mu s$ ; (g)  $t=1100 \mu s$ ; (h)  $t=1800 \mu s$

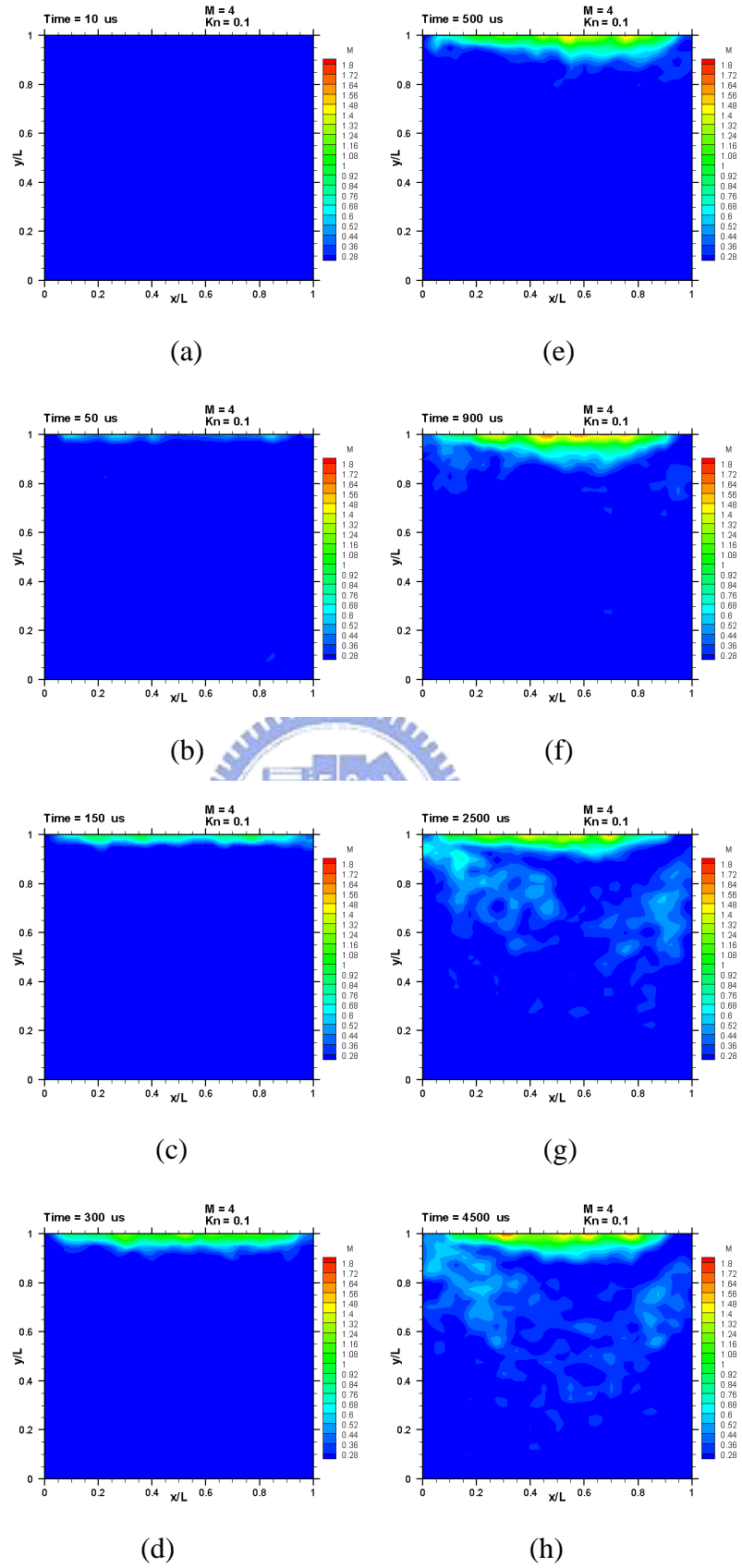


**Fig. 3.31** Contours of Mach number for  $M=4$ ,  $Kn=0.1$  at (a)  $t=10 \mu s$ ; (b)  $t=50 \mu s$ ; (c)  $t=150 \mu s$ ; (d)  $t=300 \mu s$ ; (e)  $t=500 \mu s$ ; (f)  $t=900 \mu s$ ; (g)  $t=2500 \mu s$ ; (h)  $t=4500 \mu s$

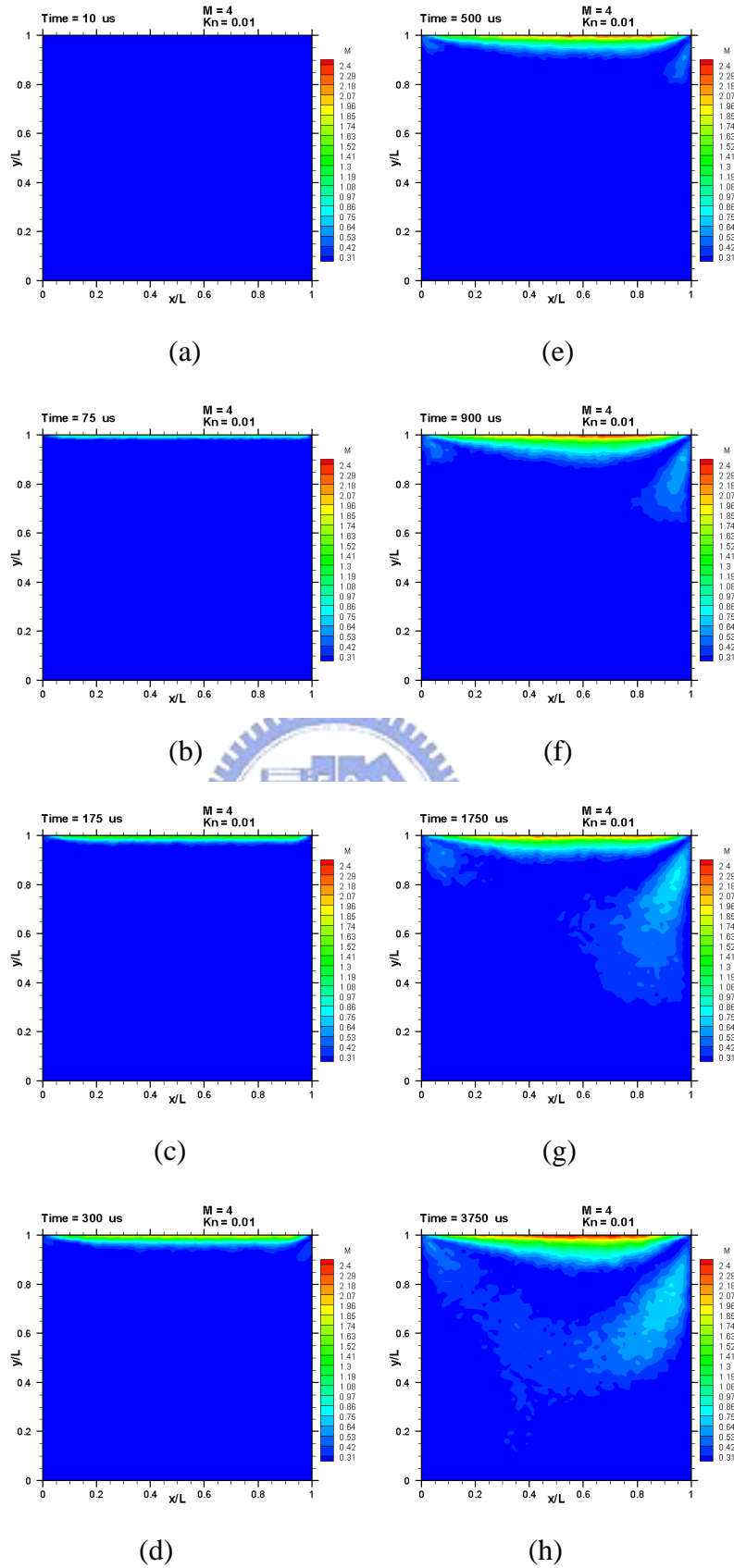


**Fig. 3.32** Contours of Mach number for  $M=4$ ,  $Kn=0.01$  at (a)  $t=10 \mu s$ ; (b)  $t=75 \mu s$ ; (c)  $t=175 \mu s$ ; (d)  $t=300 \mu s$ ; (e)  $t=500 \mu s$ ; (f)  $t=900 \mu s$ ; (g)  $t=1750 \mu s$ ; (h)  $t=3750 \mu s$

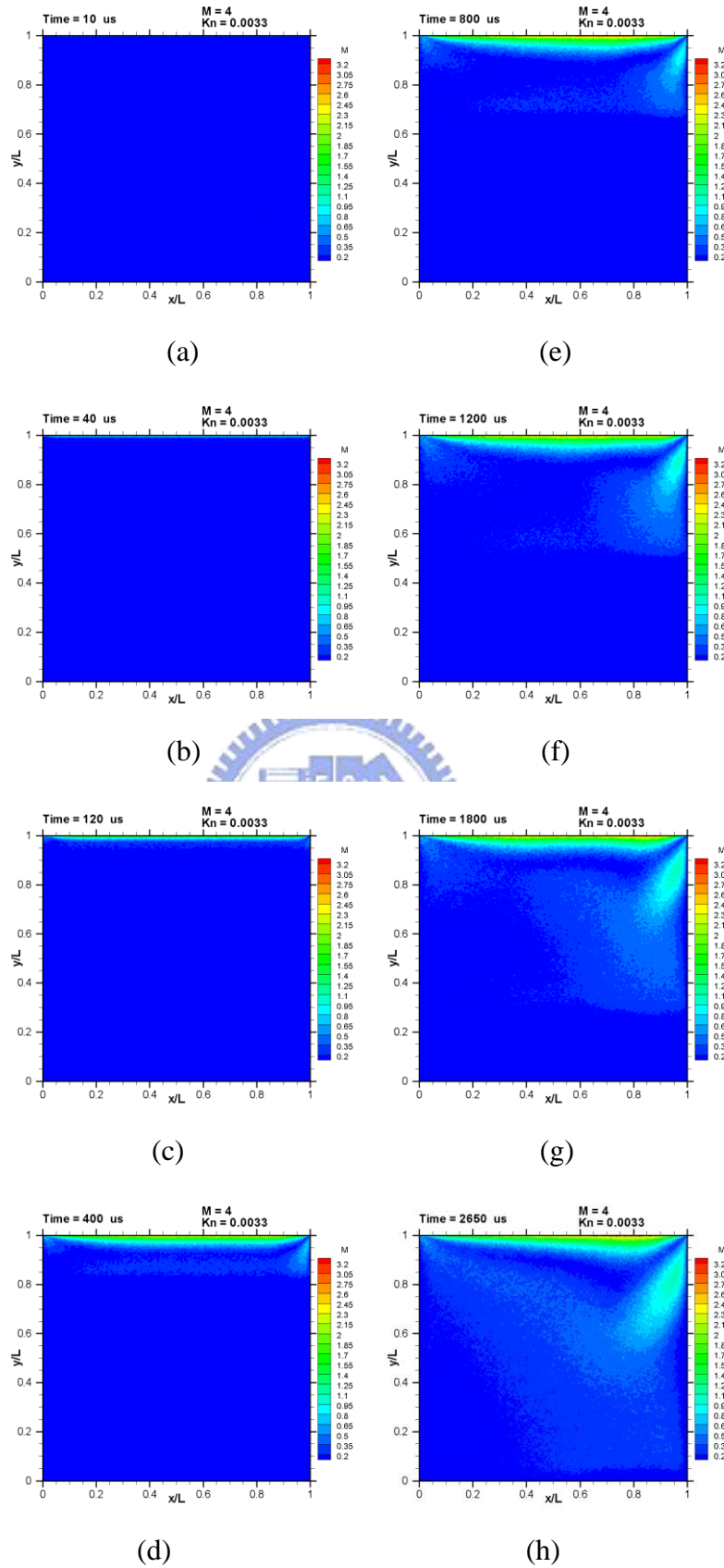


**Fig. 3.33** Contours of Mach number for  $M=4$ ,  $Kn=0.0033$  at (a)  $t=10 \mu s$ ; (b)  $t=40 \mu s$ ; (c)  $t=120 \mu s$ ; (d)  $t=400 \mu s$ ; (e)  $t=800 \mu s$ ; (f)  $t=1200 \mu s$ ; (g)  $t=1800 \mu s$ ; (h)  $t=2650 \mu s$

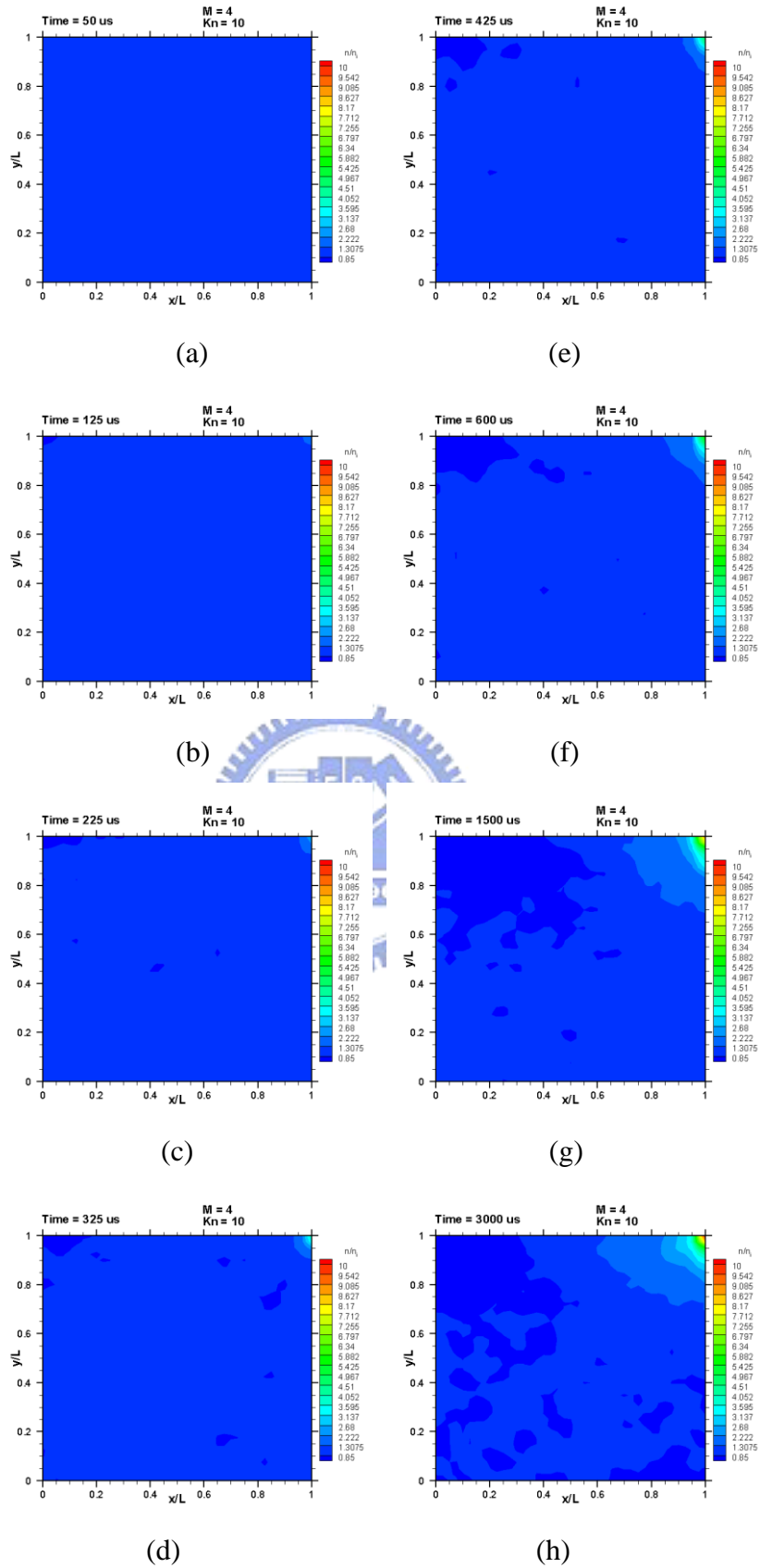


**Fig. 3.34** Contours of number density for  $M=4$ ,  $Kn=10$  at (a)  $t=50 \mu s$ ; (b)  $t=125 \mu s$ ; (c)  $t=225 \mu s$ ; (d)  $t=325 \mu s$ ; (e)  $t=425 \mu s$ ; (f)  $t=600 \mu s$ ; (g)  $t=1500 \mu s$ ; (h)  $t=3000 \mu s$



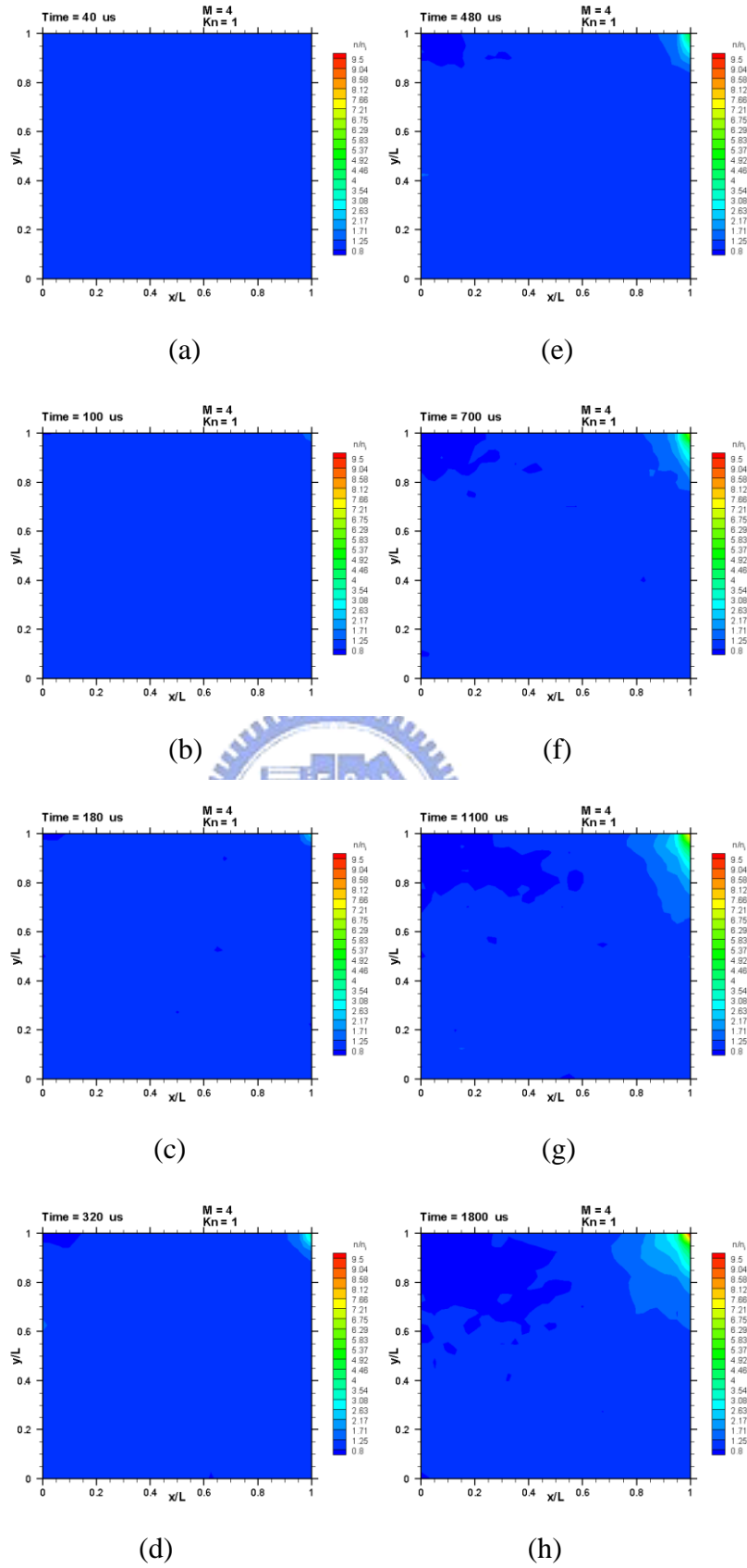


**Fig. 3.35** Contours of number density for  $M=4$ ,  $Kn=1$  at (a)  $t=40 \mu s$ ; (b)  $t=100 \mu s$ ; (c)  $t=180 \mu s$ ;  
 (d)  $t=320 \mu s$ ; (e)  $t=480 \mu s$ ; (f)  $t=700 \mu s$ ; (g)  $t=1100 \mu s$ ; (h)  $t=1800 \mu s$

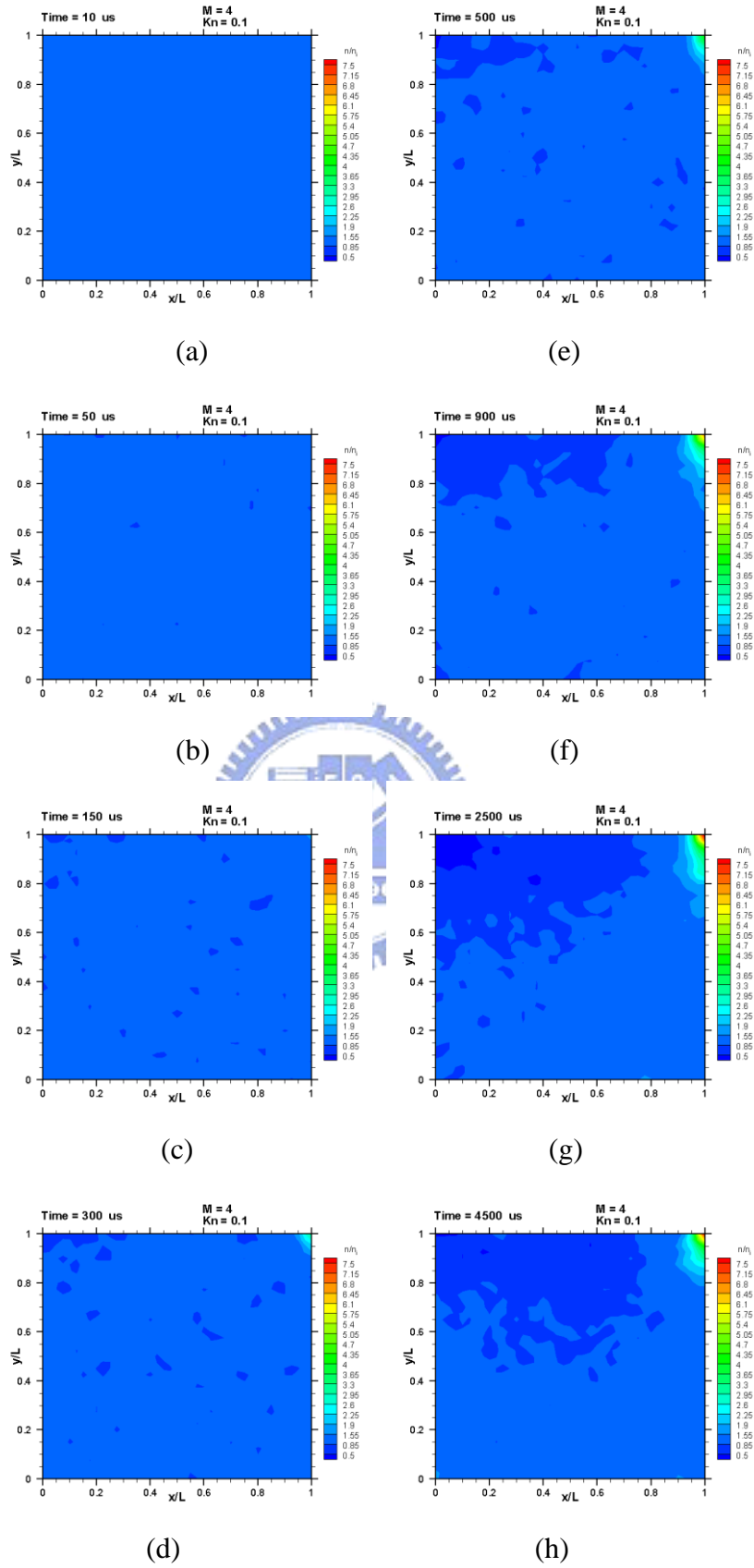


**Fig. 3.36** Contours of number density for  $M=4$ ,  $Kn=0.1$  at (a)  $t=10 \mu s$ ; (b)  $t=50 \mu s$ ; (c)  $t=150 \mu s$ ; (d)  $t=300 \mu s$ ; (e)  $t=500 \mu s$ ; (f)  $t=900 \mu s$ ; (g)  $t=2500 \mu s$ ; (h)  $t=4500 \mu s$

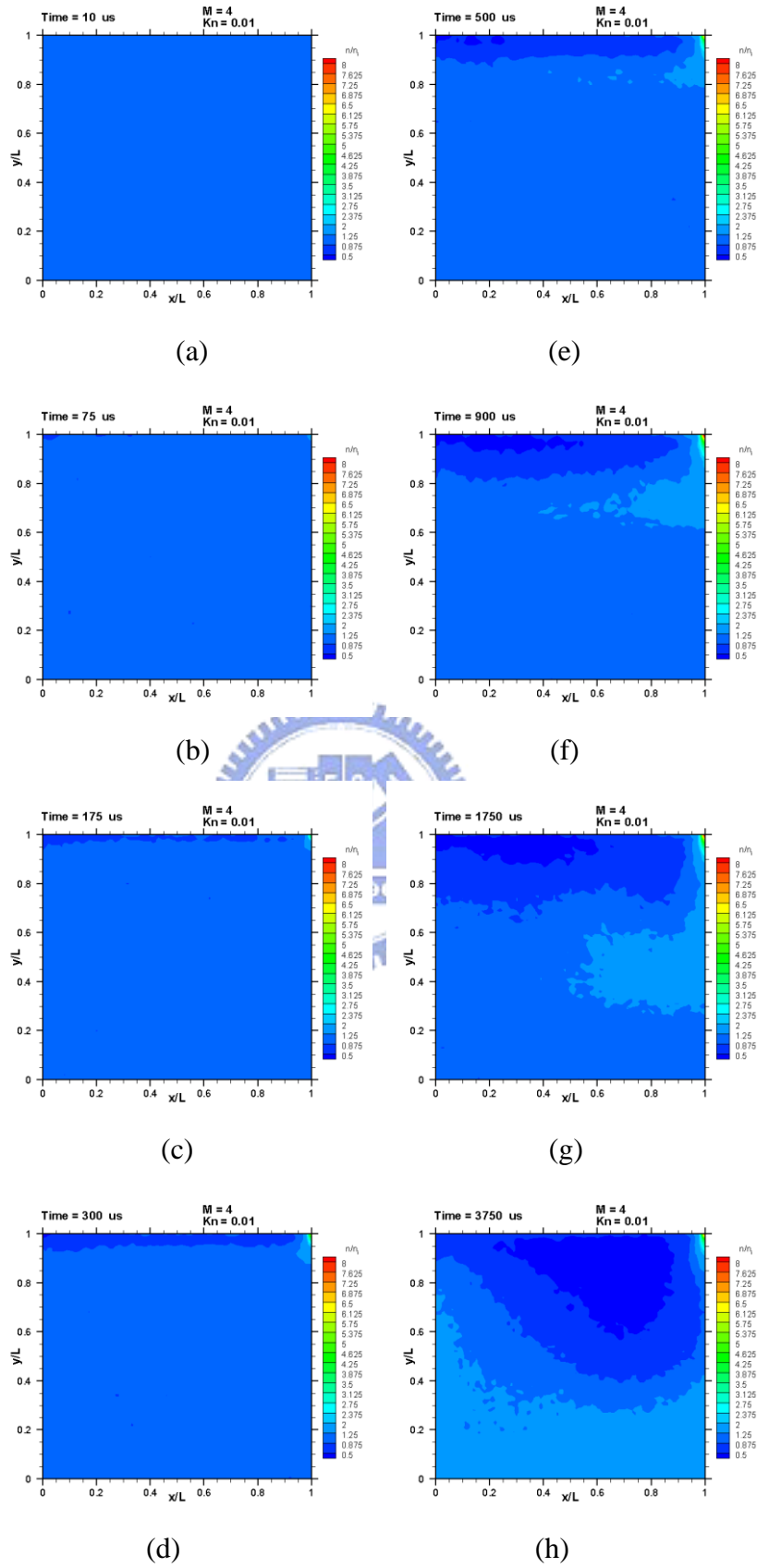


**Fig. 3.37** Contours of number density for  $M=4$ ,  $Kn=0.01$  at (a)  $t=10 \mu$ s; (b)  $t=75 \mu$ s; (c)  $t=175 \mu$ s; (d)  $t=300 \mu$ s; (e)  $t=500 \mu$ s; (f)  $t=900 \mu$ s; (g)  $t=1750 \mu$ s; (h)  $t=3750 \mu$ s

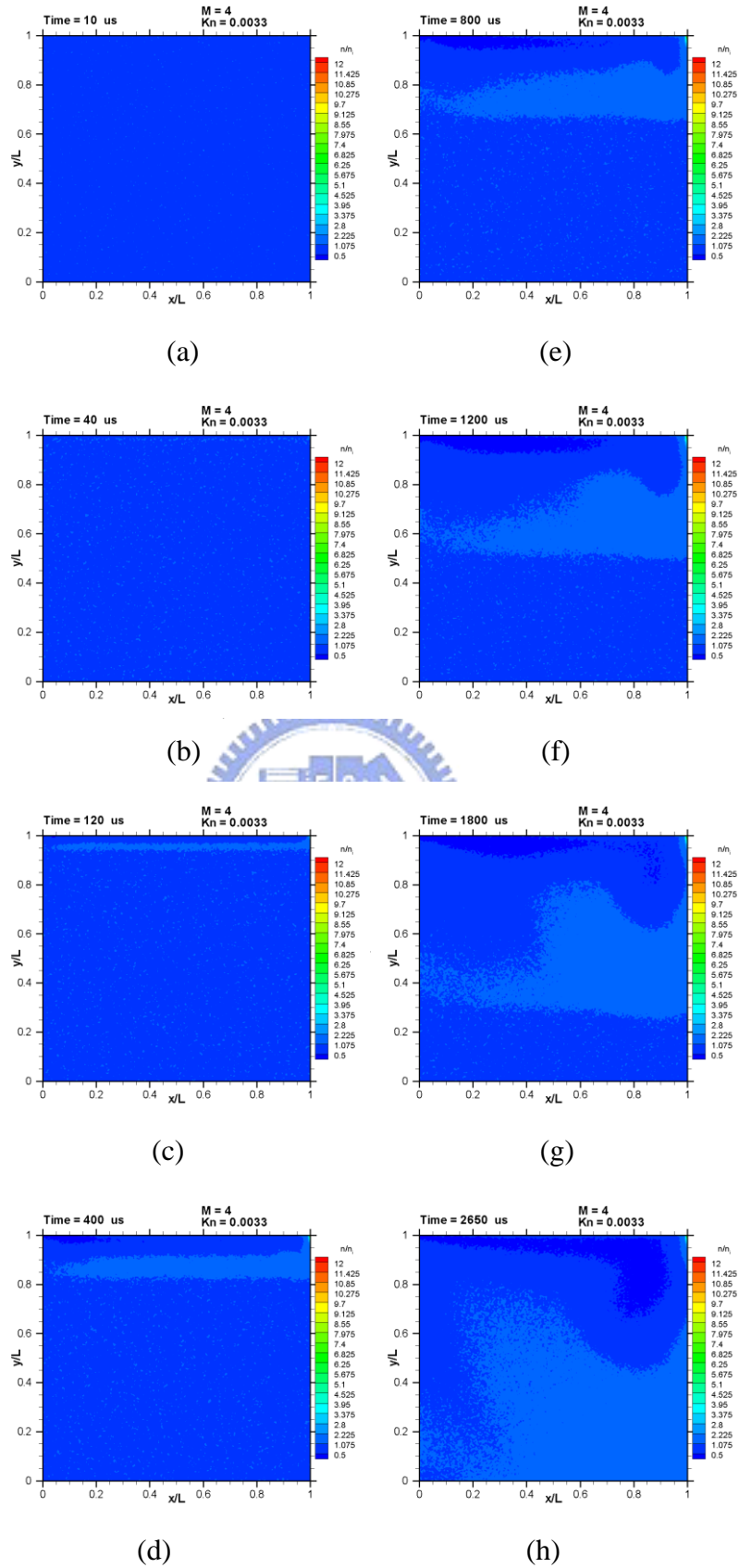


**Fig. 3.38** Contours of number density for  $M=4$ ,  $Kn=0.0033$  at (a)  $t=10 \mu$ s; (b)  $t=40 \mu$ s; (c)  $t=120 \mu$ s; (d)  $t=400 \mu$ s; (e)  $t=800 \mu$ s; (f)  $t=1200 \mu$ s; (g)  $t=1800 \mu$ s; (h)  $t=2650 \mu$ s

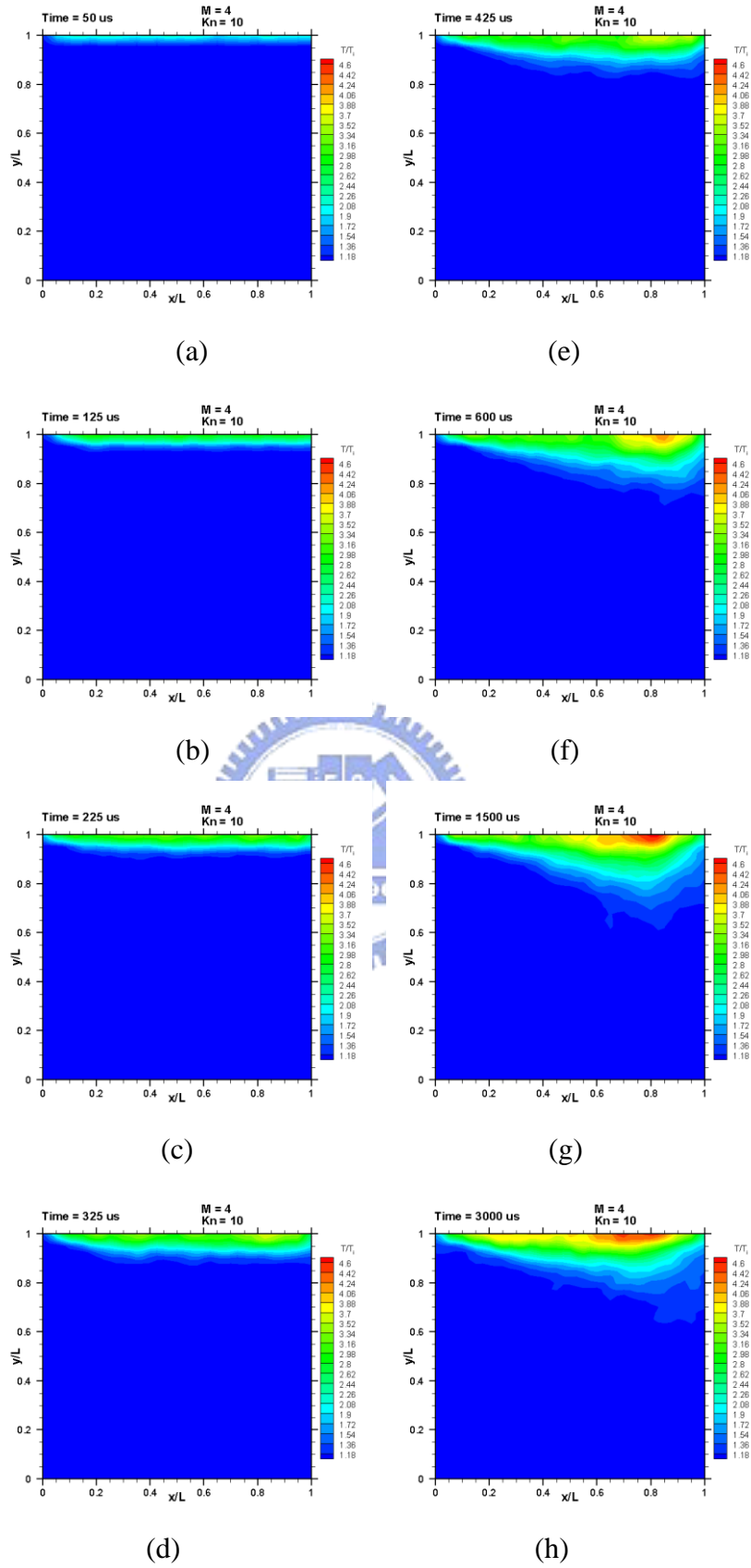


**Fig. 3.39** Contours of temperature for  $M=4$ ,  $Kn=10$  at (a)  $t=50 \mu s$ ; (b)  $t=125 \mu s$ ; (c)  $t=225 \mu s$ ; (d)  $t=325 \mu s$ ; (e)  $t=425 \mu s$ ; (f)  $t=600 \mu s$ ; (g)  $t=1500 \mu s$ ; (h)  $t=3000 \mu s$

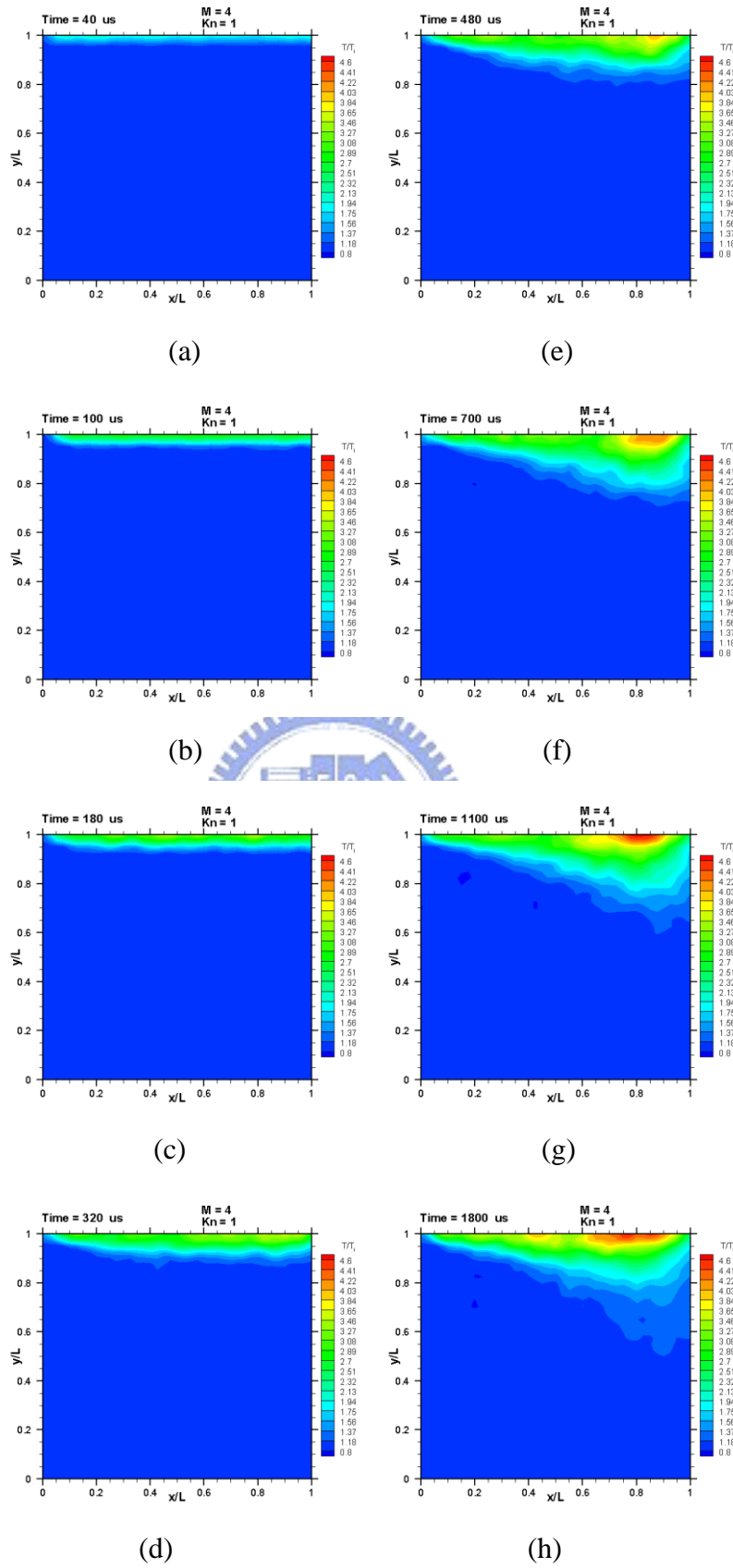


**Fig. 3.40** Contours of temperature for  $M=4$ ,  $Kn=1$  at (a)  $t=40 \mu s$ ; (b)  $t=100 \mu s$ ; (c)  $t=180 \mu s$ ; (d)  $t=320 \mu s$ ; (e)  $t=480 \mu s$ ; (f)  $t=700 \mu s$ ; (g)  $t=1100 \mu s$ ; (h)  $t=1800 \mu s$

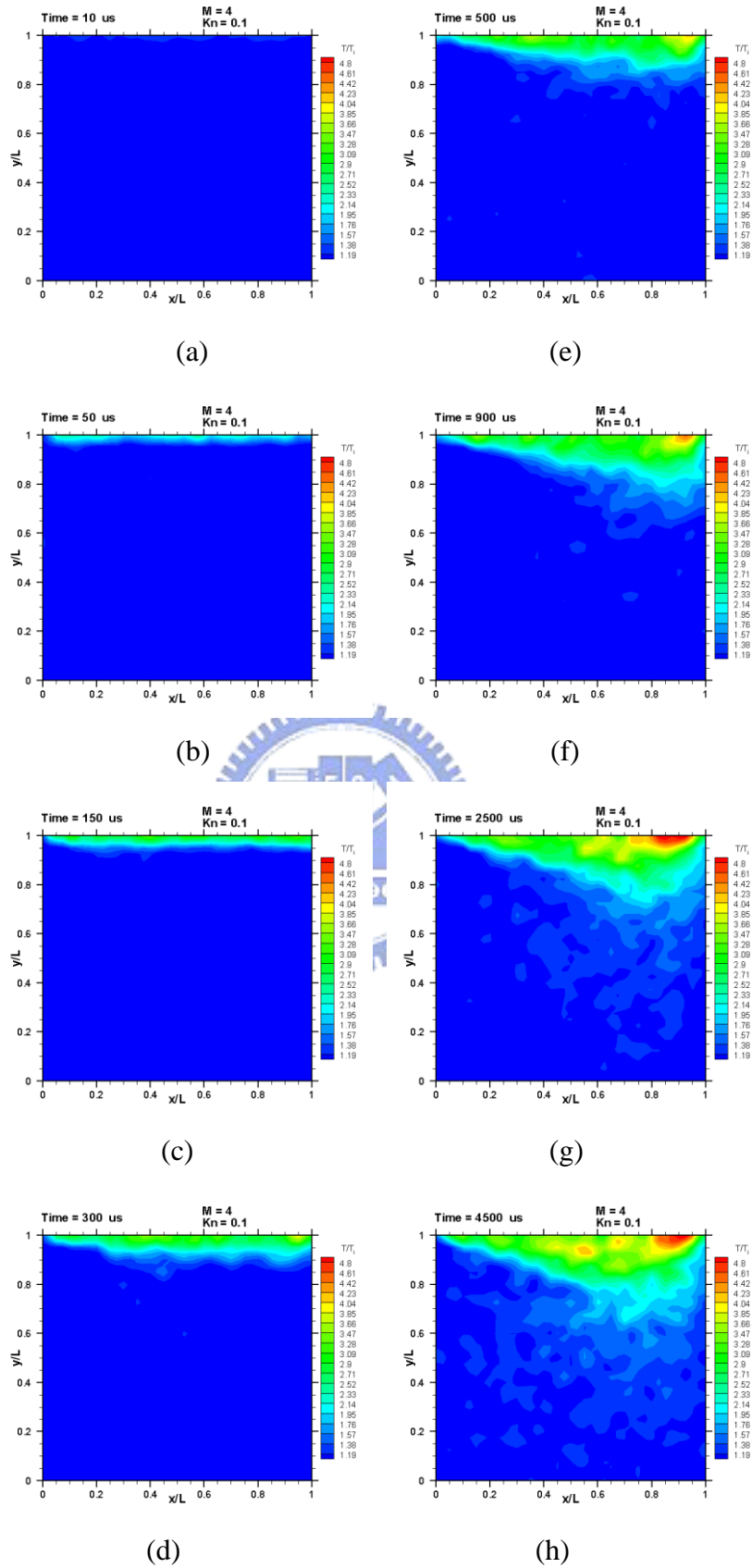


**Fig. 3.41** Contours of temperature for  $M=4$ ,  $Kn=0.1$  at (a)  $t=10 \mu s$ ; (b)  $t=50 \mu s$ ; (c)  $t=150 \mu s$ ; (d)  $t=300 \mu s$ ; (e)  $t=500 \mu s$ ; (f)  $t=900 \mu s$ ; (g)  $t=2500 \mu s$ ; (h)  $t=4500 \mu s$

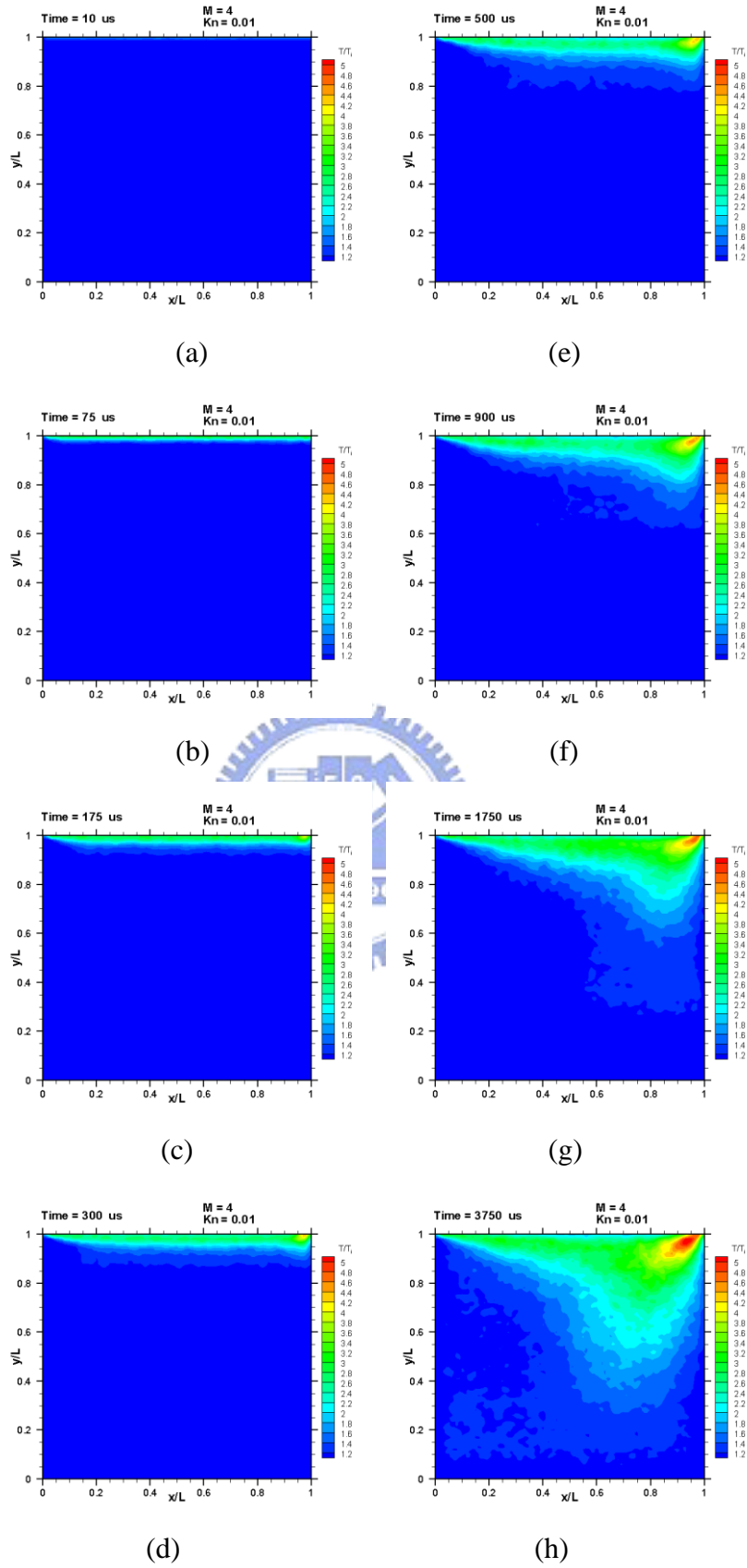


**Fig. 3.42** Contours of temperature for  $M=4$ ,  $Kn=0.01$  at (a)  $t=10 \mu s$ ; (b)  $t=75 \mu s$ ; (c)  $t=175 \mu s$ ; (d)  $t=300 \mu s$ ; (e)  $t=500 \mu s$ ; (f)  $t=900 \mu s$ ; (g)  $t=1750 \mu s$ ; (h)  $t=3750 \mu s$



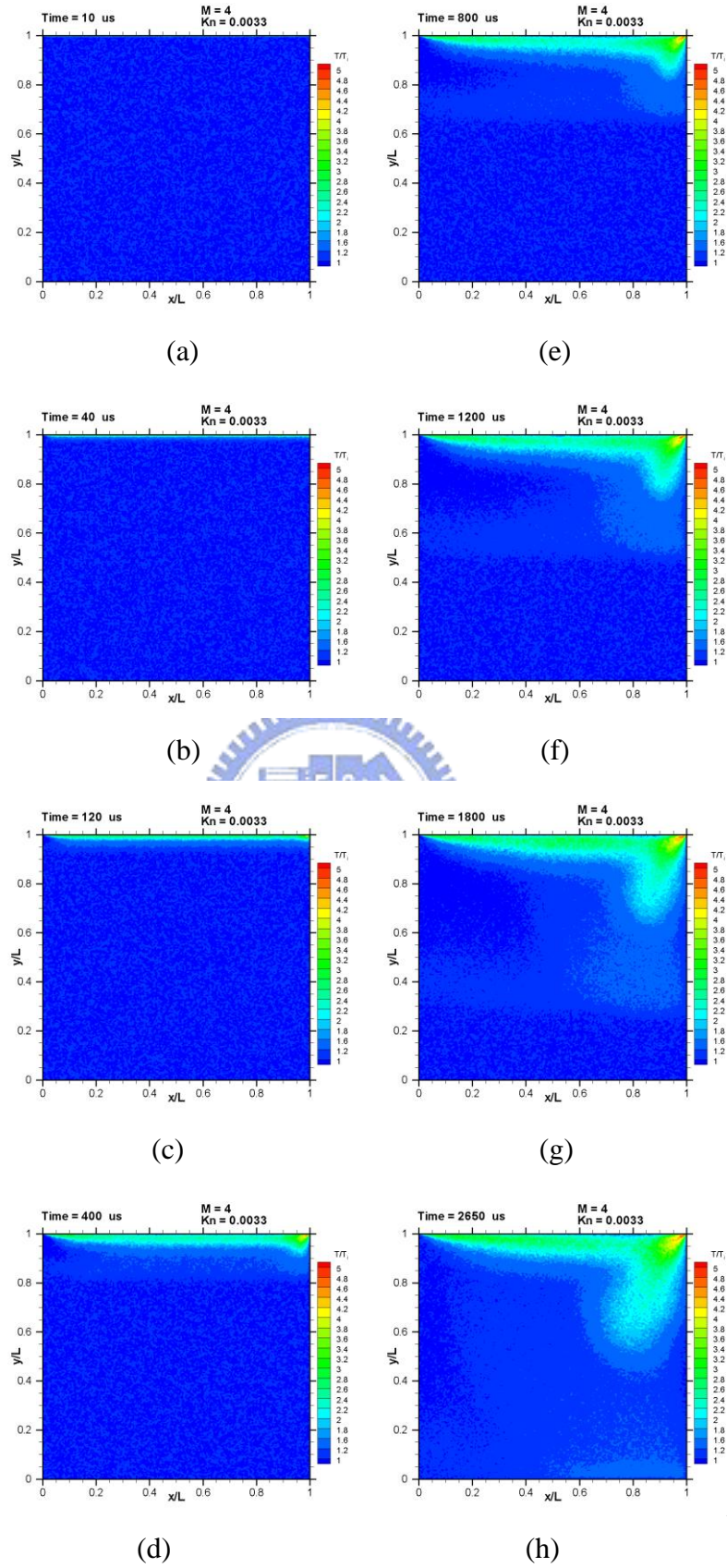


**Fig. 3.43** Contours of temperature for  $M=4$ ,  $Kn=0.0033$  at (a)  $t=10 \mu s$ ; (b)  $t=40 \mu s$ ; (c)  $t=120 \mu s$ ; (d)  $t=400 \mu s$ ; (e)  $t=800 \mu s$ ; (f)  $t=1200 \mu s$ ; (g)  $t=1800 \mu s$ ; (h)  $t=2650 \mu s$

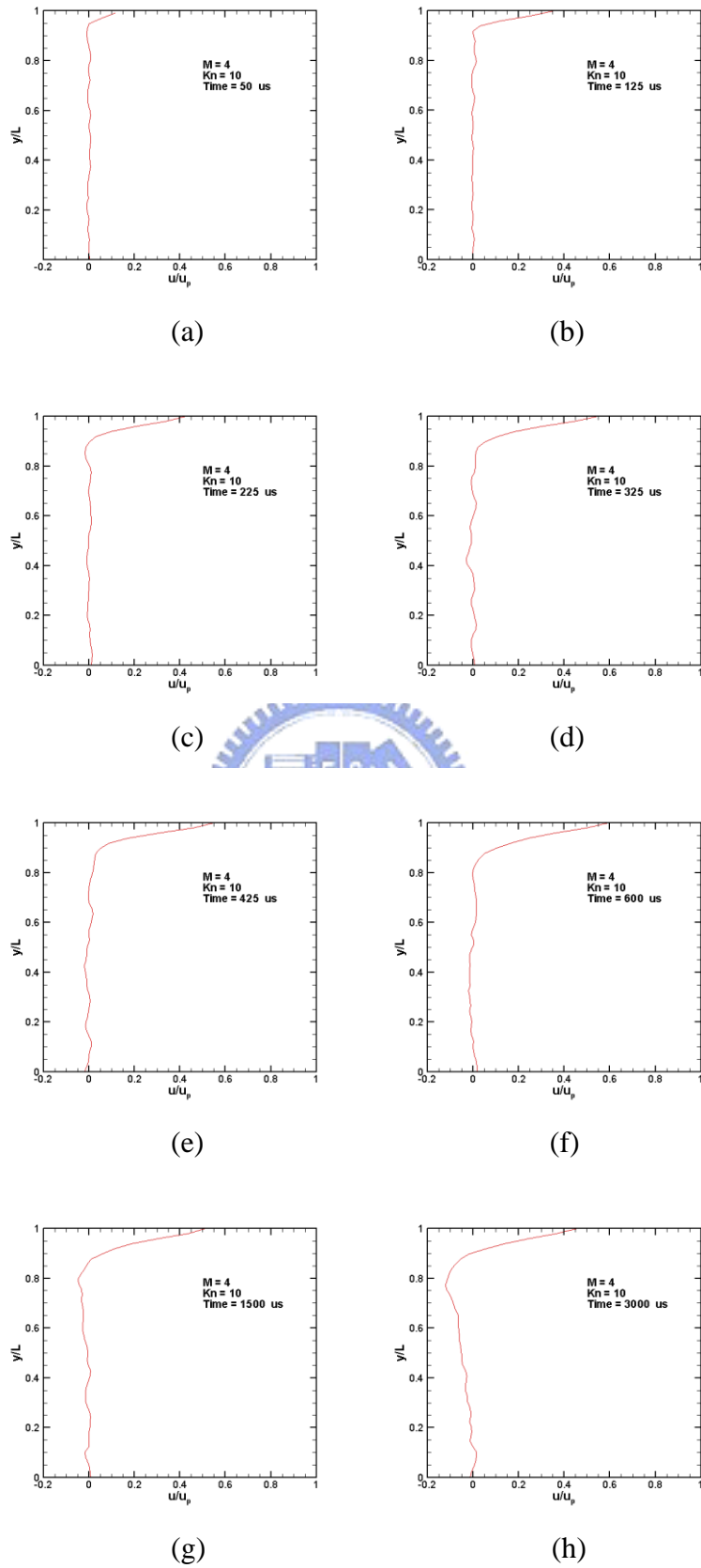


**Fig. 3.44** Profiles of  $u$ -velocity for  $M=4$ ,  $Kn=10$  along vertical lines through geometric center ( $x/L=0.5$ ) at  $t=50 \sim 3000 \mu s$ .

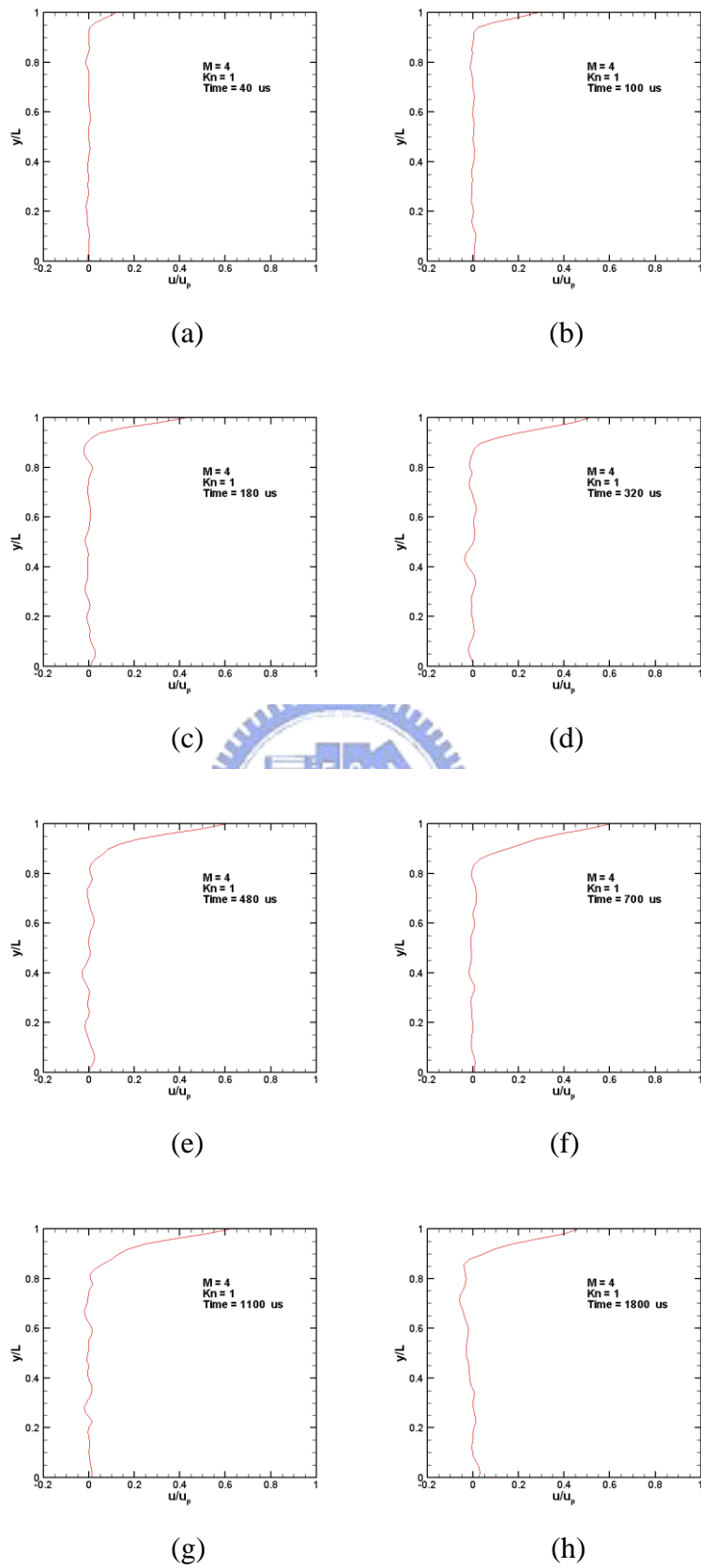


**Fig. 3.45** Profiles of u-velocity for  $M=4$ ,  $Kn=1$  along vertical lines through geometric center ( $x/L=0.5$ ) at  $t=40 \sim 1800 \mu s$ .

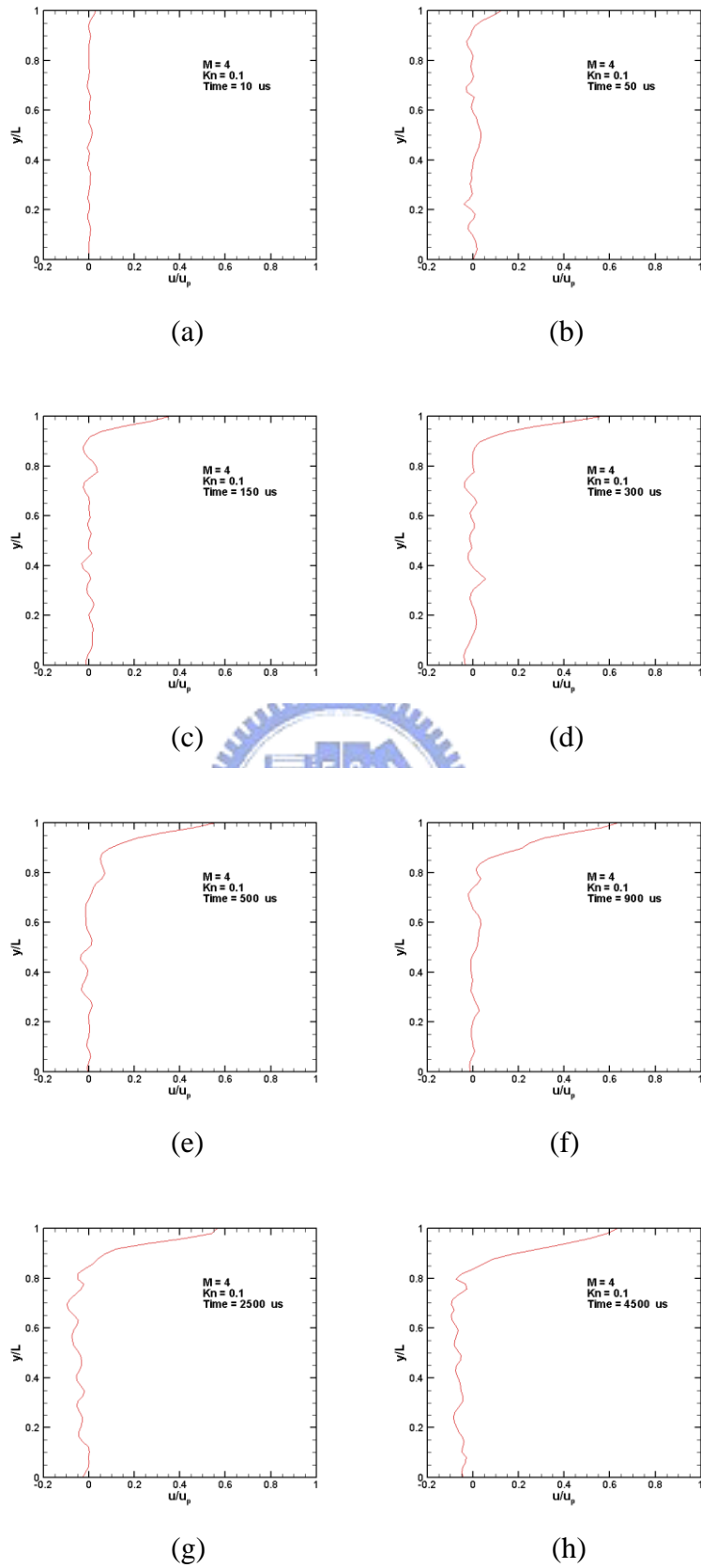


**Fig. 3.46** Profiles of u-velocity for  $M=4$ ,  $Kn=0.1$  along vertical lines through geometric center ( $x/L=0.5$ ) at  $t=10 \sim 4500 \mu$  s.

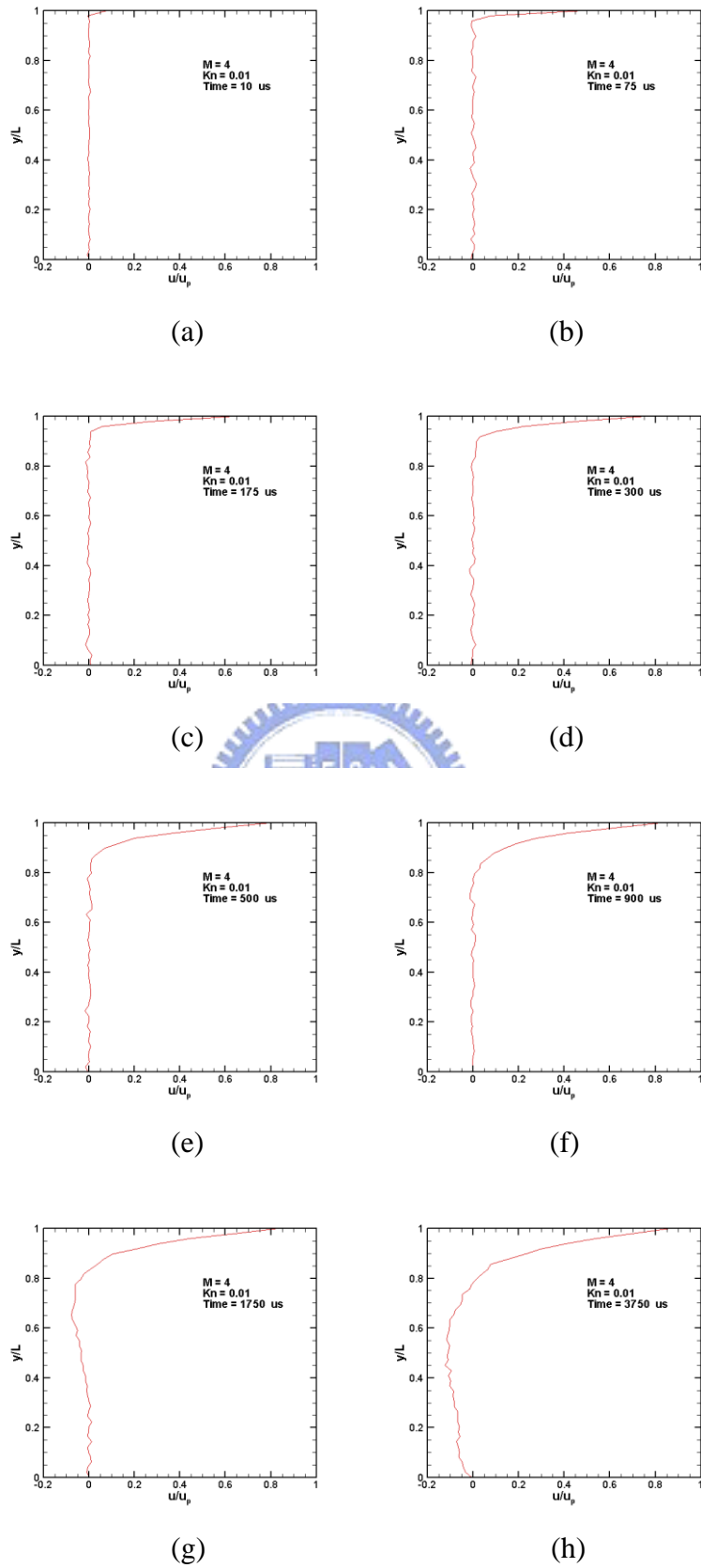


**Fig. 3.47** Profiles of u-velocity for  $M=4$ ,  $Kn=0.01$  along vertical lines through geometric center ( $x/L=0.5$ ) at  $t=10 \sim 3750 \mu s$ .

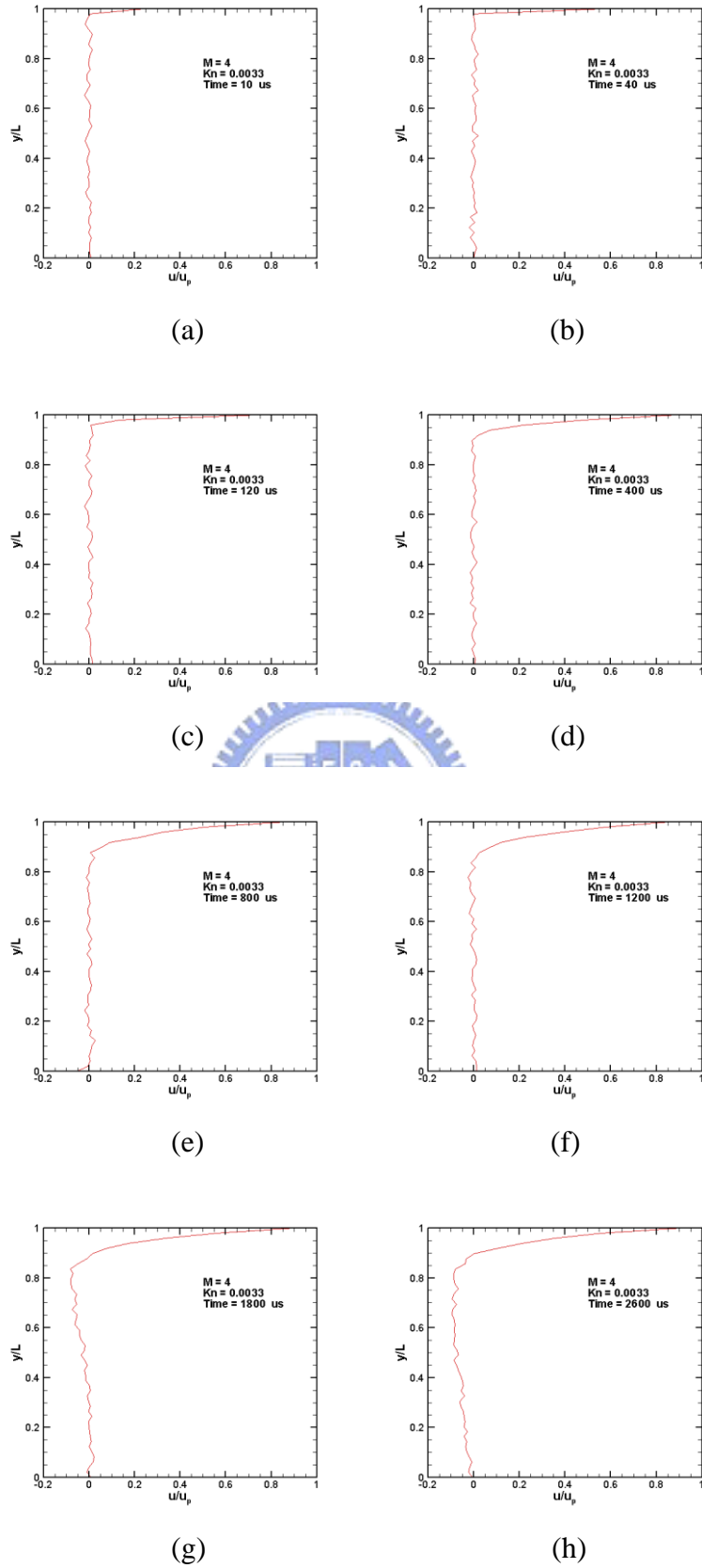


**Fig. 3.48** Profiles of  $u$ -velocity for  $M=4$ ,  $Kn=0.0033$  along vertical lines through geometric center ( $x/L=0.5$ ) at  $t=10 \sim 2600 \mu s$ .

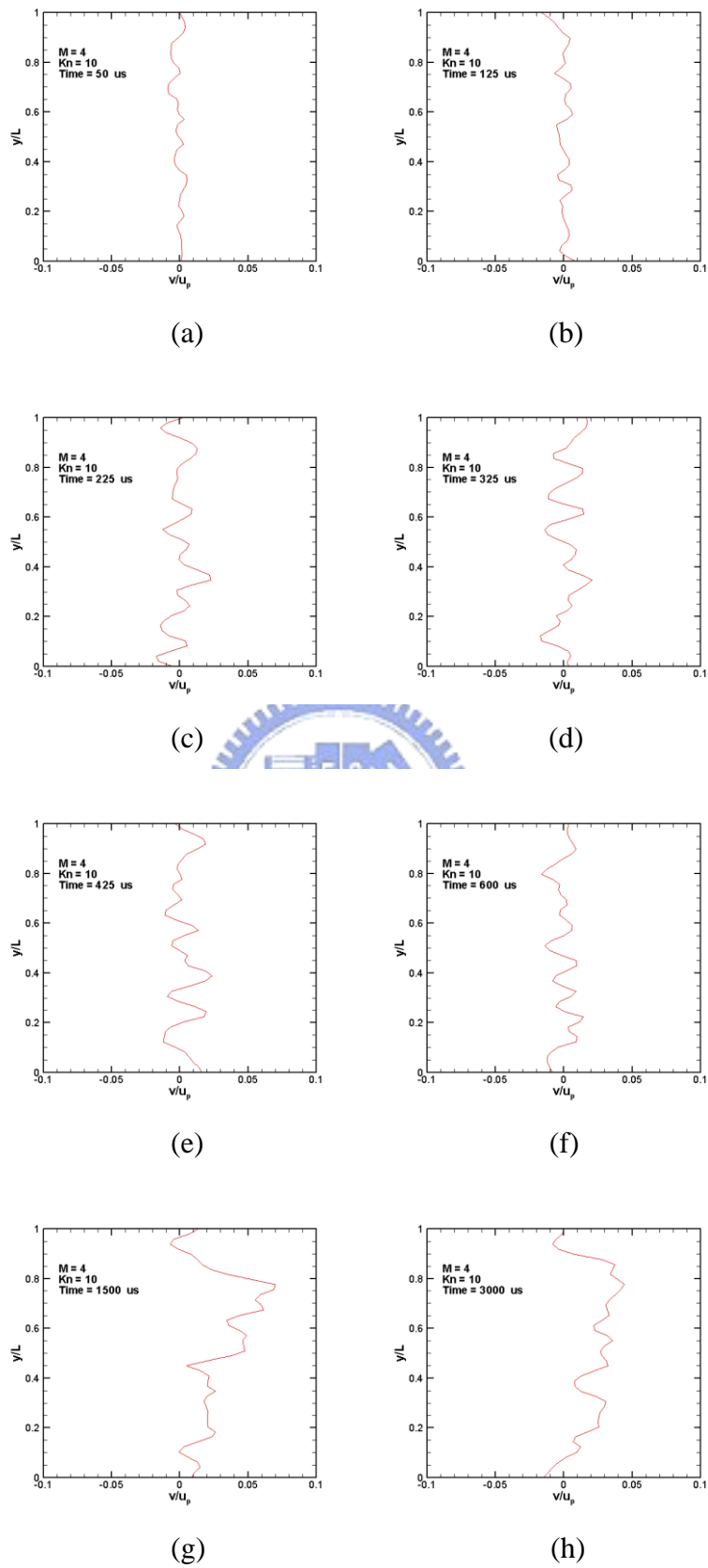


**Fig. 3.49** Profiles of v-velocity for  $M=4$ ,  $Kn=10$  along vertical lines through geometric center ( $x/L=0.5$ ) at  $t=50 \sim 3000 \mu s$ .

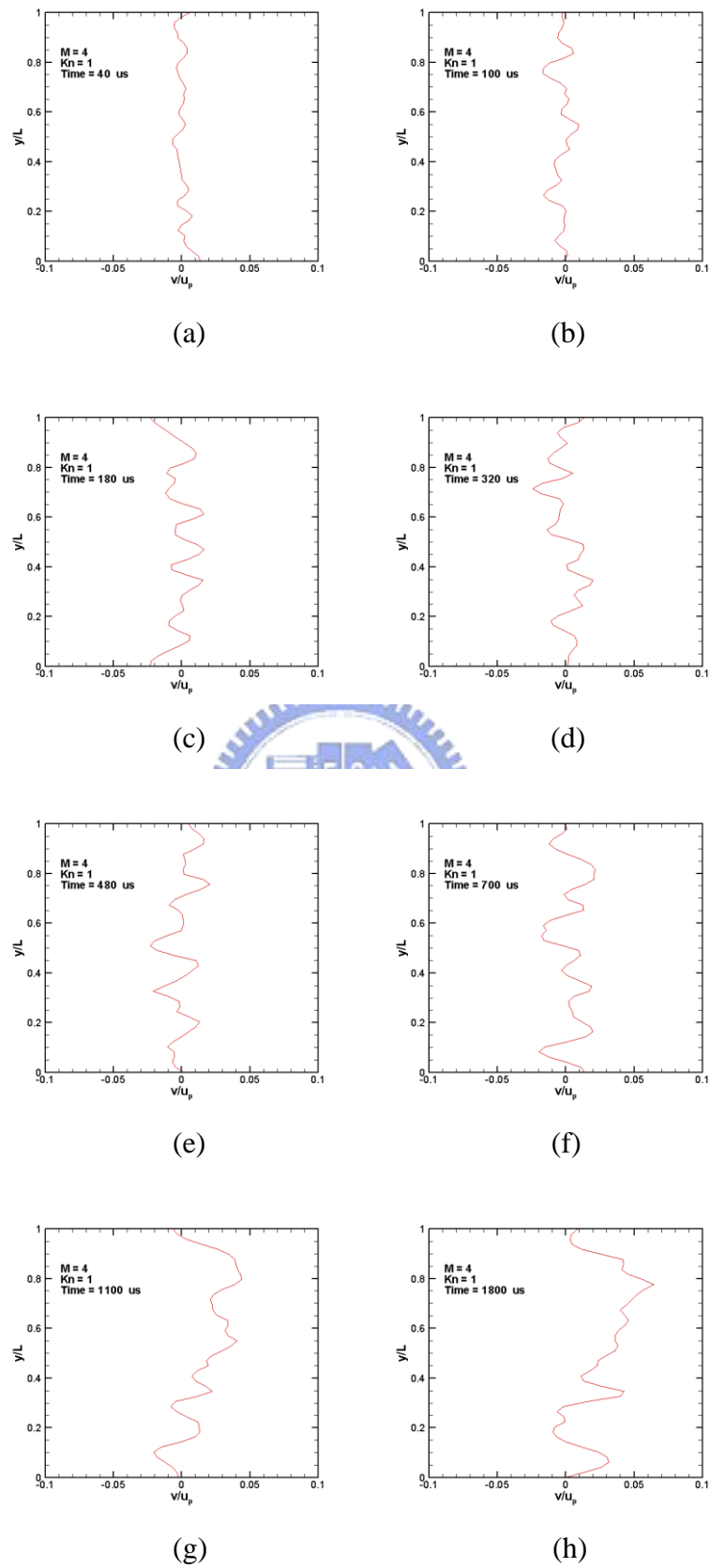


**Fig. 3.50** Profiles of v-velocity for  $M=4$ ,  $Kn=1$  along vertical lines through geometric center ( $x/L=0.5$ ) at  $t=40 \sim 1800 \mu s$ .



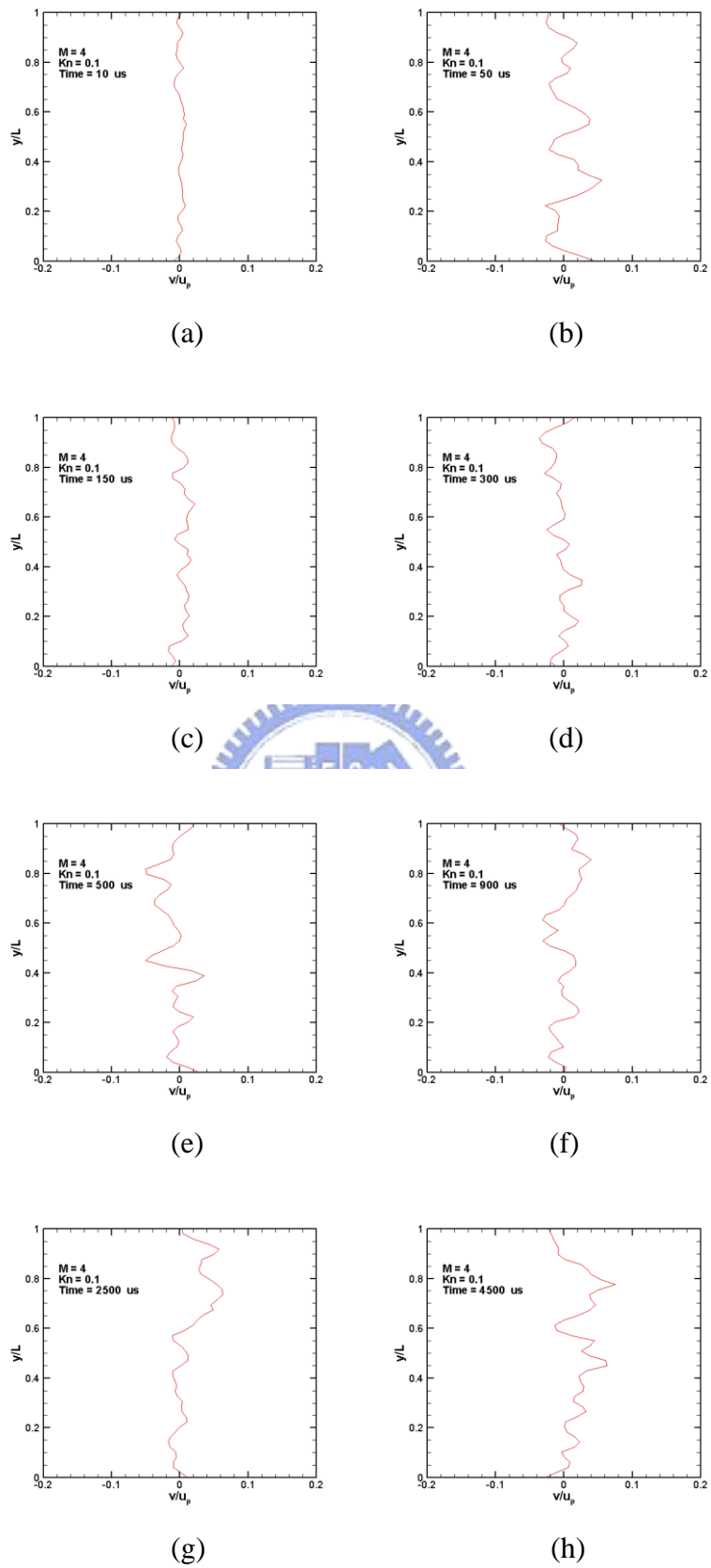


**Fig. 3.51** Profiles of v-velocity for  $M=4$ ,  $Kn=0.1$  along vertical lines through geometric center ( $x/L=0.5$ ) at  $t=10 \sim 4500 \mu$  s.

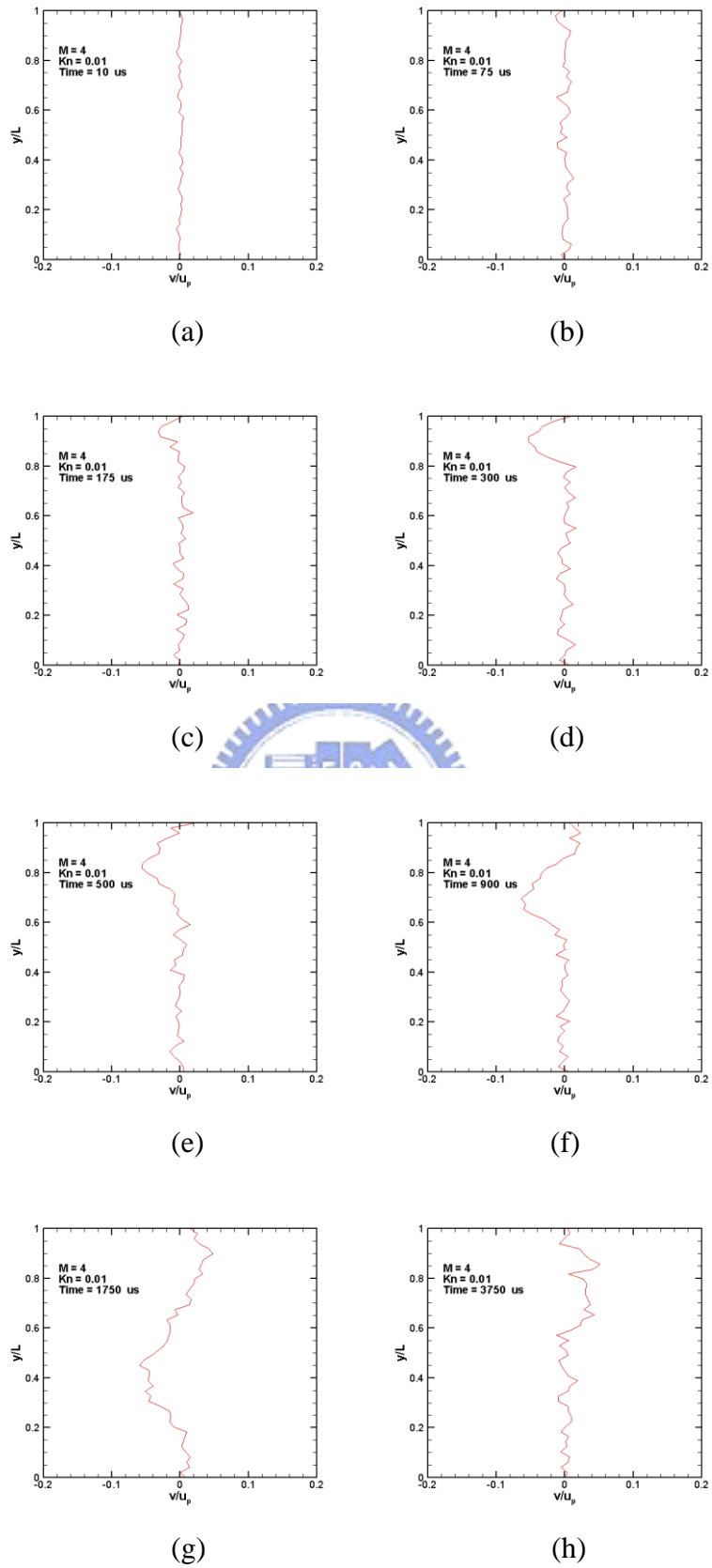


**Fig. 3.52** Profiles of v-velocity for  $M=4$ ,  $Kn=0.01$  along vertical lines through geometric center ( $x/L=0.5$ ) at  $t=10 \sim 3750 \mu s$ .

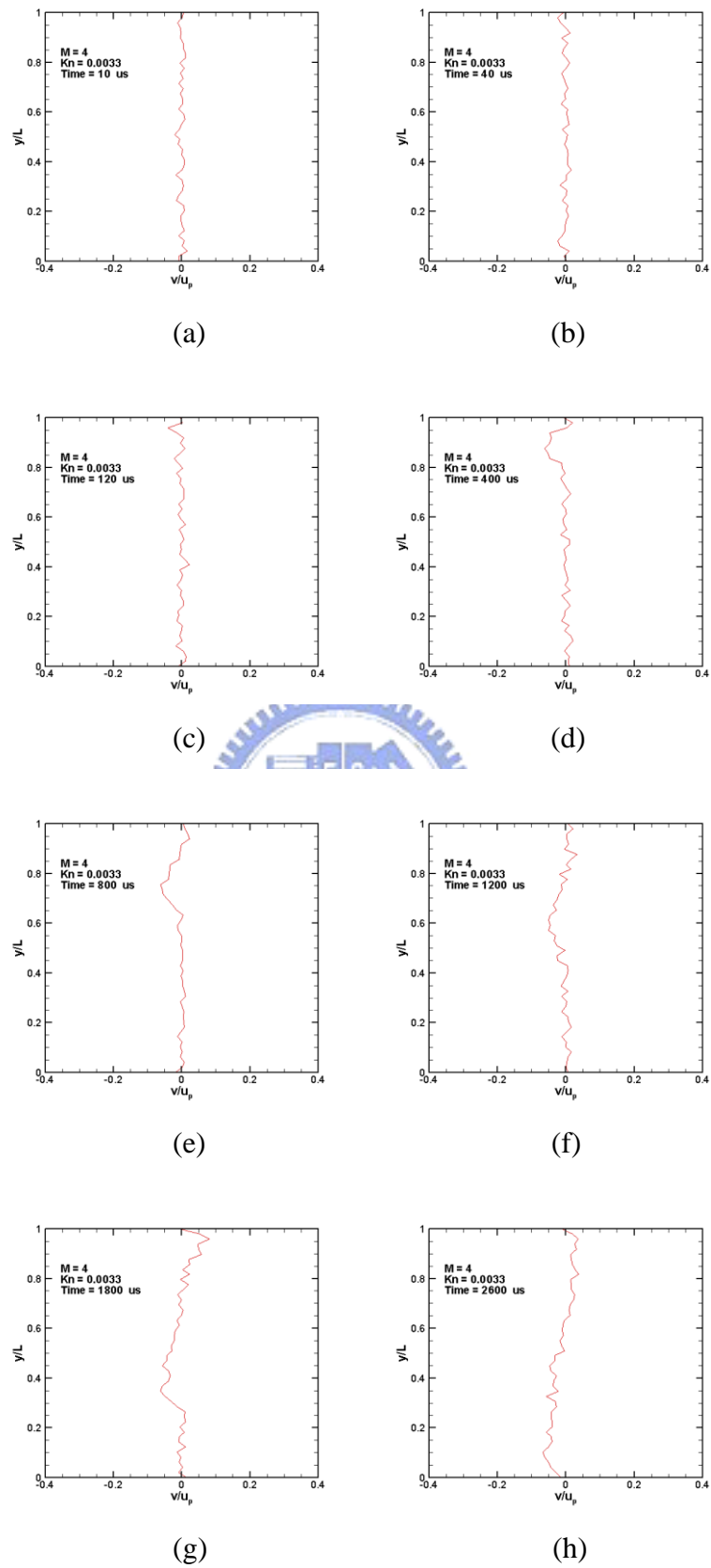


**Fig. 3.53** Profiles of  $v$ -velocity for  $M=4$ ,  $Kn=0.0033$  along vertical lines through geometric center ( $x/L=0.5$ ) at  $t=10 \sim 2600 \mu s$ .

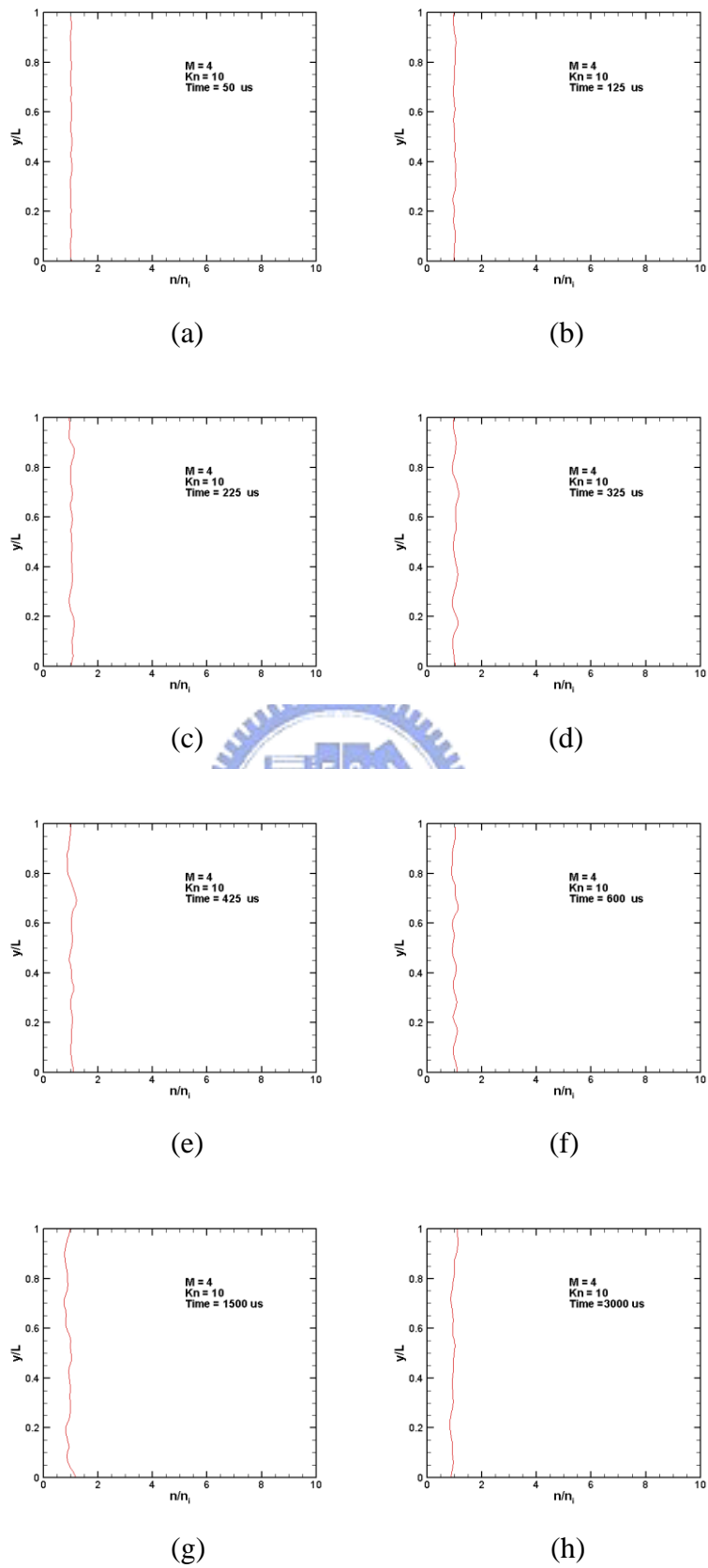


**Fig. 3.54** Profiles of number density for  $M=4$ ,  $Kn=10$  along vertical lines through geometric center ( $x/L=0.5$ ) at  $=50 \sim 3000 \mu$  s.

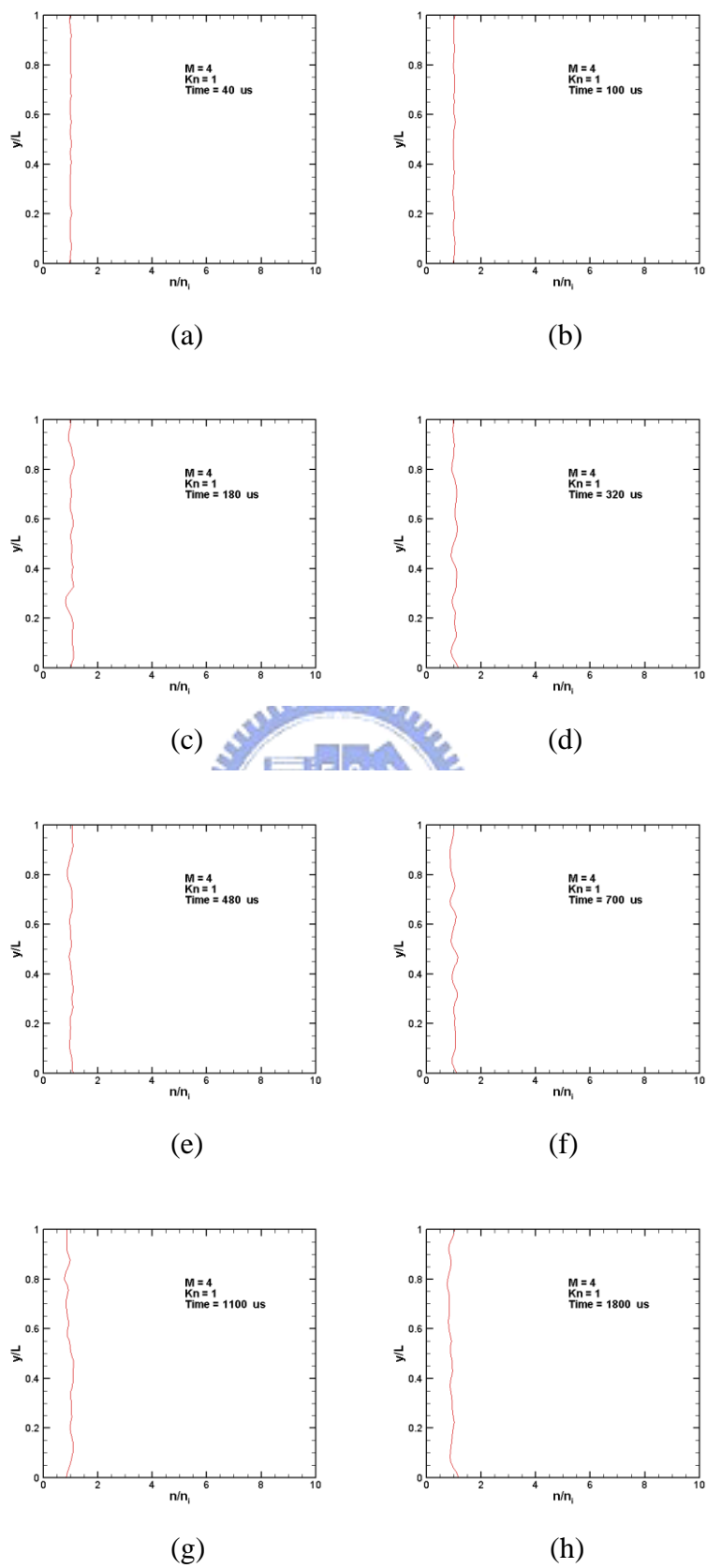


**Fig. 3.55** Profiles of number density for  $M=4$ ,  $Kn=1$  along vertical lines through geometric center ( $x/L=0.5$ ) at  $t=40 \sim 1800 \mu$  s.

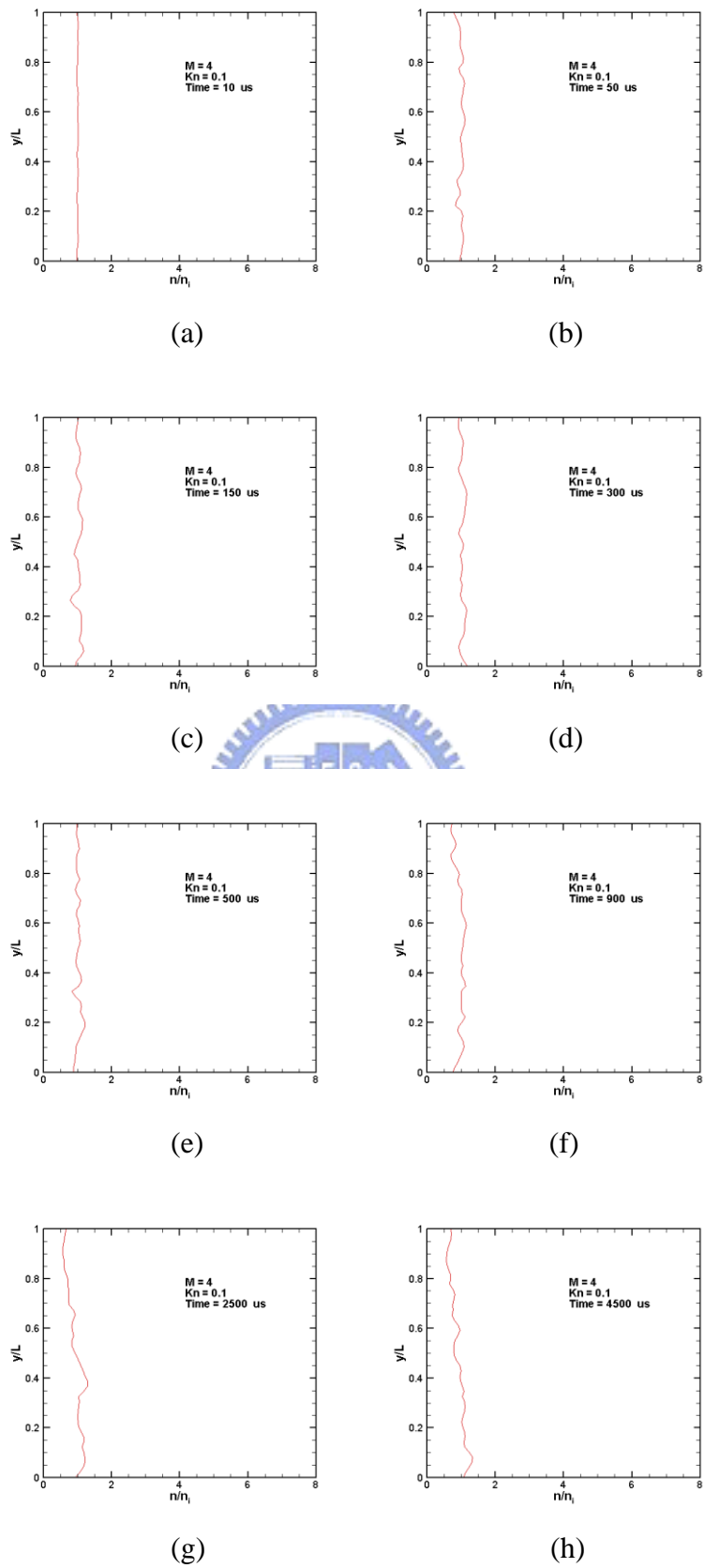


**Fig. 3.56** Profiles of number density for  $M=4$ ,  $Kn=0.1$  along vertical lines through geometric center ( $x/L=0.5$ ) at  $t=10 \sim 4500 \mu s$ .

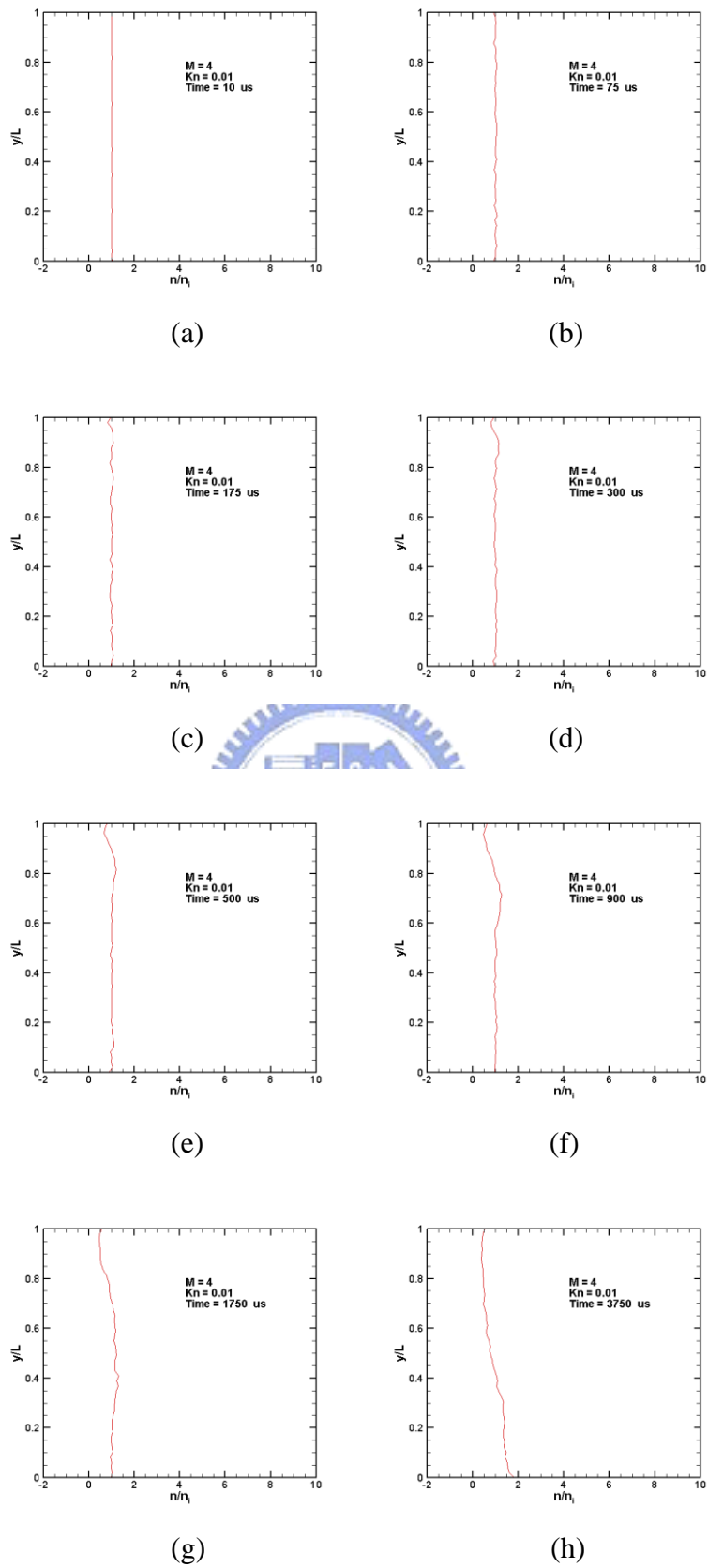


**Fig. 3.57** Profiles of number density for  $M=4$ ,  $Kn=0.01$  along vertical lines through geometric center ( $x/L=0.5$ ) at  $t=10 \sim 3750 \mu s$ .

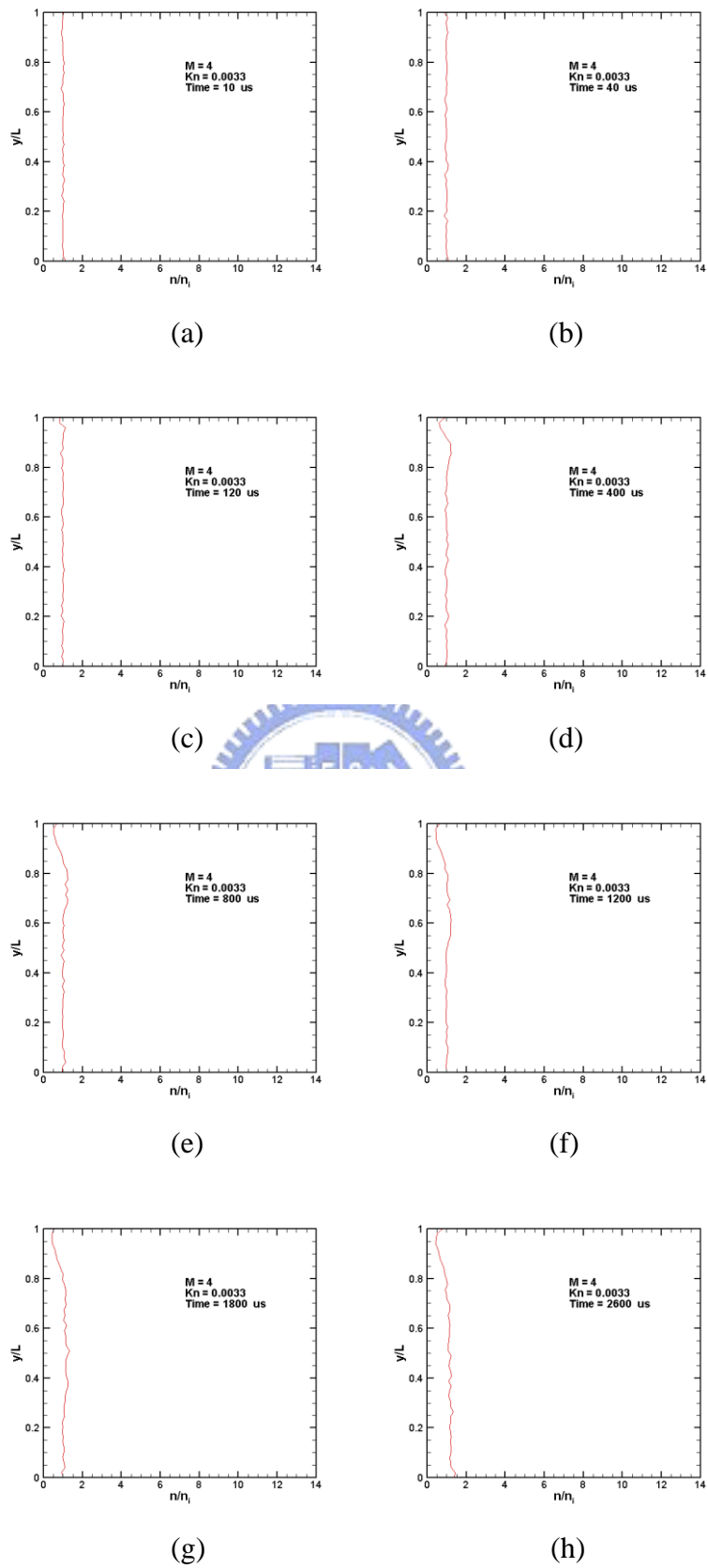


**Fig. 3.58** Profiles of number density for  $M=4$ ,  $Kn=0.0033$  along vertical lines through geometric center ( $x/L=0.5$ ) at  $t=10 \sim 2600 \mu s$ .



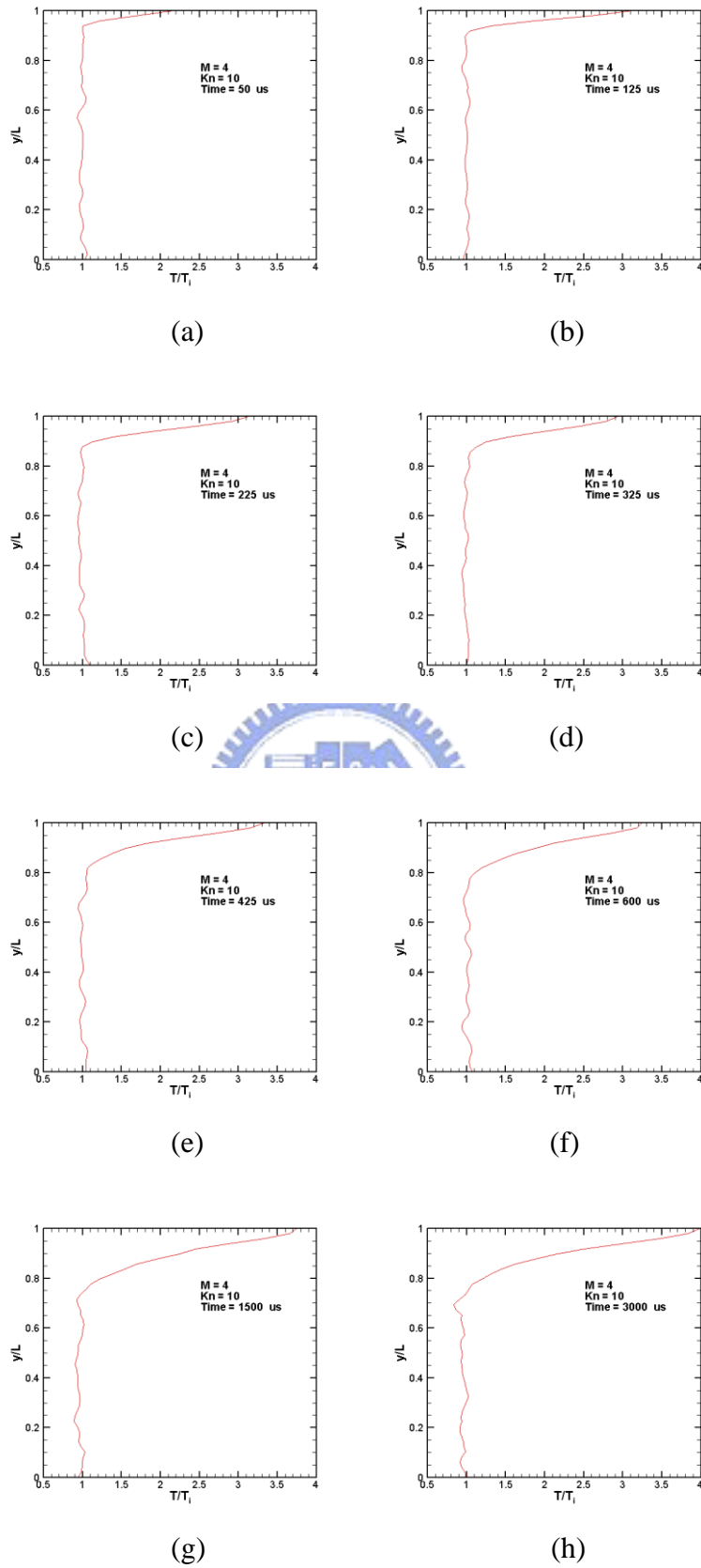


**Fig. 3.59** Profiles of temperature for  $M=4$ ,  $Kn=10$  along vertical lines through geometric center ( $x/L=0.5$ ) at  $t=50 \sim 3000 \mu s$ .

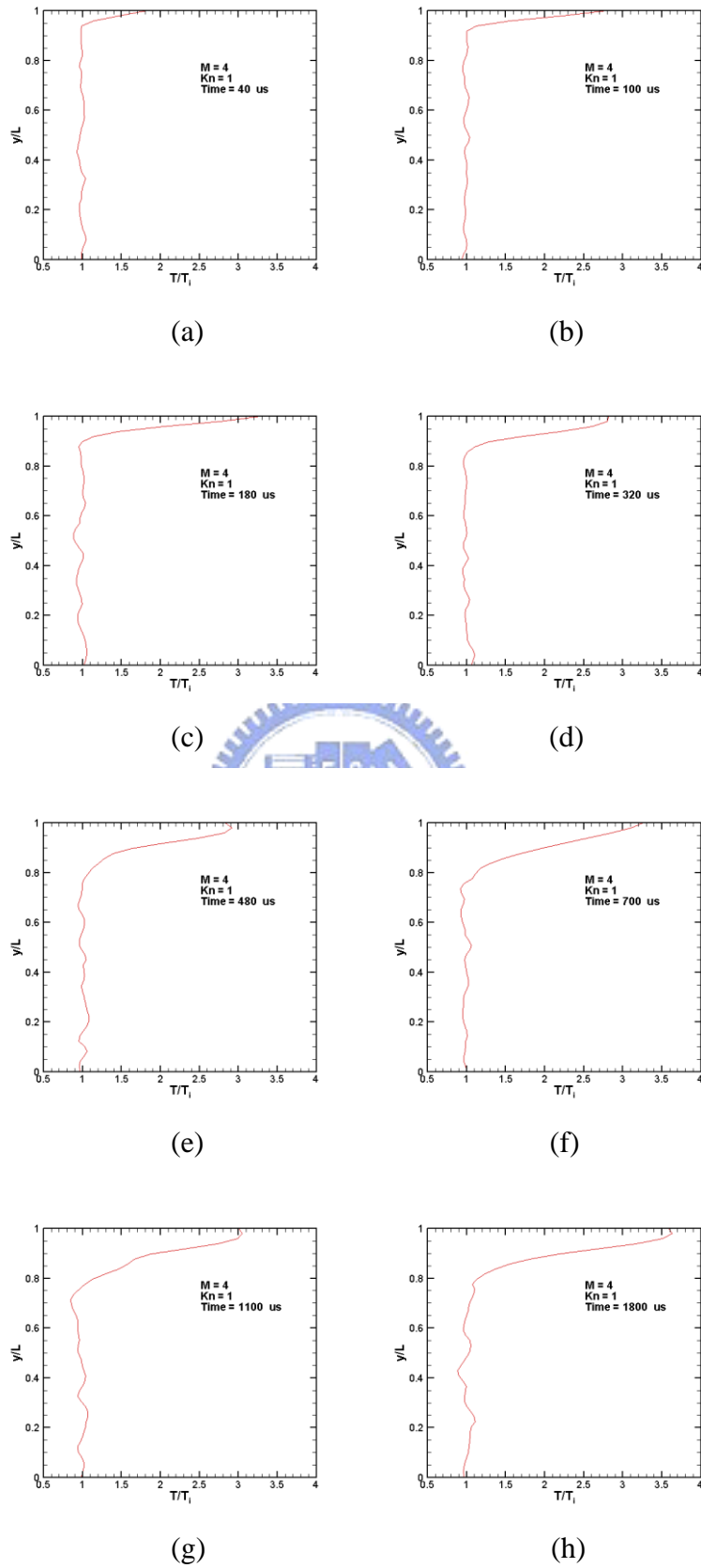


**Fig. 3.60** Profiles of temperature for  $M=4$ ,  $Kn=1$  along vertical lines through geometric center ( $x/L=0.5$ ) at  $t=40 \sim 1800 \mu s$ .

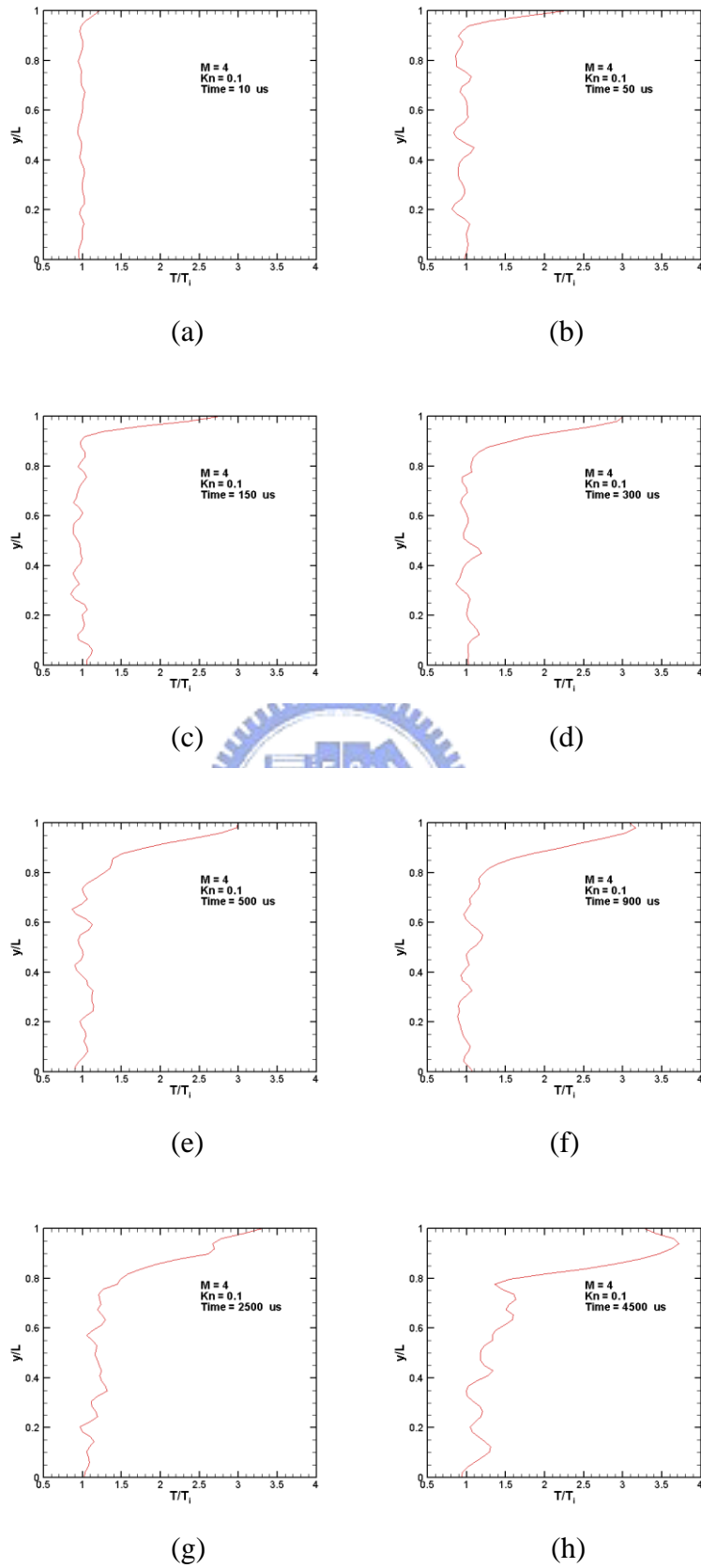


**Fig. 3.61** Profiles of temperature for  $M=4$ ,  $Kn=0.1$  along vertical lines through geometric center ( $x/L=0.5$ ) at  $t=10 \sim 4500 \mu s$ .

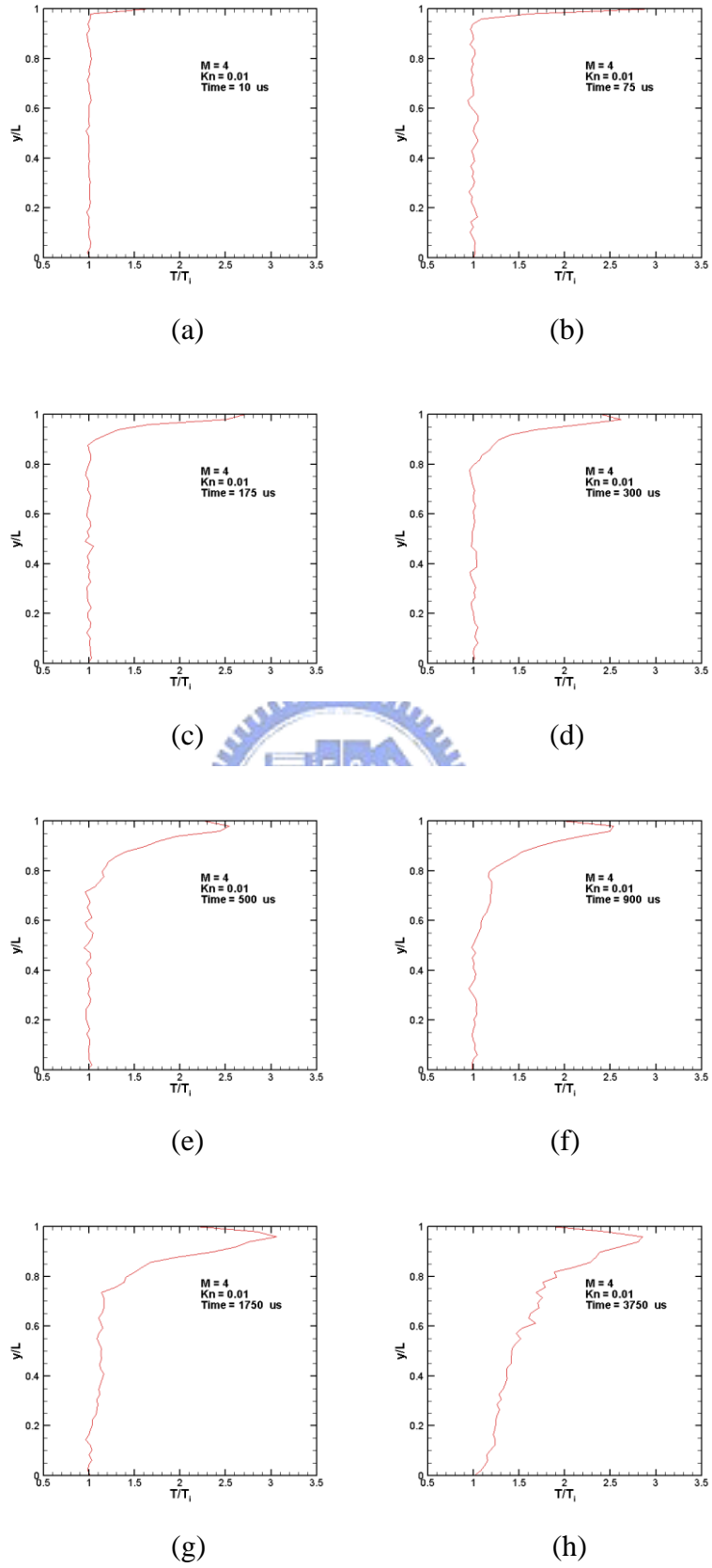


**Fig. 3.62** Profiles of temperature for  $M=4$ ,  $Kn=0.01$  along vertical lines through geometric center ( $x/L=0.5$ ) at  $t=10 \sim 3750 \mu s$ .

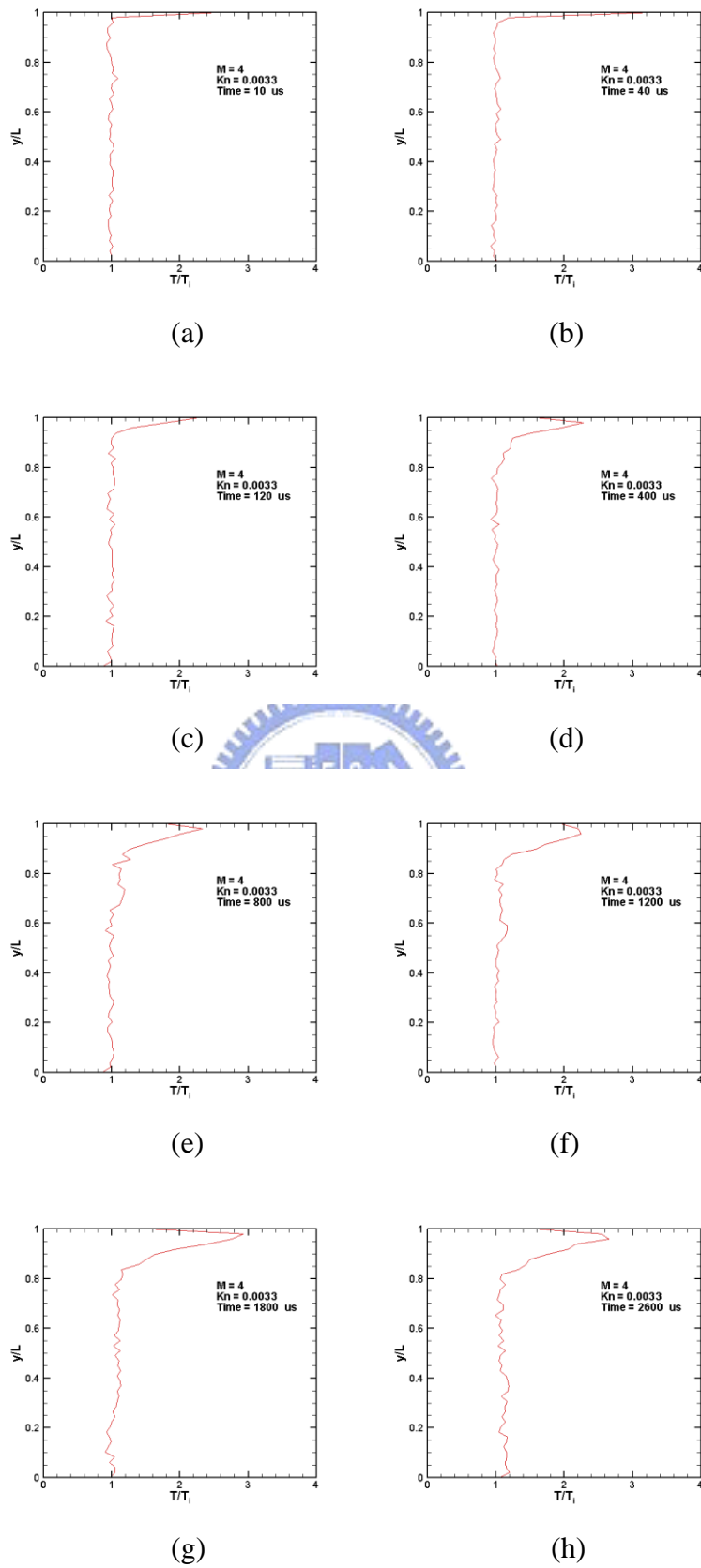


**Fig. 3.63** Profiles of temperature for  $M=4$ ,  $Kn=0.0033$  along vertical lines through geometric center ( $x/L=0.5$ ) at  $t=10 \sim 2600 \mu s$ .

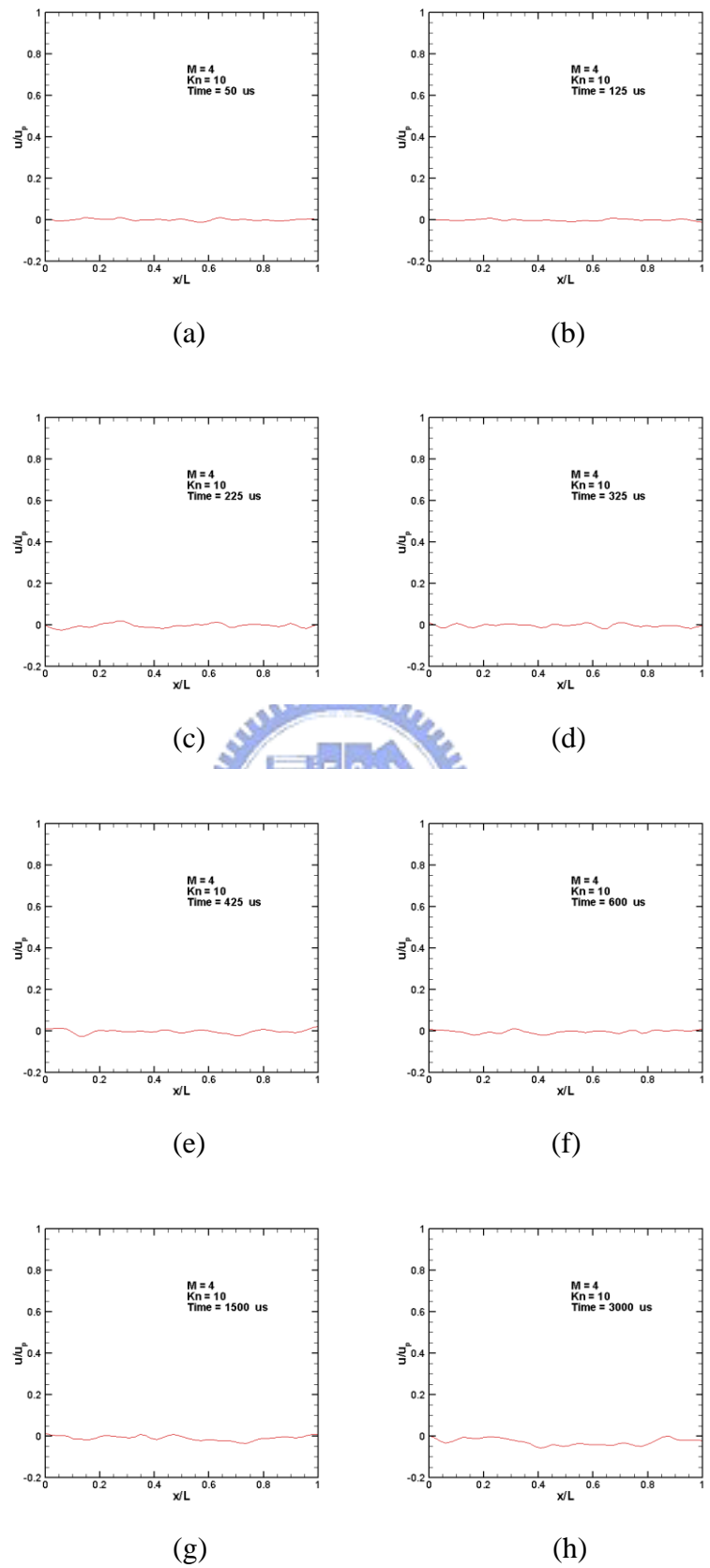
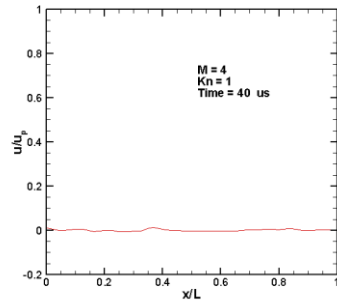
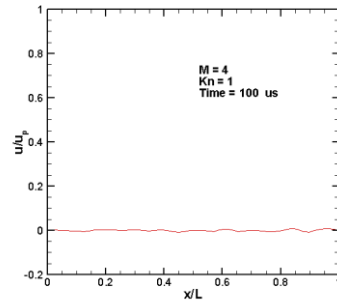


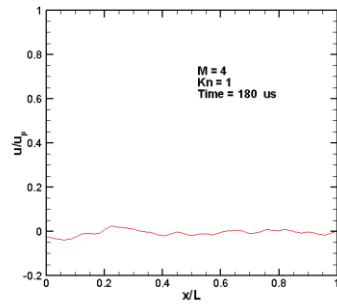
**Fig. 3.64** Profiles of u-velocity for  $M=4$ ,  $Kn=10$  along horizontal lines through geometric center ( $y/L=0.5$ ) at  $=50 \sim 3000 \mu s$ .



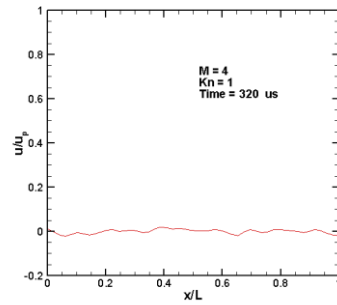
(a)



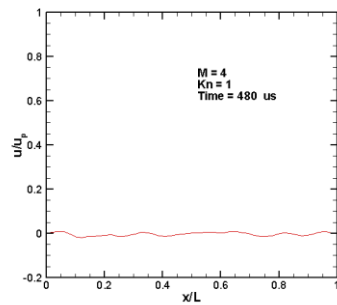
(b)



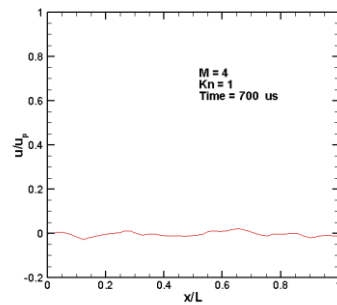
(c)



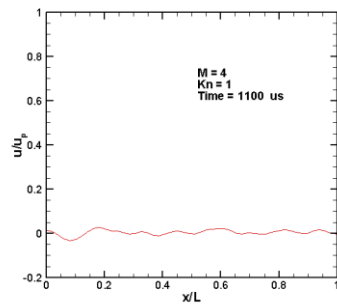
(d)



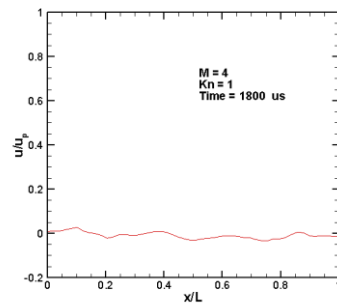
(e)



(f)



(g)



(h)

**Fig. 3.65** Profiles of  $u$ -velocity for  $M=4$ ,  $Kn=1$  along horizontal lines through geometric center ( $y/L=0.5$ ) at  $t=40 \sim 1800 \mu s$ .

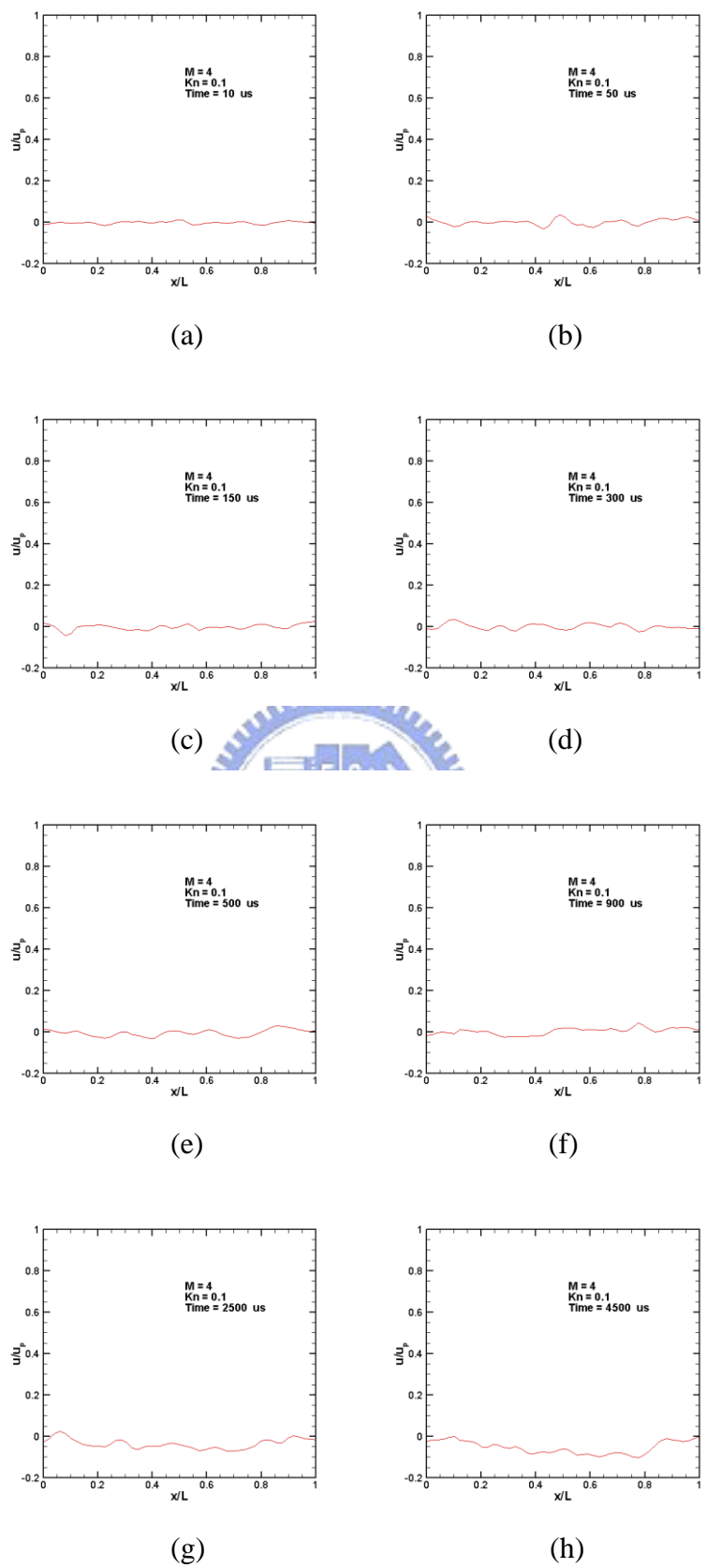


**Fig. 3.66** Profiles of u-velocity for  $M=4$ ,  $Kn=0.1$  along horizontal lines through geometric center ( $y/L=0.5$ ) at  $t=10 \sim 4500 \mu s$ .



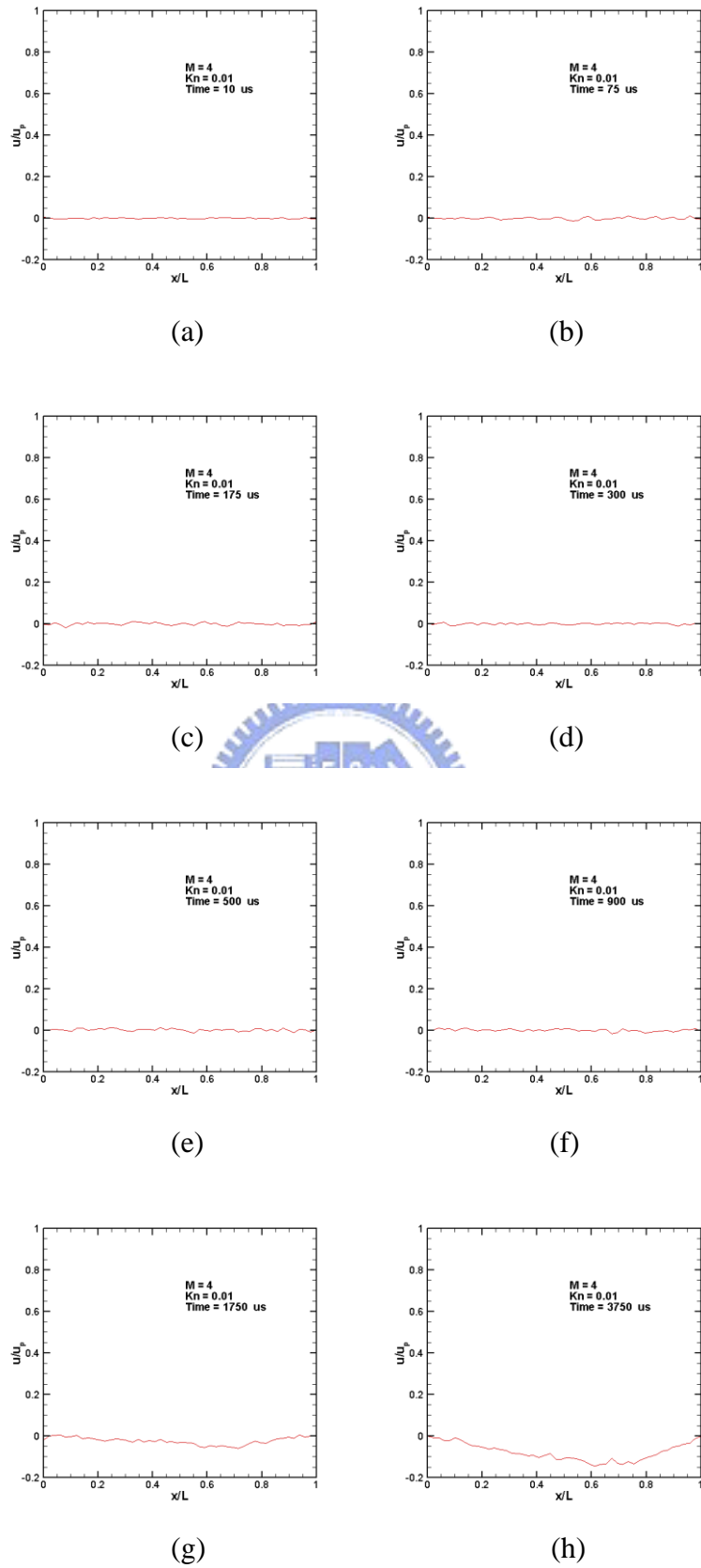


**Fig. 3.67** Profiles of u-velocity for  $M=4$ ,  $Kn=0.01$  along horizontal lines through geometric center ( $y/L=0.5$ ) at  $t=10 \sim 3750 \mu s$ .

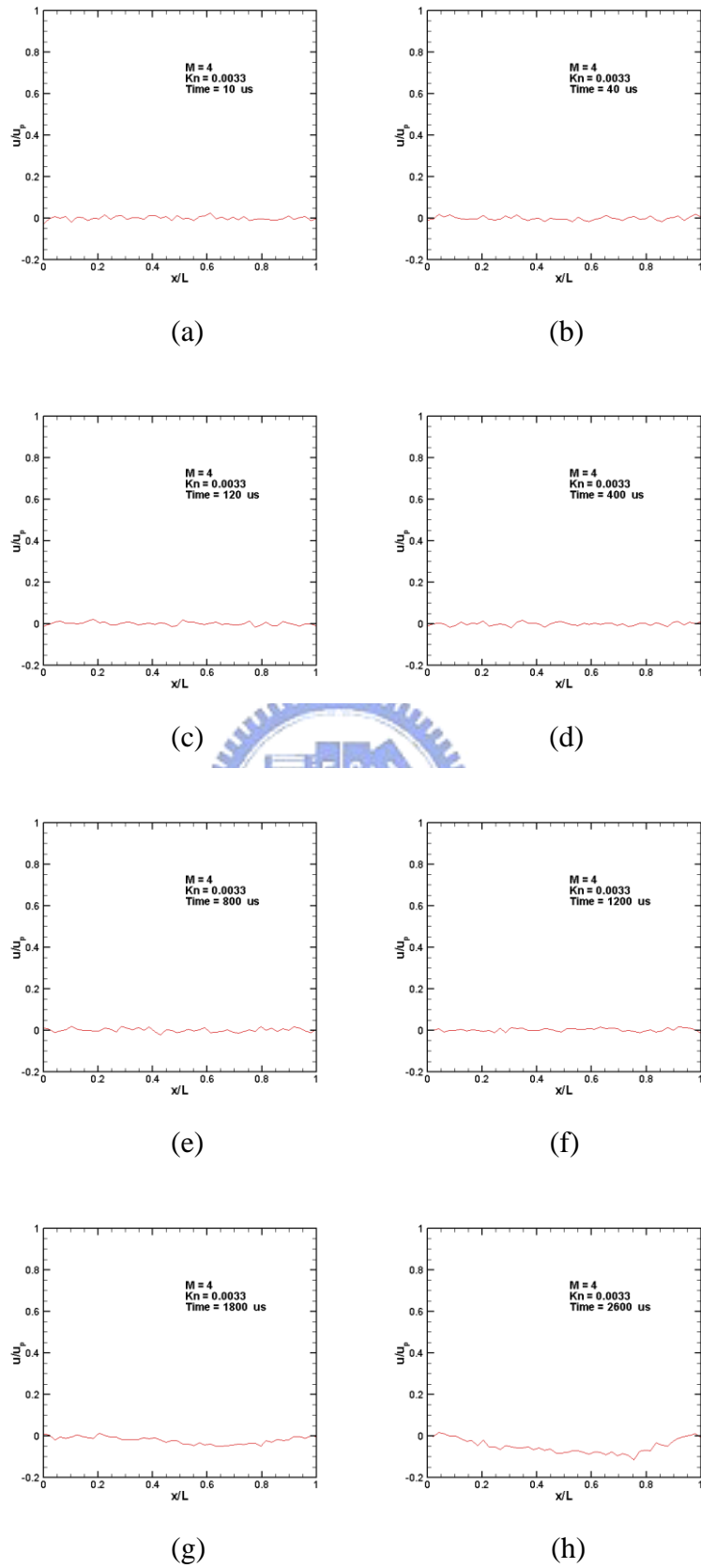


**Fig. 3.68** Profiles of  $u$ -velocity for  $M=4$ ,  $Kn=0.0033$  along horizontal lines through geometric center ( $y/L=0.5$ ) at  $t=10 \sim 2600 \mu s$ .

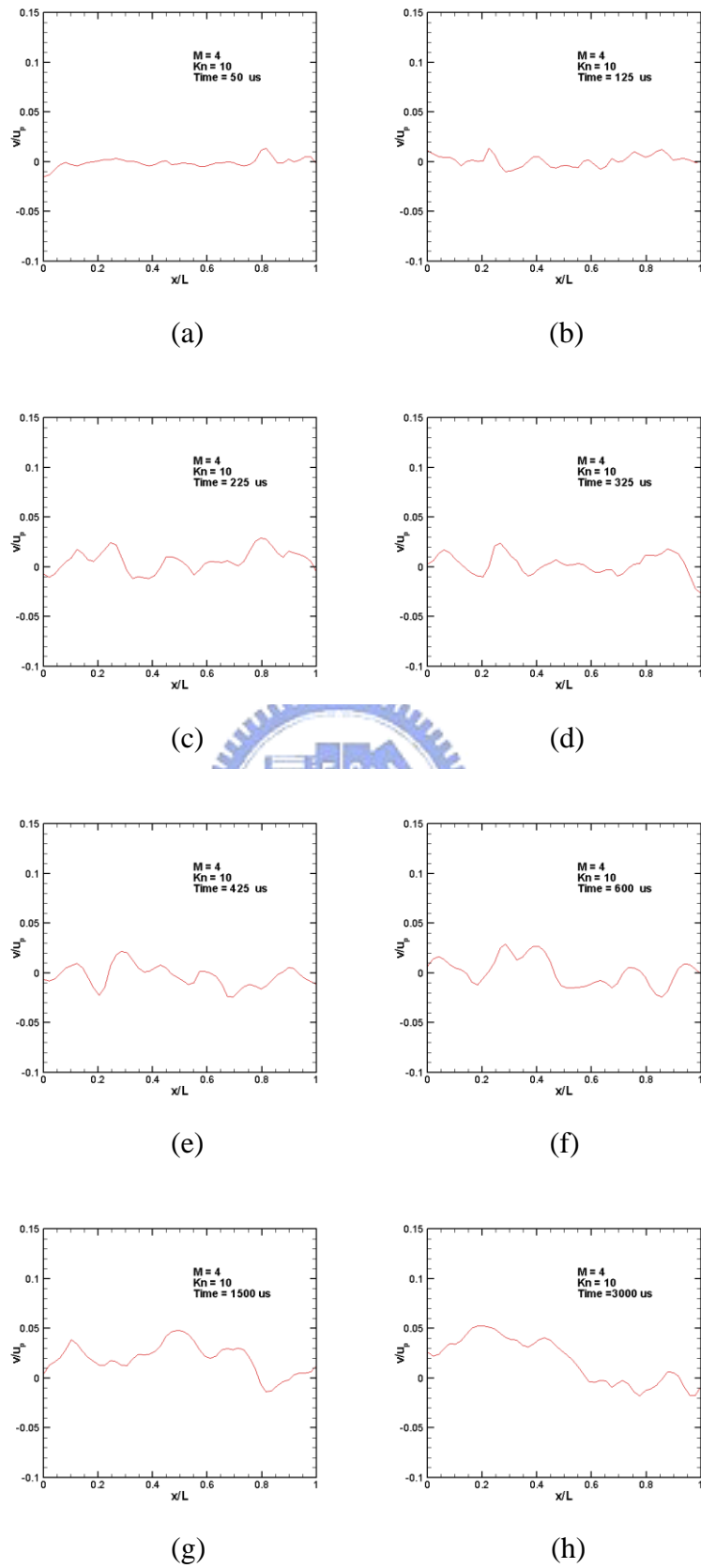


**Fig. 3.69** Profiles of v-velocity for  $M=4$ ,  $Kn=10$  along horizontal lines through geometric center ( $y/L=0.5$ ) at  $=50 \sim 3000 \mu s$ .

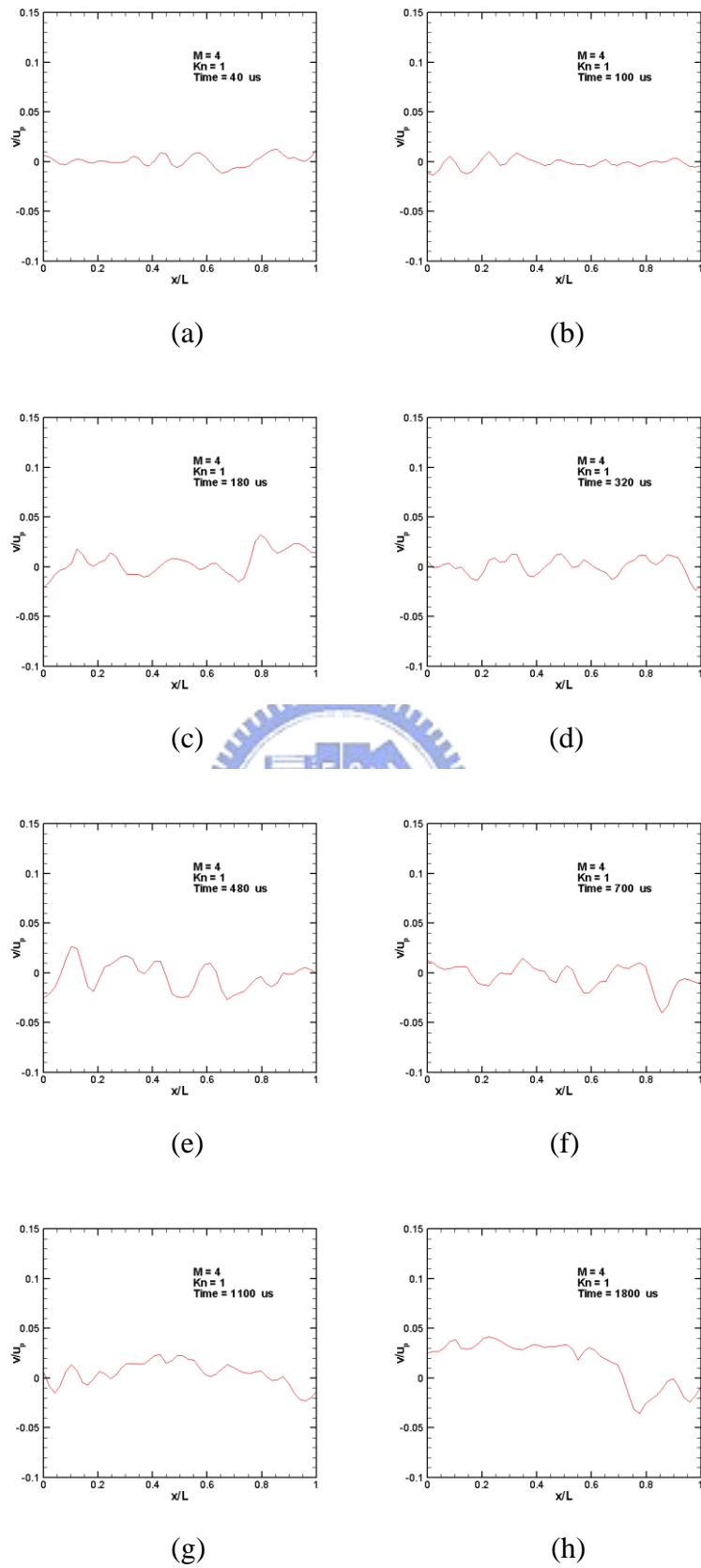


**Fig. 3.70** Profiles of v-velocity for  $M=4$ ,  $Kn=1$  along horizontal lines through geometric center ( $y/L=0.5$ ) at  $t=40 \sim 1800 \mu s$ .

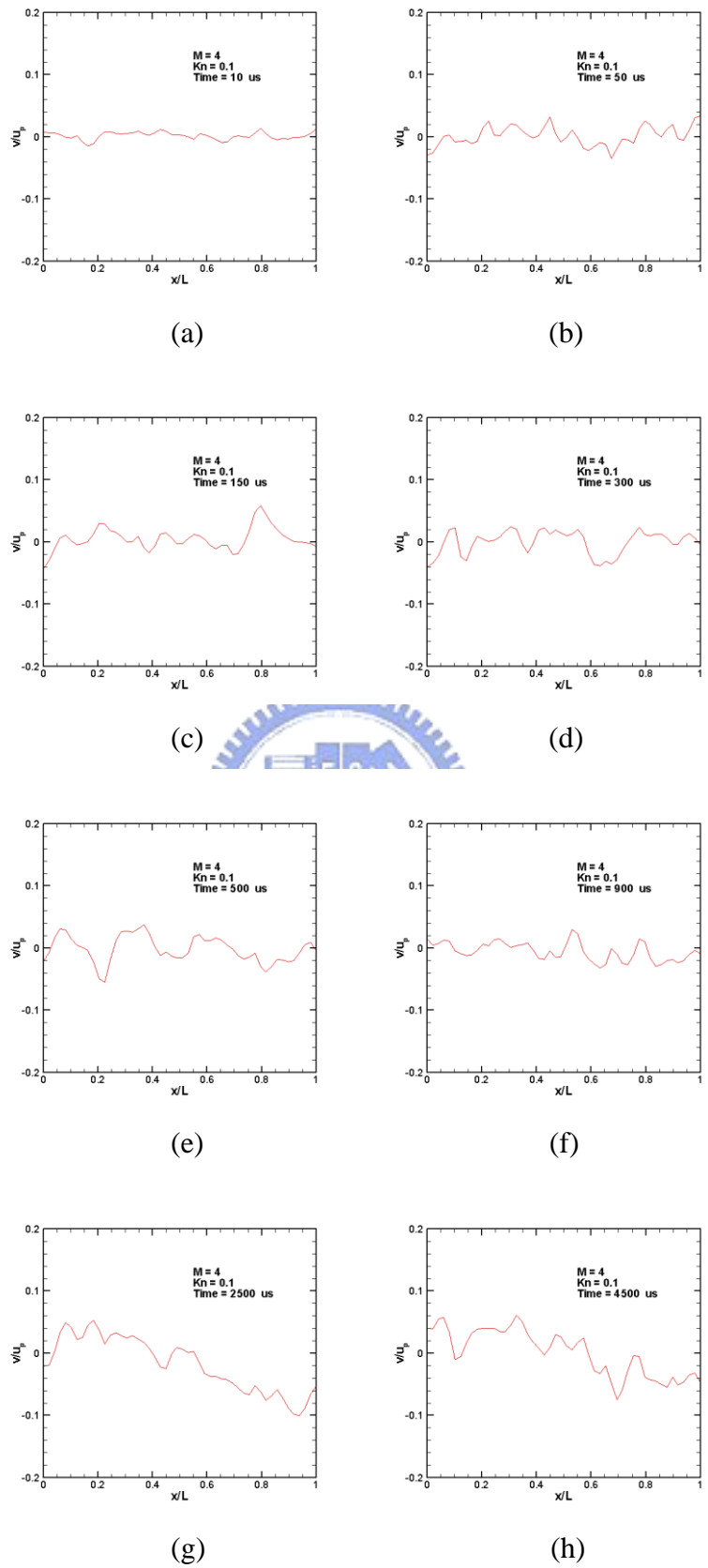


**Fig. 3.71** Profiles of v-velocity for  $M=4$ ,  $Kn=0.1$  along horizontal lines through geometric center ( $y/L=0.5$ ) at  $t=10 \sim 4500 \mu s$ .

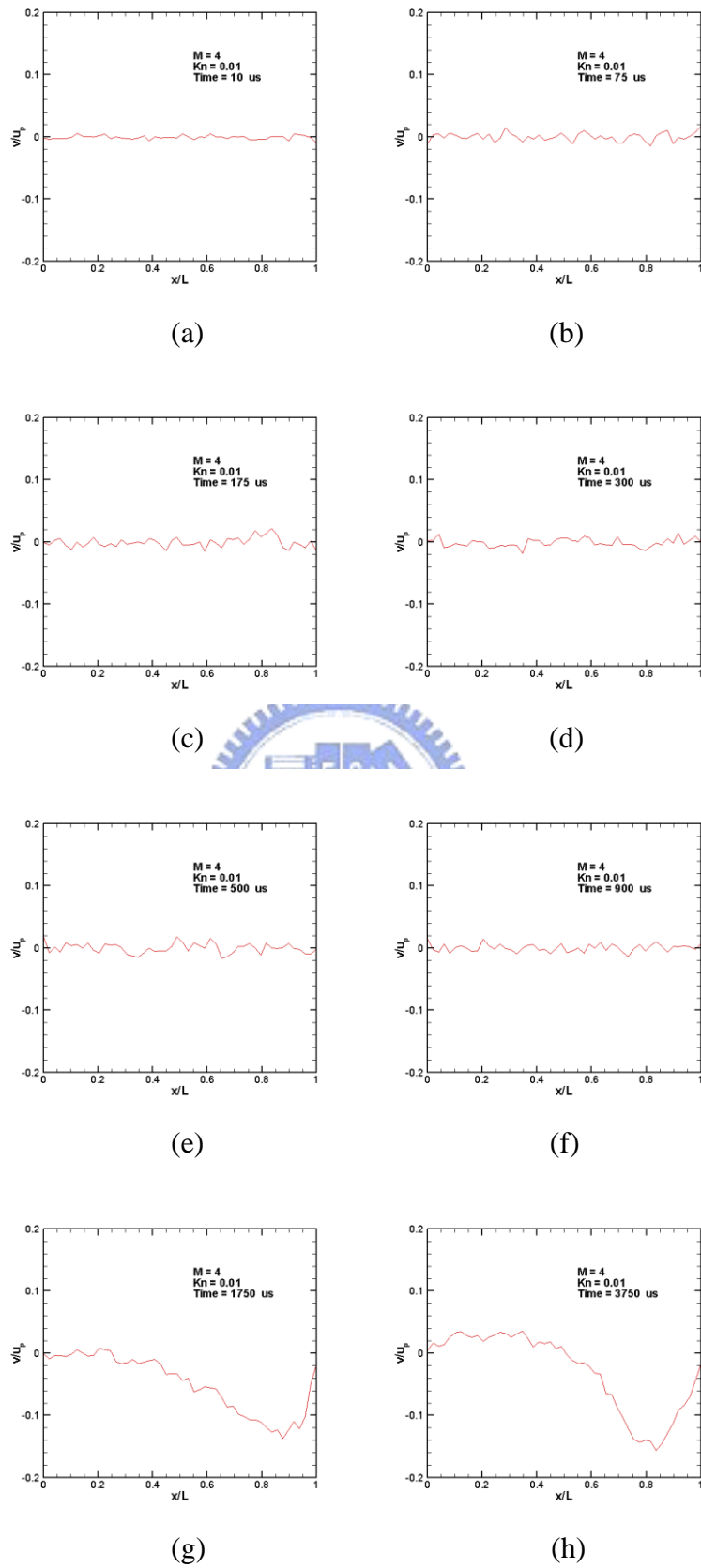


**Fig. 3.72** Profiles of v-velocity for  $M=4$ ,  $Kn=0.01$  along horizontal lines through geometric center ( $y/L=0.5$ ) at  $t=10 \sim 3750 \mu s$ .

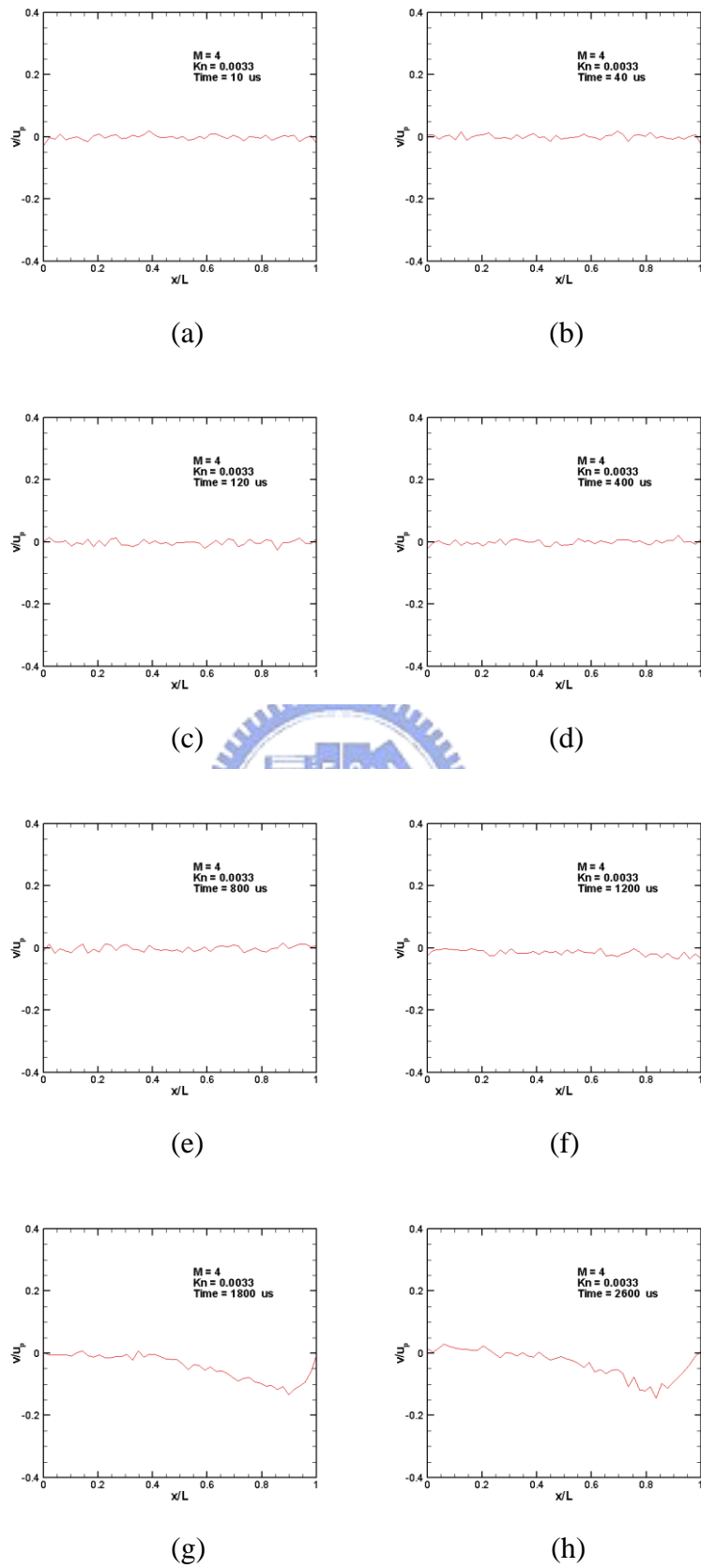


**Fig. 3.73** Profiles of v-velocity for  $M=4$ ,  $Kn=0.0033$  along horizontal lines through geometric center ( $y/L=0.5$ ) at  $t=10 \sim 2600 \mu s$ .

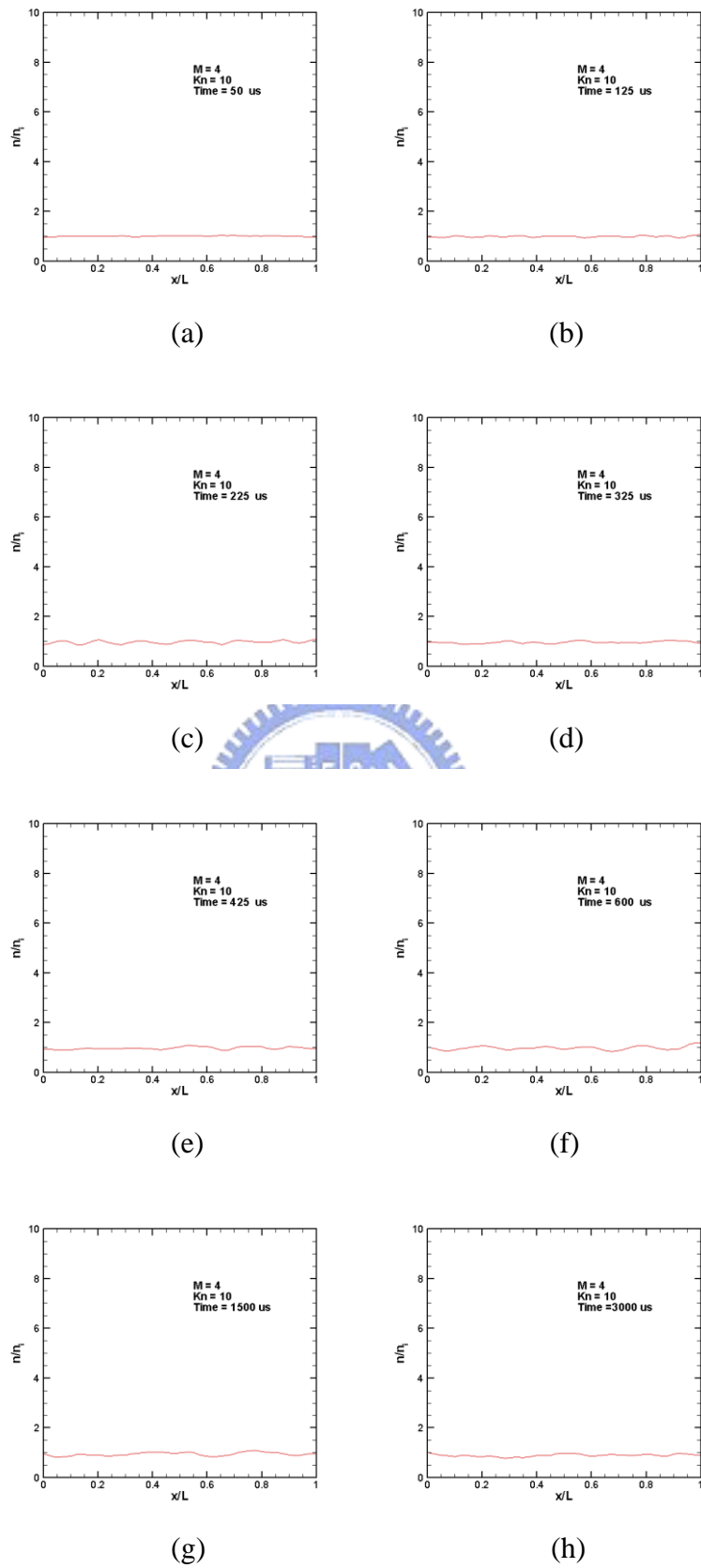


**Fig. 3.74** Profiles of number density for  $M=4$ ,  $Kn=10$  along horizontal lines through geometric center ( $y/L=0.5$ ) at  $=50 \sim 3000 \mu s$ .



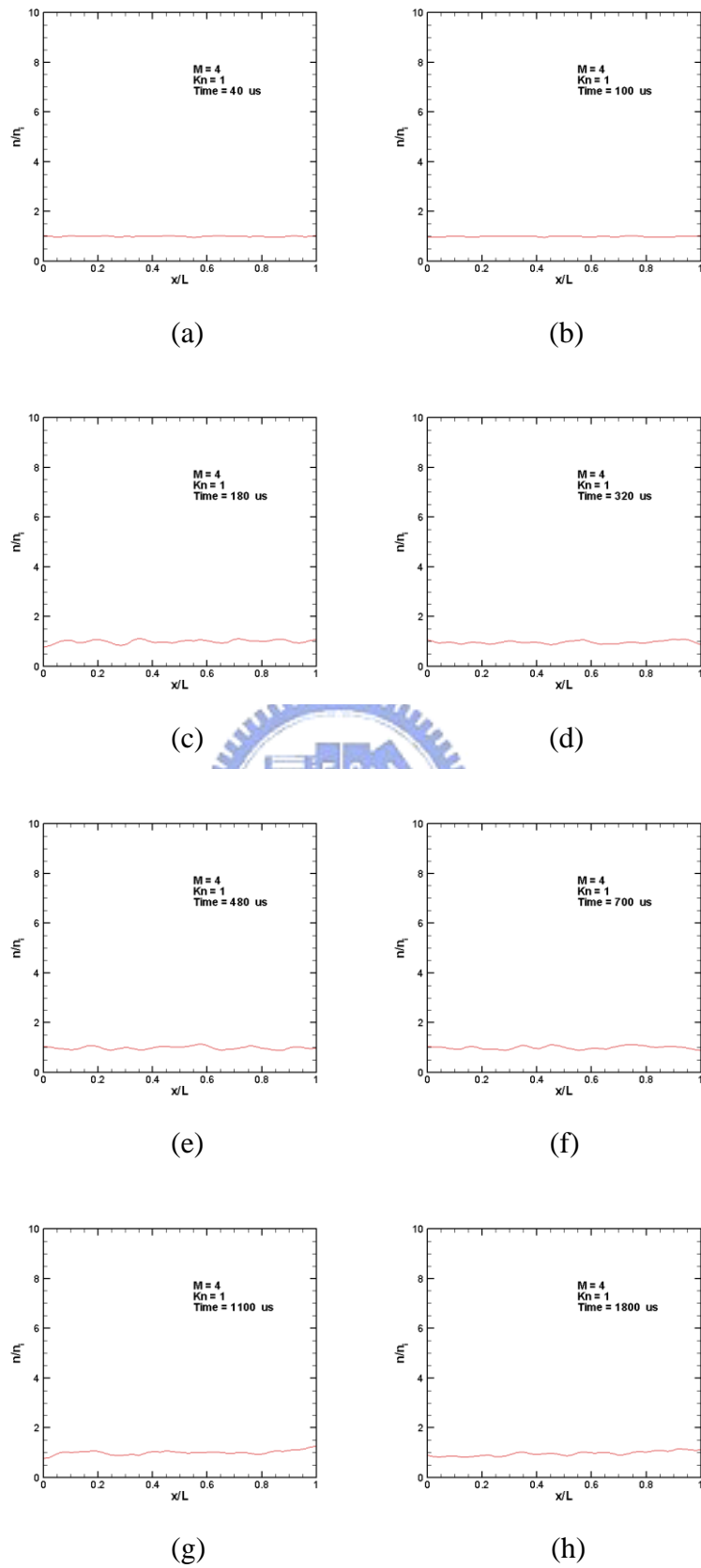


**Fig. 3.75** Profiles of number density for  $M=4$ ,  $Kn=1$  along horizontal lines through geometric center ( $y/L=0.5$ ) at  $t=40 \sim 1800 \mu$  s.

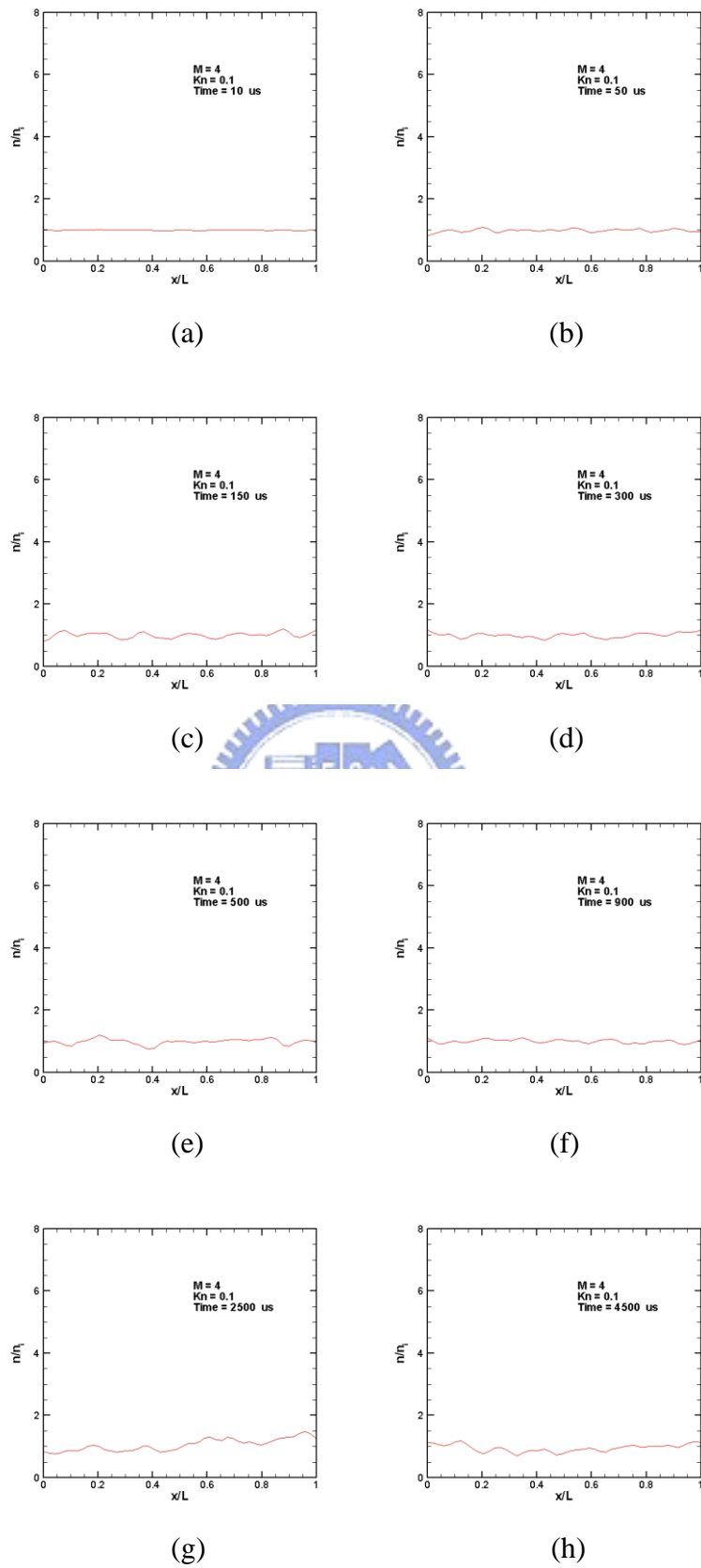


**Fig. 3.76** Profiles of number density for  $M=4$ ,  $Kn=0.1$  along horizontal lines through geometric center ( $y/L=0.5$ ) at  $t=10 \sim 4500 \mu s$ .

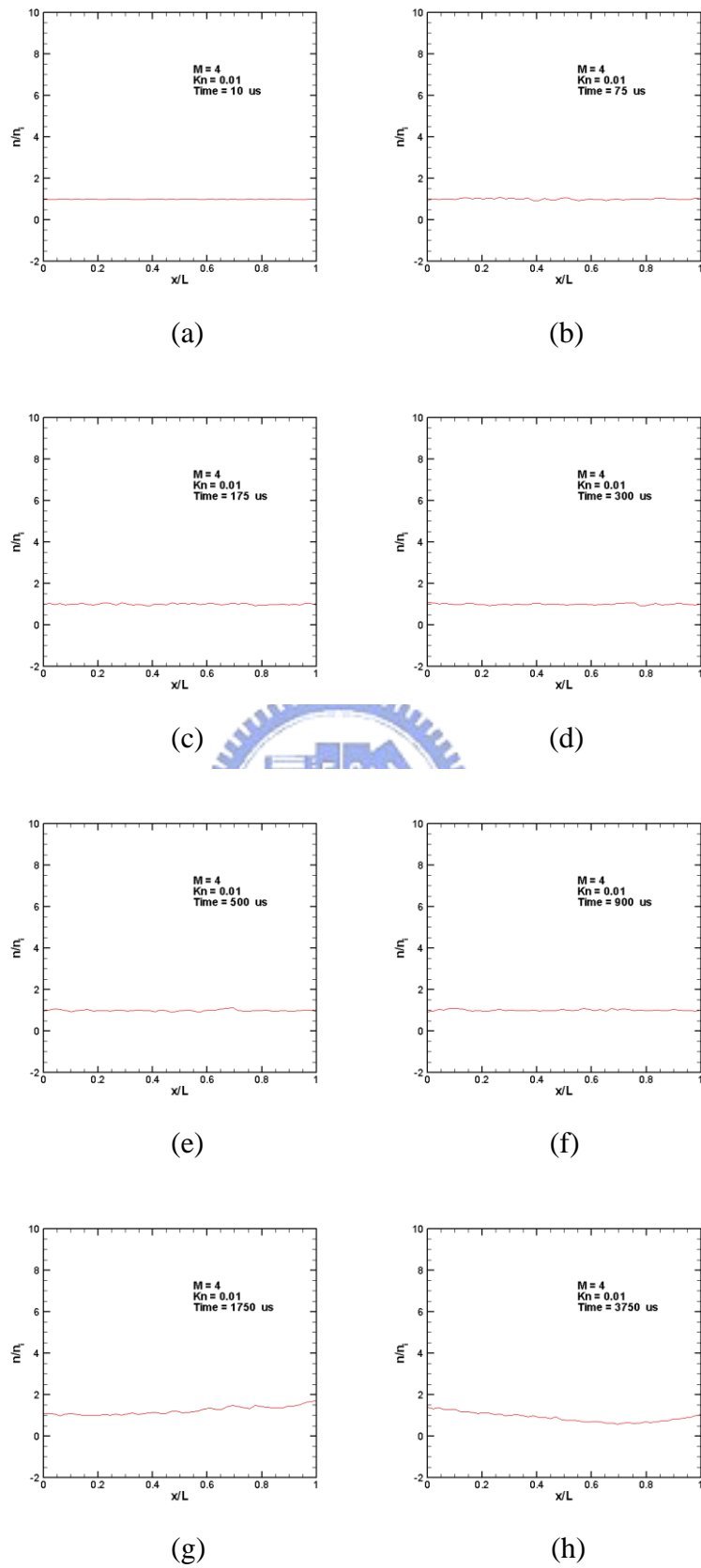


**Fig. 3.77** Profiles of number density for  $M=4$ ,  $Kn=0.01$  along horizontal lines through geometric center ( $y/L=0.5$ ) at  $t=10 \sim 3750 \mu s$ .

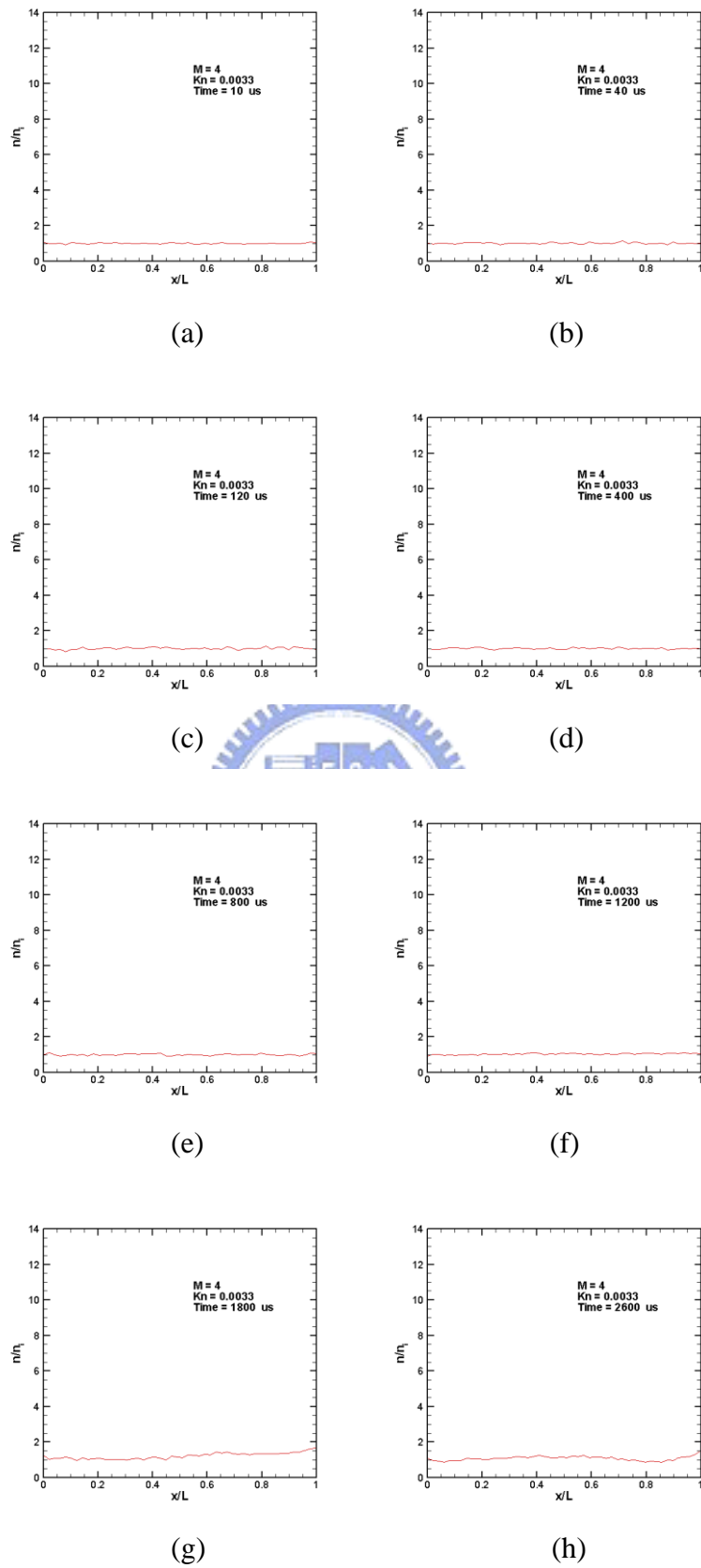


**Fig. 3.78** Profiles of number density for  $M=4$ ,  $Kn=0.0033$  along horizontal lines through geometric center ( $y/L=0.5$ ) at  $t=10 \sim 2600 \mu s$ .

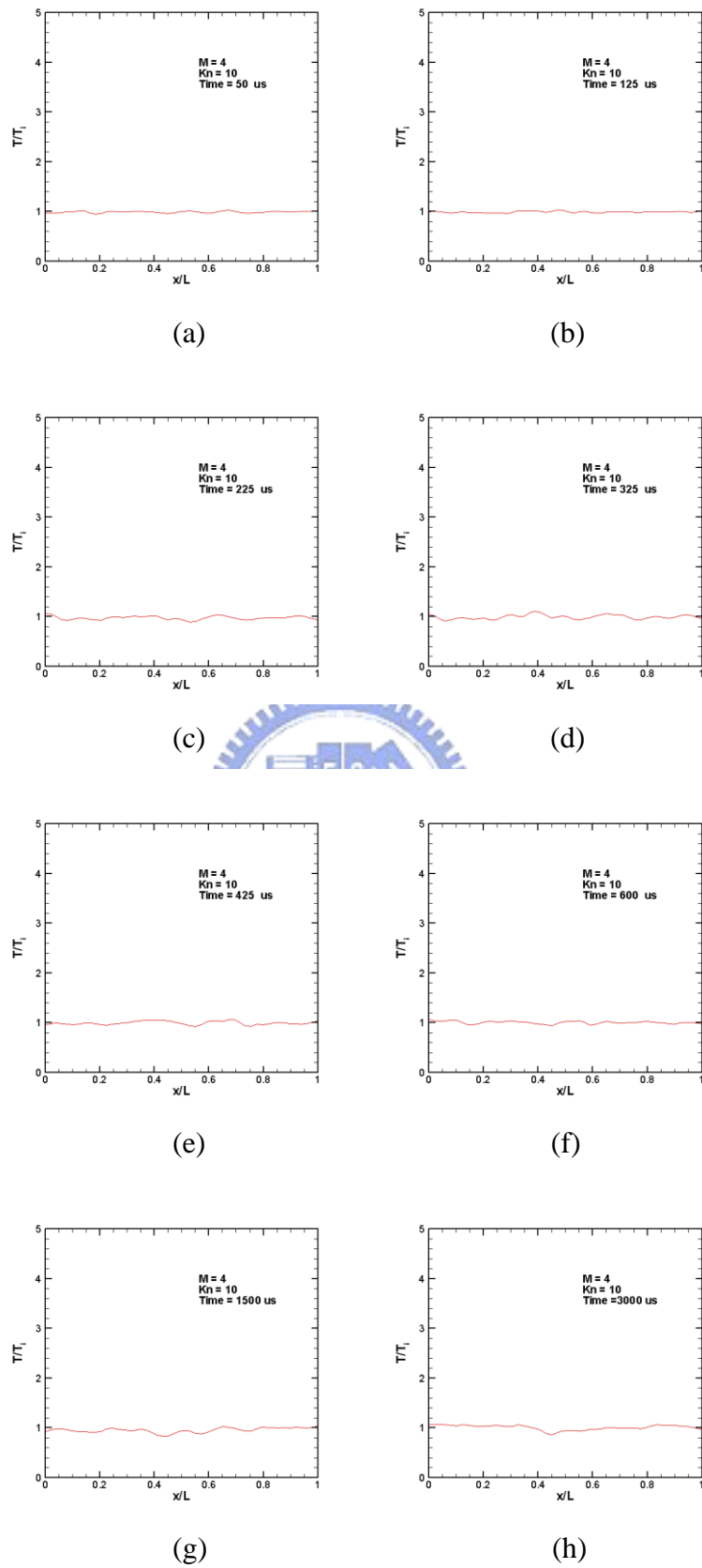


**Fig. 3.79** Profiles of temperature for  $M=4$ ,  $Kn=10$  along horizontal lines through geometric center ( $y/L=0.5$ ) at  $=50 \sim 3000 \mu s$ .

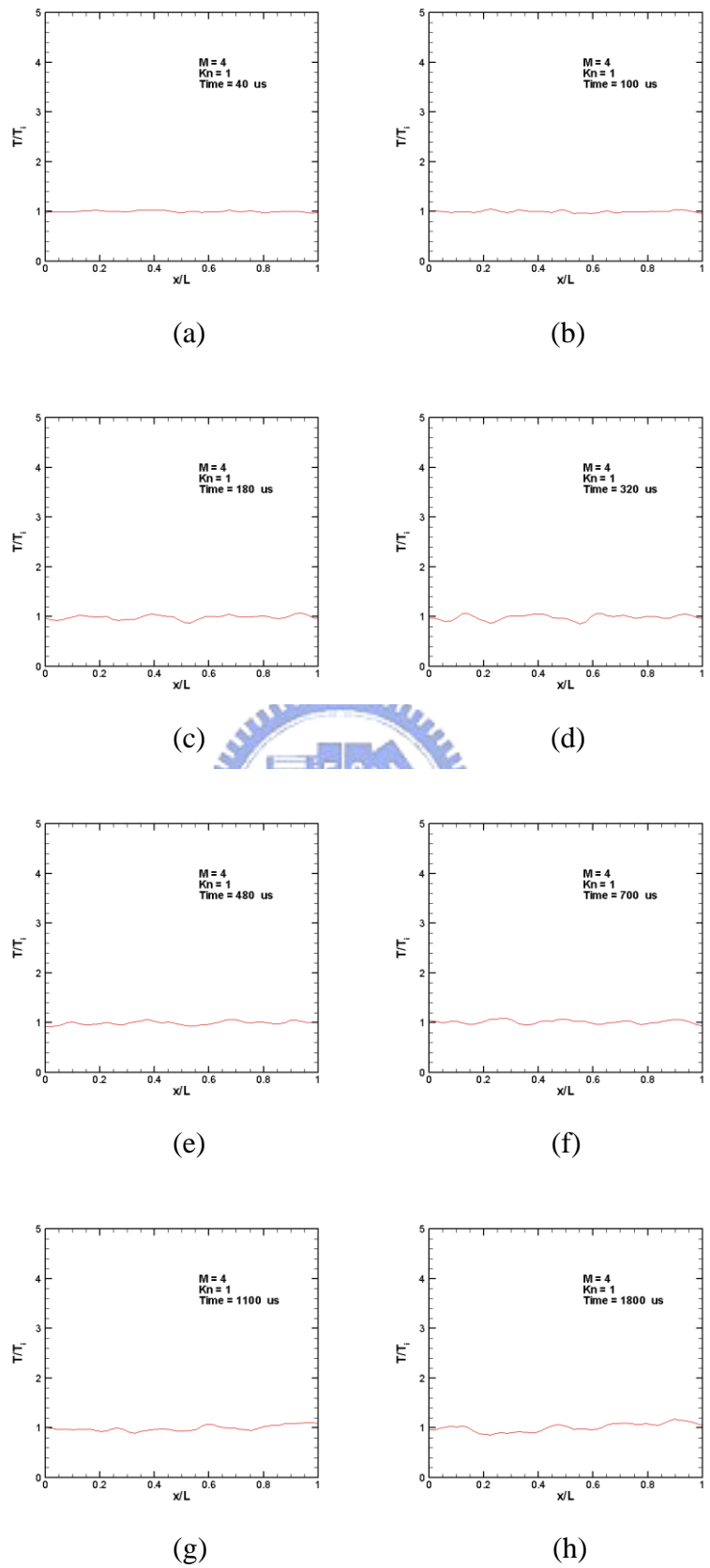


**Fig. 3.80** Profiles of temperature for  $M=4$ ,  $Kn=1$  along horizontal lines through geometric center ( $y/L=0.5$ ) at  $t=40 \sim 1800 \mu s$ .

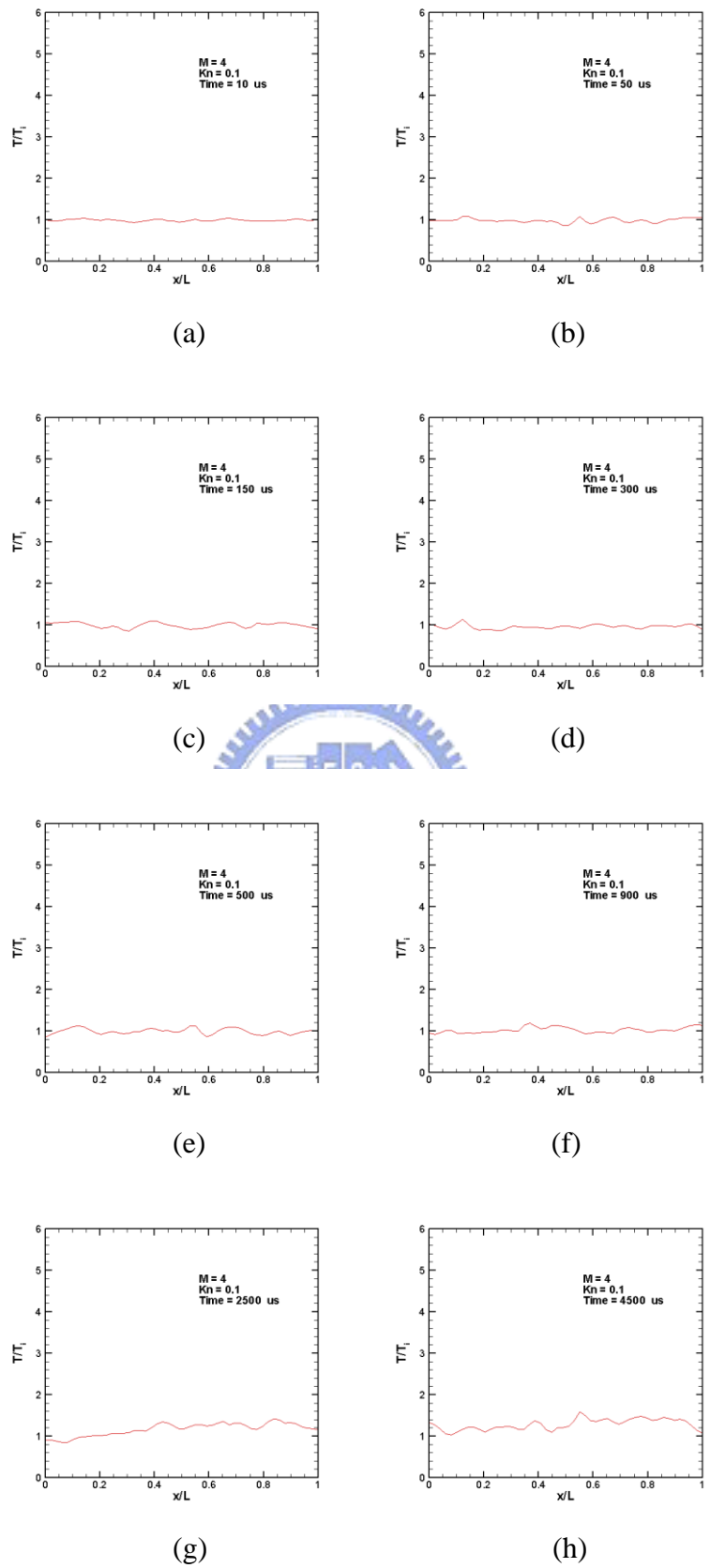


**Fig. 3.81** Profiles of temperature for  $M=4$ ,  $Kn=0.1$  along horizontal lines through geometric center ( $y/L=0.5$ ) at  $t=10 \sim 4500 \mu s$ .

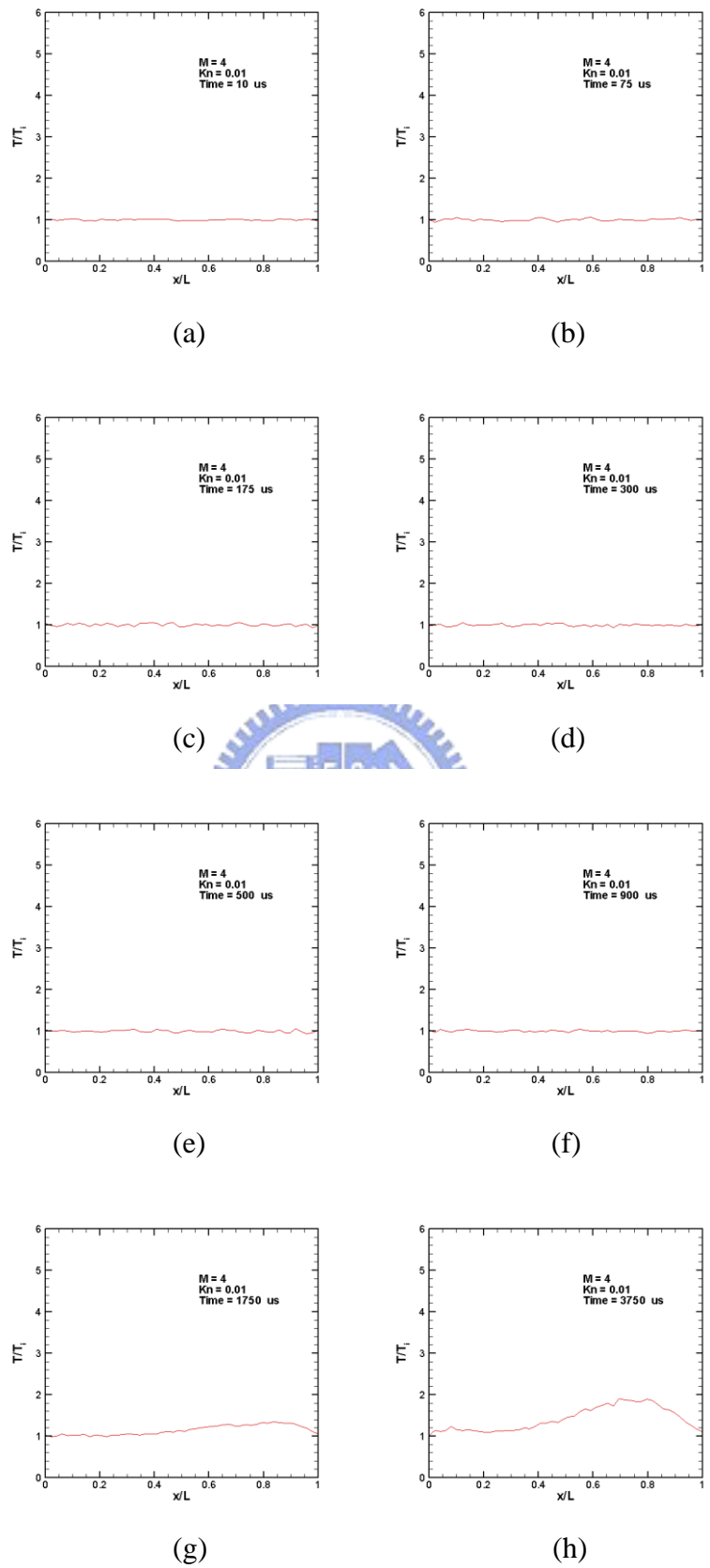


**Fig. 3.82** Profiles of temperature for  $M=4$ ,  $Kn=0.01$  along horizontal lines through geometric center ( $y/L=0.5$ ) at  $t=10 \sim 3750 \mu s$ .



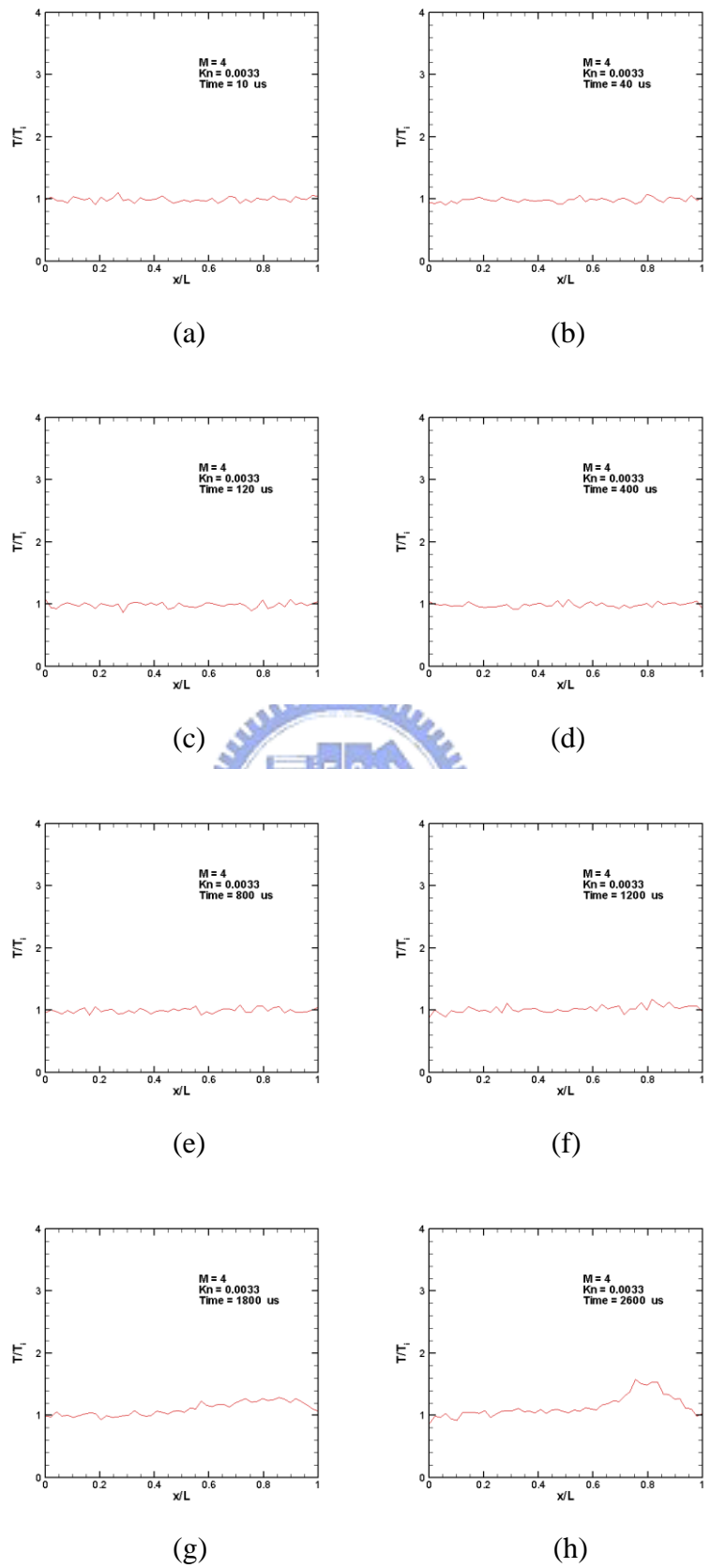


**Fig. 3.83** Profiles of temperature for  $M=4$ ,  $Kn=0.0033$  along horizontal lines through geometric center ( $y/L=0.5$ ) at  $t=10 \sim 2600 \mu s$ .

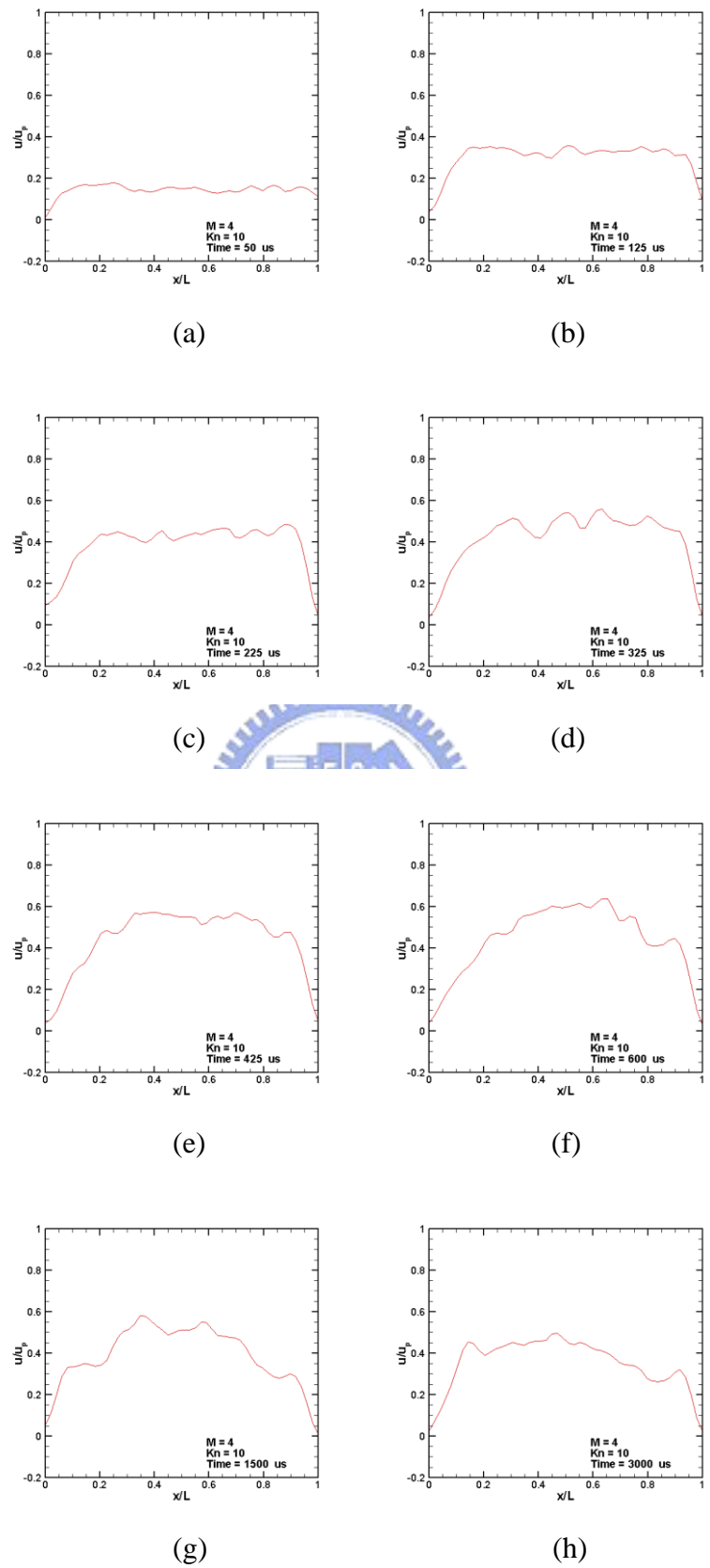


**Fig. 3.84** Profiles of  $u$ -velocity for  $M=4$ ,  $Kn=10$  along horizontal lines through upper wall ( $y/L=0.9875$ ) at  $=50 \sim 3000 \mu s$ .

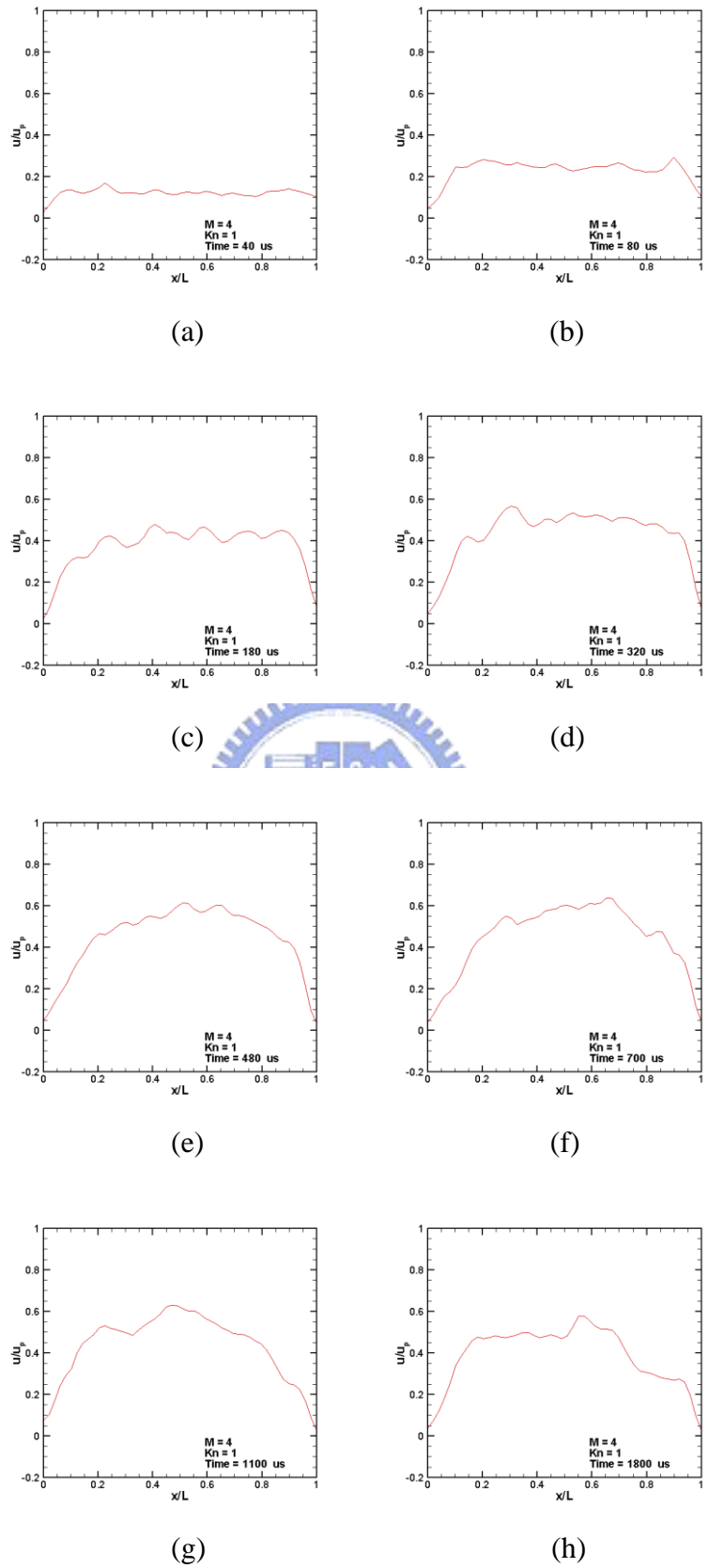


**Fig. 3.85** Profiles of  $u$ -velocity for  $M=4$ ,  $Kn=1$  along horizontal lines through upper wall ( $y/L=0.9875$ ) at  $t = 40 \sim 1800 \mu s$ .

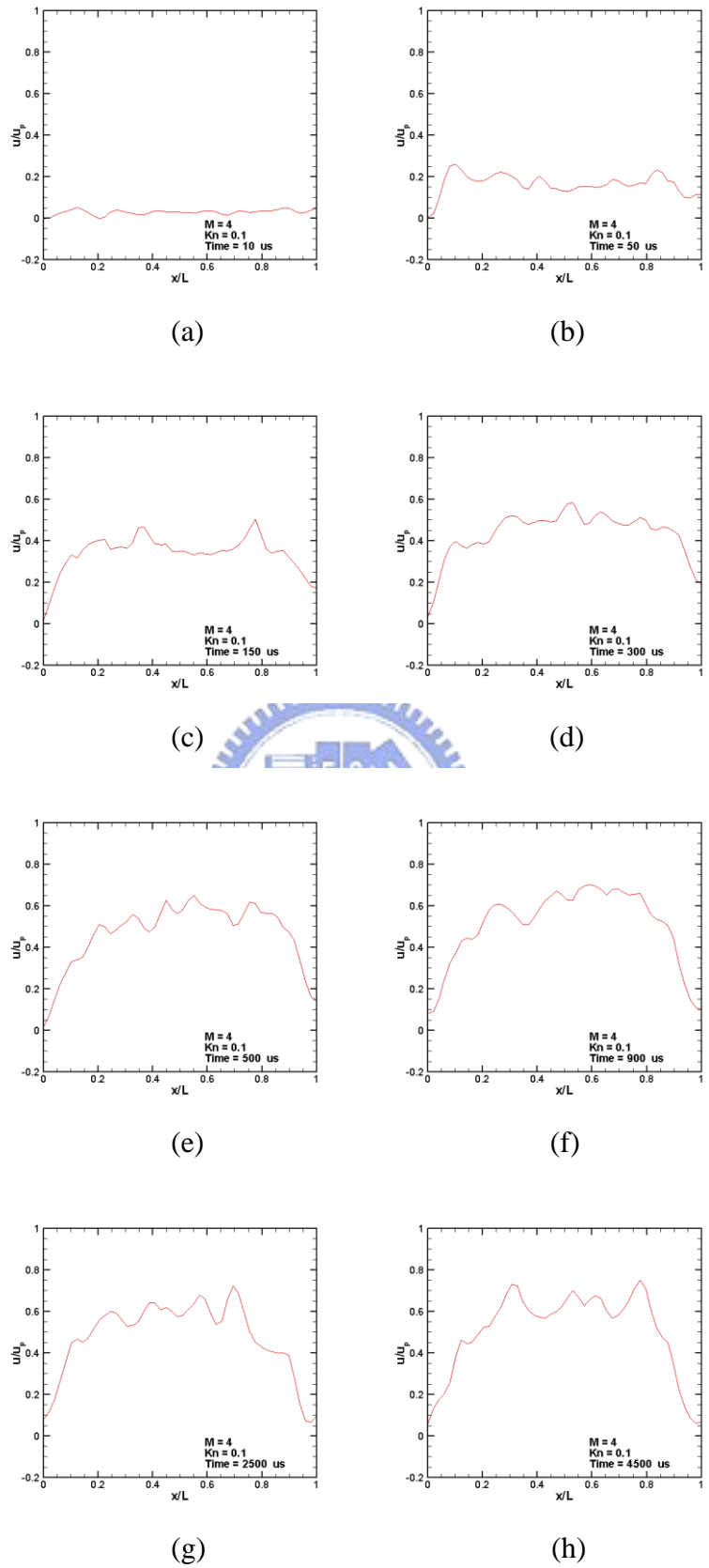


**Fig. 3.86** Profiles of  $u$ -velocity for  $M=4$ ,  $Kn=0.1$  along horizontal lines through upper wall ( $y/L=0.9875$ ) at  $t=10 \sim 4500 \mu s$ .

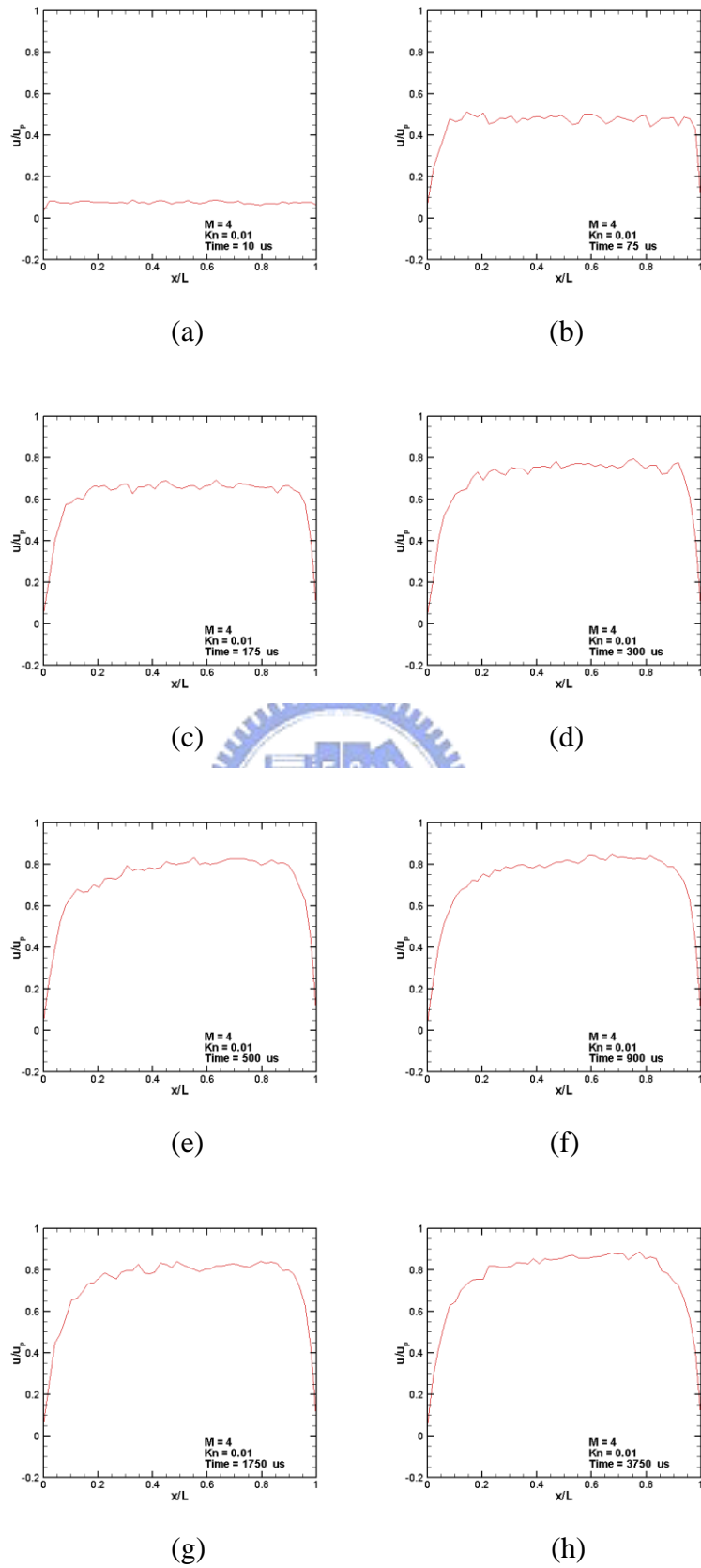


**Fig. 3.87** Profiles of  $u$ -velocity for  $M=4$ ,  $Kn=0.01$  along horizontal lines through upper wall ( $y/L=0.995$ ) at  $t=10 \sim 3750 \mu s$ .

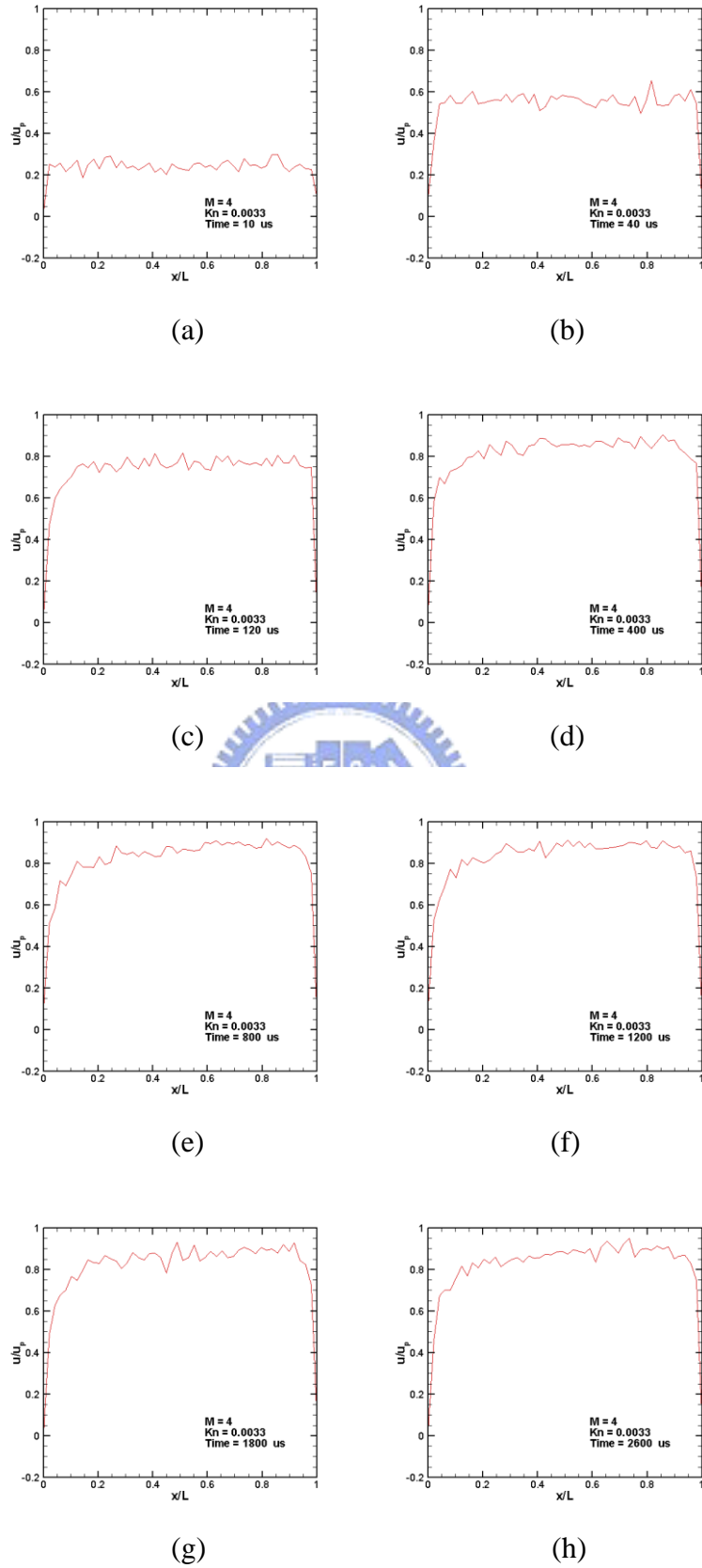


**Fig. 3.88** Profiles of  $u$ -velocity for  $M=4$ ,  $Kn=0.0033$  along horizontal lines through upper wall ( $y/L=0.9983$ ) at  $t=10 \sim 2600 \mu s$ .

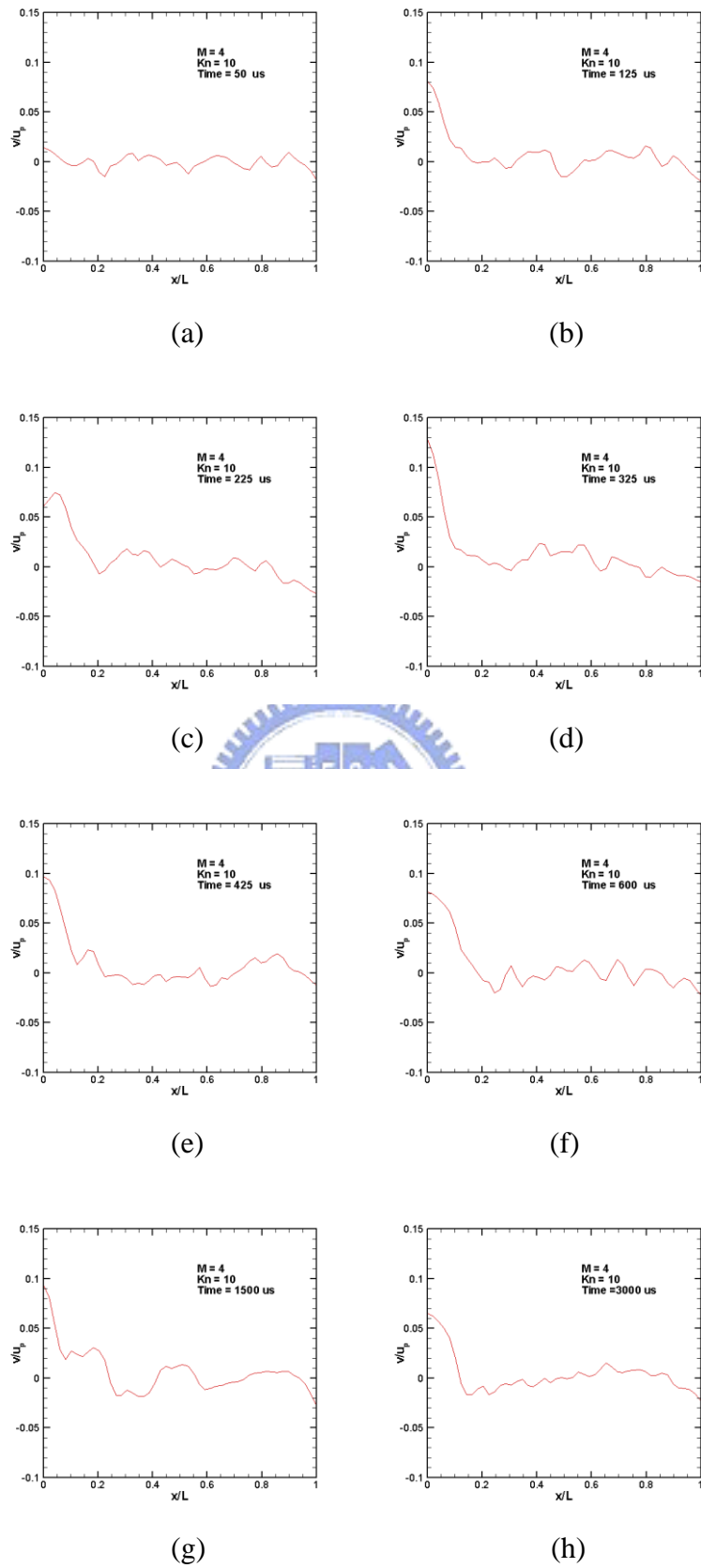


**Fig. 3.89** Profiles of v-velocity for  $M=4$ ,  $Kn=10$  along horizontal lines through upper wall ( $y/L=0.9875$ ) at  $=50 \sim 3000 \mu s$ .

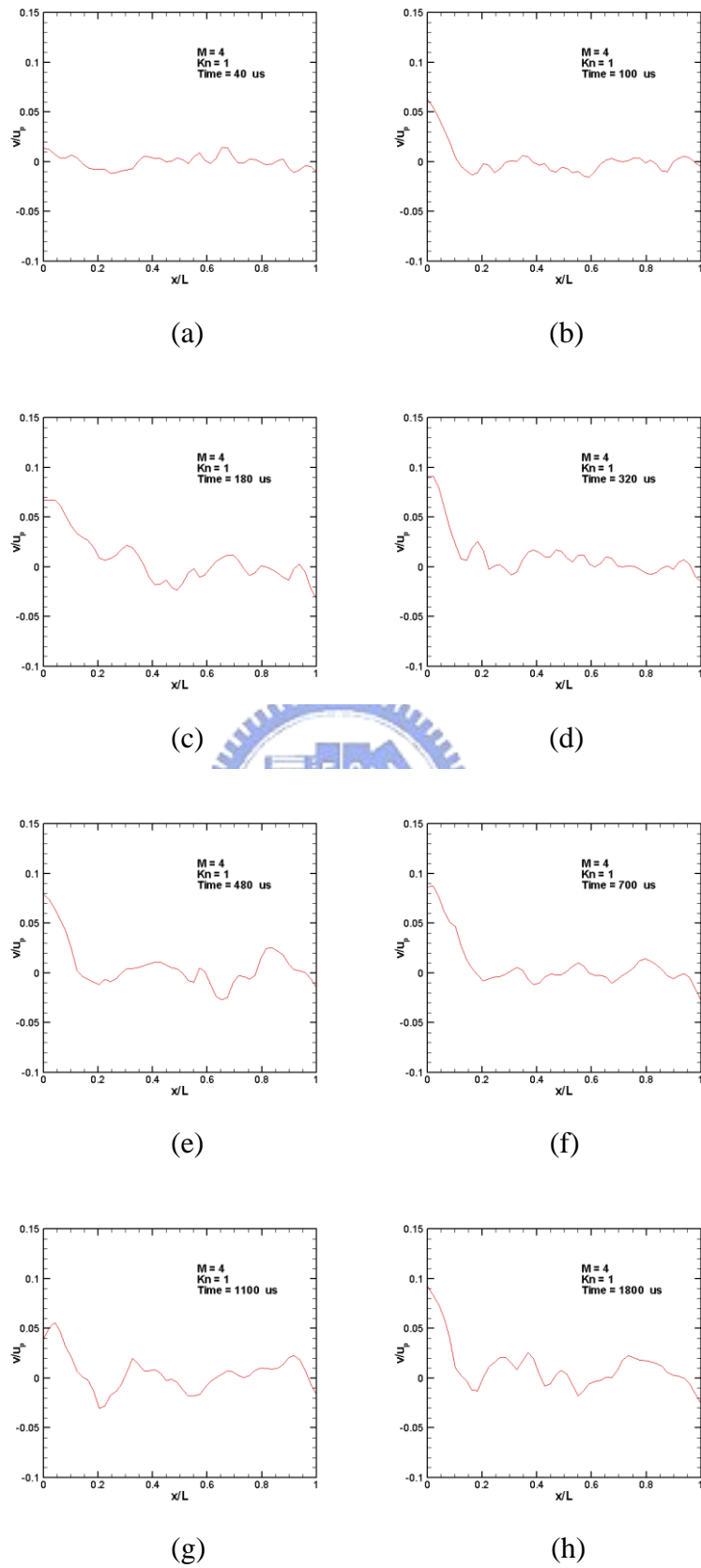


**Fig. 3.90** Profiles of  $v$ -velocity for  $M=4$ ,  $Kn=1$  along horizontal lines through upper wall ( $y/L=0.9875$ ) at  $t=40 \sim 1800 \mu s$ .



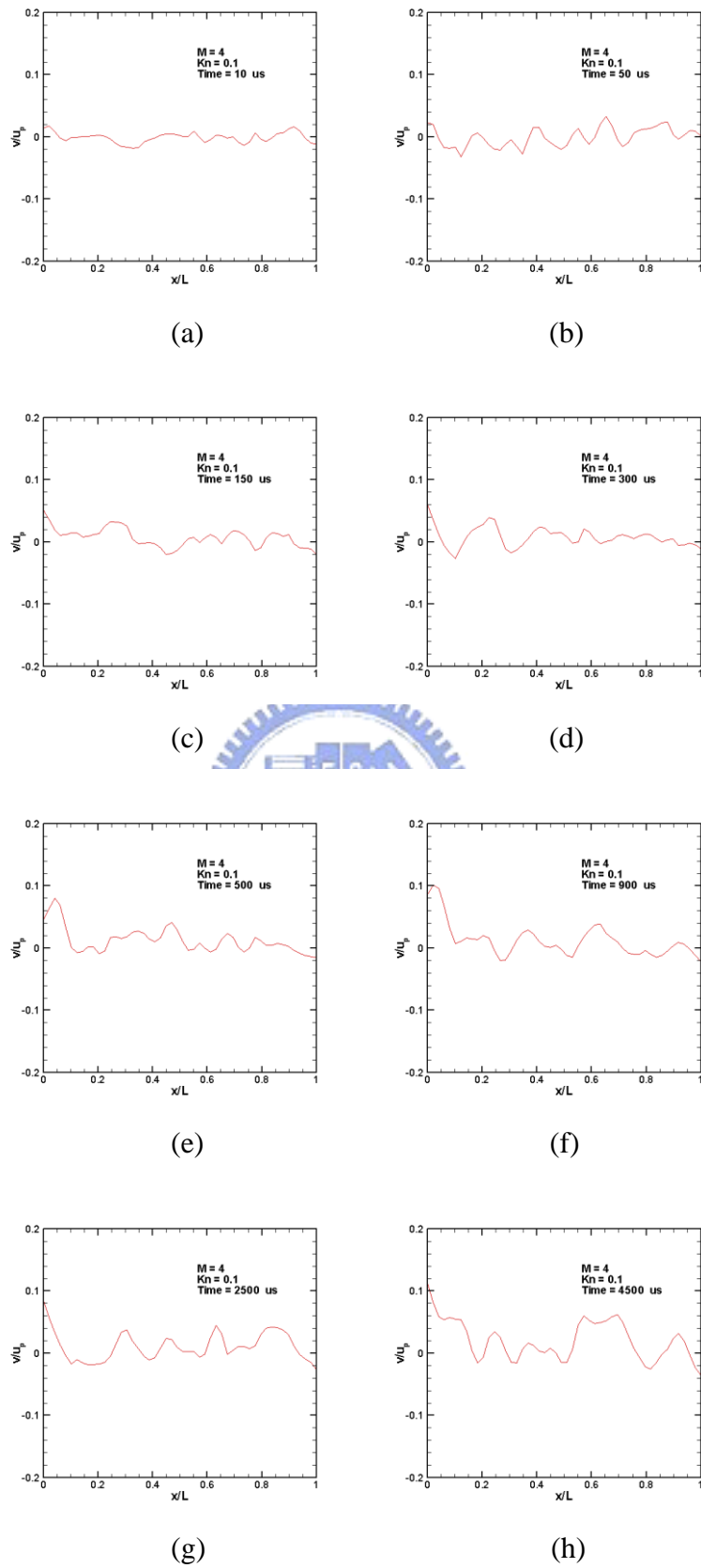


**Fig. 3.91** Profiles of  $v$ -velocity for  $M=4$ ,  $Kn=0.1$  along horizontal lines through upper wall ( $y/L=0.9875$ ) at  $t=10 \sim 4500 \mu s$ .

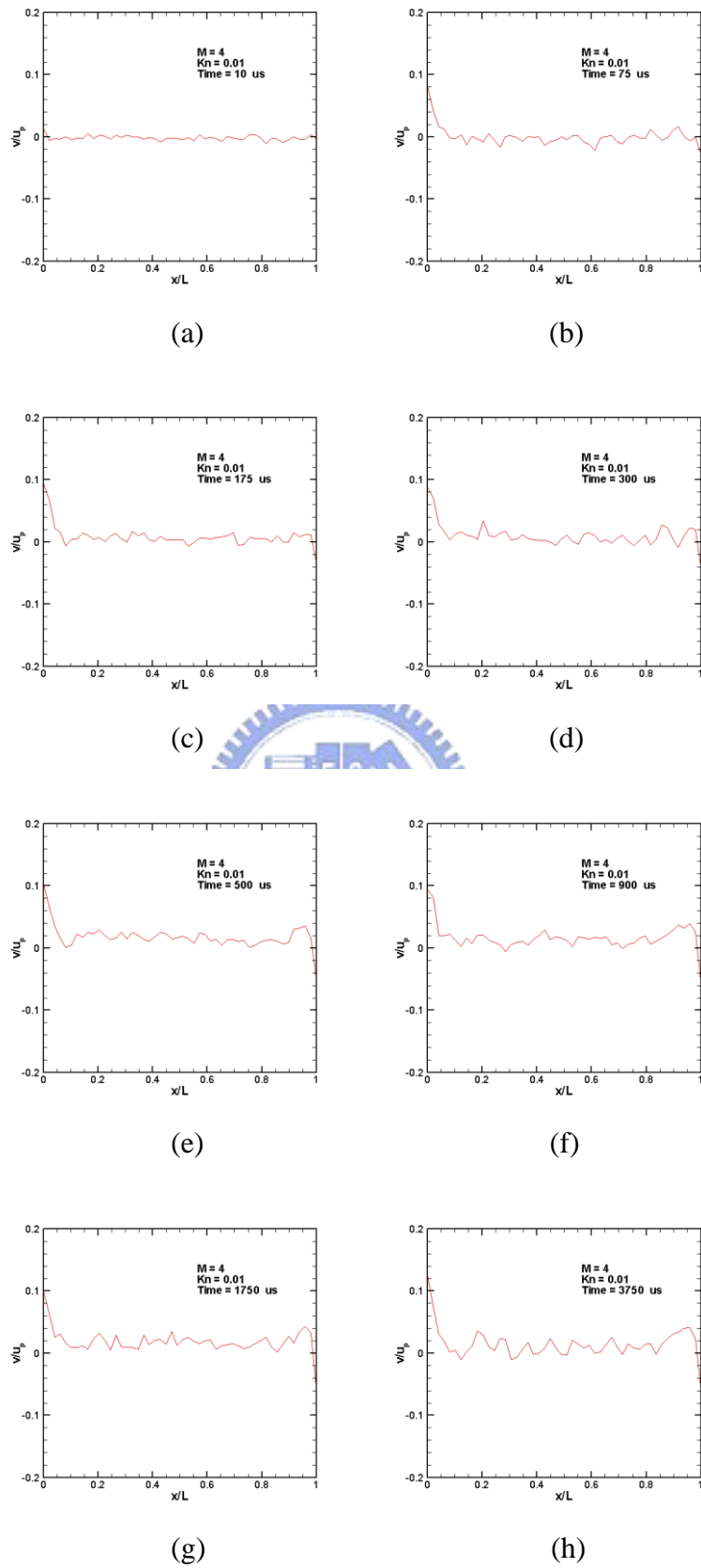


**Fig. 3.92** Profiles of  $v$ -velocity for  $M=4$ ,  $Kn=0.01$  along horizontal lines through upper wall ( $y/L=0.995$ ) at  $t=10 \sim 3750 \mu s$ .

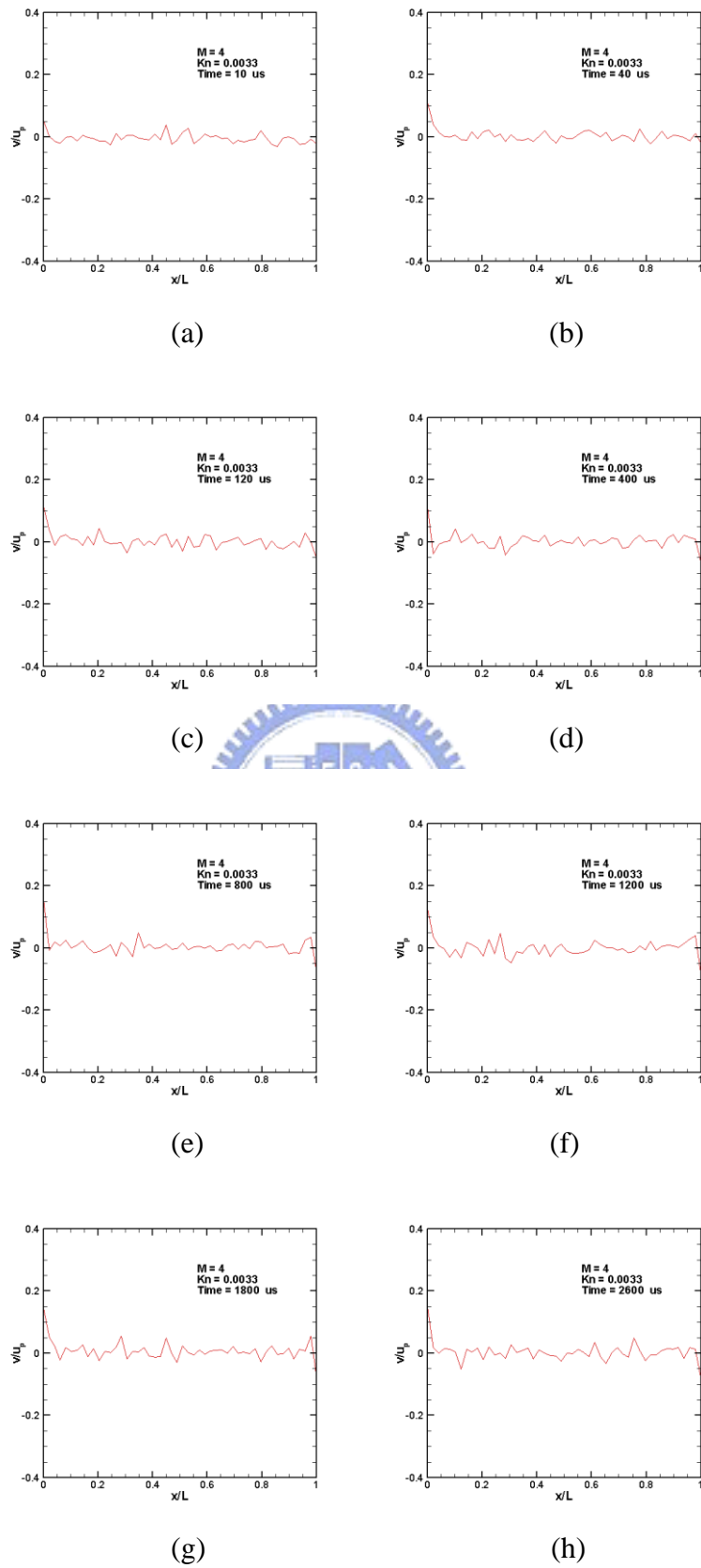


**Fig. 3.93** Profiles of v-velocity for  $M=4$ ,  $Kn=0.0033$  along horizontal lines through upper wall ( $y/L=0.9983$ ) at  $t=10 \sim 2600 \mu s$ .

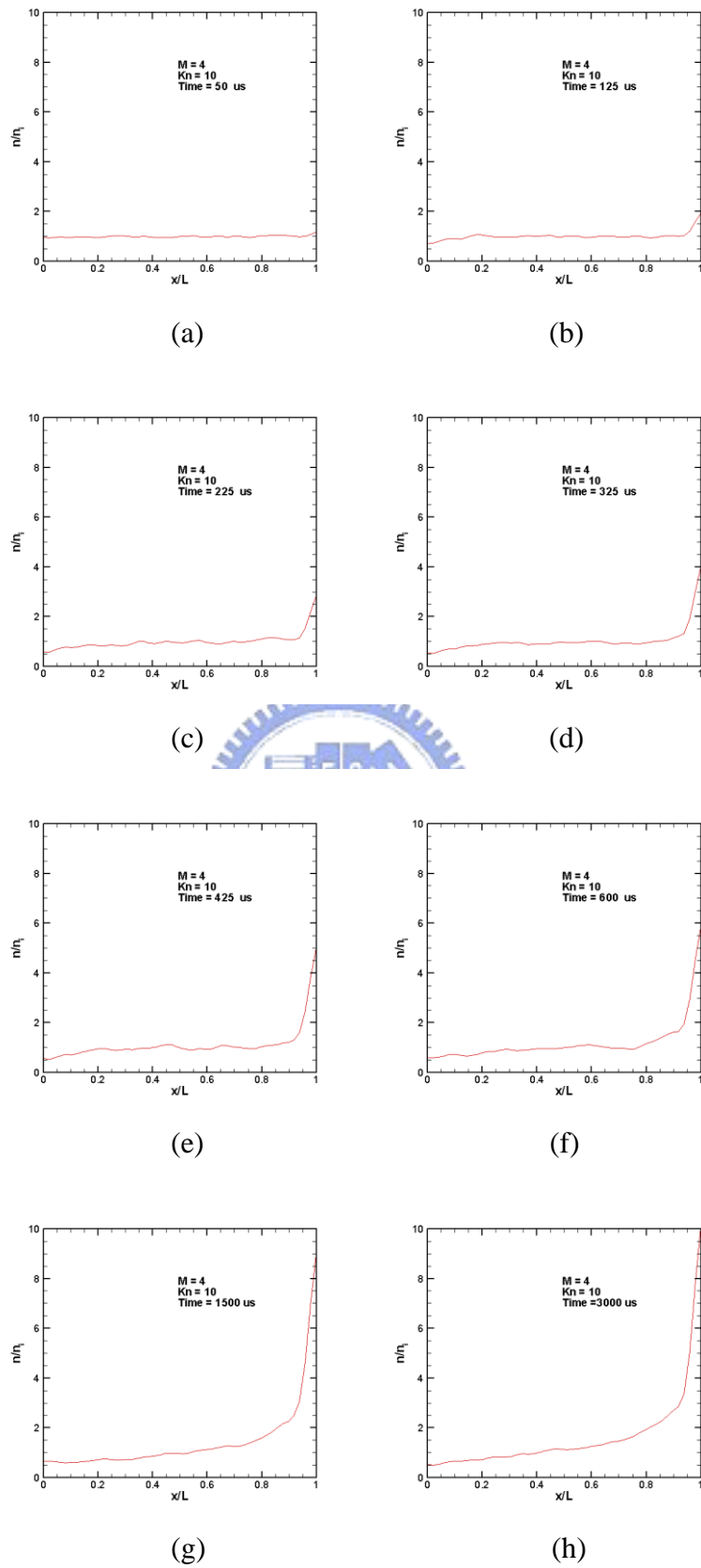


**Fig. 3.94** Profiles of number density for  $M=4$ ,  $Kn=10$  along horizontal lines through upper wall ( $y/L=0.9875$ ) at  $=50 \sim 3000 \mu s$ .

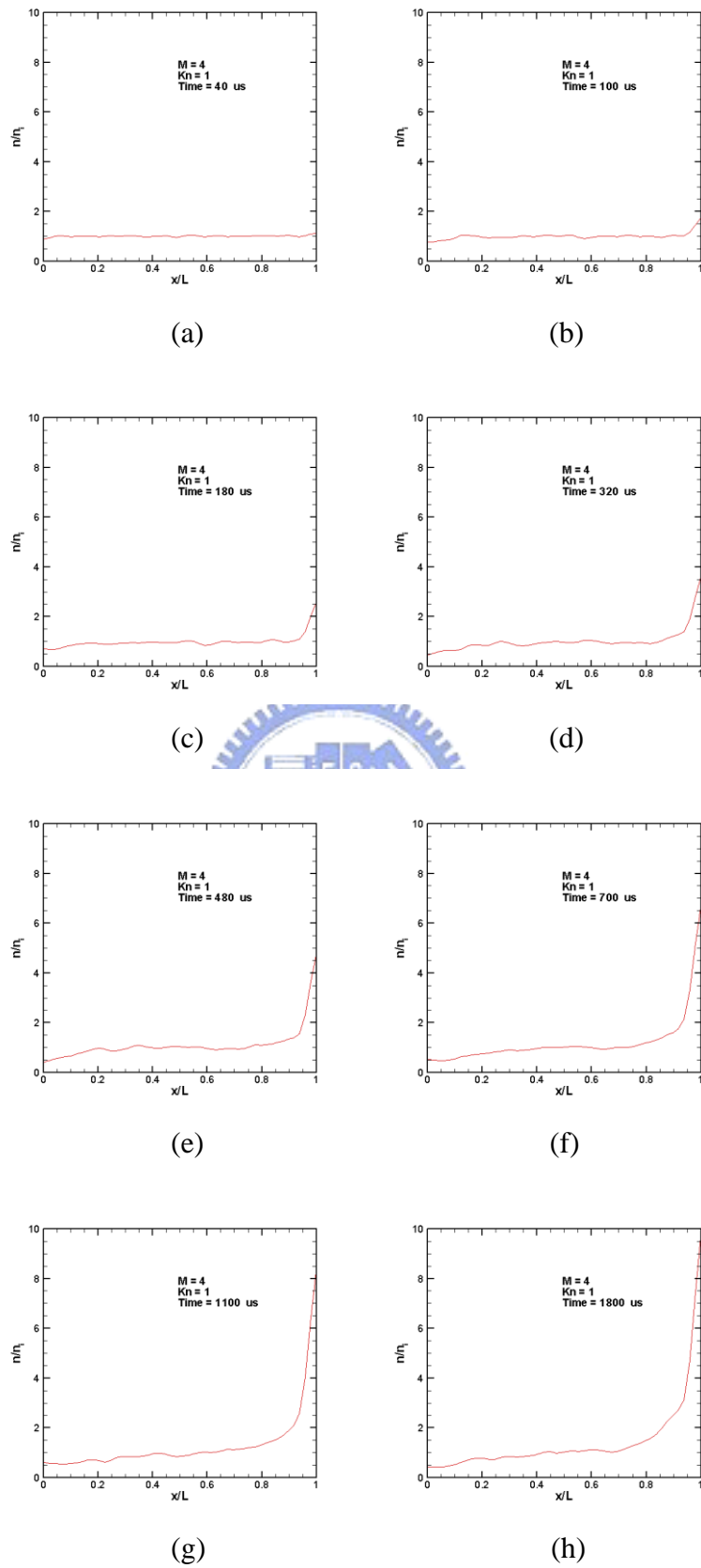


**Fig. 3.95** Profiles of number density for  $M=4$ ,  $Kn=1$  along horizontal lines through upper wall ( $y/L=0.9875$ ) at  $t=40 \sim 1800 \mu s$ .

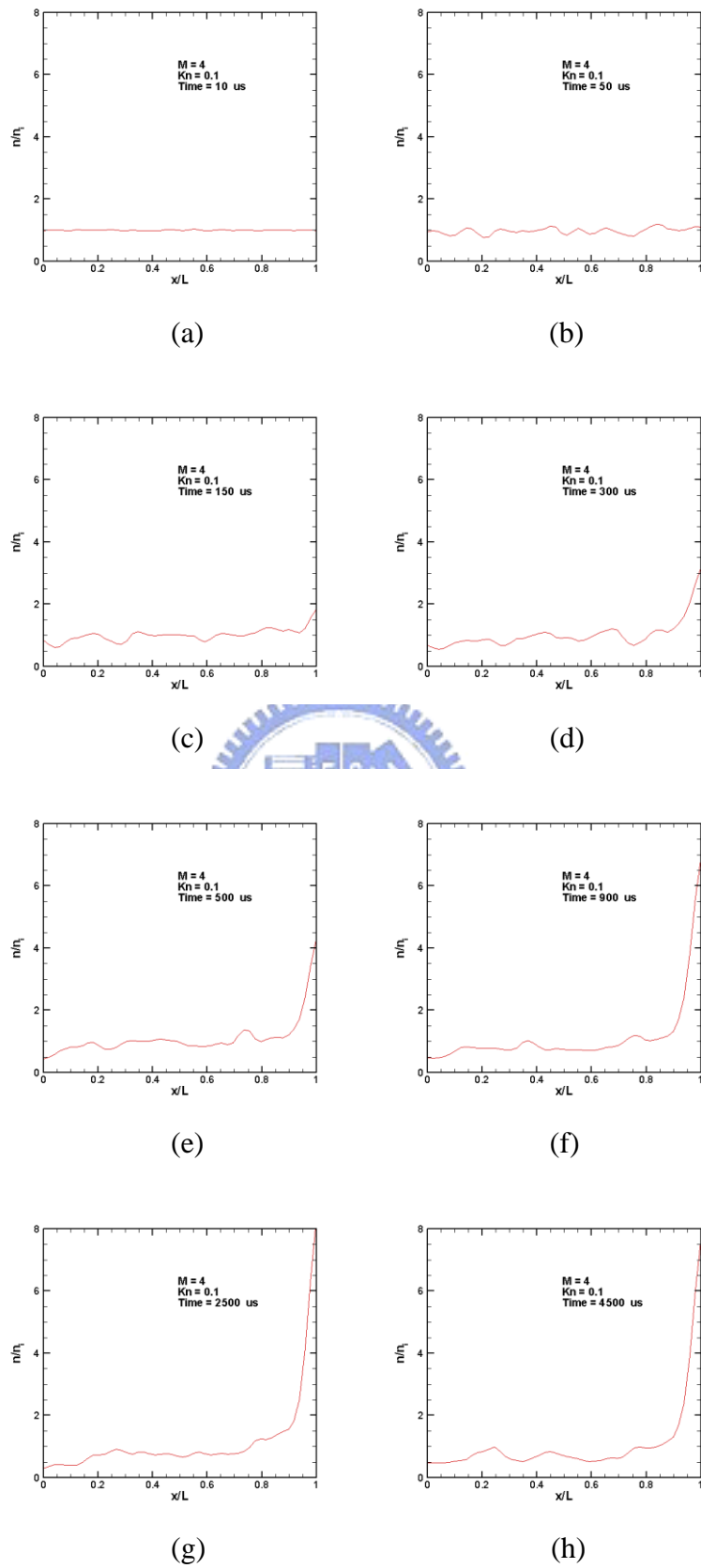


**Fig. 3.96** Profiles of number density for  $M=4$ ,  $Kn=0.1$  along horizontal lines through upper wall ( $y/L=0.9875$ ) at  $t=10 \sim 4500 \mu\text{s}$ .

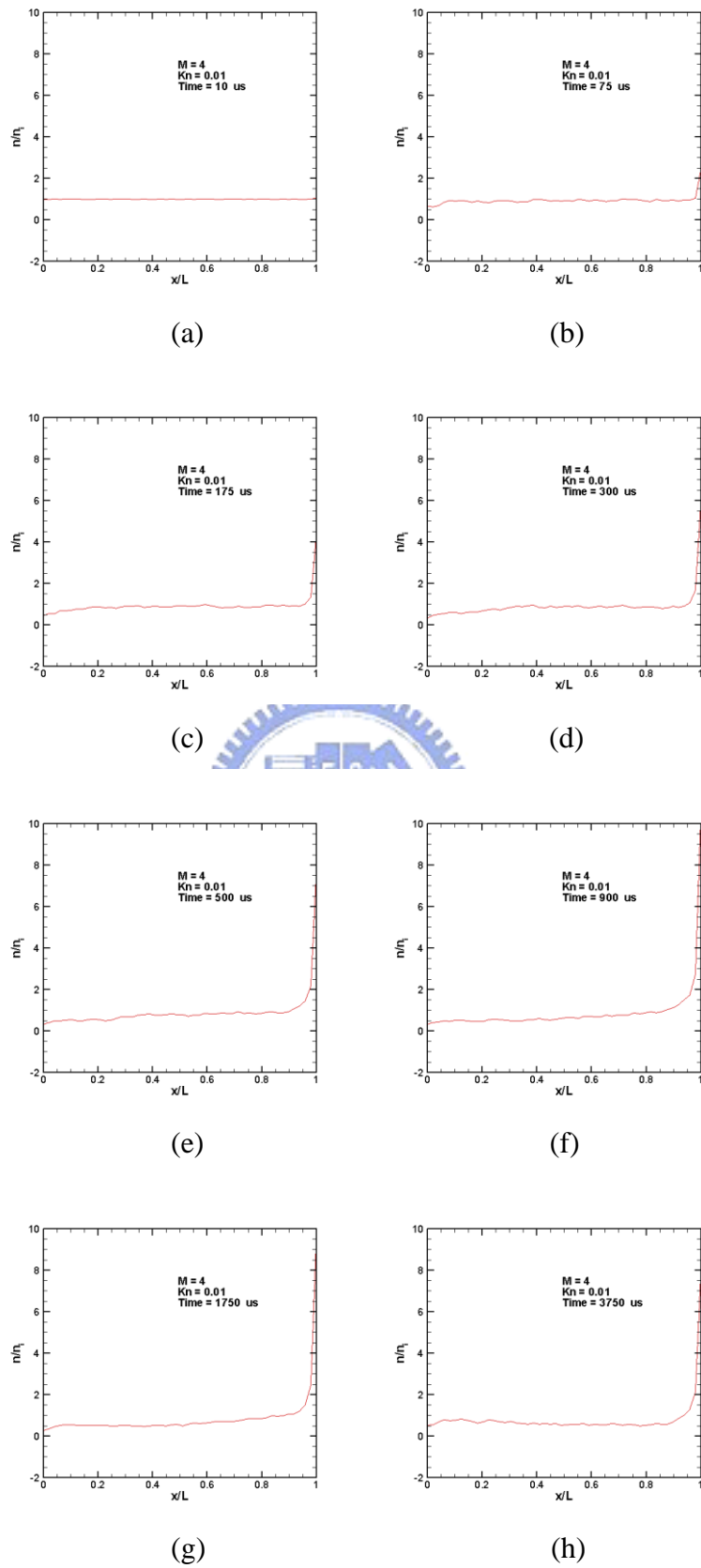


**Fig. 3.97** Profiles of number density for  $M=4$ ,  $Kn=0.01$  along horizontal lines through upper wall ( $y/L=0.995$ ) at  $t=10 \sim 3750 \mu s$ .

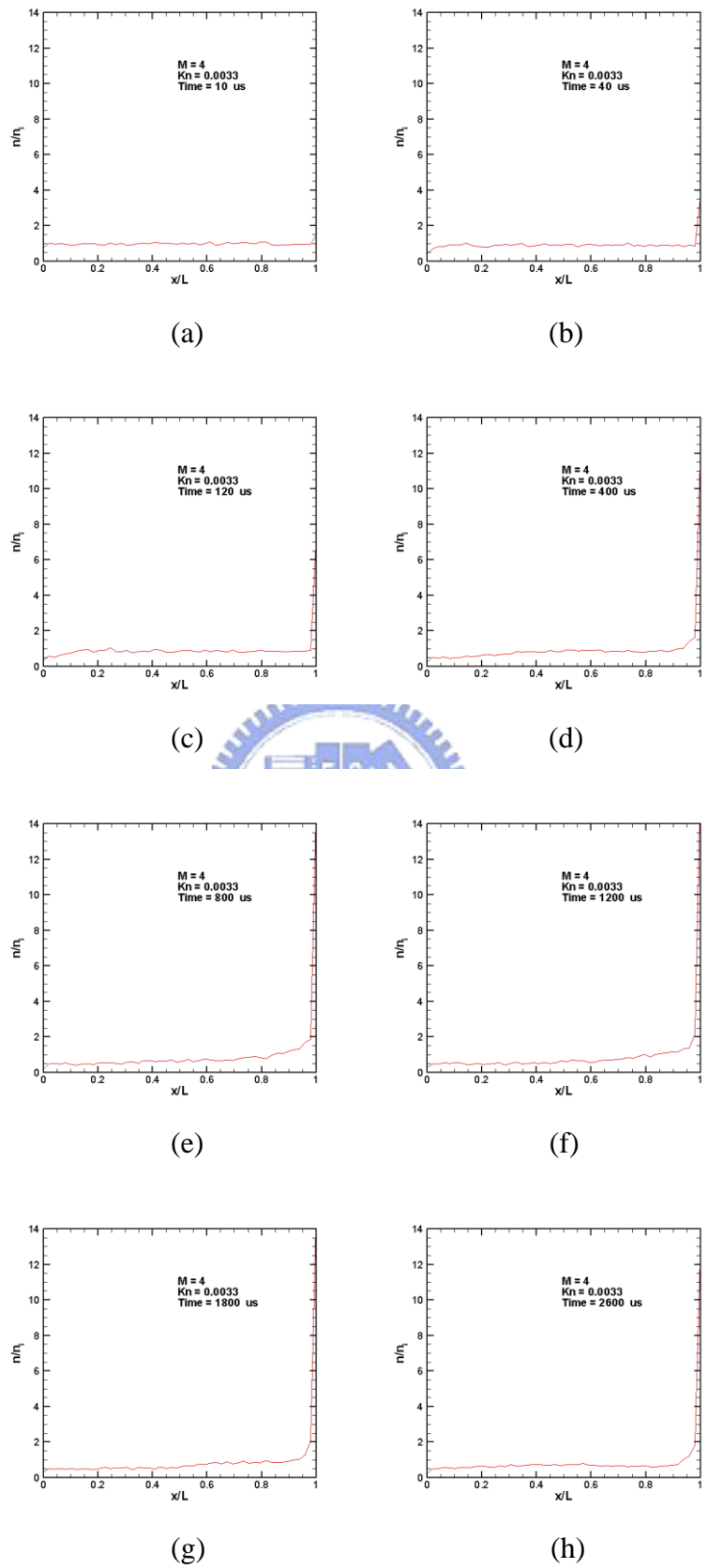


**Fig. 3.98** Profiles of number density for  $M=4$ ,  $Kn=0.0033$  along horizontal lines through upper wall ( $y/L=0.9983$ ) at  $t=10 \sim 2600 \mu s$ .



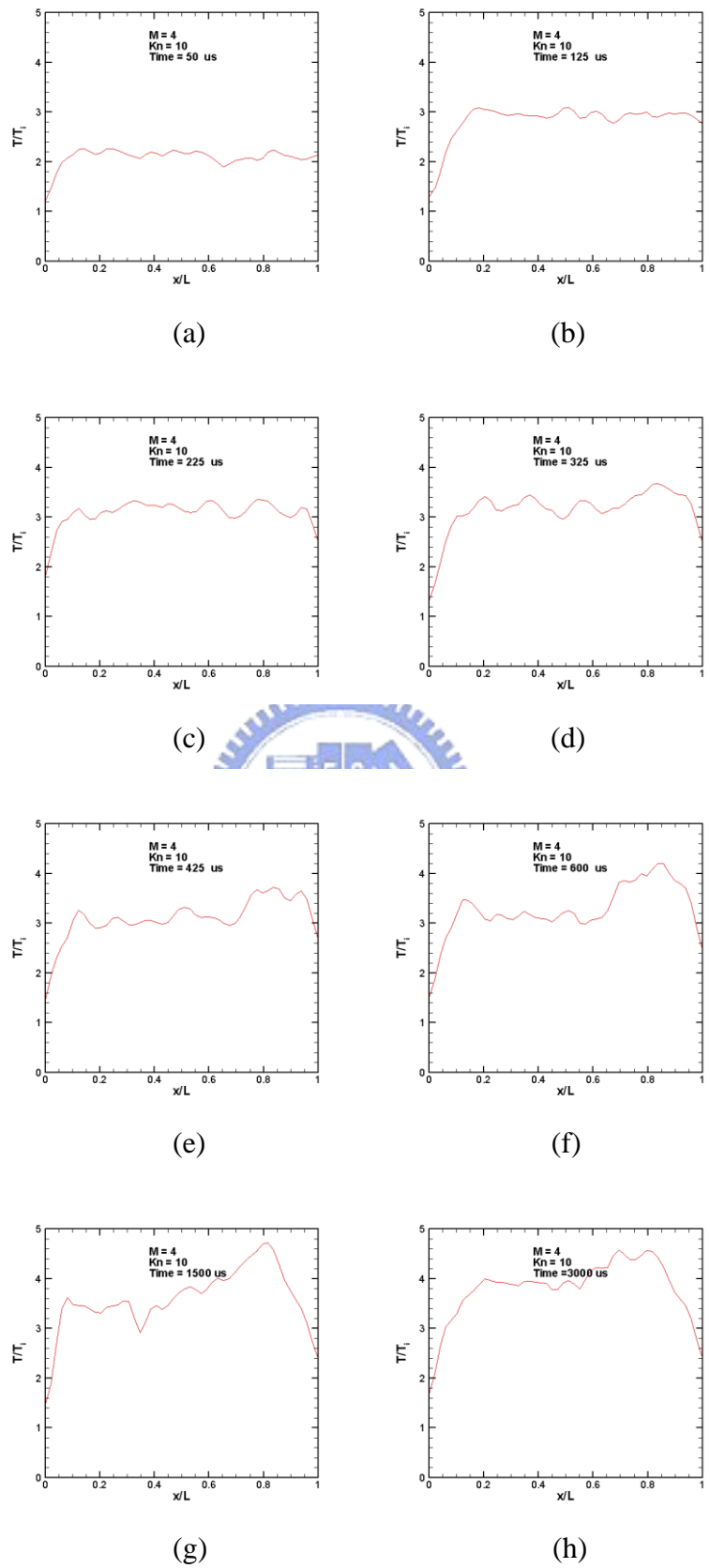


**Fig. 3.99** Profiles of temperature for  $M=4$ ,  $Kn=10$  along horizontal lines through upper wall ( $y/L=0.9875$ ) at  $=50 \sim 3000 \mu s$ .

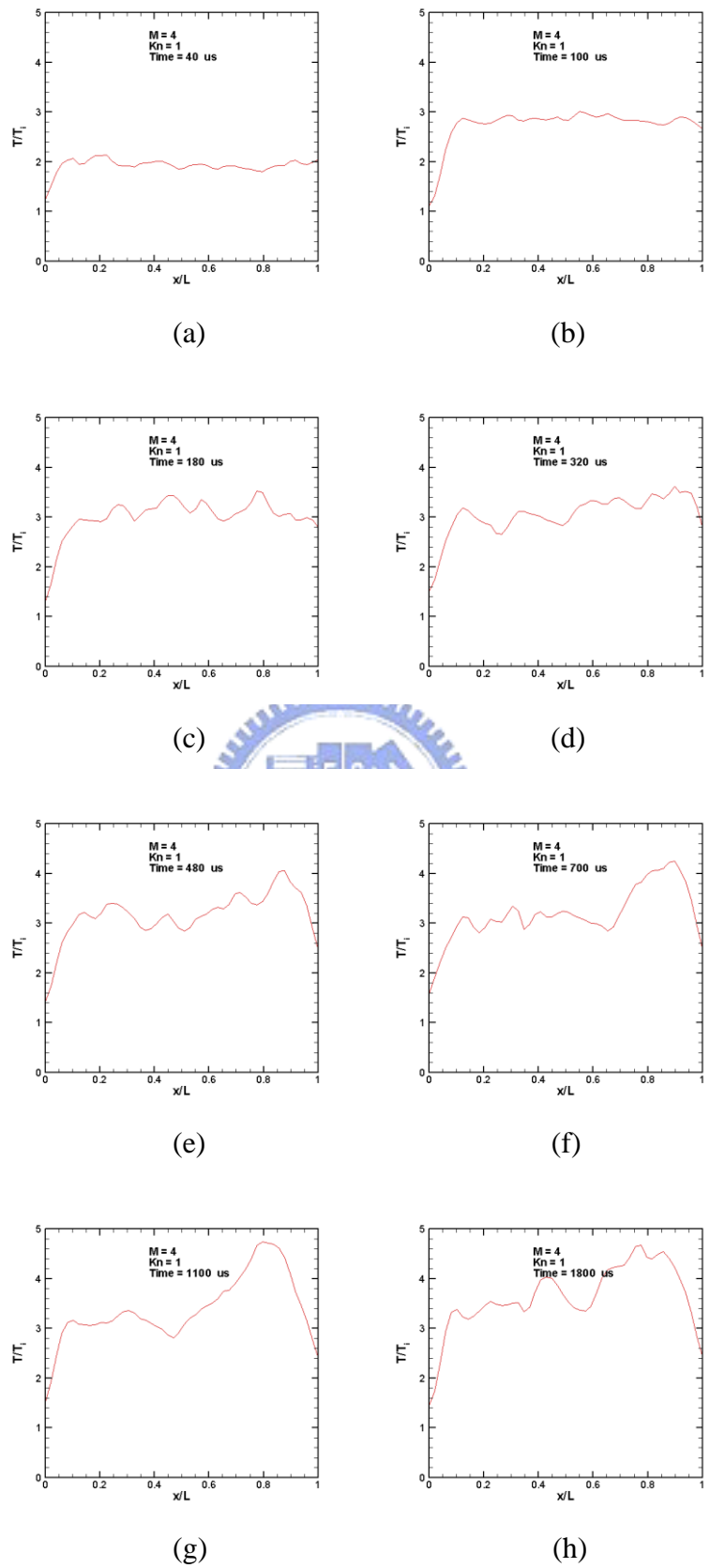


**Fig. 3.100** Profiles of temperature for  $M=4$ ,  $Kn=1$  along horizontal lines through upper wall ( $y/L=0.9875$ ) at  $t=40 \sim 1800 \mu s$ .

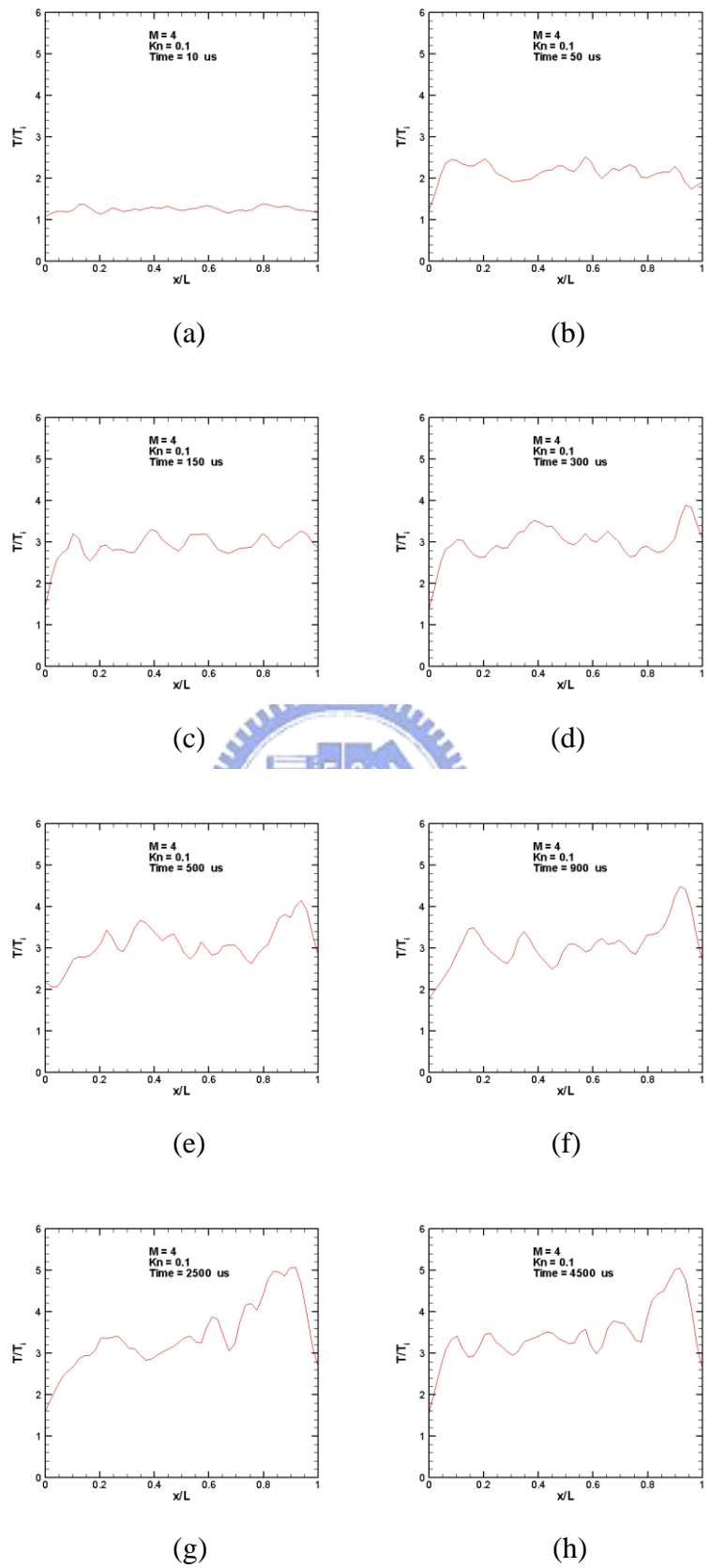


**Fig. 3.101** Profiles of temperature for  $M=4$ ,  $Kn=0.1$  along horizontal lines through upper wall ( $y/L=0.9875$ ) at  $t=10 \sim 4500 \mu s$ .

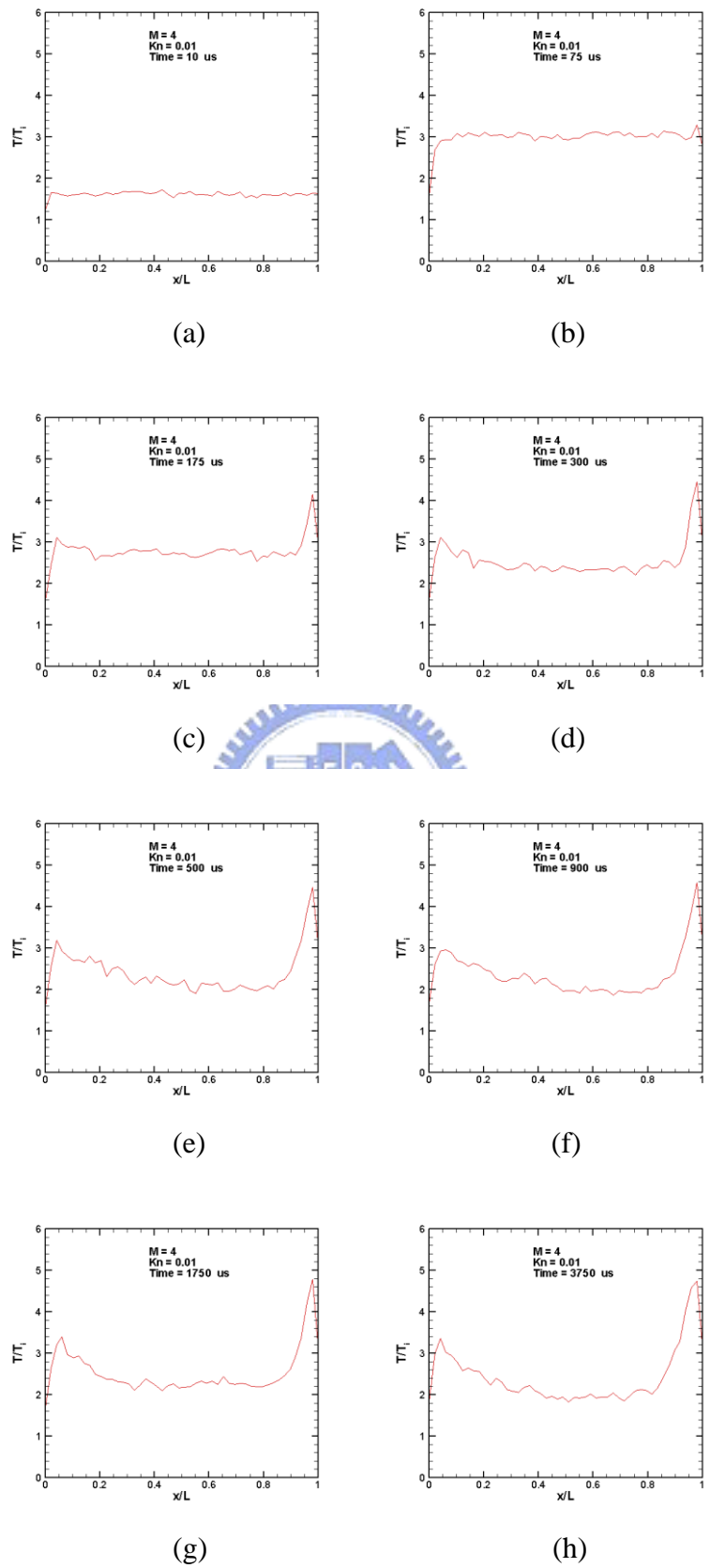


**Fig. 3.102** Profiles of temperature for  $M=4$ ,  $Kn=0.01$  along horizontal lines through upper wall ( $y/L=0.995$ ) at  $t=10 \sim 3750 \mu s$ .

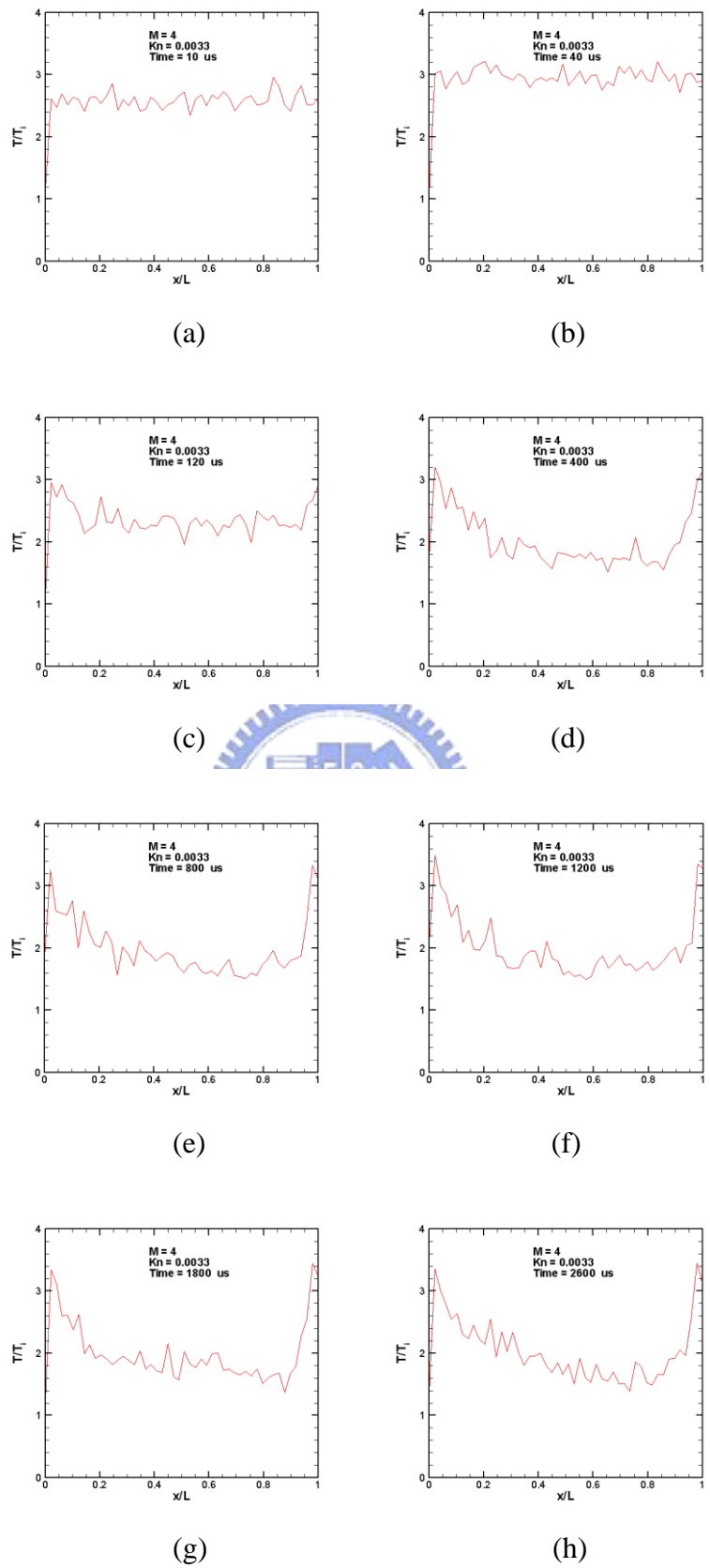
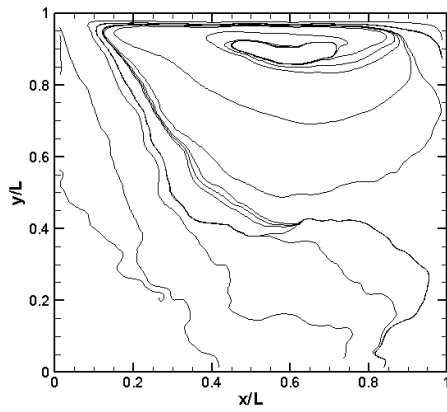
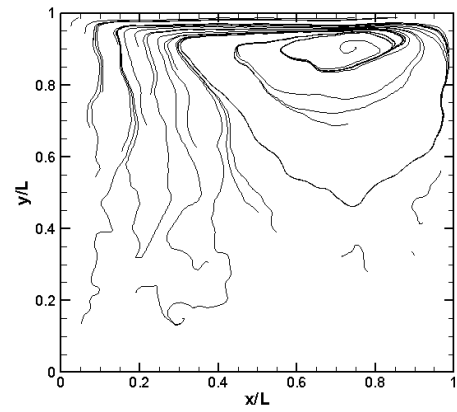


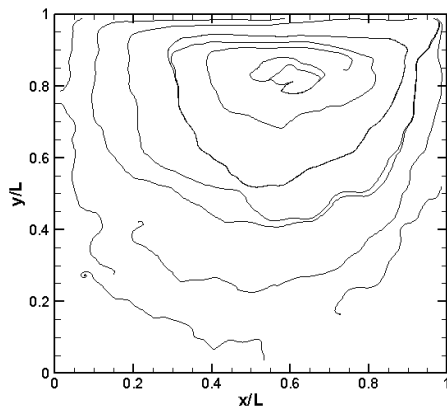
**Fig. 3.103** Profiles of temperature for  $M=4$ ,  $Kn=0.0033$  along horizontal lines through upper wall ( $y/L=0.9983$ ) at  $t=10 \sim 2600 \mu s$ .



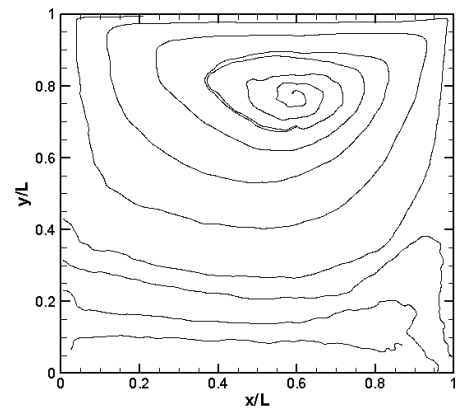
(a)



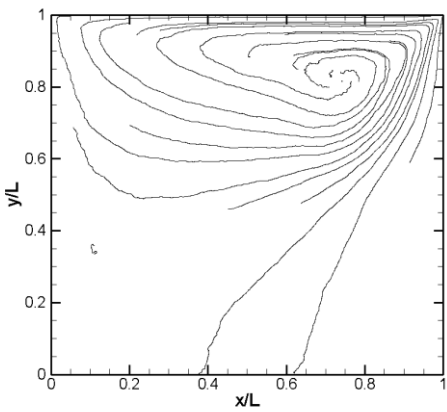
(b)



(c)



(d)



(e)

**Fig. 3.104** Streamline for  $M=4$  (a)  $Kn=10$ ; (b)  $Kn=1$ ; (c)  $Kn=0.1$ ; (d)  $Kn=0.01$ ; (e)  $Kn=0.0033$ .

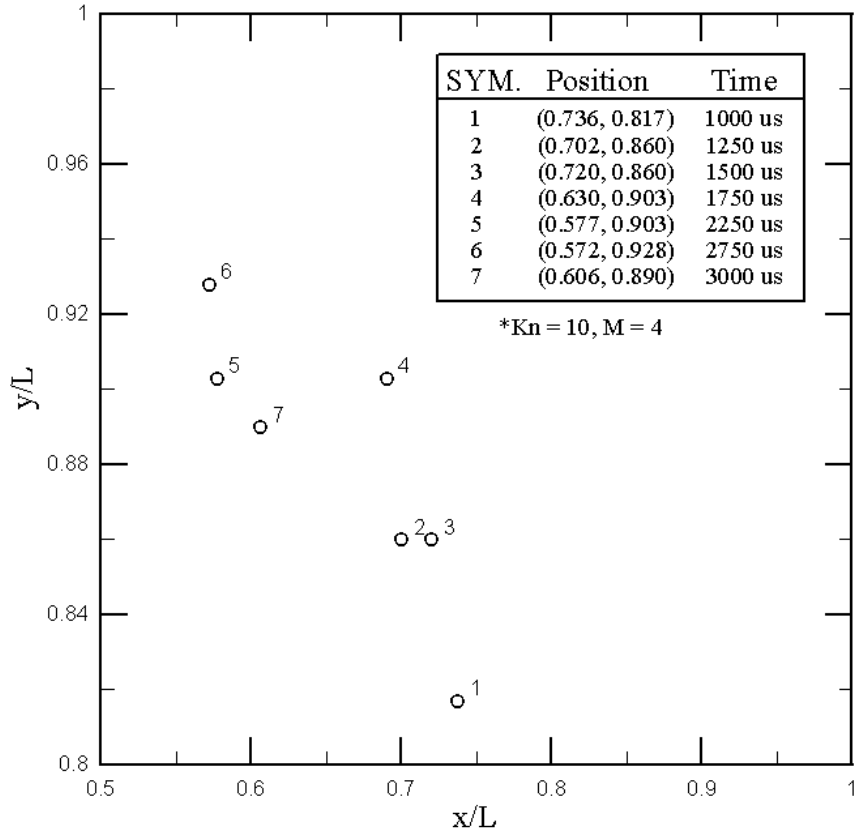


**Fig. 3.105** Positions of the center of the vortex for  $M=4$ ,  $Kn=10$  at  $1000 \sim 3000 \mu s$ .

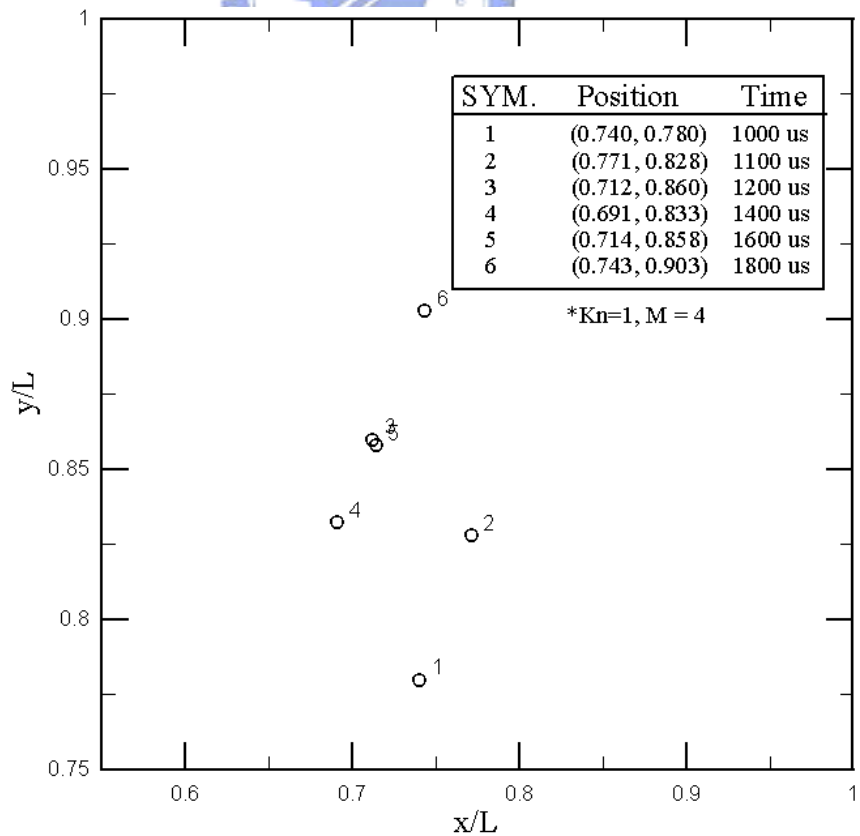


**Fig. 3.106** Positions of the center of the vortex for  $M=4$ ,  $Kn=1$  at  $1000 \sim 1800 \mu s$ .

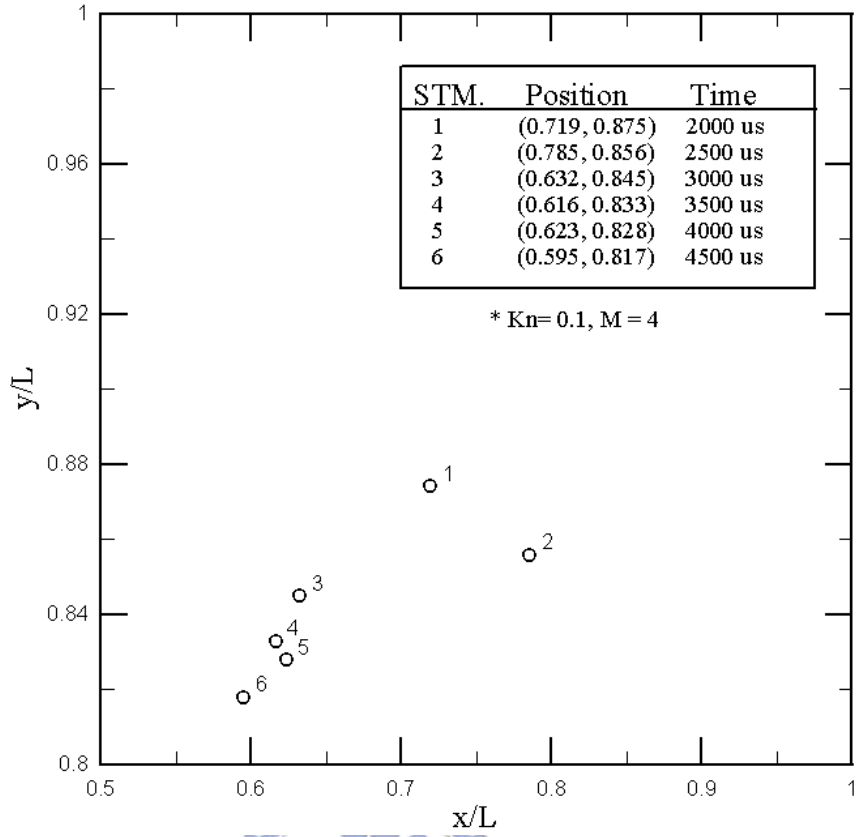


**Fig. 3.107** Positions of the center of the vortex for  $M=4$ ,  $Kn=0.1$  at  $2000 \sim 4500 \mu s$ .

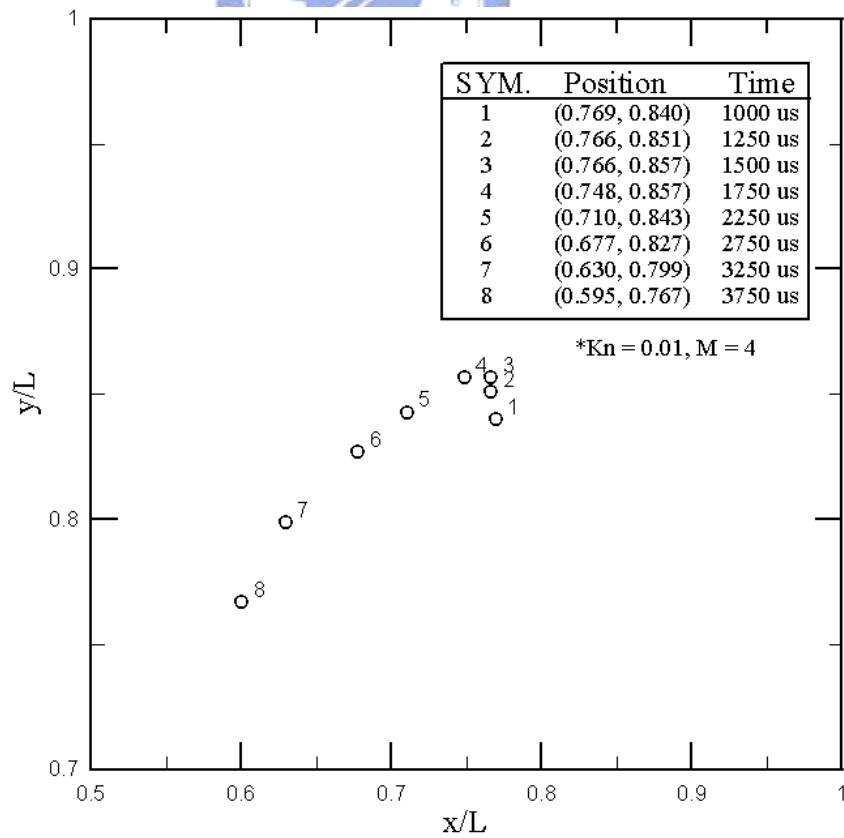


**Fig. 3.108** Positions of the center of the vortex for  $M=4$ ,  $Kn=0.01$  at  $1000 \sim 3750 \mu s$ .



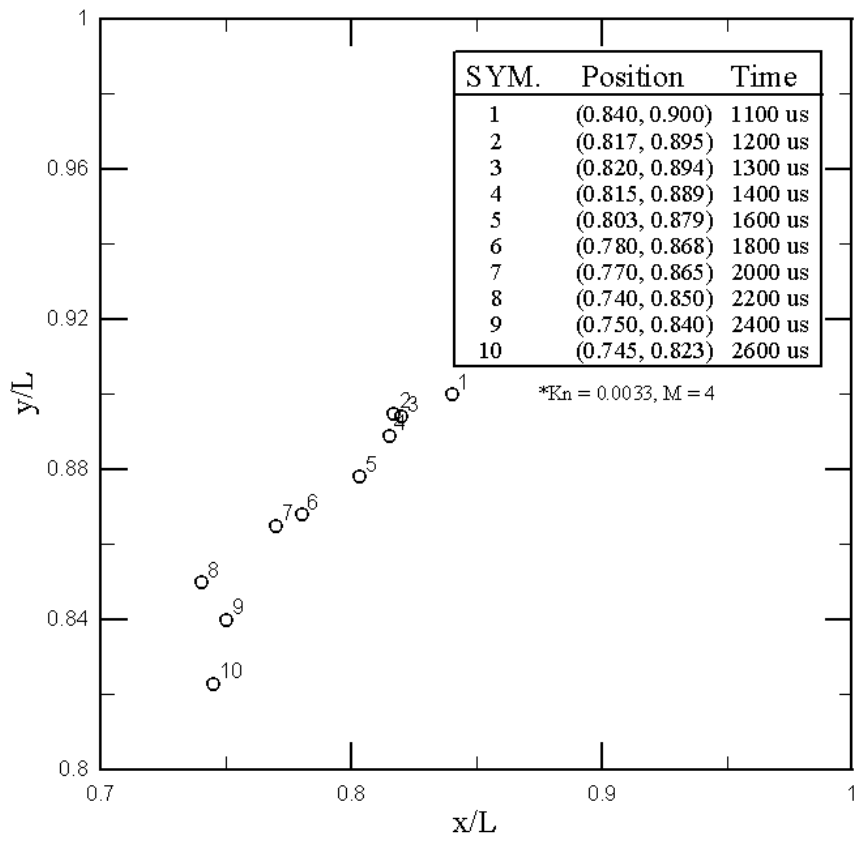


**Fig. 3.109** Positions of the center of the vortex for  $M=4, K_n=0.0033$  at  $1200 \sim 2600 \mu s$ .

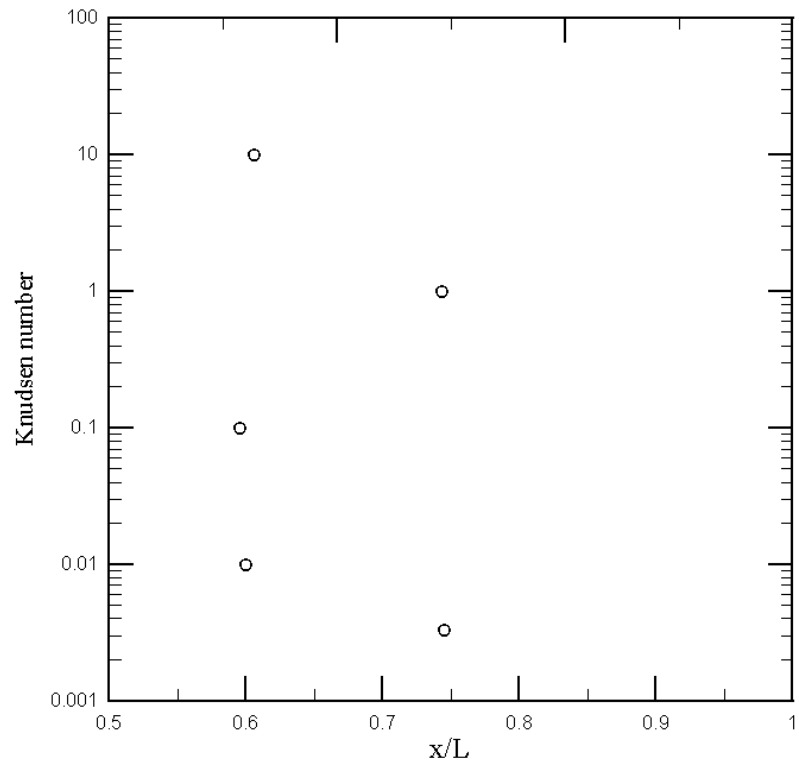


**Fig. 3.110** Positions of the center of the vortex with  $M=4$  for values of  $x/L$  and Knudsen number.

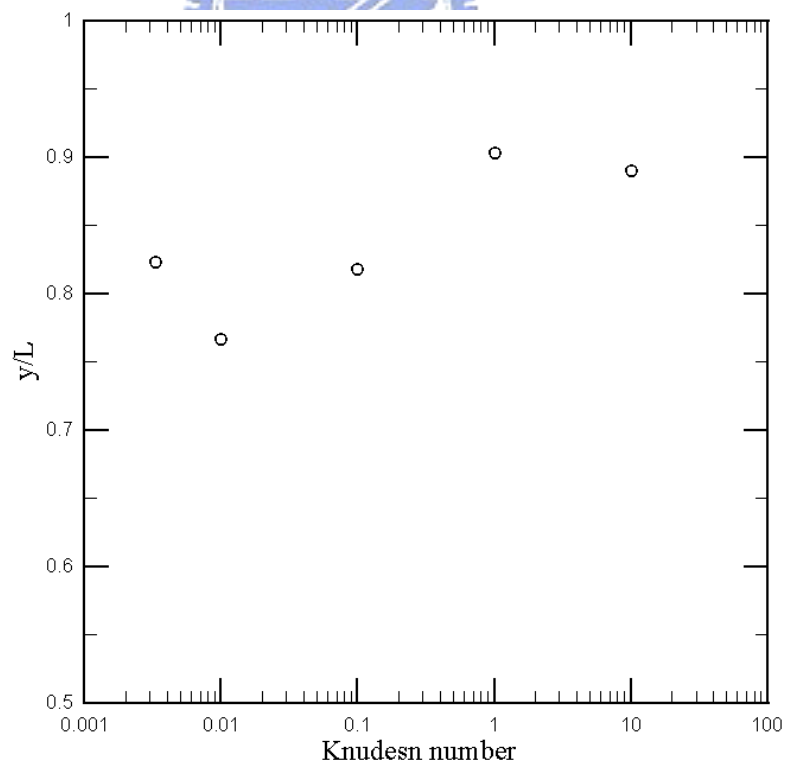


**Fig. 3.111** Positions of the center of the vortex with  $M=4$  for values of  $y/L$  and Knudsen number.